Orbital and Rotational Dynamics of Solar Power Satellites in Geosynchronous Orbits

Ian J. McNally

Submitted in fulfilment of the requirements for the
Degree of Doctor of Philosophy

Aerospace Sciences Research Division
School of Engineering
College of Science and Engineering
University of Glasgow

March 2016

“That orbed continent the fire
That severs day from night. ”
- William Shakespeare

Preface

This thesis presents work carried out by the author in the Aerospace Sciences Research Division at the University of Glasgow in the period from October 2011 to March 2016. The content is original except where otherwise stated.

Ian J. McNally

Dedication

To my parents, Nicola and John, for all you've done and the example you set. To my grandparents Betty, Ian, Isabelle, and Russell.

> "To travel hopefully is a better thing than to arrive and the true success is to labour."
>
> - Robert Louis Stevenson

Acknowledgements

First and foremost, I would like to acknowledge the support and guidance of both Dr. Daniel Scheeres and Dr. Gianmarco Radice. I have learned a great deal from working with Dr. Scheeres, whose direction and patience has been invaluable. Dr. Radice saw the potential in me to undertake a Ph.D. in the first place, and always remained a great source of support despite us being on different continents. During my first year especially, Dr. Matteo Ceriotti was also instrumental.

My fellow researchers in the field of space based solar power for their passion which has been a great source of inspiration, especially Paul Jaffe and Martin Leitgab.

I have been fortunate enough to enjoy the friendship of some very talented and special people, both in Glasgow and Boulder. Within the celestial and spaceflight mechanics laboratory, a special mention to Kohei, Aaron, and Toshi. Nicola, for always being grand 'craic'. Kiichiro, for always being willing to indulge in a shared enjoyment of the 'finer' things in life. Travis, for showing me what it truly means to be American.

For their help with the difficulties involved in arranging an prolonged research 'visit': Elaine McNamara, Heather Lambie, and Sarah Melssen.

Lastly, thanks again to my parents who have always been incredibly supportive.

This material is based upon work supported by the Engineering and Physical Sciences Research Council (EP/J500434/1, EP/P505534/1). The support of the Royal Society of Edinburgh J. M. Lessells travel scholarship is gratefully acknowledged.

Abstract

Designs for geostationary (GEO) solar power satellites (SPS) are extremely large in scale, more than one order of magnitude larger than the International Space Station. In this thesis a detailed study of the orbit dynamics of SPS is performed. Analytical equations, derived by the process of averaging of the SPS equations of motion, are used to determine the long-term orbital evolution. Previous SPS studies have simply assumed a GEO as the operational orbit, and then designed control systems for maintaining the orbit within acceptable nominal values. It is found that an alternative SPS orbital location known as the geosynchronous Laplace plane orbit (GLPO) is superior to GEO in many aspects. An SPS in GLPO requires virtually no fuel to maintain its orbit, minimises the risk of debris creation at geosynchronous altitude, and is extremely robust operationally, i.e. loss of control is inconsequential. The GLPO SPS requires approximately 10^5 kg less fuel per year compared to a GEO SPS while providing near equivalent power delivery. Although savings in orbit control are achieved, depending on the mass distribution of the SPS, attitude control costs may be incurred by placing an SPS in GLPO. Consideration of the attitude dynamics of SPS has motivated the development of a model for the rotational dynamics of a body which includes energy dissipation and the effects of external torques. Multiple spring-damper masses are used to provide a mechanism for energy dissipation. This rotational dynamics model is used to assess the naturally stable attitude configurations of a SPS design in geosynchronous orbit subject to gravity gradient torque. It is found that for a large planar array, a dynamically stable configuration requiring nominal orbit-attitude control is possible. This involves rotating around the maximum axis of inertia at the orbit rate, with the minimal axis aligned in the radial direction.

It will be shown that a SPS in this configuration while in GLPO requires virtually no orbit or attitude control. The most significant result of the research in this thesis is proving that a SPS can operate in GLPO with nominal orbit control and yet still deliver almost equivalent power to the Earth's surface as the same SPS would in a controlled GEO.

Contents

List of Figures

List of Tables

Nomenclature

CHAPTER 1: Introduction

Roman

a	Semi-major axis, m
e	Eccentricity
f	True anomaly, deg
i	Inclination, deg

Greek

μ	Standard gravitational parameter, km^3/s^2
ω	Argument of perigee, deg
Ω	Right ascension of the ascending node (RAAN), deg

Vectors

$\boldsymbol{l}$	Angular momentum of a rigid body, kg m^2/s

CHAPTER 2: Systems Analysis of the Sandwich SPS

Roman

a_{SRP}	Magnitude of the acceleration due to solar radiation pressure, m/s^2
c_{ETO}	Cost to launch SPS material plus orbit transfer propellant to LEO, $
c_{prod}	Cost of production, $
$c_{RDT\&E}$	Cost of research, development, test & evaluation, $
c_{SPS}	Total cost of SPS system, $
c_{TFU}	Cost of theoretical first unit, $
m_{IT}	Interconnecting tether mass, kg
$m_{p,OM}$	Propellant for orbit maintenance, kg
m_{ref}	Reflector mass, kg
m_{SA}	Solar array mass, kg
m_{SEP}	Solar electric propulsion system dry mass, kg
m_{SPS}	Mass of a single SPS on injection to orbit, kg
$m_{SPS,f}$	End of mission mass of SPS, kg
m_{TA}	Transmitting antenna mass, kg
m_{tank}	Propellant tank mass, kg
n	Mean motion, rad/s
n_{op}	Number of orbital planes in constellation
n_{spp}	Number of satellites per orbit plane
s_{LEO}	Specific launch cost, $ /kg
s_{MF}	Cost of manufacture per unit mass of SPS, $ / kg
$t_{A,1year}$	Total access time of entire SPS system, s
$t_{A,mission}$	Total time SPS system is beaming power to the ground, s
$t_{mission}$	Total mission lifetime, s
A_i	Acceleration component in radial, along-track, or out of plane direction (S,N,W), m/s^2
A_{min}	Minimum acceleration required to correct orbit per orbit period, m/s^2
A_{ref}	Area of reflector, m^2
A_{SA}	Area of solar arrays, m^2
A_s	Spacecraft cross sectional area with respect to the sun, m^2

A_v	Spacecraft cross sectional area with respect to the velocity direction, m^2
$A_{S,ref}$	Average cross sectional area of reflectors with respect to the incoming solar radiation, m^2
$A_{S,SP}$	Average cross sectional area of sandwich panel with respect to incoming solar radiation, m^2
A_x	Area of transmitting antenna, m^2
C	Sunlight concentration factor
C_D	Coefficient of drag
C_{ref}	Reflection coefficient of the reflectors
C_{SP}	Reflection coefficient of sandwich panel
D_x	Diameter of transmitting antenna, m
E_D	Total energy delivered to ground based receivers, J
F_A	Annual access fraction
F_T	Engine thrust, N
L_r	Launch rate per year
M_{LEO}	Total mass to be launched to LEO, kg
$M_{P,OT}$	Propellant mass for orbit transfer/s for whole SPS system, kg
M_{SPS}	Final on-orbit mass of entire SPS system, kg
N	Total number of SPSs
N_{orb}	Number of orbits per day
N_T	Total number of orbits for which orbital perturbations can be controlled using the available propellant
P	Electric power, W
P_{SPS}	Power delivered by SPS, W
P_Φ	Solar radiation constant, $kgkm^3/s^2/m^2$
Q_{in}	Heat absorbed, J
Q_{out}	Heat radiated, J
S	Learning curve slope
T	Orbital period, s
W	Solar power at 1AU, W/m^2

Greek

ε	Minimum elevation angle, deg
ζ	Engine mass to power ratio, kg/W
η_{SEP}	Electric ion engine efficiency, %
η_{SPS}	End-to-end efficiency of SPS system, %
$\mu_{M/S}$	Gravitational parameter of the Moon/Sun, km^3/s^2
ρ	Atmospheric density, kg/m^3
σ_{ref}	Reflector mass per unit area, kg/m^2
σ_{SA}	Solar array mass per unit area, kg/m^2
σ_{TA}	Transmitting antenna mass per unit area, kg/m^2
ω_E	Angular rate of Earth's rotation, rad/s
Δa_D	Change in semi-major axis over one orbit revolution, m
Δe_{SRP}	Change in eccentricity over one orbit period due to solar radiation pressure
$\Delta i_{M/S}$	Change in i over one orbit period due to luni/solar gravitational attraction, deg
$\Delta i_{2\pi}$	Change in inclination over one orbit revolution, deg
Δv	Change in velocity per orbit, m/s
Δv_a	Change in velocity for co-planar transfer, m/s
Δv_{inc}	Change in velocity for inclination change, m/s
Δv_t	Total change in velocity for orbit transfer, m/s
Δt	Single arc of thrust time, s
$\Delta V_{S,N,W}$	Components of impulse in the radial, along-track, and out-of-plane directions respectively, m/s
ΔV_{rev}	Change in velocity required each orbit to maintain a Keplerian orbit, m/s
$\Delta V_{mission}$	The total Δv requirement for the entire mission, m/s
$\Delta\omega_{J_2}$	Change in ω over one orbit period due to J_2, deg
$\Delta\omega_{M/S}$	Change in ω over one orbit period due to luni/solar gravitational attraction, deg
$\Delta\Omega_{J_2}$	Change in Ω over one orbit period due to J_2, deg
$\Delta\Omega_{M/S}$	Change in Ω over one orbit period due to luni/solar gravitational attraction, deg

CHAPTER 3: Orbital Dynamics of Geosynchronous SPSs

Roman

l	Mean longitude, rad
$\dot{l}$	Averaged rate of change of mean longitude, rad/s
m	Mass of the solar power satellite, kg
n	Mean orbital motion, rad/s
x	Inter-antenna separation distance, km
A	Average cross-sectional area of the solar power satellite with respect to the Sun, m^2
C_{20}	Earth's dimensional oblateness gravity field coefficient
C_{22}	Earth's dimensional ellipticity gravity field coefficient
D_T	Antenna diameter, km
D_R	Rectenna diameter, km
J_2	Earth's 2^{nd} degree zonal gravitational harmonic coefficient
J_{22}	Earth's 2^{nd} degree and order sectorial gravitational harmonic coefficient
P_{C-GEO}	Power received at an equatorial ground station from a solar power satellite in a controlled geostationary orbit, W
P_{U-GEO}	Power received at an equatorial ground station from a solar power satellite in an uncontrolled initially geostationary orbit, W
P_{GLP}	Power received at an equatorial ground station from a solar power satellite in a geosynchronous Laplace plane orbit, W
P_r	Power received at ground station, W
P_t	Power transmitted from the solar power satellite, W
P_Φ	Solar radiation constant, $kgkm^3/s^2/m^2$
R_E	Radius of the Earth, km
$\mathcal{R}_2$	Second degree and order gravitational perturbation potential, km^2/s^2
$\mathcal{R}_{20}$	Second degree and zeroth order perturbation potential, km^2/s^2
$\mathcal{R}_p$	Third body gravitational perturbation potential, km^2/s^2
$\mathcal{R}_{SRP}$	Solar radiation pressure perturbation potential, km^2/s^2

Greek

α	Beamed power incident angle with respect to the ground station normal, deg
β	Off-axis beam steering angle, deg
γ	Solar radiation pressure constant given by $(1+\rho)(A/m)P_\Phi$, km^3/s^2
η_t	Beam coupling efficiency
ρ	Reflectance of solar power satellite
Λ	Solar radiation perturbation parameter, deg
Φ	Laplace plane inclination with respect to the Earth's equatorial plane, deg

Vectors

$\boldsymbol{a}_2$	Acceleration due to Earth J_2, km/s^2
$\boldsymbol{a}_{22}$	Acceleration due to Earth J_{22}, km/s^2
$\boldsymbol{a}_p$	Acceleration due to third body gravitational perturbations , km/s^2
$\boldsymbol{a}_{SRP}$	Acceleration due to solar radiation pressure, km/s^2
$\boldsymbol{a}_\mu$	Acceleration due to the microwave power beam, km/s^2
$\boldsymbol{d}_e$	Sun to Earth position, km
$\boldsymbol{d}_p$	Earth to perturbing body position, km
$\boldsymbol{e}$	Orbital eccentricity
$\dot{\boldsymbol{e}}$	Secular rate of change of $\boldsymbol{e}$, 1/s
$\dot{\boldsymbol{e}}_{SRP}$	Secular rate of change of $\boldsymbol{e}$ due to solar radiation pressure, 1/s
$\dot{\boldsymbol{e}}_{20}$	Secular rate of change of $\boldsymbol{e}$ due to J_2, 1/s
$\dot{\boldsymbol{e}}_p$	Secular rate of change of $\boldsymbol{e}$ due to 3^{rd} body gravitational perturbation, 1/s
$\boldsymbol{H}$	Orbital angular momentum per unit mass, m^2/s
$\boldsymbol{h}$	Scaled orbital angular momentum given by $\boldsymbol{H}/\sqrt{\mu a}$
$\dot{\boldsymbol{h}}$	Secular rate of change of $\boldsymbol{h}$, 1/s

$\dot{\boldsymbol{h}}_{SRP}$	Secular rate of change of $\boldsymbol{h}$ due to solar radiation pressure, 1/s
$\dot{\boldsymbol{h}}_{20}$	Secular rate of change of $\boldsymbol{h}$ due to J_2, 1/s
$\dot{\boldsymbol{h}}_{p}$	Secular rate of change of $\boldsymbol{h}$ due to 3^{rd} body gravitational perturbation, 1/s
$\boldsymbol{r}$	Orbital position, km
$\boldsymbol{r}_{GS-SPS}$	Ground receiving station to solar power satellite relative position , km
$\boldsymbol{v}$	Orbital velocity, km/s

CHAPTER 4: Attitude Dynamics of Geosynchronous SPSs

Roman

$\mathrm{d}m_1$	Infinitesimal mass element in Body 1, kg
$\mathrm{d}m_2$	Infinitesimal mass element in Body 2, kg
$\mathcal{B}_1$	Body 1, the Earth
$\mathcal{B}_2$	Body 2, the Solar Power Satellite
F_{Thrust}	Average force that must be provided by thrusters to cancel gravity gradient torque, kgm/s^2
$\mathcal{I}$	Inertial reference frame
M_1	Mass of $\mathcal{B}_1$, kg
M_2	Mass of $\mathcal{B}_2$, kg
V	Mutual gravitational potential between two bodies, kgm^2/s^2
Δm_{AC}	Mass of fuel required for cancellation of gravity gradient torque, kg

Matrices/Vectors

$\boldsymbol{r}$	Radius vector between mass elements dm_1 and dm_2, m
$\boldsymbol{\rho}_1$	Radius vector from the origin of $\mathcal{B}_1$ to dm_1, m
$\boldsymbol{\rho}_2$	Radius vector from the origin of $\mathcal{B}_2$ to dm_2, m
$\boldsymbol{A}_1$	Attitude dyadic from Body 1 frame to $\mathcal{I}$
$\boldsymbol{A}_2$	Attitude dyadic from Body 2 frame to $\mathcal{I}$
$\boldsymbol{I}_i$	Inertia dyadic of body i, kgm^2
$\boldsymbol{R}$	Radius vector between the origins of bodies 1 and 2, m
$\boldsymbol{\Omega}_1$	Angular velocity of Body 1 relative to $\mathcal{I}$, rad/s
$\boldsymbol{\Omega}_2$	Angular velocity of Body 2 relative to $\mathcal{I}$, rad/s

CHAPTER 5: Accounting for Energy Dissipation

Roman

$\mathcal{R}$	Rigid body
$\mathcal{P}/\mathcal{P}_{ij}$	Internal point mass damper
$\mathcal{F}_{\mathcal{I}}$	Inertial reference frame
$\mathcal{F}_{\mathcal{P}}$	Principal axis reference frame
$\mathbf{0}$	Chosen origin of body frame
$c_{d,ij}$	Damping coefficient, kg/s
$\mathrm{d}V$	Infinitesimal element of volume in $\mathcal{R}, m^3$
f_n	Natural frequency, 1/s
$k_{d,ij}$	Spring constant, kgs^2
m_b	Mass of rigid body $\mathcal{R}$, kg
$m_{d,ij}$	Mass of point mass damper $\mathcal{P}_{ij}$, kg
m	Mass of rigid body and all point mass dampers, kg
$p_{n,ij}$	Component of damper momenta along damper axis, kgm/s
E	Total energy of the system, J
T	Kinetic energy of the system ($\mathcal{R} + \sum_{i,j=1}^{3,2} \mathcal{P}_{ij}$), J
V_{ij}	Potential energy of the spring, J

Greek

ξ_{ij}	Damper displacement from equilibrium position, m

$\dot{\xi}_{ij}$	Rate of change of damper displacement, m/s
θ_i	Nutation angle, deg
τ_D	Damping time, s
$\sigma(\underrightarrow{r})$	Mass density at $\underrightarrow{r}$, kg/m^3
Δ	Attitude deviation angle between $\boldsymbol{R}$ and $\hat{\boldsymbol{p}}_1$, deg

Vectors / Matrices

$\underrightarrow{b}_{ij}$	Position vector of point mass corresponding to a relaxed spring, i.e. for $\xi_{ij} = 0$, m
$\underrightarrow{c}$	First moment of inertia of the system with respect to $\mathbf{0}$, kg m
$\underrightarrow{c}_b$	First moment of inertia of $\mathcal{R}$ with respect to $\mathbf{0}$, kg m
$\underrightarrow{f}$	External force acting on $\mathcal{R}$, N
$\underrightarrow{f}_{d,ij}$	Force $\mathcal{R}$ exerts on $\mathcal{P}_{ij}$, N
$\underrightarrow{f}_{con,ij}$	Constraining force normal to the direction of $\mathcal{P}_ij$'s travel, N
$\underrightarrow{g}$	External torque acting on $\mathcal{R}$, Nm
$\underrightarrow{l}$	Absolute angular momentum of system $(\mathcal{R} + \sum_{i,j=1}^{3,2} \mathcal{P}_{ij})$ about $\mathbf{0}$, kgm^2/s
$\underrightarrow{l}_b$	Absolute angular momentum of rigid body $\mathcal{R}$ about $\mathbf{0}$, kgm^2/s
$\underrightarrow{\hat{n}}_{ij}$	Unit vector defining the direction of $\mathcal{P}_{ij}$'s travel
$\underrightarrow{p}_b$	Linear momentum of $\mathcal{R}$, kgm/s
$\underrightarrow{p}_{d,ij}$	Linear momentum of $\mathcal{P}_{ij}$, kgm/s
$\underrightarrow{p}$	Total linear momentum of the system $(\mathcal{R} + \sum_{i,j=1}^{3,2} \mathcal{P}_{ij})$, kgm/s
$\underrightarrow{r}$	Position vector of small volume element dV with respect to $\mathbf{0}$, m
$\underrightarrow{r}_{d,ij}$	Position vector of $\mathcal{P}_{ij}$ with respect to $\mathbf{0}$, m
$\underrightarrow{v}$	Absolute velocity of $\mathbf{0}$, m/s
$\underrightarrow{\omega}$	Absolute angular velocity of $\mathcal{R}$, rad/s
$\underrightarrow{J}$	Second moment of inertia of the system with respect to $\mathbf{0}$, kg m^2
$\underrightarrow{J}_b$	Second moment of inertia of $\mathcal{R}$ with respect to $\mathbf{0}$, kg m^2
$\underrightarrow{U}$	Identity matrix
$\boldsymbol{\mathcal{M}}$	System inertia matrix
$\boldsymbol{\mathcal{V}}$	Velocities matrix
$\boldsymbol{\varrho}$	Momenta matrix

1

Introduction

> "The energy of the sun was stored, converted, and utilized directly on a planet-wide scale. All Earth turned off its burning coal, its fissioning uranium, and flipped the switch that connected all of it to a small station, one mile in diameter, circling the Earth at half a distance from the moon. All Earth ran by invisible beams of sunpower."
>
> - Isaac Asimov

1.1 The Solar Power Satellite

The solar power satellite (SPS) is conceptually simple: a large Earth orbiting satellite designed to act as an electric power plant in orbit. The SPS consists of three main segments: a solar energy collector to convert the solar energy into direct current (DC) electricity, a DC-to-microwave converter, and a large antenna which beams the microwave power to the ground. The main benefits of collecting sunlight and converting it to electricity in space are: the sunlight is not attenuated by Earth's atmosphere, collection is not influenced by the day-night cycle, and power may be rapidly re-directed to areas of high demand. SPS also offers a CO_2 free, unlimited source of energy.

The concept of the solar power satellite originates in the 1941 short story 'Reason' by the science fiction author Isaac Asimov. The story features the protagonists being assigned to a space station which collects solar energy and beams it to numerous planets as microwaves. The idea did not garner any serious consideration until the first technical analysis of the concept was performed by Peter Glaser in 1968.[1] Glaser, who became a life long proponent of space solar power, was the first to propose that

the ideal location for a SPS to serve Earth would be in geostationary Earth orbit (GEO). Glaser later received a patent on a conceptual design in 1973.

Large scale studies were instigated by National Aeronautics and Space Administration (NASA) and the Department of Energy (DOE) in the early 1980's. Due to the physics of microwave beaming from geosynchronous altitude, the size, and hence cost of SPS were found to be prohibitive. The idea has recently resurfaced as improvements have been made in SPS enabling technologies such as photovoltaics and large space structure deployment techniques. A small portion of the extensive literature generated during this period focussed on the attitude and orbit dynamics of the extremely large SPS which were envisaged. In this literature, there is small mention of the possibility of placing SPS in the geosynchronous Laplace plane orbit (GLPO) as a method of eliminating the need for north-south station-keeping. The idea appears to have gained little traction compared to the widely accepted idea of placing SPS in GEO. The main reason for this appears to have been that for the reference system, only delivery of power to a relatively high latitude ground station (in North America) was considered. Delivery to a high latitude ground station from GLPO requires a significantly larger receiving antenna (rectenna) than from GEO. This was the justification for not considering GLPO, however, no detailed trade-off studies were performed.

1.2 Aims and Objectives

1.2.1 Aims

- Determine if the geosynchronous Laplace plane orbit (GLPO) is superior to geostationary Earth orbit (GEO) for the application of solar power satellites (SPS).
- Investigate the feasibility of operating different SPS designs in the GLPO from both an orbit and attitude dynamics perspective.

1.2.2 Objectives

- Perform a systems analysis and determine the optimal orbit for a SPS to deliver the highest Energy/Cost ratio.
- Construct an orbit propagation model which accounts for the major perturbations acting at geosynchronous altitude and is capable of fast propagation of uncontrolled SPS orbits over their full proposed lifetime of 30+ years.
- From the orbit propagations, determine if without orbit control the SPS remains in beam pointing range for a phased array antenna.
- Measure the power delivery from the SPS to a ground receiving antenna (rectenna), accounting for the power loss due to non-zero incident angle of the beamed radiation and variation in the separation distance between the SPS and rectenna.
- Assess the propellant costs for orbit and attitude control for different SPS designs in GLPO vs GEO.
- Assess the orbit and attitude stability of different SPS designs.

1.3 Contributions

- Found that GLPO offers the best energy to cost ratio for SPS systems. Systems analysis method allows SPS systems to be evaluated in terms of energy to cost ratio accounting for manufacture, launch, orbital transfer costs, orbital maintenance, and power delivery accounting for non-zero incident angle.
- Identified priorities for SPS research based upon sensitivity analysis of the systems analysis model.

- Shown that certain SPS designs are capable of operating with nominal fuel for both orbit and attitude control in a stable orbit-attitude configuration. The implication of this finding is that it removes the need for developing higher I_{sp} electric ion thrusters for SPS control, as those currently available could maintain gravity gradient SPS in the GLPO using a relatively small amount of propellant. It also removes the engineering problem of either storing large volumes of propellant (of the order 10^6 kg for an SPS lifetime), or devising a re-fuelling strategy.

- Showed that the difference in gravity gradient torque for SPS in GLPO vs GEO is minimal accounting for Earth oblateness.

- Quantified the power delivery performance from GLPO and GEO for SPS over mission lifetime.

- Confirmed the orbit stability of multiple SPS designs in the GLPO.

- Confirmed the attitude stability of the Tethered and Sun-Tower SPSs in gravity gradient orientated attitude configuration in the GLPO.

1.4 Statement of Research

A thorough analysis of the dynamics and operational implications of placing large solar power satellites in the geosynchronous Laplace plane as opposed to geostationary orbits is presented. A long term orbit propagation model is implemented using the Milankovitch orbital elements and first order averaging. The attitude dynamics of SPS in GLPO are then considered. Motivated by the issue of attitude stability for large flexible structures, such as SPS, an energy dissipation model is developed. A mechanism for energy dissipation is provided by a multiple spring-mass-damper system. External forces and torque due to gravity are incorporated to model the orbit-attitude dynamics of SPS in both GEO and GLPO. The major outcome of the

thesis is summarised in the following thesis statement.

Thesis Statement:

> There are clear and tangible benefits to utilising the geosynchronous Laplace plane orbit for the application of solar power satellites instead of geostationary Earth orbit. Orbit control fuel savings are possible and the risk of future orbital debris creation is minimised, with no significant degradation in power delivery performance.

1.4.1 Publications

- McNally, I., Scheeres, D., Radice, G., Locating large solar power satellites in the geosynchronous Laplace plane, Journal of Guidance, Control, and Dynamics, Vol. 38, No. 3 (2015), pp. 489-505
- McNally, I., Scheeres, D., Radice, G., Attitude dynamics of large geosynchronous solar power satellites, Astrodynamics Specialist Conference, San Diego, California, 2014
- McNally, I., Scheeres, D., Radice, G., Orbital dynamics of large solar power satellites: The geosynchronous Laplace plane, Spaceflight Mechanics Meeting, Sante Fe, New Mexico, 2014
- McNally, I., Scheeres, D., Radice, G., Ceriotti, M., Orbital dynamics of large solar power satellites, 64th International Astronautical Congress, Beijing, 2013
- McNally, I., Ceriotti, M., Radice, G., Systems analysis of the sandwich solar power satellite, 63rd International Astronautical Congress, Naples, 2012

1.5 Thesis Structure

In Chapter 1 the classical orbit elements are introduced following from the formulation of the two body problem. A more detailed overview of solar power satellites is provided. Finally, the dynamic and kinematic equations for the rotational motion of a generic rigid body are introduced.

In Chapter 2 an initial systems analysis study on solar power satellite systems is presented. Multi-objective optimisation using genetic algorithms is used to identify optimal parameters for SPS systems. Geosynchronous Laplace Plane orbits are confirmed to be the most cost-effective.

Chapter 3 contains an in-depth analysis of the orbital dynamics of geosynchronous orbits for SPS. Utilising the non-singular Milankovitch orbit elements, an averaged model of the dynamics is constructed for the long-term orbit propagation of geosynchronous SPS. The apparently optimal non-zero inclination orbit is named the geosynchronous Laplace plane orbit (GLPO) and the operational implications of operating in GLPO compared to GEO are considered. GLPO is found to be a feasible alternative to GEO and offers numerous benefits: an SPS in GLPO requires virtually no fuel to maintain its orbit, minimises the risk of debris creation at geosynchronous altitude, and is extremely operationally robust, i.e. loss of control is inconsequential. The GLPO SPS saves approximately 10^5 kg per year in fuel compared to a GEO SPS for near equivalent power delivery.

Although there are orbit control savings offered by locating SPS in GLPO, depending on the mass distribution and attitude configuration, there can be minor penalties in terms of attitude control costs. Chapter 4 considers the implications for attitude control against gravity gradient torque for placing Abacus SPS in GLPO rather than GEO. Coupled orbit and attitude equations of motion are derived with mutual gravitational attraction investigated. The propellant cost of maintaining attitude control is calculated for Abacus SPS operating in both GEO and GLPO.

Motivated by consideration of the attitude stability of SPS designs, a model for rotational dynamics with a mechanism for energy dissipation is developed in Chapter 5. This is then applied to the case of a geosynchronous SPS with gravity gradient and internal energy dissipation acting. The naturally stable attitude configuration for any SPS structure can be determined with this model. Configurations for SPS designs which require minimal attitude control are identified. For a triaxial SPS, the stable attitude configuration consists of rotation around the maximum axis of inertia at the orbit rate with the minimum axis of inertia Earth pointing. This is a gravity gradient stabilised satellite. For large flat platforms, such as Type I SPS, the naturally stable configuration requiring nominal orbit-attitude control is the gravity gradient stabilised orientation in a GLPO.

1.6 The Solar Power Satellite

Peter Glaser's SPS study[1] was the first proper technical analysis of SPS and prompted a wide range of technical studies in the 1970's and 1980's, such as the comprehensive 'SPS Concept Development and Evaluation Program' published by NASA and the Department of Energy (DoE).[2] As a result of these studies, a reference system was defined which consisted of a large solar array (5.3 $\times$ 10.7 km) with a large gimballed microwave transmitting antenna (1 km in diameter) as shown in Fig. 1.1. The definition of this reference system allowed many of the design parameters to be locked in which enabled more focused technical studies to be completed. One such parameter was the orbital location, GEO was chosen.

The surge in interest in space solar power at this time may in part be attributed to the previous success of the Apollo missions (and their recent end, leaving many looking for the next big space project) and rising oil prices at the time. This led to some extremely ambitious designs for solar power satellites. The so-called SPS "reference system" proposed a network of 100's of SPSs, each delivering 5 GW. It was envisaged that such a system would require the development of new higher capacity

launchers, and also on-orbit construction by 100's of astronauts. Plans for a space-station staging satellite to house the astronauts were also considered. The highly detailed nature of these studies (1000's of pages long) was impressive, yet, perhaps premature. Due to the ambition of the designs for SPS at the time, it is perhaps not surprising that these plans were shelved in 1980.[3] Oil prices had fallen to more reasonable levels and the economic case for SPSs could not be made. The technology development required and capital costs were excessive. As was the case then, and now, space solar power is not likely to replace all other forms of energy and should not be considered in this context. However, it may form an important part of the solution in the future and offers some unique advantages. For instance, with just 3 geosynchronous SPSs, over 90% of the worlds population would be within range to receive power on demand.

Since the initial studies, the concept of SPS has been periodically revisited, often motivated by concerns surrounding global climate change and the search for a reliable clean source of energy. Consequently, the SPS concept has evolved. The NASA Fresh Look study[4] produced a number of new SPS designs and resulted in a shift in emphasis towards modular and smaller SPS. Rather than focusing on designing a large scale SPS system capable of producing a significant portion of mankind's energy needs, small niche energy markets were considered for the first time. For example, delivering energy to military bases in remote or dangerous locations via small SPS systems was proposed.[5] The cost of delivering energy from SPS in this case does not need to be competitive with commercial suppliers. Instead, it must compete against the cost of generating energy in these situations via conventional means (transporting fuel to power generators) which is expensive due to the transport of the fuel through hostile territories. A roll-up rectenna could potentially be unfurled and receive power from a network of low Earth orbit SPS. This could certainly be an interesting niche market which would allow a small-scale SPS system to be implemented which would serve a useful purpose and simultaneously demonstrate the technology for a future large-scale

system.

The most recent SPS research initiative was announced in April 2015. An agreement between Northrop Grumman and Caltech was signed which involves up to $17.5M being provided over 3 years[6] to pursue SPS related research. The aim of the research program is to develop the following technologies: high-efficiency ultralight photovoltaics; ultralight deployable space structures; and phased array and power transmission.

The awareness of SPS as a potential energy source for development was raised by a recent competition across the Department of Defense, Department of State, and the U.S. Agency for International Development where entrants were tasked with proposing ideas to simultaneously advance U.S. diplomacy, defense and development (the 3 D's of foreign policy). A multi-agency-industry team with representatives from the Air Force's Air University, the Naval Research Laboratory (NRL), Northrop Grumman, NASA, the Joint Staff Logistics and Energy Division, the Defense Advanced Research Projects Administration (DARPA), the Army, and the Space Development Steering Committee presented the case for SPS to be developed. The proposal set out plans for a U.S. based research program culminating in a SPS demonstration satellite in 10 years time. The SPS proposal came 1st out of 500 entrants, winning 4 out of 7 categories. Although no follow on funding was included in the competition, it was the first time that SPS has been presented to a high level of U.S. government.

1.6.1 SPS Type Classification

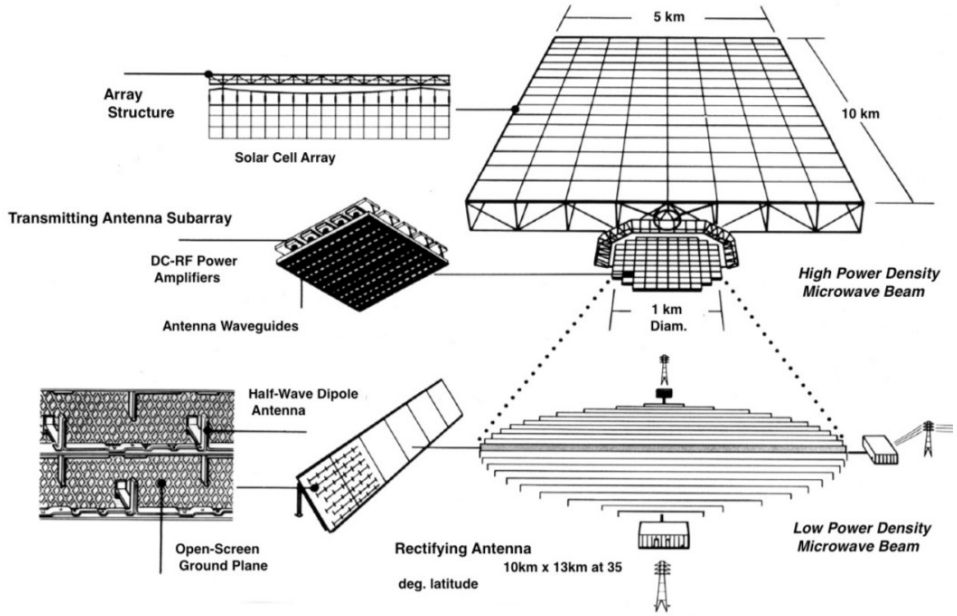

Figure 1.1: SPS reference design (Type I SPS), NASA/DOE artwork 1979-1980.

The reference system is the original of a certain class of SPS referred to as "SPS Type I: SPS Reference and Updated Reference Concepts" in the recent IAA report on SPS.[7] There are two other class of SPS defined in the IAA report, "SPS Type II: SPS Electric Laser Concepts" and "SPS Type III: SPS Sandwich and Related Concepts".

Type I involves one or two large, sun-pointed solar collection systems and one or two Earth-pointed wireless power transmission (WPT) systems (see Fig. 1.1). This is a large, 3-axis stabilised platform system architecture that involves the use of microwave radio frequency (RF) for WPT. The sun-pointing solar collector and Earth-pointing WPT system must be connected by a live rotating coupler (also known as a 'slip-ring').

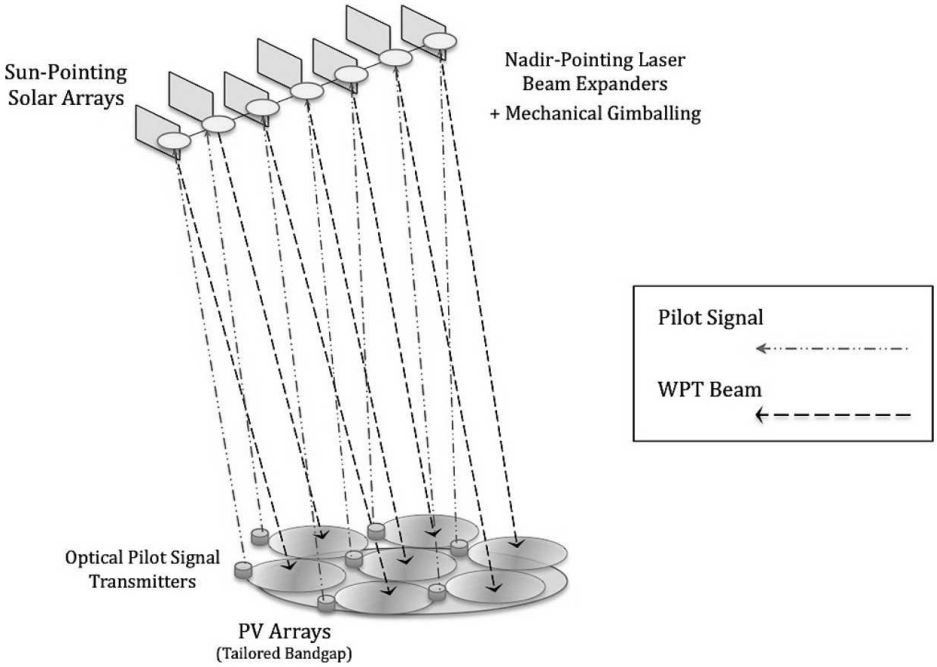

Figure 1.2: Example of a laser Type II SPS, image credit Artemis Innovation Management Solutions LLC.

Type II (see Fig. 1.2) concepts can be either: (1) electric-laser based or (2) solar-pumped laser. Within the area of laser SPS, there are several alternative systems approaches, involving either integrated platforms comprising multiple individual laser systems or constellations of free-flying laser platforms. Laser based designs are generally much smaller in scale. Microwave architectures tend to be favoured due to the superior transmission of microwave frequencies through the atmosphere (and through precipitation).

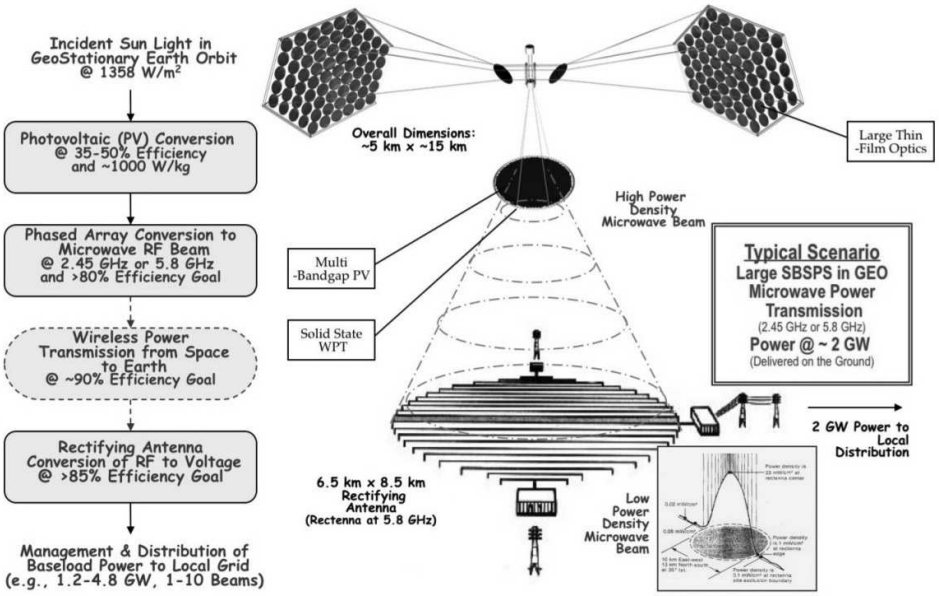

Figure 1.3: End-to-end concept of a sandwich Type III SPS.[7]

Type III (see Fig. 1.3) concepts involve a light redirection based approach to energy distribution on the SPS platform. It also depends upon the successful local integration of solar power generation, power management and distribution, and WPT systems in extremely large numbers of individual modular space systems. Type III SPS are gravity gradient stabilised. Fig. 1.3 presents a conceptual illustration of a recent sandwich type SPS.

In this thesis, Type I and III shall be focussed on. Both involve microwave transmission of power from geosynchronous orbit and, as shown in Fig. 1.1 and 1.3, both are kilometre scale satellites. Understanding the dynamics of such large structures in geosynchronous orbits is the primary aim of the thesis. Type II pose a different set of challenges, including formation flying of smaller scale SPS which is considered outside the scope of this thesis.

1.6.2 SPS Designs Past and Present

Although there is mention of 30 different SPS concepts in the literature in NASA's Fresh Look Study,[4] many of these are purely conceptual with poorly defined design

parameters or they propose the use of technology 'not yet validated in the laboratory'.[4] It is difficult to make comparisons on the costs of different SPS designs as many assume technology that is not fully developed yet. It is certainly possible, however, to compare the technical feasibility of different SPS options.

The 1979 SPS designs consisted of large, erected infrastructures. These massive units required a two-stage Earth-to-orbit (ETO) transportation system to lift the needed material as well as a large construction facility in space and hundreds of astronauts. The financial impact of this deployment scheme was significant. In 1966 dollars, more than $250 billion was estimated to be required before the first commercial kilowatt-hour could be delivered.[4] The dimensions of the NASA baseline SBSP concept from 1981 are shown in Fig. 1.4. The concept has a system mass of approximately 51,000 metric tons.

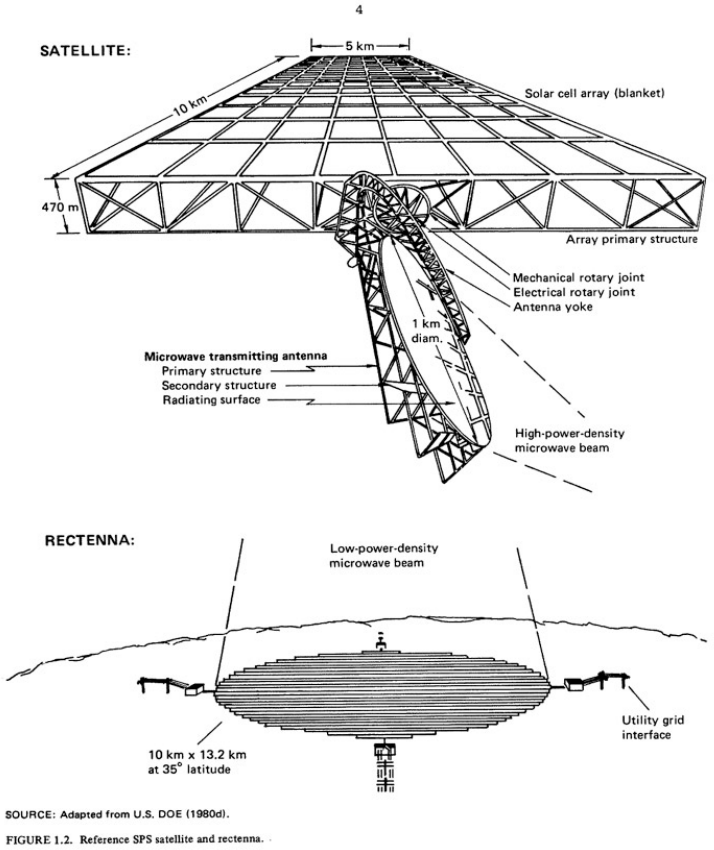

Figure 1.4: SPS reference system.

The U.S. National Research Council (NRC) and the Congressional Office of Tech-

nology Assessment (OTA) concluded that solar power satellites were technically feasible. However, they were declared 'programmatically and economically unachievable' based on the 1979 SPS Reference designs. The NRC recommended that related research continue and that the issue of solar power satellite viability should be revisited in about a decade. In reality, all serious effort on solar power from space by the U.S. government ceased.[4] The NRC report stated, 'Too little is currently known about the technical, economic, and environmental aspects of SPS to make a sound decision whether to proceed with its development and deployment. In addition, without further research an SPS demonstration or systems-engineering verification program would be a high-risk venture.'[8]

NASA decided to re-examine the various technologies, concepts and terrestrial markets that might be involved in future space solar power systems during 1995-1997 in what was known as the 'Fresh-Look' study. Its principal objective was to determine whether solar power satellites (SPS) could deliver energy to terrestrial electrical power grids at prices equal to or below ground alternatives in a variety of markets, do so without major environmental drawbacks, and which could be developed at a fraction of the initial investment projected for the SPS Reference System of the late 1970s.[4] The Fresh-Look study resulting in some new SPS concepts, and importantly, reinforced the finding of previous studies that space solar power/SPS is technically feasible. It was realised that the technology required for SPS was not anywhere near ready, and it was recommended that the emphasis on further SPS studies should be on developing the various technologies required.

In 2011 the IAA published a study that sought to direct SPS research towards the eventual realisation of SPS by performing a detailed assessment of the technical and economic feasibility of different SPS designs. Three types of SPS were identified as the most promising for further study. Also, the question of whether or not the technologies needed for various concepts was currently available, or required additional RD to achieve necessary figures of merit (FOM) and high level of maturity was addressed.

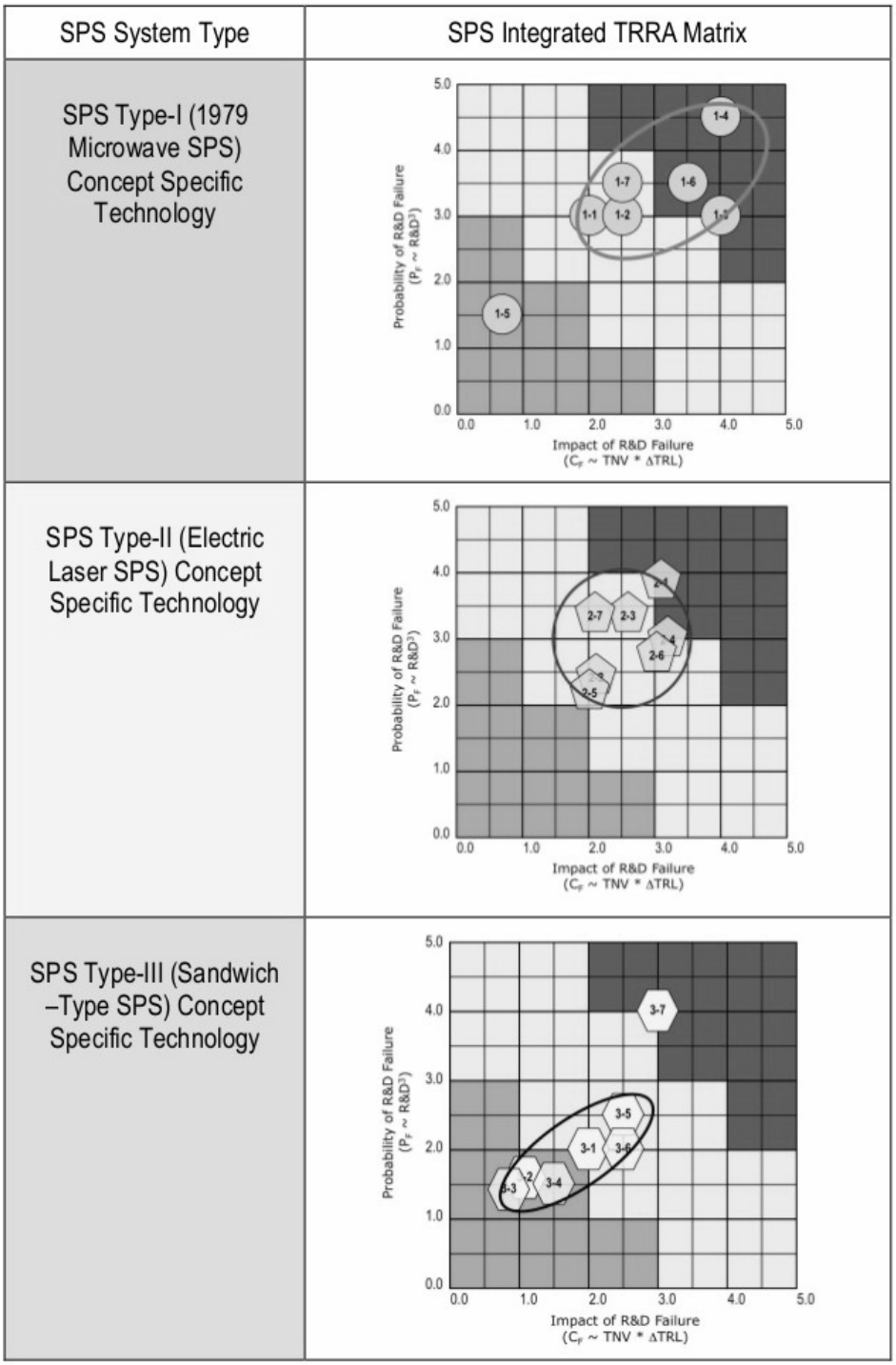

Figure 1.5: Integrated Technology Readiness and Risk Assessments (TRRAs) for the 3 types of SPS.[7]

.

Fig. 1.5 is the main result of the IAA study[7] which categorises the different types of SPS. The technology readiness level (TRL-scale for assessing technological maturity)

was assessed for the technologies required for each type of SPS. The risk associated with each technology, in terms of the probability of failure of the research and development required for that technology was calculated. Fig. 1.5 shows the probability of failure of the RD plotted against the impact of failure for the realisation of the design. The TRLs of each technology are shown as numbers (1-10:1 least mature-10 most mature) on each symbol. This allows the direct comparison of the technical feasibility of the different Types of SPS. SPS Type III are the most technically feasible overall, as the crucial technologies generally have lower probability of failure, and lower impact of failure (i.e. the technologies are clustered closer to the bottom left of the plot). This finding motivates the selection of the Type III (also referred to as sandwich SPS from here on) for the systems analysis of Chapter 2.

1.6.3 Non-Type I/Type III Designs

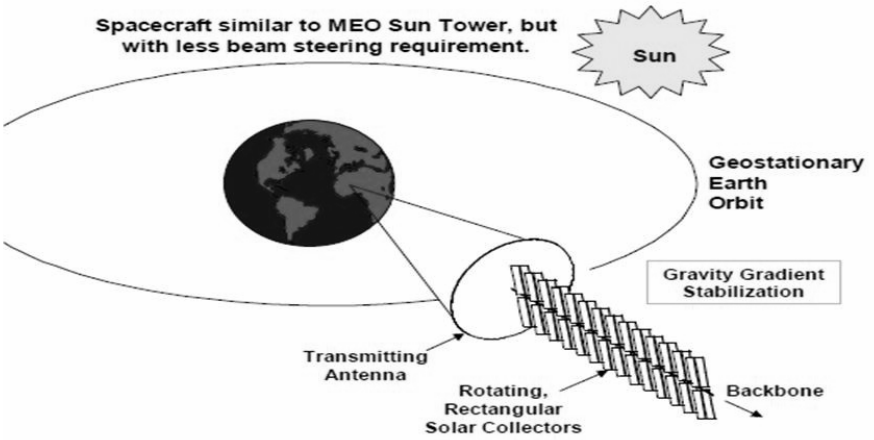

Figure 1.6: Suntower SPS

.

As recognised by the IAA study,[7] some SPS designs do not qualify as Type I, II, or III. Included here are additional SPS designs deemed of interest for investigation of their orbit and attitude dynamics.

The 'Sun Tower' concept illustrated in Fig. 1.6 and is an example of a gravity gradient stabilised SPS. The Sun tower resembles a large, Earth-pointing sunflower

in which the face of the flower is the transmitter array, and the 'leaves' on the stalk are solar collectors. The solar collectors can tilt to maximise solar collection throughout the satellite's orbit. The vertical backbone is 55 km long. This extremely long backbone is in order to avoid self-shadowing of the solar collectors.

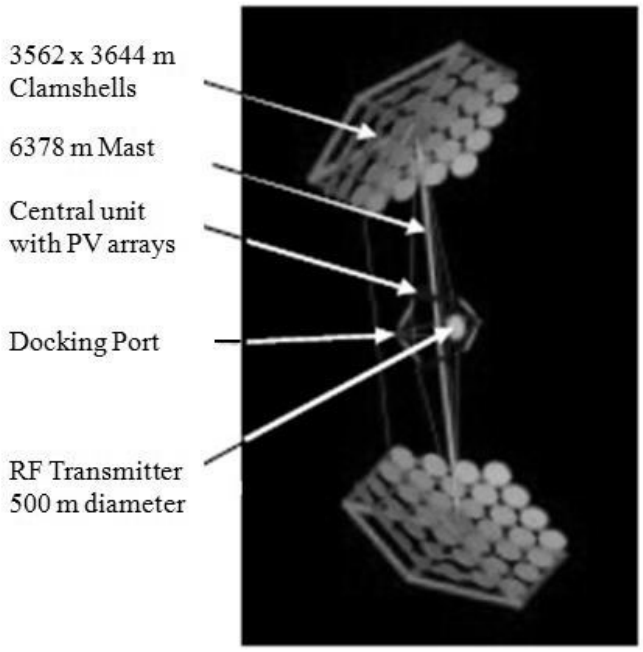

Figure 1.7: ISC SPS

.

The Integrated Symmetrical Concentrator (ISC) is an interesting alternative to the Type III/sandwich SPS. Although similar at first glance, the primary difference is the ISC has its central unit with PV arrays and microwave transmitter all in line with the reflectors. This has a significant impact on the moments of inertia compared to the Type III/sandwich SPS design, which has a T-shaped boom. The ISC cannot be gravity gradient stabilised, where as the Type III/sandwich can be. The technological area of most concern for the sandwich SPS is the issue of overheating of the sandwich module. The ISC offers an alternative design which offsets this issue by separating the PV arrays and microwave transmitter.

Recent designs focus on high modularity, but still involve very large structures

far beyond the largest structures ever built in space. The focus of this thesis is on understanding the dynamics of such large satellites, and of finding ways in which the problems surrounding orbit and attitude control might be minimised by considering the natural dynamics of such systems. The nature of SPS means that certain properties are very different compared to the average satellite. Higher area to mass ratio results in a greater perturbing effect on the orbit due to solar radiation pressure. Lower rigidity leads to more flexible structures and hence, a greater rate of energy dissipation which effects the rotational dynamics. Very large moments of inertia mean that gradient torque will be significant even for high altitude geosynchronous SPS. For these reasons it is considered necessary to not simply design an SPS and then figure out how to control it, but to instead consider the general properties of an SPS in relation to orbital and rotational dynamics, and identify the naturally stable configuration.

1.7 Two Body Problem

The simplest gravitational problem conceivable involves just two bodies, more specifically two point masses $\mathcal{B}_2$ and $\mathcal{B}_2$ orbiting each other due to their mutual gravitational attraction. This is the only gravitational problem for which a closed-form solution has been found. Comprehensive knowledge of the two body problem and its assumptions is crucial to the study of astrodynamics. $\mathcal{B}_1$ and $\mathcal{B}_2$ have masses m_1 and m_2 respectively and their relative orientations are illustrated in Fig. 1.8.

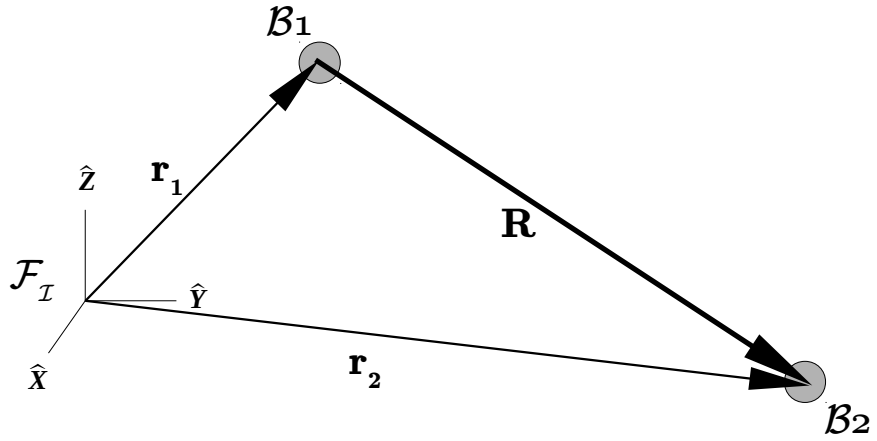

Figure 1.8: Two body problem showing the relative positions of two bodies.

Position vectors $\boldsymbol{r}_1$ and $\boldsymbol{r}_2$ give the positions of $\mathcal{B}_1$ and $\mathcal{B}_2$ relative to an inertial reference frame $\mathcal{F}_\mathcal{I}$. In applying both Newtons second law and his law of gravitation, the equations of motion for $\mathcal{B}_1$ and $\mathcal{B}_2$ may be written:

$$m_1\ddot{\boldsymbol{r}}_1 = \frac{Gm_1m_2}{R^3}\boldsymbol{R} \tag{1.1}$$

$$m_2\ddot{\boldsymbol{r}}_2 = -\frac{Gm_1m_2}{R^3}\boldsymbol{R} \tag{1.2}$$

where $\boldsymbol{R} = \boldsymbol{r}_2 - \boldsymbol{r}_1$ is the position vector from $\mathcal{B}_1$ to $\mathcal{B}_2$, R is the magnitude of $\boldsymbol{R}$, $\ddot{\boldsymbol{r}}_i$ is the inertial acceleration of $\mathcal{B}_i$ and $G = 6.6696 \times 10^{-11}$ N m^2/ kg^2 is the universal gravitational constant. The inertial acceleration $\ddot{\boldsymbol{R}}$ of $\mathcal{B}_2$ with respect to $\mathcal{B}_1$ is:

$$\ddot{\boldsymbol{R}} = \ddot{\boldsymbol{r}}_2 - \ddot{\boldsymbol{r}}_1 = -\frac{Gm_1}{R^3}\boldsymbol{R} - \frac{Gm_2}{R^3}\boldsymbol{R}$$

$$\ddot{\boldsymbol{R}} = -\frac{G(m_1+m_2)}{R^3}\boldsymbol{R} = -\frac{\mu}{R^3}\boldsymbol{R} \tag{1.3}$$

where $\mu = G(m_1 + m_2)$ and is known as the gravitational parameter. Eq. (1.3) is the fundamental equation of the 2-body problem (sometimes known as the Kepler problem) and it describes the motion of $\mathcal{B}_2$ with respect to $\mathcal{B}_1$ in an inertial reference frame. For the majority of orbital mechanics problems, the mass of the primary body is much greater than the mass of the secondary body ($m_1 >> m_2$, therefore $\mu \sim Gm_1$).

For example, in this study the primary body is always the Earth with the solar power satellite being the secondary body. Hence, we have $\mu = \mu_E \sim Gm_E$, where μ_E is the gravitational parameter of the Earth and m_E is the mass of the Earth. Unless otherwise stated, μ is assumed to be equal to μ_E. Although the two body problem does not account for perturbative effects on a bodies' motion, it is useful for gaining an understanding of the basic problem. Eq. (1.3) may be integrated to solve for the position $\boldsymbol{r}$ and velocity $\boldsymbol{v}$ of the $\mathcal{B}_2$ with respect to $\mathcal{B}_1$. The classical orbit elements are straightforwardly obtained from $\boldsymbol{r}$ and $\boldsymbol{v}$.

1.8 Classical Orbit Elements

To describe the orbit of a satellite about the Earth, it is common to use six scalar quantities known as the classical orbital elements. These consist of five elements which describe the shape, size and orientation of the satellite orbit. The sixth orbital element is required in order to specify the exact location of the satellite at a particular moment in time. The six classical orbital elements are listed in Table 1.1 and illustrated in Fig. 1.9.

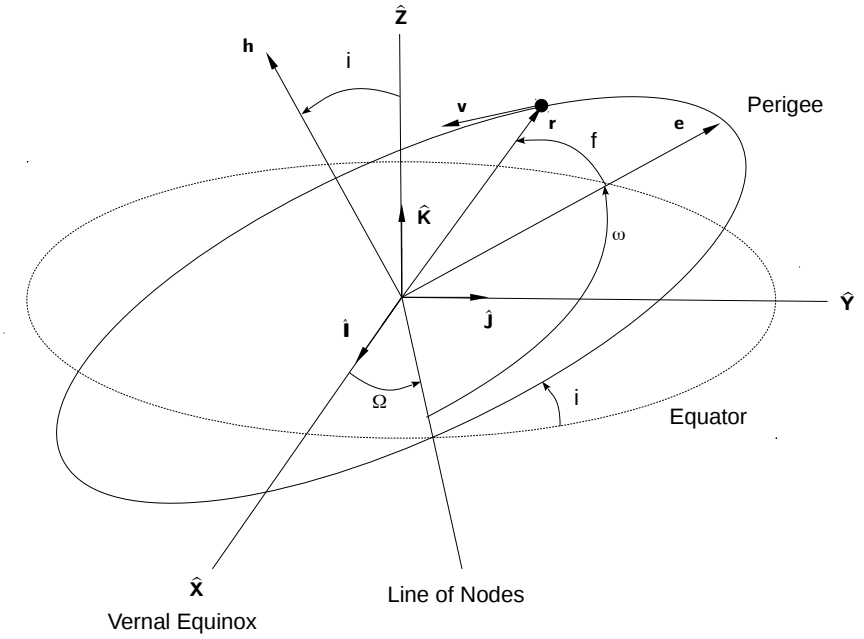

Figure 1.9: Orbit orientation shown with respect to the geocentric-equatorial reference frame, also referred to as the Earth-Centred Inertial (ECI) reference system.

Table 1.1: The classical orbit elements.

Symbol	Orbit Element
a	Semi-major axis, m
e	Eccentricity
ω	Argument of perigee, degrees
i	Inclination, degrees
Ω	Right ascension of the ascending node, degrees
f	True anomaly, degrees

The size and shape of the orbit are determined by the values of a and e, whilst f relates the position in orbit to time. The angles i and Ω give the orientation of the orbital plane with respect to the geocentric-equatorial reference frame. Finally, the angle ω defines the orientation of the orbit in its plane.

The $\hat{\boldsymbol{X}}\hat{\boldsymbol{Y}}$ plane of the Earth-Centered Inertial (ECI) frame is the Earth's equatorial plane. The $\hat{\boldsymbol{Z}}$ axis is along the Earth's polar axis of rotation. The $\hat{\boldsymbol{X}}$ axis points towards the vernal equinox, which is the point where the Sun crosses the equatorial plane from south to north on the first day of spring. Orbit propagation involves

solving for the satellites position and velocity. Often it is desirable to study the orbital elements rather than the position and velocity.

1.9 Perturbed Orbital Motion

In an ideal 2-body system, a satellite's orbit describes a conic section. For a satellite orbiting the Earth there are several forces that cause the conic section to continually change. These deviations from the ideal Kepler orbit are known as perturbations. It is important to understand how the satellites orbit differs from the mathematical ideal orbit.

Variation of parameters (VOP) is the fundamental method of perturbation theory used in celestial mechanics. VOP evolved over a period of half a century, starting with Euler and ending with Lagrange, Laplace, and Gauss.[9]

The idea behind VOP is that the inclusion of perturbing forces in the 2-body problem results in small changes (perturbations) to the constants of motion, i.e. they become time-varying parameters (or 'osculating' elements). The transformation in the 2-body problem between the constants of motion and the solution is still valid, which thereby allows the time-varying parameters to describe the solution.

1.10 Rigid Body Motion

The study of the rotational motion of a rigid body is deeply rooted in the foundations of classical physics. Aside from being of theoretical interest, the subject is essential in practical fields of astronautics and celestial mechanics.

The problem of rotation of a rigid body may be divided into two parts. The dynamic problem entails obtaining the angular velocity of the body with respect to an inertial reference frame, starting with the knowledge of the initial angular velocity and the history of the applied torque. The kinematic problem involves determining the current orientation of the body from knowledge of the initial orientation and the

history of the angular velocity.

For a generic rigid body the Eulers rotational equation of motion, in vectorial form:[10]

$$\dot{\boldsymbol{l}} = \sum \boldsymbol{g} \tag{1.4}$$

where the dot symbol denotes the time derivative with respect to an inertial reference frame, $\boldsymbol{g}$ is the resultant external torque acting on the body, and $\boldsymbol{l} = \boldsymbol{I}\boldsymbol{\omega}$ is the absolute angular momentum of the body, $\boldsymbol{I}$ is the inertia dyadic of the body with respect to its center of mass, and $\boldsymbol{\omega}$ is the angular velocity of the body with respect to an inertial reference frame. By resolving all of the vectors and the inertia dyadic along a body-fixed Cartesian coordinate system $\mathcal{B}$ with axis equal to the principal axes of inertia, Eq. (1.4) can be written in scalar form as:

$$\begin{aligned} I_1\dot{\omega}_1 &= (I_2 - I_3)\omega_2\omega_3 + g_1 \\ I_2\dot{\omega}_2 &= (I_3 - I_1)\omega_3\omega_1 + g_2 \\ I_3\dot{\omega}_3 &= (I_1 - I_2)\omega_1\omega_2 + g_3 \end{aligned} \tag{1.5}$$

where $\{I_i : i = 1,2,3\}$ are the principal moments of the rigid body, $\{\omega_i : i = 1,2,3\}$ are the components of $\boldsymbol{\omega}$ in the $\mathcal{B}$ frame, and $\{g_i : i = 1,2,3\}$ the components of the torque in the $\mathcal{B}$ frame.

The kinematics of rotation must also be considered. We introduce the attitude dyadic $\boldsymbol{A}$ which maps from a body-fixed to an inertial frame. The kinematical equation for it is given by:

$$\dot{\boldsymbol{A}} = \boldsymbol{A} \cdot \widetilde{\boldsymbol{\omega}} \tag{1.6}$$

where the $\widetilde{\ }$ symbol defines the cross product dyadic, i.e. $\widetilde{\boldsymbol{\omega}} = \omega_1(\hat{\boldsymbol{e}}_3\hat{\boldsymbol{e}}_2 - \hat{\boldsymbol{e}}_2\hat{\boldsymbol{e}}_3) + \omega_2(\hat{\boldsymbol{e}}_1\hat{\boldsymbol{e}}_3 - \hat{\boldsymbol{e}}_3\hat{\boldsymbol{e}}_1) + \omega_3(\hat{\boldsymbol{e}}_2\hat{\boldsymbol{e}}_1 - \hat{\boldsymbol{e}}_1\hat{\boldsymbol{e}}_2)$. The unit vectors $\hat{\boldsymbol{e}}_i$ are the axes of the inertial reference frame. Integration of this equation provides the current body orientation, and, together with the integrals of Eq. (1.5), completely solves the rigid body motion

problem. The attitude dyadic $\boldsymbol{A}$ is a rotation matrix relating the inertial and body-fixed reference frames. It may be used to determine the attitude orientation of the body in one of any number of attitude representations.

2

Systems Analysis of the Sandwich SPS

> "When the number of factors coming into play in a phenomenological complex is too large scientific method in most cases fails. One need only think of the weather, in which case the prediction even for a few days ahead is impossible."
>
> - Albert Einstein

To gain insight into the complex systems required to provide solar power from space, a systems analysis of a Type III SPS is performed. The aim is to identify the optimal orbital configuration for the implementation of a Type III SPS system. Of primary interest is whether geosynchronous orbits are justifiably recommended for SPSs.

2.1 Sandwich SPS Concept

Recently, an international collaborative 3 year study was completed by the International Academy of Astronautics.[7] A high-level assessment of three types of SPS was conducted. Among the outcomes, it was determined that the group of key concept specific technologies for the microwave sandwich Type III SPS are generally lower risk than those of the other concepts examined. This concept was therefore considered the most attractive/feasible overall. A working prototype of a sandwich tile module was recently developed and tested by Jaffe[11] at the Naval Research Laboratory. Based upon the IAA results and the fact that a working prototype of the critical component of the sandwich SPS exists, the sandwich SPS concept is chosen for the systems analysis performed here.

The first exhaustive examination of the sandwich module concept was by Owen Maynard in 1980. His NASA report[12] outlines many of the obstacles and sensitivities associated with the sandwich design. Large, lightweight reflectors concentrate incoming sunlight onto the top side of the sandwich structure which is covered in solar cells. The solar cells generate electricity which is converted to microwaves and beamed from the bottom Earth pointing side of the sandwich structure. The two most significant advantages of the sandwich SPS are that heavy components are reduced/made redundant (such as DC transmission lines and the rotary joint, both of which are required by other SPS concepts to transfer the electricity from the power generation to power transmission system), and a highly modular structure is possible which increases the ease of construction. However, there are also many challenges to overcome to realise the sandwich SPS. The IAA report[7] identifies the technology for thermal management of the sandwich panel array as being particularly high risk. Alternative designs based on the sandwich concept have been proposed, with slight variations on configuration.

We are specifically interested in the difference in performance of SPS microwave systems depending on their chosen orbit. The orbital and physical properties for an SPS system, for varying scenarios, shall be identified. The cost to implement each SPS system and the total energy delivered to the ground based users is evaluated. The default orbital location for SPS in previous studies is geostationary (GEO) due to the near 24 hour power delivery it offers. This choice is validated in this study, however an alternative inclined geosynchronous orbit is found to deliver superior performance over the lifetime of the SPS.

A previous study of SPS applied evolutionary algorithms (EAs)[13] to assess the optimal solutions for delivery to different ground station configurations. The focus of that study was on the potential integration of an SPS system with ground-based solar power and the cost of the combined systems (including estimates of the cost for energy storage facilities and transmission cables etc.). The effect of varying the number and

location of ground stations was analysed for a maximum of 3 ground stations, with multiple stations found to be optimal. These studies focussed on the European energy situation, hence ground station locations were limited to within Europe. This chapter shall focus on a single equatorial ground station location, instead choosing to focus on the space segment of the SPS system. The orbital dynamics of the sandwich SPS are considered, with the orbital maintenance requirements used to find the maximum mission lifetime. This is used to evaluate the total energy delivered by the system over the entire mission lifetime.

The chapter is organised as follows: in Section 2.2, the systems analysis is outlined, with sizing and costing of the SPS explained. The equations used to evaluate the total cost of the system and the total energy delivered are given. In Section 2.6 the results of the entire solution space are presented, with the best performing identified and discussed. Section 2.8 summarises the findings of the systems analysis and assesses the sensitivity of the results to various input parameters in the model.

2.2 Outline of Problem

The problem may be summarised as follows: the total cost of the SPS system C_{SPS} (which includes development, manufacture and launch) must be minimised while the total energy delivered by the SPS system to the ground-based receivers over the mission lifetime E_D must be maximised. As such the objective functions are given by:

$$\text{Min: } F_1 = C_{SPS}$$

$$\text{Max: } F_2 = E_D$$

Both objective functions are evaluated with respect to 2 decision variables which define the shape and orientation of the orbit. These are semi-major axis a and inclination i, the ranges considered are given in Table 2.1.

Table 2.1: Decision variables and bounds. These values are used for all test cases unless stated otherwise.

Symbol	Decision Variable	Lower Bound	Upper Bound
a	Semi-major axis, km	7000	50000
i	Inclination, deg	0	180

The allowed ranges of the decision variables are chosen such that a wide array of possible solutions are available. The simplicity of the problem formulation allows all different combinations of decision variables to be assessed. The method used for evaluating each objective function is given in the following sections.

2.3 SPS Sizing

A preliminary mass budget is required for the SPS. The initial mass of a single SPS on injection into operational orbit is given by:

$$m_{SPS} = m_{p,OM} + m_{SEP} + m_{tank} + m_{SA} + m_{IT} + m_{ref} + m_{TA} \tag{2.1}$$

where each mass component is defined in Table 2.2.

Table 2.2: SPS mass components.

Parameter	Mass Component
$m_{p,OM}$	Propellant for orbit maintenance
m_{SEP}	Solar electric propulsion system
m_{tank}	Propellant tank
m_{SA}	Solar arrays
m_{IT}	Interconnecting tether
m_{ref}	Reflectors
m_{TA}	Transmitting antenna

The mass of the propellant tank, m_{tank}, is a function of the propellant mass.[14]

$$m_{tank} = 0.1 m_{p,OM}$$

where $m_{p,OM}$ is the mass of propellant for orbital maintenance and over the mission

lifetime, $m_{p,OM} = 0.05 m_{SPS,f}$ is assumed, where $m_{SPS,f}$ is the end of mission mass of the SPS. m_{SEP} is the mass of the solar electric propulsion system, and is calculated using the properties shown in Table 2.3 from Wie and Roithmayr's study of the 1.2GW Abacus SPS.[15,16]

Table 2.3: Properties of the electric propulsion system.

Parameter	Value
Power/Thrust	30 kW/N
m_{SEP}/Power	5 kg/kW

The method for orbit control assumes that the velocity changes required to correct the orbit are delivered in one single arc of full thrust. This arc is a fraction of the orbital period T,$\Delta t = 0.25T$. This assumption is made to approximate the properties of electric ion thrusters performing orbit maintenance thrusts. To calculate the minimum thrust required of the propulsion system it is necessary to find the Δv correction required per orbit. The method for calculating Δv is given later in Section 2.5.2 and is divided by the thrust arc time, Δt, to find the minimum acceleration required, A_{min}. The minimum thrust requirement of the propulsion system is then:

$$F_T = m_{SPS} A_{min}$$

where the approximation that m_{SEP} is not included in m_{SPS} is made. The total power required for the propulsion system is then:

$$P = \frac{F_T V_e}{2\eta_{SEP}}$$

where $V_e = I_{sp} g_0$ is exhaust velocity, I_{sp} the specific impulse of the engine, g_0 the gravitational acceleration (9.8 m/s^2), and η_{SEP} is engine efficiency, taken to be 80%.[16] The dry mass of the electric propulsion system, m_{SEP}, is then calculated using the

value of mass to power ratio of $\zeta = 5$kg/kW as suggested by Wie and Roithmayr.[15,16]

$$m_{SEP} = \zeta P$$

m_{SA} is the mass of the solar arrays which cover the top surface of the sandwich panel:

$$m_{SA} = \sigma_{SA} A_{SA}$$

where $\sigma_{SA} = 1.7$ kg/m^2 as suggested for future MBG solar arrays.[17] Similarly, the mass of the large lightweight reflectors is given by:

$$m_{ref} = \sigma_{ref} A_{ref}$$

where $\sigma_{ref} = 0.45$ kg/m^2 is used according to Seboldt and Reichert[18] for future deployable/inflatable areas (suggested range 0.2-0.7 kg/m^2). m_{IT} is the mass of the interconnecting tether which joins the reflectors to the sandwich panel. A similar model is assumed as for the Integrated Symmetrical Concentrator SPS, which is very similar to the sandwich SPS. This involves a tether mass per unit length of $\sigma_{IT} = 25$ kg/m.[19] The length of tether material required is assumed to be $l_{IT} \simeq 6D_x$ as in the ISC design.[19]

The diameter of the transmitting antenna D_x is sized to obtain good power beaming efficiency. The parameter τ is defined by Goubau and Schwering:[20]

$$\tau = \frac{\sqrt{A_x A_r}}{\lambda_\mu (a - R_E)} \tag{2.2}$$

where A_x and A_r are the areas of the transmitting antenna and rectenna respectively, a is semi-major axis, R_E is the radius of the Earth and λ_μ is the wavelength of the microwave beam. For high efficiency transmission we take $\tau = 2$. As shown in Figure 2.1, $\tau = 2$ gives an efficiency of $\sim 95\%$.

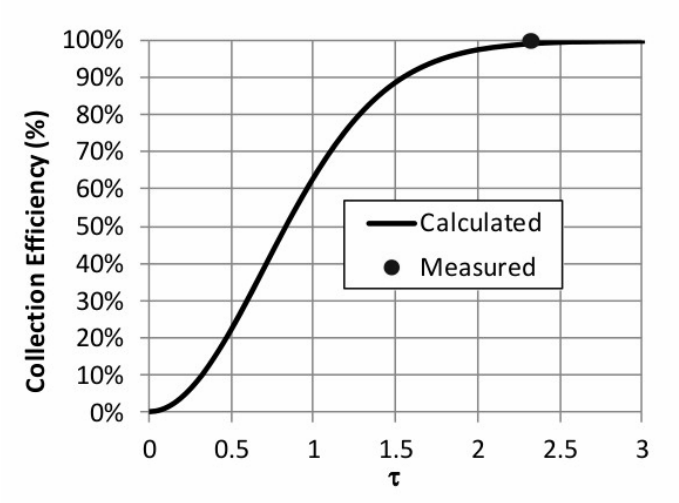

Figure 2.1: Power collection efficiency as a function of τ with optimum power taper over the transmitting aperture.[21]

.

Substituting in $\tau = 2$ and rewriting as a function of the diameters of the transmitting antenna D_x and rectenna D_r gives:

$$D_x = \frac{8\lambda_\mu(a - R_E)}{\pi D_r}$$

where a is semi-major axis, and R_E is the radius of the Earth. We assume an upper limit of $D_r = 10$ km on the ground which allows us to calculate D_x as a function of a. For $f = 2.45$GHz this gives $D_x = 19.0$ m for $a = 7,000$ km and $D_x = 2860.9$ m for $a = 100,000$ km.

It is now possible to calculate the areas of the transmitting antenna and reflectors, A_x and A_{ref} respectively. Assuming a circular transmitting antenna:

$$A_x = \pi(\frac{D_x}{2})^2$$

The mass of the transmitting antenna can then be calculated:

$$m_{TA} = \sigma_{TA} A_x$$

The value of $\sigma_{TA} = 20.2$ kg/m^2 was used to be in agreement with the sandwich prototype value of $\sigma_{TA+SA} = 21.9$ kg/m^2 of Jaffe[11] (i.e. since we have used $\sigma_{SA} = 1.7$ kg/m^2). This value of σ_{TA} is also in agreement with McSpadden and Mankin's suggested range of $\sigma_{TA} = 4 - 40 kg/m^2$.[22] The solar arrays cover the top of the sandwich panel, hence $A_{SA} = A_x$. The area of lightweight reflectors to concentrate the sunlight is calculated with the sunlight concentration factor, C:

$$A_{ref} = A_{SA} C$$

The value of C as suggested by NRL[23] is the maximum feasible due to thermal inbalance, i.e. for high C the sandwich panel absorbs more heat than it can radiate. To ensure this is not the case, the following constraint was applied:

$$\text{Constraint: } Q_{out} - Q_{in} >= 0$$

where $Q_{out/in}$ is the heat radiated/absorbed. The maximum operating temperature determines the values of the heat radiated/absorbed and is determined by the maximum feasible operating temperature of the electronics/PV arrays. This is taken to be $T_{max} = 373$K. The areas A_x and A_{ref} are used to calculate the average cross-sectional area with respect to the Sun vector, A_s and the velocity vector, A_v, to evaluate the effect of solar radiation pressure and atmospheric drag respectively. A_{ref} is also used to calculate the power delivered by the SPS:

$$P_{SPS} = \eta_{SPS} W A_{ref} \tag{2.3}$$

where $W = 1358$ W/m^2 is the power density at 1AU. η_{SPS} is the SPS end-to-end efficiency and is calculated depending on the efficiencies of the various components of the SPS system, as summarised in Table 2.4. The values given in Table 2.4 are as suggested for a sandwich SPS by the IAA[7] and give a value of $\eta_{SPS} = 0.2$ as a

technically feasible goal. Jaffe's prototype sandwich module[11] was found to deliver $\eta_{SPS} = 0.08$. As recognised by Jaffe, there is significant room for improvement on the prototype, therefore a value of $\eta_{SPS} = 0.14$ shall be used which is halfway between the IAA goal and Jaffe's prototype efficiency. The P_{SPS} is used to calculate objective function 2 E_D in Section 2.5.3.

Table 2.4: Conversion efficiencies for the sandwich SPS.

Conversion Stage	Efficiency
MBG PV arrays	35%
DC-RF	80%
Power distribution & control	95%
Transmission to Earth	90%
Rectenna RF-DC	85%

2.4 Objective 1: Financial Cost

The cost calculated here accounts for the differences in launch costs for different sizes of SPSs, as well as different orbital locations.

2.4.1 Earth to Orbit (ETO)

One of the main drivers for the cost of any potential SPS system is the cost of launch. The price of the Space X Falcon Heavy launcher is used as a reference value, giving a specific launch cost of $s_{LEO} = \$1410/\text{kg}$ to a 300 km $i_0 = 28.5°$ orbit.[24]

2.4.2 In-Space Transportation (IST)

The mass required to construct the SPS must be transferred from the initial 300 km $i_0 = 28.5°$ orbit to the final operational orbit. Previous studies have found on-board solar electric propulsion to be the best option for launch of the Sun-Tower GEO SPS, both in terms of overall transfer time and financially.[25] On-board electric low thrust propulsion is used to transfer each SPS module (sized according to maximum launch

capability of 63,800 kg). The properties of the electric propulsion system are given earlier in Table 2. A low-thrust non-coplanar transfer must be completed to achieve the desired orbital inclination. To minimise the overall Δv required, the semi-major axis is increased before any inclination change is performed. The change in inclination over an orbital revolution can be calculated with the following according to the work of Wiesel and Alfano.[26]

$$\Delta i_{2\pi} = \frac{4a^2 a_v}{\mu}\left[\frac{1}{\sqrt{c_v}}E(c_v) + \left(\sqrt{c_v} - \frac{1}{\sqrt{c_v}}\right)K(c_v)\right] \tag{2.4}$$

The parameter a_v is the acceleration, c_v represents the thrust direction, $c_v = 0$ for in-plane thrust, $c_v = 1$ for thrust perpendicular to orbital plane. To change inclination most efficiently, one must thrust perpendicular to the orbital plane. Hence, $c_v = 1$ is substituted into Eq. (2.4) to calculate the Δv for a required inclination change. For $c_v = 1$, the elliptical integrals of the 1st and 2nd kind are $E(1) = 1$, $K(1) = 0$. The rate of change of inclination ($\mathrm{d}i/\mathrm{d}t$) is obtained by dividing Eq. (2.4) by the orbital period, T. This allows the time for orbit transfer to be calculated:

$$t_{trans} = \Delta i/(\mathrm{d}i/\mathrm{d}t) \tag{2.5}$$

The Δv required to achieve the required inclination change Δi is:

$$\Delta v_{inc} = \frac{\mathrm{d}i}{\mathrm{d}t}\frac{\pi}{2}\sqrt{\frac{\mu}{a}}$$

The total Δv required to transfer from the initial equatorial 300km orbit to the final, operational orbit using low-thrust propulsion is given by:

$$\Delta v_t = \Delta v_a + \Delta v_{inc}$$

where Δv_a is the Δv required to perform the co-planar transfer between the initial and

final orbits. The effect of eclipses and atmospheric drag during the orbital transfer are not considered in this study.

2.4.3 Launch Cost

The final on-orbit mass for the entire SPS system is calculated using Eq. (2.1). The total mass that must be launched to LEO may then be calculated:

$$m_{LEO} = m_{SPS} \exp\left(\frac{\Delta v_t}{g_0 I_{sp}}\right)$$

The propellant required for the orbital transfer for the whole SPS system is calculated:

$$m_{p,OT} = m_{LEO} - m_{SPS}$$

The additional propellant tankage required to store the orbital transfer propellant is $0.1 m_{p,OT}$. Therefore the total cost to launch the SPS material plus orbital transfer propellant to LEO is given by:

$$C_{ETO} = s_{LEO}(m_{LEO} + 0.1 m_{p,OT})$$

2.4.4 Manufacturing Cost

It is difficult to make a rough order of magnitude estimate of the manufacturing cost of an individual SPS based upon data from past missions. According to Wertz,[27] an average value of cost/kg for communications satellites is $200,000/kg. However, this is based upon one-off communications satellites. This order of $/kg would render any commercial SPS economically unfeasible. The recent IAA study[7] suggests that for SPS to be realised, the cost per kg of SPS hardware should be in the range $400-800/kg. This is drastically lower than previous missions; however, it is feasible for a highly modular SPS, with a large number of small units mass produced. We choose

the more conservative value of $s_{MF} = \$5,000/\text{kg}$ which Jaffe[11] suggests as realistic with incremental improvements (for reference, Jaffe's sandwich module prototype was built at a cost of $s_{MF} = \$10,000/\text{kg}$). The cost of production is calculated as:

$$C_{Prod} = s_{MF} m_{SPS}$$

2.4.5 Total Cost of SPS System

Finally, the total cost of the SPS system is given by:

$$C_{SPS} = C_{Prod} + C_{ETO} \tag{2.6}$$

The first objective is to minimise the total cost of the SPS system.

2.5 Objective 2: Total Energy Delivered

To evaluate the effectiveness of the SPS system, the total energy delivered by the system over its entire mission lifetime is assessed.

2.5.1 Access Time

To calculate the overall energy delivered by the SPS system to the ground station, it is necessary to calculate the total time in which the satellite is able to beam power to the Earth, depending upon its orbits. For this study, circular orbits are assumed for simplicity and to reduce the computational load at the same time. The perturbations acting upon the satellite are assumed to be controlled, and therefore the satellite maintains its orbit. The satellite is considered to be accessing the GS if it satisfies two conditions: firstly there must be a line of sight between the Earth to SPS vector and the Earth to Sun vector, i.e. the satellite must be in sunlight (an oblate earth is assumed); secondly, the angle between the SPS to GS vector and the normal to the

GS must be less than or equal to 90- ε, where the minimum elevation angle, $\varepsilon = 30°$, is assumed as in previous SPS studies.[28] The position of the spacecraft is propagated along its orbit in time, and the two conditions are checked at each time-step. The orbital elements are considered constant, apart from the true anomaly which changes with time. The Earth to SPS vector is calculated simply by transforming the orbital elements. The ground station vector is calculated at initial time from the latitude and longitude, and transformed to the Earth centred inertial frame. The second condition may then be evaluated, i.e. the scalar product of the normal vector to the ground station and the GS to SPS vector is used to determine whether the satellite is in view of the GS. The total access time of the system is calculated by assessing the two conditions for access between the GS and the SPS. The access time over one year is used to calculate the access fraction:

$$F_A = t_{A,1year}/1 \text{ year} \tag{2.7}$$

where $t_{A,1 \text{ year}}$is the access time of the system over one year. The access fraction is then used to calculate the total time for which the SPS system is beaming energy to the ground, $t_{A,mission}$, derived later.

Maximising Access Time

If we consider how to maximise the time that a satellite is in view with its ground station (the access time), clearly, the only way to guarantee that it is always in range (neglecting whether it's in sunlight or not) is to make the orbital rate of the satellite equal to the Earth's rotation rate. If these rates are not equal then at some point the satellite will drift out of range of the ground station. For a single satellite and ground rectenna, GSO is the only way to maintain almost 100 percent access. To determine the semi-major axis for GSO we equate the Earth's rotation rate and the orbital rate

for a circular orbit:

$$\frac{2\pi}{P_{ERot}} = \sqrt{\frac{\mu}{a^3}} \tag{2.8}$$

where $P_{ERot} = 86164s$ is the Earth's rotation period. We can rearrange for a:

$$a = \left(\frac{\mu P_{ERot}^2}{4\pi^2}\right)^{\left(\frac{1}{3}\right)} = 42,164\text{km} \tag{2.9}$$

It is expected that solutions with $a = 42,164$ km should provide significantly higher access time and hence deliver more energy over their mission lifetime.

2.5.2 Orbit Control

As in previous studies[15,16,19] it is assumed that attitude can be controlled simultaneously to the orbit at no additional cost using orbit control thrusters. Perturbations due to the J_2 gravitational term, solar radiation pressure (SRP), atmospheric drag, and 3rd body gravitational attractions are considered. The total Δv required to correct the SPS orbit for perturbations each orbit is calculated using the following method. The Gauss form of the Lagrange planetary equations is applied to the analysis of the small orbital manoeuvres required to correct for the effect of perturbations each orbit, see Eq. (2.10). The change of an orbital element due to a small impulsive thrust may be found by integration of the Gauss equations, where the orbital elements on the right-hand side of the equations are considered to be constant and:

$$\frac{\lim}{t \to 0}\left(\int_0^t a_i \mathrm{d}t\right) = \Delta V_i$$

where the index i refers the indices S, N, W, which represent the components of the acceleration/impulse in the radial, along-track and out-of-plane directions respectively.[29] Eq. (2.10) is the linearised relation between small impulsive burns and the

resulting small changes in orbital elements. The orbital elements on the right-hand side of Eq. (2.10) are of the desired orbit. The left-hand side are small changes in the orbital elements caused by the various perturbations.

$$
\begin{aligned}
\Delta a &= 2\sqrt{\frac{a^3}{\mu(1-e^2)}}[\Delta V_S e \sin f + \Delta V_N(1+e\cos f)] \\
\Delta e &= \sqrt{\frac{a(1-e^2)}{\mu}}\left[\Delta V_S \sin f + \Delta V_N\left\{\frac{2\cos f + e(1+\cos f^2)}{1+e\cos f}\right\}\right] \\
\Delta i &= \sqrt{\frac{a(1-e^2)}{\mu}}\Delta V_W \frac{2\cos\omega + f}{1+e\cos f} \\
\Delta\omega &= \sqrt{\frac{a(1-e^2)}{\mu}}\left[-\Delta V_S\frac{\cos f}{e} + \Delta V_N\left\{\frac{\sin f(2+e\cos f)}{e(1+e\cos f)}\right\} - \Delta V_W\frac{\cot i\sin(\omega+f}{1+e\cos f}\right] \\
\Delta\Omega &= \sqrt{\frac{a(1-e^2)}{\mu}}\Delta V_W\frac{\sin(\omega+f)}{\sin i(1+e\cos f)}
\end{aligned}
\tag{2.10}
$$

where $\Delta V_S, \Delta V_N, \Delta V_W$ are impulsive burns in the radial (S), along-track (N), and out-of-plane (W) directions.

Earth's Oblateness (J_2)

The gravitational potential due to the non-spherical Earth causes periodic variations of all the orbital elements. However, the secular variations in Ω and ω caused by the Earth's oblateness are the dominant effects. The changes in ω and Ω over one orbital period, T, are as given by Vallado[29] but simplified for circular orbits:

$$
\begin{aligned}
\Delta\omega_{J_2} &= \frac{3nR_E^2 J_2}{4a^2}(4-5\sin^2 i)T \\
\Delta\Omega_{J_2} &= -\frac{3nR_E^2 J_2\cos i}{2a^2}T
\end{aligned}
\tag{2.11}
$$

where n is the mean motion, R_E is the radius of the Earth.

Third-Body Perturbations

The secular changes per orbital revolution in ω and Ω caused by lunar attraction are as given by Wertz:[27]

$$\Delta\omega_M = 0.00169\frac{\pi}{180}(4 - 5\sin^2 i)/N_{orb}^2$$
$$\Delta\Omega_M = -(0.00338\frac{\pi}{180}\cos i)/N_{orb}^2$$

where N_{orb} is the number of orbits per day, and $\Delta\omega_M$ and $\Delta\Omega_M$ are in rad/orbit. Similarly for solar attraction:

$$\Delta\omega_S = 0.00077\frac{\pi}{180}(4 - 5\sin^2 i)/N_{orb}^2$$
$$\Delta\Omega_S = -(0.00154\frac{\pi}{180}\cos i)/N_{orb}^2$$

Finally, luni-solar perturbations also cause a long-term periodic variation in i. Elementary analysis where orbits are assumed to be circular gives the following for the maximum amplitude of variation in i per orbit:

$$\Delta i_M = \frac{3\pi\mu_M a^3}{2\mu r_M^3}\sin i_M$$
$$\Delta i_S = \frac{3\pi\mu_S a^3}{2\mu r_S^3}\sin i_S \tag{2.12}$$

where $\mu_{M/S}$ is the gravitational parameter of the Moon/Sun, and $i_{M/S}$ is the angle between the orbital plane and the plane of the Moon/Sun. If these perturbations are left uncontrolled, changes in inclination would cancel out over long intervals of time. However, they are controlled in this case.

Solar Radiation Pressure (SRP)

To calculate the effect of SRP, firstly, it is necessary to calculate the average cross-sectional area of the sandwich panel, $A_{S,SP}$, and the reflectors, $A_{S,ref}$ with respect to the incoming solar radiation. The magnitude of the acceleration due to SRP is then:

$$a_{SRP} = \frac{P_\Phi}{m_{SPS}}(A_{S,SP}C_{SP} + A_{S,ref}C_{ref}) \tag{2.13}$$

where $P_\Phi = 4.5 \times 10^{-6}$ Nm^{-2} is the solar pressure constant, $C_{SP} = 1.3$ and $C_{ref} = 1.7$ are the reflection coefficients assumed for the sandwich panel and reflectors respectively. The change per orbit of eccentricity caused by SRP is given by Wie:[30]

$$\Delta e_{SRP} = \frac{3\pi a_{SRP}}{n^2 a N_{orb}} \tag{2.14}$$

where n is the mean motion, N_{orb} is number of orbits per day.

Atmospheric Drag

The predominant effect of drag is to shrink the orbit. An exponential model of atmospheric density, ρ, is assumed. The linearised equations used for the effect of drag on the satellites orbital elements over one orbital revolution are as given by Vallado[29] but in the simplified form for circular orbits for semi-major axis:

$$\begin{aligned} \Delta a_D &= -\frac{2\pi Q A_v C_D a^2 \rho}{m_{SPS}} \\ Q &= 1 - \frac{2\omega_E \cos i}{n} \end{aligned} \tag{2.15}$$

where Q is a factor which includes the rotation of the atmosphere ($0.9 \leq Q \leq 1.1$), A_v is the cross-sectional area with respect to the satellites velocity vector, C_D is coefficient of drag, and ω_E is the rotational velocity of the Earth.

Calculation of Δv and Lifetime

All the components from different perturbations contributing to a change in an orbital element are summed:

$$\begin{aligned} \Delta a &= \Delta a_D \\ \Delta e &= \Delta e_{SRP} \\ \Delta i &= \Delta i_M + \Delta i_S \\ \Delta \omega &= \Delta \omega_{J_2} + \Delta \omega_M + \Delta \omega_S \\ \Delta \Omega &= \Delta \Omega_{J_2} + \Delta \Omega_M + \Delta \Omega_S \end{aligned} \tag{2.16}$$

The Δv to correct that particular orbital element is calculated using Eq. (2.10). It is assumed that the manoeuvre is performed at the optimal true anomaly, f, and along the optimal direction (S, N or W) for that orbital element. For example, to change the semi-major axis, the optimum manoeuvre has to be executed at perigee ($f = 0$) along the in-track direction. Therefore, to change the orbit by a specified value, Δa, the minimum Δv required is:

$$\Delta V_{(N,a)} = \frac{\Delta a}{2a}\sqrt{\frac{\mu(1-e)}{a(1+e)}}$$

which is derived from Eq. (2.10) where it is assumed that $e \neq 0, i \neq 0$ (to avoid singularities) and that the linearized expressions are accurate for small values of e

and i. This procedure is followed for each orbital element:

$$\begin{aligned}
\Delta V_{N,e} &= \frac{1}{2}|\Delta e|\sqrt{\frac{\mu}{a}} \\
\Delta V_{N,\omega} &= \frac{1}{2}|\Delta\omega|e\sqrt{\frac{\mu}{a}} \\
\Delta V_{W,i} &= \Delta i\sqrt{\frac{\mu}{a}} \\
\Delta V_{W,\Omega} &= |\Delta\Omega|\sin i\sqrt{\frac{\mu}{a}}
\end{aligned} \tag{2.17}$$

The magnitude of the combined Δvs required per orbit is calculated as follows:

$$\Delta V_{rev} = |\Delta V_{N,a} + \Delta V_{N,e} + \Delta V_{N,\omega}| + |\Delta V_{W,i} + \Delta V_{W,\Omega}| \tag{2.18}$$

where ΔV_{rev} is the Δv required each revolution to maintain the Keplerian orbit. This method of calculating the value of the Δv allows the possibility of different perturbations cancelling each other out. From the assumption that the propellant mass, $m_{p,OM} = 0.05 m_{SPS,f}$, it is possible to calculate the total Δv requirement for the entire mission.

$$\Delta V_{mission} = -I_{sp} g_0 \ln\left(\frac{m_{SPS,f}}{m_{SPS}}\right) \tag{2.19}$$

The value found using Eq. (2.19) is independent of the value of m_{SPS} as $m_{SPS,f} = 0.945 m_{SPS}$. The total number of orbits N_T for which the orbital perturbations can be controlled using the available propellant is given by:

$$N_T = \frac{\Delta V_{mission}}{\Delta V_{rev}}$$

Subsequently the total mission lifetime can be calculated:

$$t_{mission} = N_T T$$

where T is the orbital period. This is the total time that the system of SPSs can

maintain their orbits and hence the total time over which power can be delivered to the ground.

2.5.3 Energy Delivered

Due to eclipse and the SPS system not necessarily being in continuous view of the ground stations, the SPS system will only deliver power according to its access fraction, F_A (Eq. (2.7)). The total time for which the SPS system is beaming energy to the ground is therefore:

$$t_{A,mission} = F_A t_{mission} \tag{2.20}$$

To calculate the energy delivered over the mission lifetime, the mean power received at the rectenna from the SPS must be calculated:

$$P_r = P_{SPS} \cos \alpha^2 \tag{2.21}$$

where P_r is averaged to account for times when there is no power being beamed (i.e. $\alpha > 60°$). This accounts for the loss in power received for non-zero incidence angle of the beamed radiation when the SPS is not directly over the GS, i.e. in cases where the SPS is in a non-synchronous orbit or in an inclined synchronous orbit.

Finally, the total energy delivered to the ground over the mission lifetime by the SPS system can be calculated:

$$E_D = P_r t_{A,mission} \tag{2.22}$$

The second objective is to maximise this value.

2.6 Systems Analysis Results

The aim of the analysis that follows is to explore the affect that placing the SPS in different orbits has on the total energy delivered and the overall cost of the system. The full range of possible orbit inclinations $i = 0 - 180^{\circ}$ are considered and semi-major axis in the range $a = 7,000 - 100,000$ km.

2.6.1 Full Solution Space

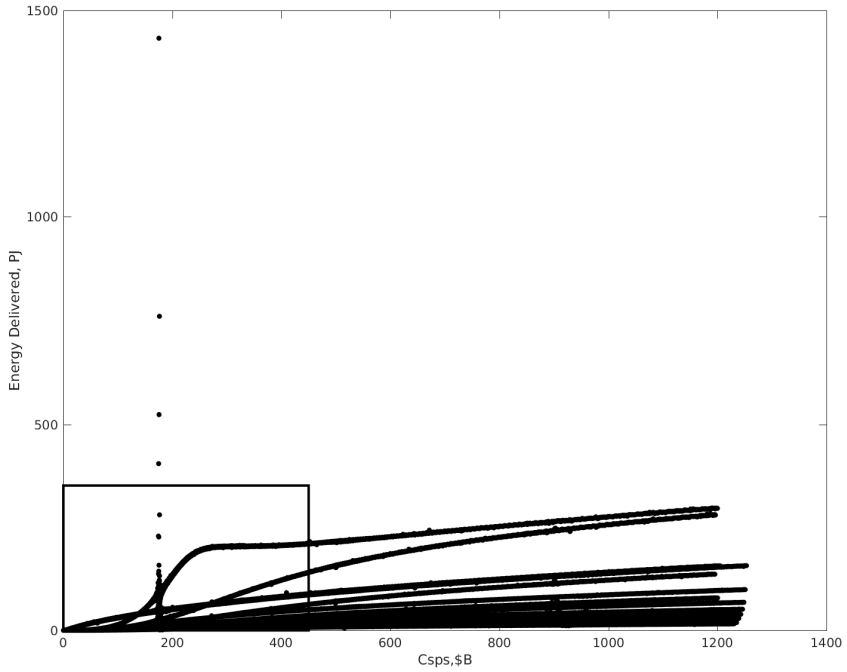

Figure 2.2: All data points within the range $a = 7,000 - 100,000$ km and $i = 0 - 180^{\circ}$.

The two objective functions (E_D and C_{SPS}) are evaluated over the entire solution space such that an optimal orbit can be identified for the sandwich microwave SPS. To save computational effort the resolution of the first search is kept low and shows the full range of $a = 7,000 \rightarrow 100,000$ km and $i = 0 \rightarrow 180^{\circ}$. Each plot point in Figure 2.2 is a solution for a different combination of a and i, so the energy and cost are plotted for

all possible combinations of orbit size and orientation (assuming circular orbits). The solutions range in cost from $\sim \$70\text{M} - \$1250\text{B}$. The higher energy solutions (shown in Figure 2.2) with Energy Delivered $\sim> 250$ PJ are all within a few kilometres of geosynchronous orbit, a_{GSO}. The near GSO solutions clearly provide significantly more energy, however, firstly we shall focus on the low cost and low energy region highlighted in Figure 2.2 and zoomed into in Figure 2.3.

2.6.2 Low Cost Low Energy Solutions

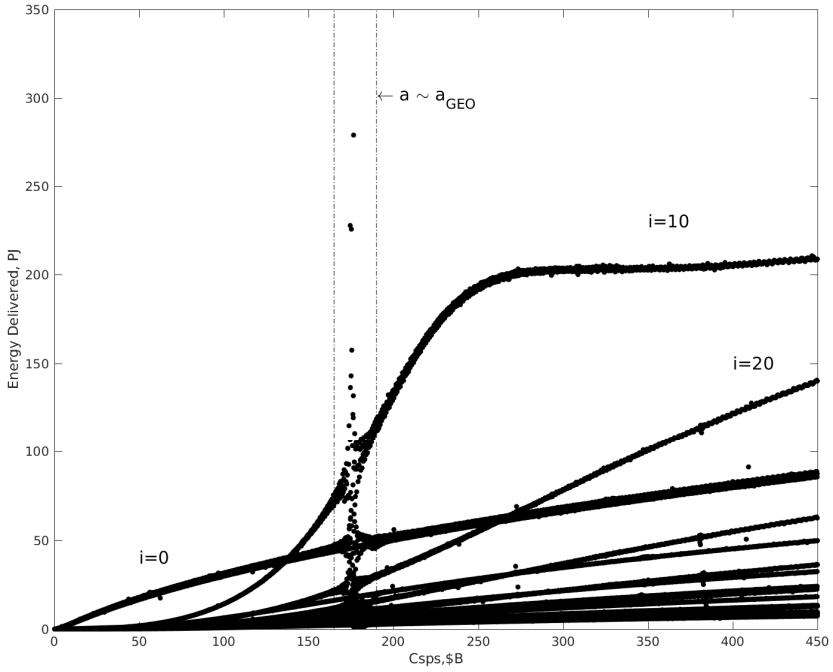

Figure 2.3: All data points within the range 7,000-100,000km zoomed in. Each band of points is for a different i and shows solutions for the different values of a.

.

In Figure 2.3 there are different bands of solutions for each value of i. The lower inclination solutions generally provide more energy due to a lower angle of incidence for the beamed power, α. The breaking apart of each band occurs for $a \sim a_{GSO}$ (i.e. where much higher and lower energy values are created).

At low values of a (and consequently lower cost) equatorial orbits perform best, see the bottom left corner of Figure 2.3. Before a_{GSO} is reached the $i = 10^\circ$ solutions outperform the equatorial ones. This turns out to be because the Laplace surface is closer to $i = 10^\circ$ than $i = 0^\circ$ at this point.

The top performing solutions for non-GSO deliver approximately $5 - 10\%$ of the energy that the equivalent cost GSO solution provides. This proves that for all values of i in this plot, the only reasonable choice is GSO altitude (highlighted in Figure 2.3). These solutions are investigated later using a higher resolution search of this region of the solution space.

At much higher values of a the $i = 20^\circ$ band will eventually outperform the $i = 10^\circ$ band as the Laplace surface at these altitudes becomes close to the ecliptic plane ($i = 23.5^\circ$). At higher cost and lower E_D than GSO options, these solutions are not considered further.

The lower than GSO altitude options are cheaper than GSO, hence, they may be useful for SPS pilot plants or niche markets requiring low levels of power.

GSO offers a large pay off in terms of E_D. For this reason, from this point forward a narrow range of a close to $a = 42,164$ km is considered, i.e. near GSO altitude.

2.6.3 Near Geosynchronous Solutions

The highest energy solution for each different i shown in Figure 2.4 is $a = 42,164$ km Figure 2.4. The best inclination to have a GSO SPS is at $i = 7.5^\circ$. This is recognised as the geosynchronous Laplace plane orbit (GLPO) where the Earth oblateness and luni-solar third body perturbations approximately cancel each other out. The additional mission lifetime offered by the savings in orbit maintenance fuel in this orbit outweigh the reduction in power received caused by the non-zero orbit inclination. This is the most significant finding of this systems analysis. Due to the fact that we assume a fixed orbit maintenance propellant fraction of 5% the overall mass of the system, GLPO's mission lifetime is 3.3 times that of an SPS in GEO. This agrees approximately with

the difference in maximum E_D offered by GLPO vs GEO in Figure 2.4.

The affect of the orbit inclination transfer cost from the initial insertion orbit to the operational orbit is considered. In Figure 2.4 the lowest cost option is $i = 27.5°$ because that requires the smallest Δv_i from the initial LEO at $i_0 = 28.5°$. The higher energy and lower cost options are considered in more detail.

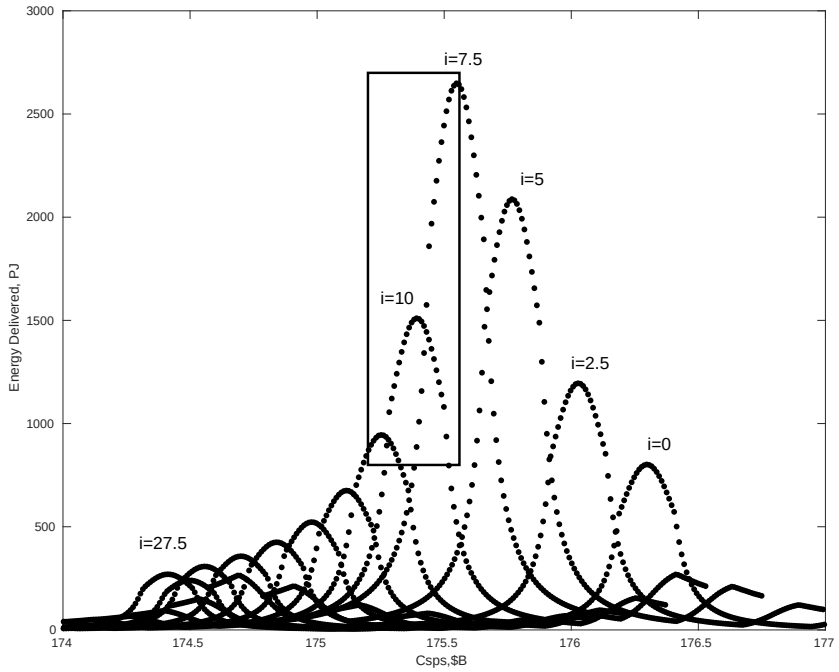

Figure 2.4: All data points within the range $a = 42,064 - 42,264$km and $i = 0 - 30°$.

.

The primary affect of i on cost is due to the cost of the orbit transfer inclination change required (Eq. (2.6)), assuming a LEO insertion into $i_0 = 28.5°$. Table 2.5 shows the ΔV_i values for the different orbital inclinations which accounts for the ordering of the different i solutions in terms of cost seen in Figure 2.4. The cost of propellant for the inclination orbital transfer is the determining factor in where the particular band of i lies on the cost axis. The cheapest option is to leave the SPS in the same i as the initial insertion orbit, as then $\Delta V_i = 0$. The ordering of the cost of different i bands is explained by the Table 2.5 showing $|i_o - i|$. Although they invoke a higher transfer cost penalty, significantly higher values of E_D can be attained with lower i's.

Table 2.5: Orbit transfer inclination delta v at a_{GSO}.

$i(^\circ)$	$\lvert i_0 - i \rvert (^\circ)$	Δv_i (m/s)
27.5	1.0	84
10	2.5	1559
7.5	3.5	1770
5	18.5	1981
2.5	21.5	2192
0	28.5	2402

The maximum E_D for any band of i solutions (which are all different values of a), depends upon the the total mission access time as determined by the orbital maintenance ΔV_{rev} and the average power attained accounting for the non-zero incident angle of the beamed power. The impact of the value of i on the energy delivered is twofold. First, the orbit maintenance ΔV_{rev} is strongly related to i, which given the assumption of a fixed mass fraction of fuel (5%), limits the lifetime of the spacecraft. The lower the ΔV_{rev}, the longer the spacecraft can continue beaming power. Secondly, the value of i impacts the incident angle of the beamed radiation at the rectenna. Higher inclination orbits result in a higher incident angle and hence, reduced levels of received power. To the author's knowledge, no previous analysis has incorporated these two affects to compare SPS performance in orbits with different a and i.

The solutions highlighted by the box in Figure 2.4 are all identified as being superior to GEO ($i = 0^\circ$,$a = 42,164$ km) and include options with $a \neq 42,164$km. This is significant, as previously, SPS studies have simply assumed GEO. Note the solutions in between $i = 7.5^\circ$ and $i = 0^\circ$ are also superior to GEO but are not considered as they provide the same energy as the solutions highlighted but for higher cost (this is dependent on the $i_0 = 28.5^\circ$ of the initial LEO).

2.6.4 Maximum Energy Solution: The GLPO

The mass components of the maximum energy GLPO solution ($a = 42,164$ km,$i = 7.5^\circ$) are shown in Table 2.6.

The total mass of the SPS approximately the same as the similar ISC design ($m_{sps} = 2.25 \times 10^7$ kg). This is despite the larger transmitting antenna required by the 2.45GHz ($D_x \sim 1000$ m) sandwich SPS compared to the 5.8GHz ISC ($D_x \sim 500$ m). The ISC design was formulated in 2000, in the ensuing years various advancements have been made in light weight photo-voltaics and reflector material which are accounted for in the systems analysis model.

Table 2.6: Maximum energy delivered solution SPS mass components.

Parameter	Mass Component	Value (kg)	% of total mass
$m_{p,OM}$	Propellant for orbit maintenance	1.32×10^6	5.0
m_{SEP}	Solar electric propulsion system	9.05×10^3	0.0
m_{tank}	Propellant tank	2.63×10^5	1.0
m_{SA}	Solar arrays	1.66×10^6	6.3
m_{IT}	Interconnecting tether	1.67×10^5	0.6
m_{ref}	Reflectors	1.32×10^6	5.0
m_{TA}	Transmitting antenna	1.98×10^7	74.7
m_{LEO}	Launch mass to LEO	3.02×10^7	114.0
m_{sps}	Total SPS mass	2.65×10^7	

The break down of the costs of the GLPO sandwich SPS are given in Table 2.7. The system delivers an average power level of 540 MW. The solution was confirmed to satisfy the recommended safety level of power density at the rectenna of ≤ 23 mW/cm^2,[7] by calculating P_{sps}/A_r.

Table 2.7: Maximum energy delivered solution SPS cost components.

Parameter	Cost Component	Value ($)
C_{ETO}	Cost of launch to LEO	43.1B
C_{Prod}	Cost of production of SPS	132.5B
C_{SPS}	Total SPS cost	175.6B

The GLPO sandwich microwave SPS provides a cost per installed kW of $\sim$ \$325,000/kW. This is approximately two orders of magnitude larger than the currently available energy sources shown in Figure 2.5. As realistic figures were used for the input parameters to the model, it is reasonable to conclude that SPS is not economically competitive at this moment in time. The economics just do not work

for baseload power.

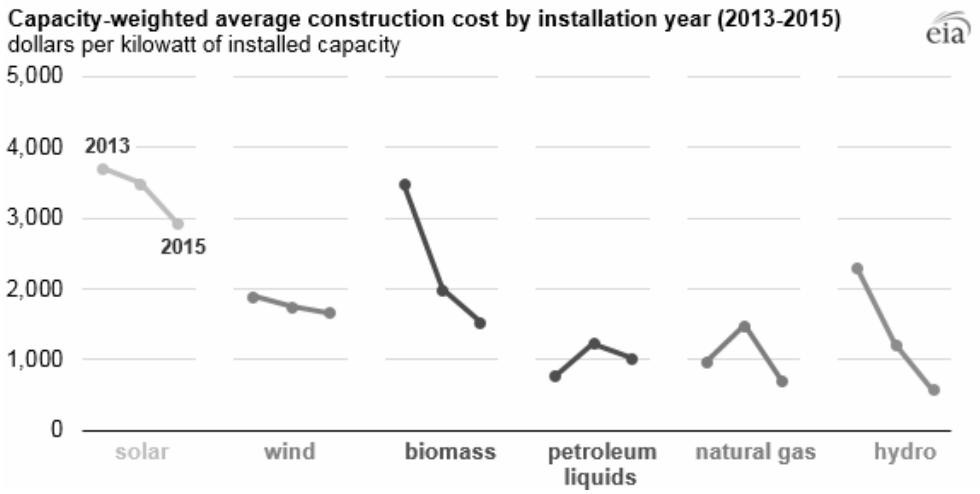

Figure 2.5: Cost of different energy sources.[31]

.

However, to be clear, that does not warrant dismissing the concept entirely. This study has purposely used current values for various input parameters or realistic projections (see Table 2.8). It is widely acknowledged that improvements in multiple areas are necessary to make SPS a competitive source of baseload power. We can investigate which parameters should be prioritised for improvement through performing a sensitivity analysis.

2.7 Sensitivity Analysis

Table 2.8 gives the full list of inputs for the parameters for which a value was chosen rather than strictly defined. In the case where no guide to the possible parameter range is found in the literature, a range of $\pm 20\%$ from the nominal value was used. The sensitivity index is calculated for each parameter using the variance based method of sensitivity analysis of Sobol.[32,33,34] The open source tool SALib[35] is used to perform this analysis. The sensitivity of each input is often represented by a numeric value, called the sensitivity index. Sensitivity indices come in several forms:

1. First-order indices: measure the contribution to the output variance by a single

model input alone.

2. Second-order indices: measure the contribution to the output variance caused by the interaction of two model inputs.

3. Total-order index: measure the contribution to the output variance caused by a model input, including both its first-order effects (the input varying alone) and all higher-order interactions.

We consider only the total order index here in order to account for first and higher order interactions between the input parameters.

Table 2.8: Input parameters information. The reference used for the source of the nominal value/range is given for each parameter where available.

Symbol	Nominal Value	Range	Units	Reference
C	3	1-5	-	-
I_{sp}	5,000	3,000-20,000	s	[16]
σ_{SA}	1.7	1.36-2.04	kg /m^2	[17]
σ_{ref}	0.45	0.2-0.7	kg /m^2	[18]
σ_{TA}	20.2	4 - 40	kg /m^2	[11,22]
σ_{IT}	25	20-30	kg / m	[19]
η_{SPS}	0.14	0.08-0.2	-	[11]
s_{MF}	5,000	100-10,000	\$ / kg	[11]
s_{LEO}	1410	100-1,410	\$ / kg	[24]
ϵ	30	24-36	degrees	[28]
i_0	28.5	0-90	degrees	[24]
ζ	5	4-6	kg / kW	[16]
η_{SEP}	0.8	0.64 - 0.96	-	[16]
D_r	10,000	4,200-15,000	m	[36]
Δt_{frac}	0.25	0.2-0.3	-	-

The systems analysis model is run for all the inputs generated from the bounds in Table 2.8 using the theory of Sobol.[32] The outputs for each systems analysis run are then used as input into SALib[35] to calculate the sensitivity indices. The sensitivity analysis is performed on the maximum energy GLPO solution.

Note, the range for D_r is calculated to limit the power density at the rectenna to safe levels.

2.7.1 Energy Delivered

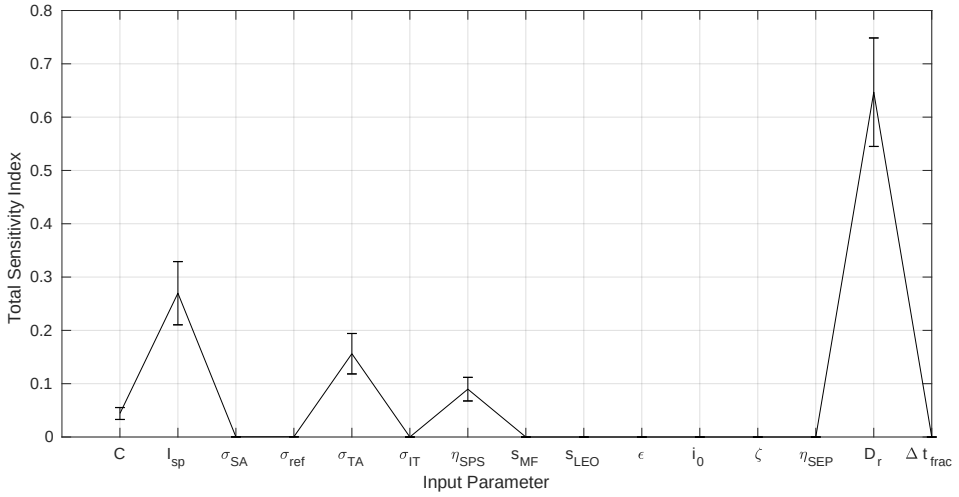

Figure 2.6: Total sensitivity indices for all input parameters for GLPO. 95% confidence bands are shown.

.

In Figure 2.6 we can see that the value of E_D is most sensitive to the diameter of the rectenna, D_r. D_r determines the size of the system at a given altitude as D_x is calculated from Eq. (2.3) which is a function of D_r and a. The larger we make D_r, the smaller D_x can be to maintain a high efficiency link. However, the power collected by the SPS is dependent on D_x due to the sandwich design of $A_x = A_{SA}$. Hence, if we have a large D_r, and consequently small D_x, we have a large rectenna which is collecting a small amount of power. Conversely, if a very small D_r is chosen then a large D_x is required. This becomes expensive and less feasible to launch and construct, while also leading to exceeding safe power density levels at the small rectenna.

E_D is second most sensitive to the I_{sp} of the electric ion thrusters. The more efficient the thrusters, the longer the orbit can be maintained and the more energy can be delivered to the ground rectenna. It should be noted that other factors which may affect the lifetime of the SPS, for example photovoltaic degradation, are not accounted for in this model. The lifetimes in some cases are unrealistic ($t_{mission} \sim 160$

years for GLPO). Clearly, other factors such as economics, competing prices, wearing out of components, changing operational costs, profitability, would preclude such an extended lifetime. We could have either reduced the propellant mass fraction or instead fixed the operational lifetime and allowed the propellant mass fraction to vary.

E_D is also sensitive to the density of the transmitting antenna σ_{TA}. This is in fact due to the affect of the SRP perturbation. The transmitting antenna is the major contributor to the overall mass of the system (74.7% for the GLPO example in Table 2.6). The perturbing acceleration due to SRP is given by Eq. (3.3) in which $a_{SRP} \propto 1/m_{sps}$. The smaller the value of σ_{TA}, the smaller m_{sps}, and the larger the delta v required to cancel SRP. Over the range of σ_{TA} considered, the impact on mission lifetime is significant:

GLPO

$$t_{mission}(\sigma_{TA} = 40) = 4.26 \times t_{mission}(\sigma_{TA} = 4)$$

This indicates the importance of the affect of SRP on SPS. SPS have inherently high area-to-mass-ratios (HAMRs) which in GLPO makes it the dominant perturbation (as oblateness and luni-solar gravitation approximately cancel each other). When the SPS is in GEO, the SRP perturbation magnitude is comparable to luni-solar and oblateness, hence, has σ_{TA} has less of an impact:

GEO

$$t_{mission}(\sigma_{TA} = 40) = 1.27 \times t_{mission}(\sigma_{TA} = 4)$$

The E_D is also sensitive to the overall efficiency of the SPS system η_{sps} as one might expect. The E_D is less sensitive to improvements in the level of sunlight concentration possible.

2.7.2 Cost of the SPS

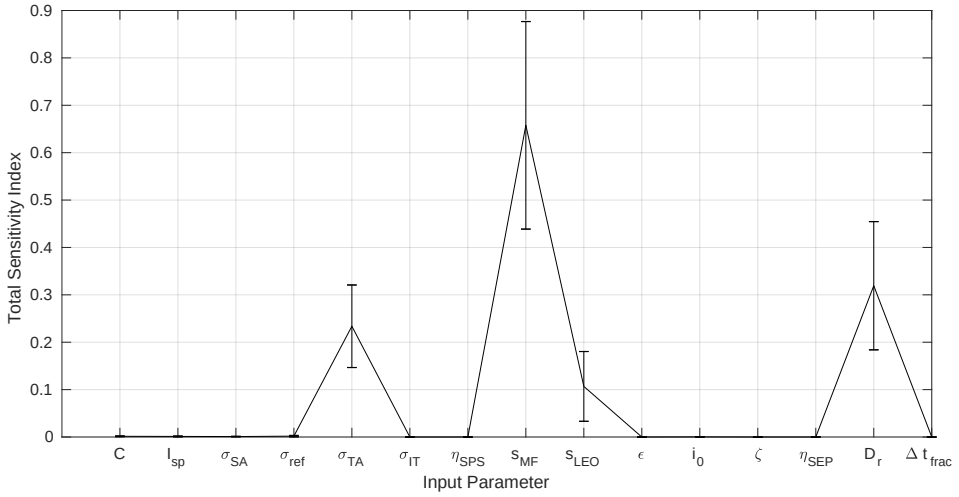

Figure 2.7: Total sensitivity indices for all input parameters for GLPO. 95% confidence bands are shown.

.

In Figure 2.6 we can see that the value of C_{SPS} is most sensitive to the cost per kg of manufacture of the in-space components s_{MF}. This is a strong indication that modularity of a SPS is very important in determining the cost of the system. Greater modularity allows the benefits of mass production of components to be realised in a lower s_{MF}. This finding endorses the approach of the Alpha-SPS designed by John Mankins.[37] The Alpha-SPS design is constructed of 8 different modular elements. These elements can be combined in different ways to build all the components needed for a functioning SPS. This allows the mass production of each of the 8 components, and theoretically a cost per kg of $s_{MF} = \$500 - 1000/\text{kg}$ to be achieved.[37]

The cost is second most sensitive to D_r. This is primarily due to the impact of D_r on the size of the SPS, and more specifically on the size of the transmitting antenna through Eq. (2.3).

C_{SPS} is also sensitive to σ_{TA}. The reason that the cost is sensitive to σ_{TA} is because the overall mass of the SPS is dominated by the m_{TA}. The cost of the SPS

is dependent upon m_{sps} as the $C_{ETO} \propto m_{sps}$ and $C_{Prod} \propto m_{sps}$.

The parameter that C_{SPS} is next most sensitive to is the specific launch cost to LEO, s_{LEO}. In comparison to the other input parameters just discussed, the cost is not as sensitive to s_{LEO}. It is due to the advancements made by private industry in recent years[24] which set the upper limit of s_{LEO} at \$1410/kg, which is considerably lower than the upper limits assumed for the likes of s_{MF}.

2.7.3 Energy to Cost Ratio

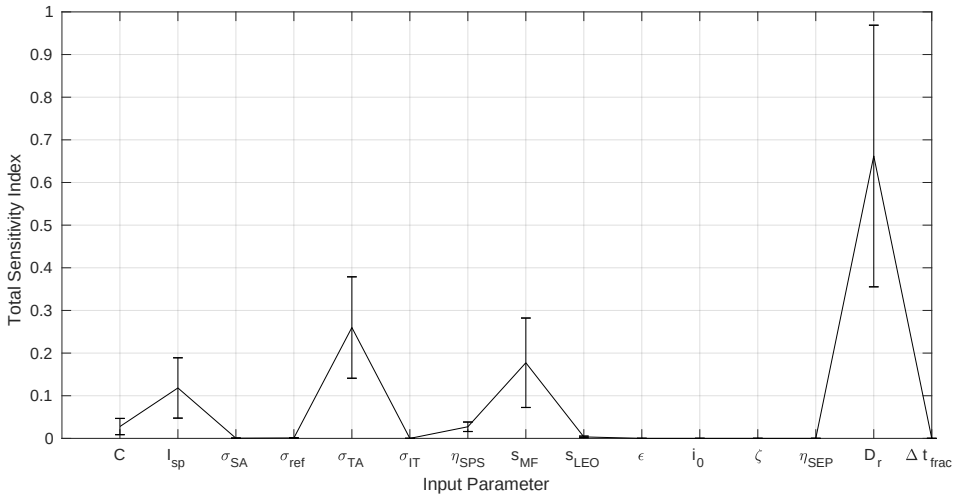

Figure 2.8: Total sensitivity indices for all input parameters for GLPO. 95% confidence bands are shown.

.

Figure 2.8 shows the sensitivity of the output E_D/C_{SPS} to the various input parameters for GLPO. This gives a good indication of which areas SPS research should focus on to make a more economically viable SPS when both cost and energy delivered are considered.

The output is most sensitive to D_r indicating that this is a crucial parameter that both the energy and cost of the system are sensitive to.

The mass and cost of manufacture of the transmitting antenna are also important factors to address to make SPS a viable energy source. This is understandable when

one considers that the TA makes up 74.8% of the overall SPS mass in our maximum energy solution.

Lastly is the specific impulse I_{sp} of the electric ion thrusters used both for orbital transfer and maintenance. The importance of this variable may be overstated in this analysis due to the assumption that the orbit is fully controlled. The control strategy is certainly conservative in this study. However, the sensitivity to I_{sp}, coupled with the maximum energy solutions all being Laplace plane indicates that finding an orbit with minimal delta v requirements and developing high I_{sp} electric ion thrusters is certainly worthwhile for the overall performance of the SPS.

The output is not very sensitive to the specific launch cost s_{LEO}, i.e. the cost per kg of launch to LEO. The range selected for s_{LEO} (see Table 2.8) uses the quoted price[24] for the Space X Falcon Heavy for the upper bound. This indicates that the launch cost is not the current showstopper for SPS. In any case, the cost of launch is predicted to come down further and so does not need an SPS driven effort to do so.

2.8 Discussion

A comprehensive systems analysis model has been presented for assessing the energy delivered per cost of the sandwich SPS.

The Geosynchronous Laplace Plane orbit (GLPO) has been found to be the optimal orbit for a sandwich SPS, capable of delivering the most energy for the lifetime of the satellite. This includes accounting for:

- the loss of power delivered from an inclined orbit vs GEO due to the higher value of incidence angle of the beamed radiation at the ground rectenna
- the impact of orbit perturbations on the lifetime of the satellite assuming a 5% propellant mass fraction for all solutions
- the orbital transfer cost from LEO $i_0 = 28.5°$

The significant increase in mission lifetime offered by GLPO and other GSO inclined orbits results in considerably higher levels of energy being delivered to the ground station compared to a GEO sandwich SPS.

This finding motivates an in-depth analysis of the dynamics of SPS in the GLPO to determine if operating an SPS in this alternative orbit is feasible from both an orbit and an attitude dynamics stand-point. The sensitivity analysis performed highlighted that the perturbation due to SRP can have a significant impact on the orbit maintenance propellant consumption. SRP should be carefully considered in the orbit and attitude dynamics studies. This motivates examining SPS with a wide range of AMRs in the orbit dynamics study in the following chapter.

A range of near geosynchronous inclined orbits near to GLPO were also shown to outperform the traditionally proposed GEO location for SPS. This indicates that the SPS orbit may not need to be fully controlled in GLPO in order to obtain a high performing SPS system. The next chapter contains analysis of the uncontrolled orbit dynamics of SPS starting in either GLPO and GEO, and the resulting power delivery performance for comparison.

The sensitivity analysis undertaken implies that the E_D/C_{sps} ratio of the system is most sensitive to the rectenna diameter D_r. If you make D_r too small, then D_x becomes large to maintain high efficiency transmission. A larger D_x means a larger area to collect power and therefore a higher P_{sps}. This becomes a problem when the power is high and the rectenna area is small as the power density becomes too large. There is a trade-off here. If motivated by minimising the size of the in-space antenna D_x we may make D_r too large, then it is difficult to justify the land usage for the consequently low power density being received. Also, due to the sandwich's design which involves the solar array area being on top of the transmitting antenna, a smaller transmitting antenna means less solar arrays and less power. Overall, the sensitivity analysis indicates that size of the rectenna and the transmitting antenna are the most important features in determining the performance of the system.

2.8.1 Impact of SPS Design on Results

The analysis of this chapter focussed on the sandwich SPS which is a Type III SPS. Type III was chosen due to the IAA finding that Type III SPS are the most feasible due to the technology readiness level of the critical technologies.[7] The Sandwich SPS is a gravity gradient stabilised design. The IAA[7] study's finding of Type III SPS as the most technically feasible is partially due to Type III's use of passive gravity gradient stabilisation.

The differences in design features of the different SPSs come down to the input parameters. The sensitivity analysis on these input parameters indicates the particular parameters to which the performance of the SPS system is most sensitive. For a GLPO sandwich 2.45 GHz SPS the most sensitive parameters are D_r, σ_{TA}, s_{MF}, and I_{sp}. Two of these are essentially tied to the transmitting antenna which would be exactly the same for a Type I SPS beaming power at the same frequency. The sensitivity to I_{sp} is related to the relationship between lifetime and orbit maintenance delta-v. In the orbit dynamics, the only distinguishing feature related to the specific SPS design is the area to mass ratio (AMR).

This is the main distinguishing property for the orbit dynamics and is quantified by the SPS's Λ value which determines the impact of the SRP perturbation. For this reason, Chapter 3 considers 3 SPS designs with a wide range of Λ values. It finds that the Λ value has little impact on the performance of the uncontrolled SPS system but does affect the attitude control costs which is considered in Chapter 4.

The input parameter that the output is most sensitive to is D_r, which is independent of the particular design type of a microwave SPS, and instead entirely dependent on the microwave frequency used. The degree to which the output is sensitive to D_r may be dependent on the choice of microwave frequency. The systems analysis presented is for $f_\mu = 2.45$ GHz. The two main candidate frequencies for microwave SPS are 2.45 GHz and 5.8 GHz. Different SPS designs select either 2.45 or 5.8 GHz.

Therefore we rerun the sensitivity analysis for $f_\mu = 5.8$ GHz in Fig. 2.10. No change in the ordering of the magnitudes of the sensitivity indices is observed for the alternative frequency. This indicates that the insights gained from the systems analysis apply to SPS designs regardless of whether they have $f_\mu = 2.45$ GHz or $f_\mu = 5.8$ GHz.

The attitude control for different SPS designs would introduce differences due to their different mass distributions and attitude configurations, but is not considered in this chapter's cost effective analysis.

The rest of the input parameters in Fig. 2.9 would not be significantly impacted by the choice of SPS design (Type I vs Type III). We see for instance that the results are not particularly sensitive to the sunlight concentration factor, which is $C = 1$ for Type I SPS and $C = 3 - 5$ for Type III SPS.

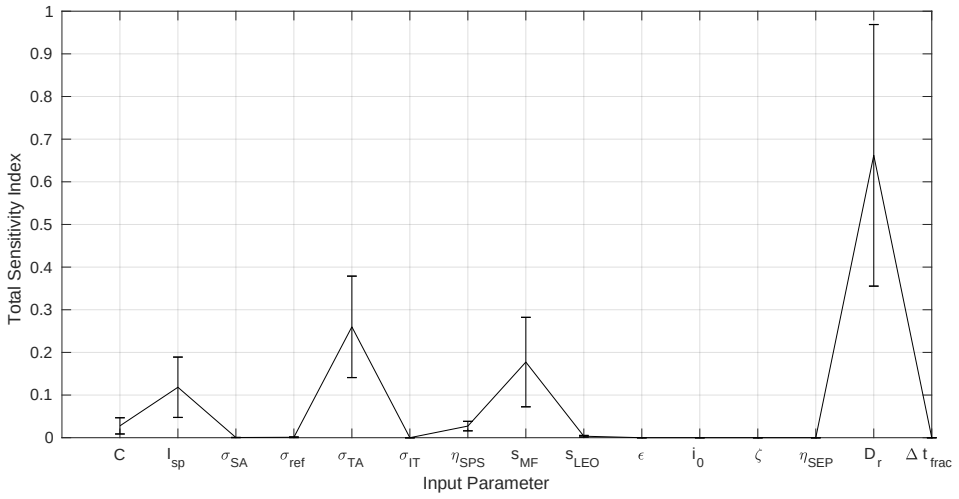

Figure 2.9: Total sensitivity indices for all input parameters ($f_\mu = 2.45$ GHz.)

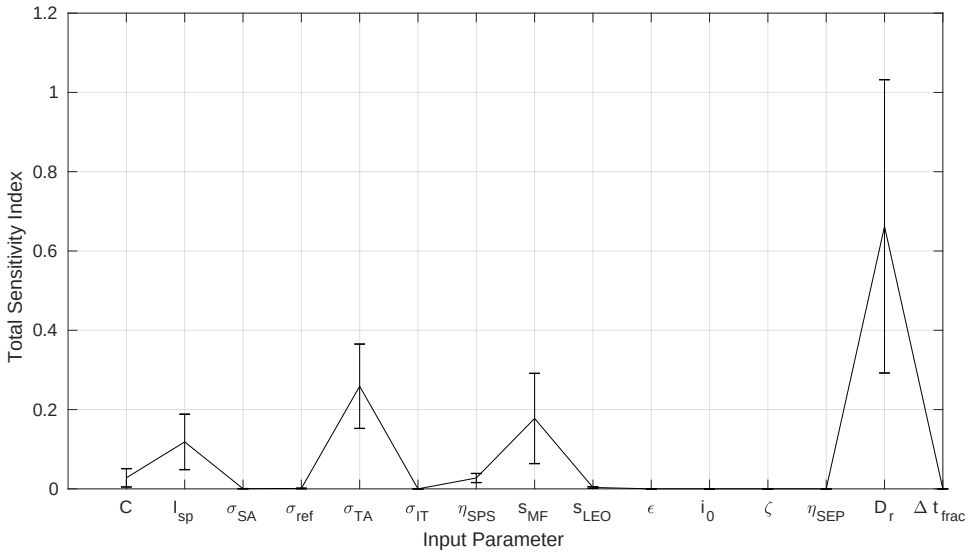

Figure 2.10: Total sensitivity indices for all input parameters ($f_\mu = 5.8$ GHz)

.

3

Orbital Dynamics of Geosynchronous SPSs

> "Among the primary arguments for solar energy conversion in space for use on Earth is the nearly constant availability of solar radiation in GEO as compared with solar radiation received on Earth. Futhermore, solar energy available in GEO will be at least four times the solar energy available even in favorable locations on Earth because of interruptions caused by weather and night."
>
> - Peter Glaser

The literature suggests the most effective orbital location for the operation of SPS structures is in equatorial geostationary Earth orbit (GEO).[1,2,7] This ensures 24-hour power supply, with only small outages around the equinoxes and simplified transmitting antenna/ receiving antenna geometry.

The primary purpose of this chapter is the investigation of an alternative orbital location for SPS referred to herein as the geosynchronous Laplace plane orbit (GLPO). Although the proposal to place SPS in this orbit is not original, having been mentioned in a small number of the studies in the 1970's,[38,39] it was not widely considered. One of stated reasons[39] for dismissal of the GLPO option was due to the choice of delivering power to a particular geographic location. Delivery of power to this location from GLPO would result in an increased area of receiving antenna compared to from GEO. On the basis of the additional cost this would incur, GLPO was dismissed. However, delivering power to lower latitudes does not incur the same increases in rectenna size from GLPO. Although Graf[38] demonstrated the long-term stability of GLPO, no detailed analysis of GLPO and the impact on potential SPS performance caused by moving the orbit location from GEO was performed. This chapter analyses the

potential benefits and drawbacks of GLPO as an alternative orbital location to GEO.

The remainder of this chapter is outlined as follows. Firstly, a comprehensive understanding of the effect of perturbations on orbits of large SPS structures over a time-frame commensurate with proposed SPS lifetimes (30-40 years) is obtained. An averaged model of the dynamics is used. The integration of the averaged equations of motion is several hundred times faster than the integration of the nonaveraged equations of motion for orbit propagations over the timescales considered. The results of the orbital dynamics study are used to assess the performance of a SPS over mission lifetime. The following three cases are studied and compared: an SPS in a controlled GEO; an SPS initially in GEO but left uncontrolled; and finally, an uncontrolled SPS placed in a GLPO.

The GLPO SPS provides comparable performance in terms of power delivered to the controlled GEO SPS while requiring nominal fuel to maintain its orbit. Additional benefits are the reduction of the risk from orbital debris, improved operational robustness, and avoidance of conflict/interference with GEO communication satellites.

3.1 Solar Power Satellite Designs

Since the 1970's SPS reference system studies, the idea of SPS has been periodically revisited. The 'Fresh Look' study, conducted by NASA during 1995-1997 and reported by Mankins,[4] and more recent studies by NASA as part of the SSP (Space Solar Power) Exploratory Research and Technology (SERT) program studies in the early 2000's produced a variety of new configurations of solar power satellites. Three of the SPS designs that resulted from the more recent NASA studies are considered here, shown in Fig. 3.1 (ISC is an example of a sandwich SPS design). These designs are chosen for being representative of a range of area-to-mass ratios. All SPS designs have a high-area-to-mass ratio (HAMR) as compared with conventional satellites, this leads to an increased effect on the orbit due to solar radiation pressure (SRP). Consequently, this is the parameter which distinguishes their orbital dynamics.

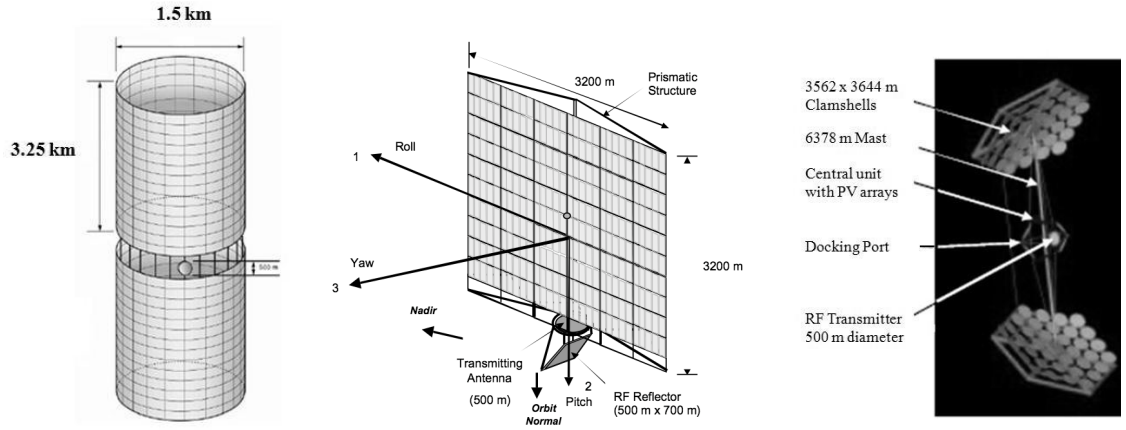

(a) Cylindrical SPS. (b) Abacus (c) Integrated Symmetrical Concentrator (ISC).

Figure 3.1: SPS designs,[40] where PV: photovoltaic and RF: radio frequency.

3.2 Retro-Directive Phased Array Antennas

One of the primary reasons GEO was first suggested for SPS in past studies[1,41,2] was due to the simple geometry between transmitting antenna and receiving antenna (rectenna) on the ground. Minimal repointing of the power beam is required, therefore removing the need to mechanically reorient the transmitter and rectenna throughout an orbital period. However, a method of wireless power transmission has been developed using a so-called retro-directive phased array that allows for the beam to be electronically steered with no major mechanical repointing necessary, hence, off-axis power beaming is possible. Consequently, orbits other than the conventional GEO become more feasible. This thesis shall focus on the orbit dynamics of SPS, and as such it is sufficient to select a reference system retro-directive phased array antenna, as developed by Frank Little et al.,[42] the details of which are given in Table 3.1. The parameters given in Table 3.1 are illustrated in Fig. 3.2. The important beam steering parameter, β, is the maximum off-axis beaming angle possible for the reference system considered. The retro-directive phased array power transmission system is assumed for all three SPS designs.

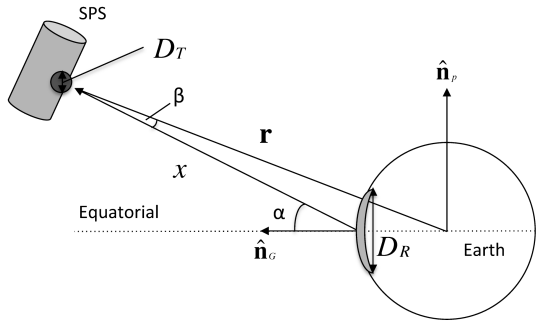

Figure 3.2: SPS-ground rectenna geometry.

3.3 Orbital Location

Previous SPS orbit dynamics studies[19,16] assumed SPS to be located in GEO and designed control systems for maintaining the orbit. However, this may not be the best option in terms of orbital dynamics of the system. An alternative system with an SPS located in a GLPO is considered.

3.3.1 Geostationary

A satellite in GEO is stationary with respect to a point on the Earth's surface. Its altitude is such that its orbital rate is equal to the rotational rate of the Earth. This occurs for an altitude of 35,786 km. It has approximately zero inclination and eccentricity. As well has providing near 24 hour access (with only short outages around the equinoxes), GEO minimises scanning losses as minimal slewing of the

Table 3.1: Retro-directive phased array antenna reference system[42]

Property	Symbol	Value
Antenna Diameter	D_T	0.5 km
Rectenna Diameter	D_R	8.85 km
Power Transmitted	P_t	1.78 GW
Frequency	ν_μ	5.8 GHz
Wavelength	λ_μ	5.17 cm
Separation	x	$35,786km + \Delta x$
Beam Steering	β	$\pm 3^\circ$

power beam is necessary. The main disadvantages are: the high cost of launch to GEO, the divergence of the power beam over the large distance from GEO to the ground-based rectenna drives the overall system size up, and finally, the potential conflict with the communication satellite industry which heavily utilises GEO.

3.3.2 The Laplace Plane

While studying Saturn's satellites in 1805, Laplace[44] recognised that the combined effect of a planet's oblateness and the solar tide induced a so-called 'proper' inclination in satellite orbits with respect to the planetary equator. He found that the proper inclination depended upon the distance of the satellite from the planet, increasing with increasing distance. This proper inclination defines a plane between the orbital plane of the planet around the sun and the planet's equatorial plane. This is what is now known as the Laplace plane (see Fig. 3.3). The normal to the local Laplace plane, $\hat{\boldsymbol{Z}}$, lies between, and is coplanar with, the planets spin pole, $\hat{\boldsymbol{n}}_p$, and the normal to the ecliptic, $\hat{\boldsymbol{n}}_{ecl}$. The angular momentum vector, $\boldsymbol{h}$, or the normal to an arbitrary objects orbit plane, will precess around $\hat{\boldsymbol{Z}}$, at approximately constant inclination, i_L, sweeping out a cone. The Earth's obliquity, ϵ, is simply the angle between the vectors $\hat{\boldsymbol{n}}_p$ and $\hat{\boldsymbol{n}}_{ecl}$. The Laplace plane angle, Φ, represents the angle between $\hat{\boldsymbol{n}}_p$ and the $\hat{\boldsymbol{Z}}$ axis. Recent contributions to the understanding of the Laplace plane and the effect of solar radiation pressure on the Laplace plane have been made by Tamayo et al.,[43] Rosengren et al.[45] and Ulivieri et al.[46] The Laplace plane is essentially a region of

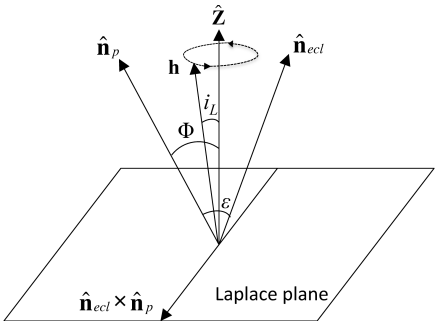

Figure 3.3: The Laplace plane. Based on figure from Tamayo et al.[43]

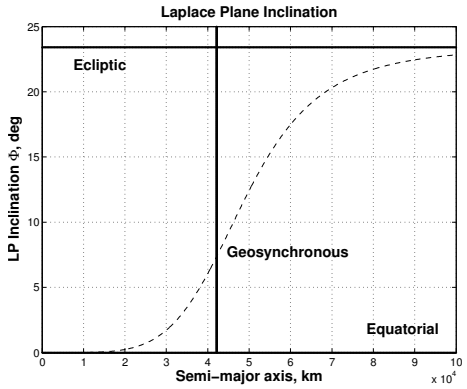

Figure 3.4: Laplace plane inclination with respect to the Earth's equatorial plane for various semimajor axis.[47]

space where the secular evolution of the combined effects of the luni-solar gravitational and Earth planetary oblateness perturbations cancel each other out. Consequently, the orientation of orbits lying within this plane vary minimally.

The approximate inclination of the Laplace plane with respect to the equatorial plane can be calculated according to the theory of Allan and Cook,[47] with the results for different semimajor axis shown in Fig. 3.4. For SPSs, it is beneficial to maintain the geosynchronous nature of the orbit to allow for 24 hour power beaming. From Fig. 3.4, the Laplace plane inclination, Φ, at the altitude required for geosynchronous is approximately 7.5°.

3.3.3 Previous Investigation of Geosynchronous Laplace Plane SPS

The possibility of locating SPS in the Laplace plane has been investigated before by Graf,[38] and in a study by Rockwell[39] both in 1978. Graf[38] studied the long-term evolution of the eccentricity and inclination of GLPO orbits for SPS using analytical methods. The ground-tracks of these orbits for varying argument of perigee were found. Graf also considered the possibility of an orbit with non-zero initial eccentricity, for which it appears the amplitude of the yearly oscillations in eccentricity are decreased for the first decade or so. However, no analysis was made of the consequences for the operation of an SPS in such an orbit, compared to the conventional

GEO. The Rockwell study[39] considered GLPO, but instead recommended the use of GEO for SPS due to the NASA reference system design requirement of delivering power to a site at 34° latitude. Delivering power to this relatively high latitude requires a rectenna 13.9% larger for SPS located in GLPO compared with an SPS in GEO. It appears that it was partly on this basis that GEO was chosen. Using a semi-analytical orbit propagation technique, more accurate and longer-term predictions of SPS orbits than Graf are obtained and various parameters related to the performance of the SPS system are assessed.

3.4 Orbital Modeling

In order to justify the large initial investment, a large scale SPS should have an operating lifetime of at least 30 years. Perishable items such as the solar arrays may be replenished periodically but the main structure could be in orbit for even longer. Therefore, when considering the orbital dynamics it is desirable to understand the evolution of the orbit over timescales of this order. Hence, an averaged formulation developed by Rosengren and Scheeres[48] for the propagation of high-area-to-mass ratio (HAMR) objects in Earth orbit which accounts for solar radiation pressure, Earth oblateness, and luni-solar gravitational perturbations, is used. This is a first-order averaged model given in terms of the Milankovitch orbit elements.[49] The method of Rosengren and Scheeres shall be outlined here (for further detail consult[48]). This approach allows one to easily capture both the qualitative and quantitative effects of perturbations on the orbits of SPS over long time spans commensurate with proposed SPS lifetimes. To enhance confidence in the results obtained from the averaged equations of motion, numerical integration of the full nonaveraged equations of motion is also performed. The integration of the averaged equations of motion is several hundred times faster than the integration of the nonaveraged equations of motion for orbit propagations over the time scales considered.

To perform the orbit modeling it is first necessary to define the reference frames and

notation to be used. To describe the motion of the Earth about the sun a heliocentric orbit frame is defined ($\hat{\boldsymbol{E}}_e, \hat{\boldsymbol{E}}_{e_\perp}, \hat{\boldsymbol{H}}_e$), where $\hat{\boldsymbol{E}}_e$ points towards the orbit perihelion, $\hat{\boldsymbol{H}}_e$ is the orbit normal, and in the heliocentric plane of motion $\hat{\boldsymbol{E}}_{e_\perp} = \widetilde{\hat{\boldsymbol{E}}}_e \cdot \hat{\boldsymbol{H}}_e$.* The changing position vector between the Earth and the sun is given as $\boldsymbol{d}_e = d_e \hat{\boldsymbol{d}}_e$, with the magnitude and direction functions of Earth true anomaly f_e:

$$d_e = \frac{a_e(1-e_e^2)}{1+e_e \cos f_e} \tag{3.1}$$

$$\hat{\boldsymbol{d}}_e = \cos f_e \hat{\boldsymbol{E}}_e + \sin f_e \hat{\boldsymbol{E}}_{e_\perp} \tag{3.2}$$

where a_e is Earth's heliocentric semimajor axis, and e_e is the corresponding eccentricity of the Earth's orbit.

The moon's actual orbit is extremely complicated. For the purpose of this study, a simplified Moon orbit is assumed where the Moon is on an osculating elliptical orbit and the lunar node precesses clockwise in the ecliptic plane with a period of 18.61 years. This is sufficient to identify qualitatively the regularities of the motion and is an accurate enough depiction of lunar motion to obtain quantitative predictions of long-term orbital changes in the satellites motion. Therefore a geocentric orbit frame is defined ($\hat{\boldsymbol{E}}_m, \hat{\boldsymbol{E}}_{m_\perp}, \hat{\boldsymbol{H}}_m$), where $\hat{\boldsymbol{E}}_m$ is the unit vector in the direction of the moon's orbit perigee, $\hat{\boldsymbol{E}}_{m_\perp} = \widetilde{\hat{\boldsymbol{H}}}_m \cdot \hat{\boldsymbol{E}}_m$, and $\hat{\boldsymbol{H}}_m$ is the moon's angular momentum unit vector. These vectors are resolved using the moon's ecliptic orbital elements in which $\Omega_m(t) = \Omega_{m_0} + \dot{\Omega}_m(t-t_0)$, where $\dot{\Omega}_m = -2\pi / P_{saros}$ and P_{saros} is the sidereal period of nodal regression in seconds. The position vector from the Earth to the Moon is then $\boldsymbol{d}_m = d_m \hat{\boldsymbol{d}}_m$, where d_m and $\hat{\boldsymbol{d}}_m$ are given by Eqs. (3.1) and (3.2), respectively, but using the moon's orbital parameters. Finally, the position vector of the sun from the Earth is simply given by $\boldsymbol{d}_s = -\boldsymbol{d}_e$.

*The notation $\widetilde{\boldsymbol{a}}$ denotes the cross-product dyadic, which is defined as: $\widetilde{\boldsymbol{a}} \cdot \boldsymbol{b} = \boldsymbol{a} \cdot \widetilde{\boldsymbol{b}} = \boldsymbol{a} \times \boldsymbol{b}$

3.5 Nonaveraged Model

3.5.1 Solar Radiation Pressure

The cannonball model is used, which is the simplest model for solar radiation pressure (SRP) acceleration and assumes that the spacecraft presents a constant area perpendicular to the object-sun line (with uniform optical properties), and that the total momentum transfer is insolation plus reflection. The net acceleration due to SRP will act in the opposite direction to the object-sun line and will have the general form as given by Scheeres ([50] pp. 55-57, Sec. 2.6.2):

$$\begin{aligned} \boldsymbol{a}_{SRP} &= -(1+\rho)(A/m)P_{\Phi}\frac{\boldsymbol{d}_s - \boldsymbol{r}}{|\boldsymbol{d}_s - \boldsymbol{r}|^3} \\ &= -\gamma\frac{\boldsymbol{d}_s - \boldsymbol{r}}{|\boldsymbol{d}_s - \boldsymbol{r}|^3} \end{aligned} \tag{3.3}$$

where ρ is the reflectance of the spacecraft, A is the average cross-sectional area with respect to the sun, m is the mass, P_{Φ} is the solar radiation constant approximately equal to 1×10^8 kgkm^3/(s$^2 \cdot$ m^2), $\gamma = (1+\rho)(A/m)P_{\Phi}$, and $\boldsymbol{r}$ is the position vector of the satellite relative to the Earth. This simple form of the SRP acceleration can be rewritten as a potential:

$$\mathcal{R}_{SRP} = -\gamma\frac{1}{|\boldsymbol{d}_s - \boldsymbol{r}|} \tag{3.4}$$

where $\boldsymbol{a}_{SRP} = \partial\mathcal{R}_{SRP}/\partial\boldsymbol{r}$. Because Earth-orbiting satellites where $r \ll d_s$ are being considered, the potential may be simplified by expanding $1/|\boldsymbol{d}_s - \boldsymbol{r}|$ and keeping the first term that contains position vector $\boldsymbol{r}$, to give:

$$\mathcal{R}_{SRP} = -\frac{\gamma}{d_s^3}\boldsymbol{d}_s \cdot \boldsymbol{r} \tag{3.5}$$

For a given satellite semimajor axis a, an angle known as the SRP perturbation angle can be defined as:[51]

$$\tan\Lambda = \frac{3\gamma}{2}\sqrt{\frac{a}{\mu\mu_s a_e(1-e_e^2)}} \tag{3.6}$$

where μ and μ_s are the gravitational parameters of the Earth and sun, respectively. SRP perturbation becomes strong as $\Lambda \to \pi/2$ and weak as $\Lambda \to 0$. Therefore, the angle Λ characterises the strength of the SRP perturbation. Values of Λ for the three SPS designs are calculated in Table 3.2.

Table 3.2: Area-to-mass ratios, reflectance coefficients and the corresponding values for SRP perturbation angle for different SPS designs.

SPS	A/m (m^2/kg)	ρ	Λ $(^\circ)$
Cylindrical	0.15	0.3	0.12
Abacus	0.40	0.3	0.33
ISC	0.87	1.0	1.09

3.5.2 Earth Mass Distribution

The effects of only the C_{20} and C_{22} terms of the harmonic expansion of Earth's gravitational potential are considered here, because these are sufficient to capture the main effects of Earth's nonsphericity on high-altitude orbits. The standard manner to represent the potential function of the second degree and order of gravity field perturbation is using a body-fixed frame with latitude angle δ measured from the equatorial plane and the longitude λ measured in the equatorial plane from the axis of minimum moment of inertia, as given by Scheeres ([50] pp. 42-57, Sec. 2.5.1):

$$\mathcal{R}_2 = -\frac{\mu C_{20}}{2r^3}\left(1-3\sin^2\delta\right) + \frac{3\mu C_{22}}{r^3}\cos^2\delta\cos 2\lambda \tag{3.7}$$

where μ is the Earth's standard gravitational parameter, $C_{20} = -J_2 R_E^2$ is the oblateness gravity field coefficient, R_E is the mean equatorial radius of Earth, and C_{22} is the ellipticity gravity field coefficient. The potential function can be rewritten as a general vector expression:

$$\mathcal{R}_2 = -\frac{\mu C_{20}}{2r^3}\left(1 - 3(\hat{\boldsymbol{r}}\cdot\hat{\boldsymbol{p}})^2\right) + \frac{3\mu C_{22}}{r^3}\left[(\hat{\boldsymbol{r}}\cdot\hat{\boldsymbol{s}})^2 - (\hat{\boldsymbol{r}}\cdot\hat{\boldsymbol{q}})^2\right] \tag{3.8}$$

where it is assumed that the unit vectors $\hat{\boldsymbol{p}}, \hat{\boldsymbol{q}}, \hat{\boldsymbol{s}}$, are aligned with the Earth's maximum, intermediate and minimum axes of inertia. The perturbing acceleration may then be calculated by $\boldsymbol{a}_2 = \partial\mathcal{R}_2/\partial\boldsymbol{r}$:

$$\begin{aligned}\boldsymbol{a}_2 = {} & \frac{3\mu C_{20}}{2r^4}\{\left[1 - 5(\hat{\boldsymbol{r}}\cdot\hat{\boldsymbol{p}})^2\right]\hat{\boldsymbol{r}} + 2(\hat{\boldsymbol{r}}\cdot\hat{\boldsymbol{p}})\hat{\boldsymbol{p}}\} \\ & - \frac{3\mu C_{22}}{r^4}\{5\left[(\hat{\boldsymbol{r}}\cdot\hat{\boldsymbol{s}})^2 - (\hat{\boldsymbol{r}}\cdot\hat{\boldsymbol{q}})^2\right]\hat{\boldsymbol{r}} - 2\left[(\hat{\boldsymbol{r}}\cdot\hat{\boldsymbol{s}})\hat{\boldsymbol{s}} - (\hat{\boldsymbol{r}}\cdot\hat{\boldsymbol{q}})\hat{\boldsymbol{q}}\right]\}\end{aligned} \tag{3.9}$$

where only the first term is included for the averaging process. The second term is due to the ellipticity of the Earth's equator and cannot be included in the averaged model. It is later included in the nonaveraged model to check the stability of the solution to this perturbing acceleration.

3.5.3 Third-Body Gravitational Attraction: Moon and Sun

The effect of the moon and the sun's gravity must be considered when modeling SPS orbits. Taking the Earth as the center of the dynamic system, the perturbing acceleration from a body with gravitational parameter μ_p is given by Scheeres ([50] pp. 53-55, Sec. 2.6.1):

$$\boldsymbol{a}_p = -\mu_p\left[\frac{\boldsymbol{r} - \boldsymbol{d}_p}{|\boldsymbol{r} - \boldsymbol{d}_p|^3} + \frac{\boldsymbol{d}_p}{|\boldsymbol{d}_p|^3}\right] \tag{3.10}$$

where $\boldsymbol{d}_p$ is the position vector of the disturbing body relative to the Earth ($\boldsymbol{d}_s$ or $\boldsymbol{d}_m$). For later use in the averaged perturbation analysis, it is useful to recast this as a perturbing potential:

$$\mathcal{R}_p = \mu_p\left[\frac{1}{|\boldsymbol{r} - \boldsymbol{d}_p|} + \frac{\boldsymbol{d}_p\cdot\boldsymbol{r}}{|\boldsymbol{d}_p|^3}\right] \tag{3.11}$$

where $\boldsymbol{a}_p = \partial\mathcal{R}_p/\partial\boldsymbol{r}$. In this case, the satellite's distance from the Earth is small compared to the distance between the Earth and the third body in both cases (i.e. $r/d_p \ll 1$), hence the perturbing potential can be represented as an infinite series using the Legendre expansion (Scheeres[50] pp. 53-55, Sec. 2.6.1), giving:

$$\mathcal{R}_p = \frac{\mu_p}{d_p}\left[\sum_{i=0}^{\infty}\left(\frac{r}{d_p}\right)^i P_{i,0}\left(\frac{\boldsymbol{r}\cdot\boldsymbol{d}_p}{rd_p}\right) - \frac{\boldsymbol{d}_p\cdot\boldsymbol{r}}{d_p^2}\right] \tag{3.12}$$

Retaining only the first nonconstant term and substituting in the Legendre polynomial $P_{2,0}(x) = 1/2(3x^2-1)$:

$$\mathcal{R}_p = \frac{\mu_p}{2d_p^3}\left[3(\boldsymbol{r}\cdot\hat{\boldsymbol{d}}_p)^2 - r^2\right] \tag{3.13}$$

Under these simplifying assumptions, the 3rd body perturbing acceleration reduces to

$$\boldsymbol{a}_p = \frac{\mu_p}{d_p^3}\left[3(\boldsymbol{r}\cdot\hat{\boldsymbol{d}}_p)\hat{\boldsymbol{d}}_p - \boldsymbol{r}\right] \tag{3.14}$$

3.5.4 Microwave Beaming

Because of the high power of the microwave beam, the SPS microwave transmitter will actually perturb the orbit when beaming power. There is a reactive force in the opposite direction to the beaming direction. This direction is given by the ground station (GS) to SPS unit vector direction, $\hat{\boldsymbol{r}}_{GS-SPS}$. The perturbation acceleration is dependent on the power transmitted, P_t, and the mass of the SPS, m, and is given by

$$\boldsymbol{a}_\mu = \frac{P_t}{cm}\hat{\boldsymbol{r}}_{GS-SPS} \tag{3.15}$$

where c is the speed of light. The SPS would only beam power when in sunlight, however, eclipses for satellites at geosynchronous altitude are minimal and shall not be considered here. Therefore, the microwave beam is considered continuous. This perturbation will not be included in the averaged analysis, however, its effect shall be analysed with the nonaveraged model.

3.5.5 Nonaveraged Equations of Motion

The preceding perturbing force models may be combined to define the equations of motion for an SPS in high Earth orbit, accounting for solar radiation pressure, Earth oblateness, and lunisolar gravitational perturbations. They can be stated in an inertially fixed Earth-centered frame in relative form:

$$U(\boldsymbol{r}) = \frac{\mu}{r} + \mathcal{R}_{SRP}(\boldsymbol{r}) + \mathcal{R}_2(\boldsymbol{r}) + \mathcal{R}_s(\boldsymbol{r}) + \mathcal{R}_m(\boldsymbol{r}) \tag{3.16}$$

$$\ddot{\boldsymbol{r}} = \frac{\partial U}{\partial \boldsymbol{r}} \tag{3.17}$$

where $\mathcal{R}_s$ and $\mathcal{R}_m$ are the third-body perturbation acceleration potential functions for the sun and the moon, respectively. Performing the partial derivatives of the potential functions, the equation of motion may be expressed in terms of the perturbing accelerations:

$$\ddot{\boldsymbol{r}} = -\frac{\mu}{r^3}\boldsymbol{r} + \boldsymbol{a}_{SRP} + \boldsymbol{a}_2 + \boldsymbol{a}_s + \boldsymbol{a}_m \tag{3.18}$$

This equation may be solved by numerical integration, which is performed to enhance confidence in the averaged method used. The additional perturbations due to the microwave beam and the J_{22} term are included later to confirm the stability of the Laplace plane solution with respect to these forces.

3.6 Averaging of Dynamic Equations

The concept of averaging allows the secular effects of the orbital perturbations on the satellite motion to be evaluated. The short-term variations caused by the various perturbations are averaged out, leaving just the secular terms. For this to be valid, the perturbing forces must be small enough so that, over one orbital period, the deviations of the true trajectory from the Keplerian trajectory are relatively small. The Milankovitch elements have not been used widely in celestial mechanics in recent

history, however, they have recently been reformulated by Rosengren and Scheeres[49] and offer much simpler and more elegant equations than the classical orbit element Lagrange formulation, and they also avoid singularities. In this case, where the perturbations considered are in the form of potentials, the semimajor axis a does not undergo secular change, hence, the angular momentum per unit mass vector $\boldsymbol{H}$ can be divided by $\sqrt{\mu a}$, giving vector $\boldsymbol{h}$. With vector $\boldsymbol{h}$ and eccentricity vector $\boldsymbol{e}$, the secular Milankovitch equations are compact and symmetrical in form. In terms of position vector $\boldsymbol{r}$ and velocity vector $\boldsymbol{v}$, they can be expressed as[47]

$$\boldsymbol{h} = \frac{1}{\sqrt{\mu a}} \widetilde{\boldsymbol{r}} \cdot \boldsymbol{v} \tag{3.19}$$

$$\boldsymbol{e} = \frac{1}{\mu} \widetilde{\boldsymbol{v}} \cdot \widetilde{\boldsymbol{r}} \cdot \boldsymbol{v} - \frac{\boldsymbol{r}}{|\boldsymbol{r}|} \tag{3.20}$$

The first-order averaged equations in Lagrangian form may then be stated as[49,47,52]

$$\dot{\overline{\boldsymbol{h}}} = \widetilde{\overline{\boldsymbol{h}}} \cdot \left(\frac{\partial \overline{\mathcal{R}}^*}{\partial \overline{\boldsymbol{h}}} \right)^T + \widetilde{\overline{\boldsymbol{e}}} \cdot \left(\frac{\partial \overline{\mathcal{R}}^*}{\partial \overline{\boldsymbol{e}}} \right)^T \tag{3.21}$$

$$\dot{\overline{\boldsymbol{e}}} = \widetilde{\overline{\boldsymbol{e}}} \cdot \left(\frac{\partial \overline{\mathcal{R}}^*}{\partial \overline{\boldsymbol{h}}} \right)^T + \widetilde{\overline{\boldsymbol{h}}} \cdot \left(\frac{\partial \overline{\mathcal{R}}^*}{\partial \overline{\boldsymbol{e}}} \right)^T \tag{3.22}$$

where the overbar indicates an averaged value [*] and $\overline{\mathcal{R}}^* = \overline{\mathcal{R}}(\boldsymbol{h}, \boldsymbol{e}) / \sqrt{\mu a}$ is the scaled averaged potential. Each averaged perturbing potential is calculated with

$$\overline{\mathcal{R}}(\boldsymbol{h}, \boldsymbol{e}) = \frac{1}{2\pi} \int_0^{2\pi} \mathcal{R}(\boldsymbol{\alpha}, M) \mathrm{d}M \tag{3.23}$$

where $\boldsymbol{\alpha}$ is an arbitrary set of orbital elements excluding the mean anomaly, and $\overline{\mathcal{R}}(\boldsymbol{h}, \boldsymbol{e})$ is independent of the fast variable M. The individual perturbation potentials given by Equations (3.5),(3.8) and (3.13) are substituted into Equation (3.23). These are then scaled by $\sqrt{\mu a}$ to obtain the individual $\overline{\mathcal{R}}^*$ values for each perturbing force,

[*]From this point onward, the overbar operator has been omitted from the Milankovitch elements $\boldsymbol{h}$ and $\boldsymbol{e}$, because all variables are averaged variables in what follows.

which may then be substituted into Equations (3.21) and (3.22) to obtain the secular variation in $\boldsymbol{h}$ and $\boldsymbol{e}$ due to each perturbation. The overall secular variation in $\boldsymbol{h}$ and $\boldsymbol{e}$ is calculated by summing the contributions from each perturbing force.

3.6.1 Averaged SRP

To calculate the averaged potential for solar radiation pressure, Eq. (3.5) is substituted into Eq. (3.23):

$$\begin{aligned}\overline{\mathcal{R}}_{SRP} &= \frac{1}{2\pi}\int_0^{2\pi} \mathcal{R}_{SRP}\mathrm{d}M \\ &= -\frac{\gamma}{d_s^2}\hat{\boldsymbol{d}}_s \cdot \bar{\boldsymbol{r}}\end{aligned} \tag{3.24}$$

The satellite-sun vector is considered fixed over the averaging time scale, therefore, only the average over the position vector must be computed, a classically known result:

$$\bar{\boldsymbol{r}} = \frac{1}{2\pi}\int_0^{2\pi} \boldsymbol{r}\mathrm{d}M = -\frac{3}{2}a\boldsymbol{e} \tag{3.25}$$

Consequently,

$$\overline{\mathcal{R}}^*_{SRP} = \frac{3}{2}\sqrt{\frac{a}{\mu}}\frac{\gamma}{d_s^2}\hat{\boldsymbol{d}}_s \cdot \boldsymbol{e} \tag{3.26}$$

This scaled, averaged SRP perturbation potential is then substituted in the secular Milankovitch equations (3.21) and (3.22), resulting in

$$\dot{\boldsymbol{h}}_{SRP} = -\frac{3}{2}\sqrt{\frac{a}{\mu}}\frac{\gamma}{d_s^2}\widetilde{\hat{\boldsymbol{d}}}_s \cdot \boldsymbol{e} \tag{3.27}$$

$$\dot{\boldsymbol{e}}_{SRP} = -\frac{3}{2}\sqrt{\frac{a}{\mu}}\frac{\gamma}{d_s^2}\widetilde{\hat{\boldsymbol{d}}}_s \cdot \boldsymbol{h} \tag{3.28}$$

3.6.2 Averaged J_2

Only the averaged C_{20} dynamics are considered here. Although the C_{22} can also introduce long-term effects, the averaged effect of this perturbation cannot be treated

with the method adopted here. Therefore, the following is obtained:

$$\overline{\mathcal{R}}_{20} = -\frac{\mu C_{20}}{2}\left[\overline{\frac{1}{r^3}} - 3\hat{\boldsymbol{p}}\cdot\overline{\frac{\hat{\boldsymbol{r}}\hat{\boldsymbol{r}}}{r^3}}\cdot\hat{\boldsymbol{p}}\right] \tag{3.29}$$

Substituting in the following averaging results

$$\overline{\frac{1}{r^3}} = \frac{1}{a^3h^3} \tag{3.30}$$

$$\overline{\frac{\hat{\boldsymbol{r}}\hat{\boldsymbol{r}}}{r^3}} = \frac{1}{2a^3h^3}\left[\boldsymbol{U} - \hat{\boldsymbol{h}}\hat{\boldsymbol{h}}\right] \tag{3.31}$$

where $\boldsymbol{U}$ is the identity dyadic and has the property $\boldsymbol{U}\cdot\boldsymbol{a} = \boldsymbol{a}\cdot\boldsymbol{U} = \boldsymbol{a}$, gives

$$\overline{\mathcal{R}}^*_{20} = \frac{nC_{20}}{4a^2h^3}\left[1 - 3(\hat{\boldsymbol{p}}\cdot\hat{\boldsymbol{h}})^2\right] \tag{3.32}$$

where n is the mean motion of the satellite and $h = \sqrt{1-e^2}$. This scaled, averaged J_2 perturbation potential is then substituted in the secular Milankovitch equations (3.21) and (3.22), resulting in

$$\dot{\boldsymbol{h}}_{20} = \frac{3nC_{20}}{2a^2h^5}(\hat{\boldsymbol{p}}\cdot\boldsymbol{h})\widetilde{\hat{\boldsymbol{p}}}\cdot\boldsymbol{h} \tag{3.33}$$

$$\dot{\boldsymbol{e}}_{20} = \frac{3nC_{20}}{4a^2h^5}\left\{\left[1 - \frac{5}{h^2}(\hat{\boldsymbol{p}}\cdot\boldsymbol{h})^2\right]\widetilde{\boldsymbol{h}} + 2(\hat{\boldsymbol{p}}\cdot\boldsymbol{h})\widetilde{\hat{\boldsymbol{p}}}\right\}\cdot\boldsymbol{e} \tag{3.34}$$

3.6.3 Singly Averaged Third Body

There are two time scales over which the dynamic motion occurs for the third-body perturbations, the period of the orbiter, and the period of the disturbing body. In the case considered here, the orbital rate n of the orbiter is considerably greater than the angular rate N_p of the disturbing bodies (moon and sun), and therefore it is acceptable to hold N_p constant while averaging over n.

The perturbing potential in Eq. (3.13) can be averaged over the unperturbed two-

body motion of the Earth. This results in singly averaged third-body equations:

$$\overline{\mathcal{R}}_p = \frac{\mu_p}{2d_p^3}\left[3\hat{\boldsymbol{d}}_p \cdot \overline{\boldsymbol{rr}} \cdot \hat{\boldsymbol{d}}_p - \overline{r^2}\right] \tag{3.35}$$

where, from Scheeres ([50] pp. 363-366, Appendix C),

$$\overline{r^2} = a^2\left(1 + \frac{3}{2}e^2\right) \tag{3.36}$$

$$\overline{\boldsymbol{rr}} = \frac{1}{2}a^2\left[5\boldsymbol{ee} - \boldsymbol{hh} + (1-e^2)\boldsymbol{U}\right] \tag{3.37}$$

Substituting Eqs. (3.36) and (3.37) into (3.35), disregarding the constant term, and scaling by $\sqrt{\mu a}$ gives

$$\overline{\mathcal{R}}_p^* = \frac{3\mu_p}{4nd_p^3}\left[5(\hat{\boldsymbol{d}}_p \cdot \boldsymbol{e})^2 - (\hat{\boldsymbol{d}}_p \cdot \boldsymbol{h})^2 - 2e^2\right] \tag{3.38}$$

This is the scaled averaged disturbing potential for any third body (here only the moon and the sun are considered). Consequently, the secular equations for the third-body gravitational perturbation are

$$\dot{\overline{\boldsymbol{h}}}_p = \frac{3\mu_p}{2nd_p^3}\hat{\boldsymbol{d}}_p \cdot (5\boldsymbol{ee} - \boldsymbol{hh}) \cdot \widetilde{\hat{\boldsymbol{d}}_p} \tag{3.39}$$

$$\dot{\overline{\boldsymbol{e}}}_p = \frac{3\mu_p}{2nd_p^3}\left[\hat{\boldsymbol{d}}_p \cdot (5\boldsymbol{eh} - \boldsymbol{he}) \cdot \widetilde{\hat{\boldsymbol{d}}_p} - 2\widetilde{\boldsymbol{h}} \cdot \boldsymbol{e}\right] \tag{3.40}$$

where $\boldsymbol{ee}, \boldsymbol{hh}, \boldsymbol{eh},$ and $\boldsymbol{he}$ are dyads. The overbar has been reintroduced to distinguish between the singly averaged and the doubly/triply averaged results that follow.

3.6.4 Doubly Averaged Third Body

Because it is assumed that the third bodies are in elliptic orbits, and because there is sufficient distance between the two aforementioned time scales, another averaging may

be performed over the third body's motion. This is achieved simply by substituting Eqs. (3.39) and (3.40) into the averaging equation (3.23) to obtain

$$\dot{\bar{\bar{\boldsymbol{h}}}}_p = \frac{1}{2\pi}\int_0^{2\pi} \dot{\bar{\boldsymbol{h}}}_p \mathrm{d}M_p \tag{3.41}$$

$$= -\frac{3\mu_p}{2n}\left[5\boldsymbol{e}\cdot\overline{\left(\frac{\hat{\boldsymbol{d}}_p\hat{\boldsymbol{d}}_p}{d_p^3}\right)}\cdot\widetilde{\boldsymbol{e}} - \boldsymbol{h}\cdot\overline{\left(\frac{\hat{\boldsymbol{d}}_p\hat{\boldsymbol{d}}_p}{d_p^3}\right)}\cdot\widetilde{\boldsymbol{h}}\right] \tag{3.42}$$

$$\dot{\bar{\bar{\boldsymbol{e}}}}_p = \frac{1}{2\pi}\int_0^{2\pi} \dot{\bar{\boldsymbol{e}}}_p \mathrm{d}M_p \tag{3.43}$$

$$= -\frac{3\mu_p}{2n}\left[5\boldsymbol{e}\cdot\overline{\left(\frac{\hat{\boldsymbol{d}}_p\hat{\boldsymbol{d}}_p}{d_p^3}\right)}\cdot\widetilde{\boldsymbol{h}} - \boldsymbol{h}\cdot\overline{\left(\frac{\hat{\boldsymbol{d}}_p\hat{\boldsymbol{d}}_p}{d_p^3}\right)}\cdot\widetilde{\boldsymbol{e}} + \overline{\left(\frac{1}{d_p^3}\right)}2\widetilde{\boldsymbol{h}}\cdot\boldsymbol{e}\right] \tag{3.44}$$

Again, substituting in the averaged values as given in Eqs. (3.30) and (3.31),

$$\dot{\bar{\bar{\boldsymbol{h}}}}_p = -\frac{3\mu_p}{4na_p^3h_p^3}\hat{\boldsymbol{H}}_p\cdot(5\boldsymbol{e}\boldsymbol{e} - \boldsymbol{h}\boldsymbol{h})\cdot\widetilde{\hat{\boldsymbol{H}}}_p \tag{3.45}$$

$$\dot{\bar{\bar{\boldsymbol{e}}}}_p = -\frac{3\mu_p}{4na_p^3h_p^3}\left[\hat{\boldsymbol{H}}_p\cdot(5\boldsymbol{e}\boldsymbol{h} - \boldsymbol{h}\boldsymbol{e})\cdot\widetilde{\hat{\boldsymbol{H}}}_p - 2\widetilde{\boldsymbol{h}}\cdot\boldsymbol{e}\right] \tag{3.46}$$

where $\hat{\boldsymbol{H}}_p$ is the perturbing body's angular momentum unit vector. These doubly averaged equations can also be used for evaluating the effects of lunisolar gravitational perturbations $\dot{\boldsymbol{h}}_m$, $\dot{\boldsymbol{e}}_m$, $\dot{\boldsymbol{h}}_s$, and $\dot{\boldsymbol{e}}_s$.

3.6.5 Moon's Nodal Motion Averaging

The doubly averaged equations may be averaged again over the moon's nodal motion, therefore,

$$\dot{\bar{\bar{\bar{\boldsymbol{h}}}}}_m = \frac{1}{2\pi}\int_0^{2\pi} \dot{\bar{\bar{\boldsymbol{h}}}}_m \mathrm{d}\Omega_m \tag{3.47}$$

$$\dot{\bar{\bar{\bar{\boldsymbol{e}}}}}_m = \frac{1}{2\pi}\int_0^{2\pi} \dot{\bar{\bar{\boldsymbol{e}}}}_m \mathrm{d}\Omega_m \tag{3.48}$$

where Ω_m is the moon's right ascension of the ascending node (RAAN) in the ecliptic frame. Carrying out the averaging process leads to

$$\dot{\bar{\bar{\boldsymbol{h}}}}_m = -\frac{3\mu_m}{4na_m^3h_m^3}(\cos^2 i_m - \frac{1}{2}\sin^2 i_m)\left[5\boldsymbol{e}\cdot\hat{\boldsymbol{n}}_{ecl}\widetilde{\hat{\boldsymbol{n}}}_{ecl}\cdot\boldsymbol{e} - \boldsymbol{h}\cdot\hat{\boldsymbol{n}}_{ecl}\widetilde{\hat{\boldsymbol{n}}}_{ecl}\cdot\boldsymbol{h}\right] \tag{3.49}$$

$$\begin{aligned}\dot{\bar{\bar{\boldsymbol{e}}}}_m = -\frac{3\mu_m}{4na_m^3h_m^3}\Big[&\frac{5}{2}\sin^2 i_m\boldsymbol{e}\cdot(\widetilde{\boldsymbol{h}} - \hat{\boldsymbol{n}}_{ecl}\widetilde{\hat{\boldsymbol{n}}}_{ecl}\cdot\boldsymbol{h}) + 5\cos^2 i_m\boldsymbol{e}\cdot\hat{\boldsymbol{n}}_{ecl}\widetilde{\hat{\boldsymbol{n}}}_{ecl}\cdot\boldsymbol{h}\\ &+\frac{1}{2}\sin^2 i_m\boldsymbol{h}\cdot(\hat{\boldsymbol{n}}_{ecl}\widetilde{\hat{\boldsymbol{n}}}_{ecl}\cdot\boldsymbol{e} - \widetilde{\boldsymbol{e}}) - \cos^2 i_m\boldsymbol{h}\cdot\hat{\boldsymbol{n}}_{ecl}\widetilde{\hat{\boldsymbol{n}}}_{ecl}\cdot\boldsymbol{e} - 2\widetilde{\boldsymbol{h}}\cdot\boldsymbol{e}\Big]\end{aligned} \tag{3.50}$$

where $\hat{\boldsymbol{n}}_{ecl}$ is the normal to the ecliptic plane, and i_m is the inclination of the moon's orbit with respect to the ecliptic plane. These triply averaged equations may also be used for evaluating the effects of lunar gravitational perturbations $\dot{\boldsymbol{h}}_m$ and $\dot{\boldsymbol{e}}_m$. The form of these triply averaged secular equations for lunar gravity perturbation has not been presented before to the author's knowledge.

3.6.6 Secular Equations of Motion

The secular evolution of the Milankovitch orbital elements including the effects of J_2, SRP and lunisolar perturbations can hence be stated as

$$\dot{\boldsymbol{h}} = \dot{\boldsymbol{h}}_{SRP} + \dot{\boldsymbol{h}}_{20} + \dot{\boldsymbol{h}}_s + \dot{\boldsymbol{h}}_m \tag{3.51}$$

$$\dot{\boldsymbol{e}} = \dot{\boldsymbol{e}}_{SRP} + \dot{\boldsymbol{e}}_{20} + \dot{\boldsymbol{e}}_s + \dot{\boldsymbol{e}}_m \tag{3.52}$$

These equations cannot be solved analytically, however, they may be integrated numerically with the advantage of being hundreds of times faster to integrate than the full equations of motion. The SRP dynamics are given by Eqs. (3.27) and (3.28). The Earth oblateness dynamics are given by Eqs. (3.60) and (3.61). The lunisolar dynamics may be represented by either the singly averaged Eqs. (3.39) and (3.40), or by the doubly averaged Eqs. (3.62) and (3.63). The triply averaged equations for lunar motion (3.49) and (3.50) may also be used.

3.6.7 Averaged Position Vector from Averaged Milankovitch Elements

The position vector of the satellite is obtained from the averaged values of $\boldsymbol{e}$ and $\boldsymbol{h}$ to evaluate the SPS performance. The effects of the perturbations on the mean motion of the satellite may be accounted for by consideration of the averaged rate of change of the mean longitude of the orbiter, which is given by Rosengren and Scheeres:[49]

$$\dot{\bar{l}} = n_0 - \frac{\boldsymbol{h} + h\hat{\boldsymbol{n}}_p}{h + \hat{\boldsymbol{n}}_p \cdot \boldsymbol{h}} \cdot \left(\frac{\partial \overline{\mathcal{R}}^*}{\partial \boldsymbol{h}} \right)^T + \left(\frac{h}{1+h} \boldsymbol{e} + \frac{\hat{\boldsymbol{n}}_p \cdot \boldsymbol{e}}{h(h + \hat{\boldsymbol{n}}_p \cdot \boldsymbol{h})} \boldsymbol{h} \right) \cdot \left(\frac{\partial \overline{\mathcal{R}}^*}{\partial \boldsymbol{e}} \right)^T \tag{3.53}$$

where mean longitude $l = M + \Omega + \omega$. The partials of the scaled potentials are given by

$$\frac{\partial \overline{\mathcal{R}}^*}{\partial \boldsymbol{h}} = \frac{\partial \overline{\mathcal{R}}^*_{SRP}}{\partial \boldsymbol{h}} + \frac{\partial \overline{\mathcal{R}}^*_{20}}{\partial \boldsymbol{h}} + \frac{\partial \overline{\mathcal{R}}^*_{s}}{\partial \boldsymbol{h}} + \frac{\partial \overline{\mathcal{R}}^*_{m}}{\partial \boldsymbol{h}} \tag{3.54}$$

$$\frac{\partial \overline{\mathcal{R}}^*}{\partial \boldsymbol{e}} = \frac{\partial \overline{\mathcal{R}}^*_{SRP}}{\partial \boldsymbol{e}} + \frac{\partial \overline{\mathcal{R}}^*_{20}}{\partial \boldsymbol{e}} + \frac{\partial \overline{\mathcal{R}}^*_{s}}{\partial \boldsymbol{e}} + \frac{\partial \overline{\mathcal{R}}^*_{m}}{\partial \boldsymbol{e}} \tag{3.55}$$

The individual partials of the perturbation potentials are given in the Appendix A. Note that, for the doubly and triply averaged third-body models, the potentials must doubly and triply averaged, respectively. For example, if the doubly averaged luni-solar Eqs. (3.62) and (3.63) are used, then $\overline{\mathcal{R}}_p$ is replaced with $\overline{\overline{\mathcal{R}}}_p$ in the preceding Eqs. (3.54) and (3.55). Integrating Eq. (3.53) gives

$$l = (n_0 + \Delta n)t \tag{3.56}$$

where $n_0 = \sqrt{\mu / a_0^3}$ with a_0 the value of initial semimajor axis, which gives an average mean motion commensurate with the rotation rate of the Earth. This can be solved for by setting $\dot{\bar{l}} = 2\pi / P_{sidereal}$ in Eq. (3.53) and solving for a_0, where the partials given in the Appendix A are functions of a_0. The second and third terms in Eq. (3.53) are equal to Δn and t is the time since epoch. To proceed, the mean anomaly is

determined by

$$M = l - (\Omega + \omega) \tag{3.57}$$

where Ω and ω are obtained straightforwardly from $\boldsymbol{e}$ and $\boldsymbol{h}$. Assuming two-body motion, Kepler's equation is used to determine the true anomaly f. Then, the averaged position vector can be calculated from Scheeres ([50] pp. 357-359, Appendix A):

$$\bar{\boldsymbol{r}} = r\left[\cos f\hat{\boldsymbol{e}} + \sin f\hat{\boldsymbol{e}}_{\perp}\right] \tag{3.58}$$

where

$$r = \frac{a(1-e^2)}{1+e\cos f} \tag{3.59}$$

and $\hat{\boldsymbol{e}}$ is the unit vector in the direction of the periapsis from the Earth's centre, and $\hat{\boldsymbol{e}}_{\perp} = \widetilde{\hat{\boldsymbol{e}}} \cdot \hat{\boldsymbol{h}}$, where $\hat{\boldsymbol{h}}$ is the angular momentum unit vector. The averaged position vector $\bar{\boldsymbol{r}}$ is required to evaluate the performance of the SPS and whether or not it stays within range of the rectenna on the ground.

3.6.8 Linear Stability Analysis of GLP Solution

Allan and Cook[47] examined the Laplace plane and considered the lunisolar gravitation and Earth Oblateness and SRP perturbations. They also chose to consider a geosynchronous satellite. Tremaine[52] considered solar gravitation and planetary oblateness, not just for Earth but for other solar system planets with different planetary obliquities. He presented linear stability analysis of the classic case (solar gravitation and planetary oblateness).

Rosengren et al.[53] presented the equilibrium condition for the Laplace plane for lunar and solar gravitation, oblateness and SRP. Rosengren and Scheeres[54] reproduce the classic Laplace plane linear stability analysis of Tremaine[52] and also present linear stability analysis of what they call the modified Laplace plane which includes SRP.[54]

A linear stability analysis of the Laplace equilibrium solution is undertaken with

luni-solar gravitation, Earth oblateness and SRP. We derive the linearised equations of motion from which we obtain the eigenvalue equations. We are primarily interested in the equilibrium solution at geosynchronous altitude for our SPS application.

Equilibrium Conditions

The perturbation equations for third body gravitation, planetary oblateness and SRP are restated here for convenience:

Planetary Oblateness – Singly Averaged

$$\dot{\boldsymbol{h}}_{20} = \frac{3nC_{20}}{2a^2h^5}(\hat{\boldsymbol{p}}\cdot\boldsymbol{h})\widetilde{\hat{\boldsymbol{p}}}\cdot\boldsymbol{h} \tag{3.60}$$

$$\dot{\boldsymbol{e}}_{20} = \frac{3nC_{20}}{4a^2h^5}\left\{\left[1-\frac{5}{h^2}(\hat{\boldsymbol{p}}\cdot\boldsymbol{h})^2\right]\widetilde{\boldsymbol{h}}+2(\hat{\boldsymbol{p}}\cdot\boldsymbol{h})\widetilde{\hat{\boldsymbol{p}}}\right\}\cdot\boldsymbol{e} \tag{3.61}$$

Third Body Gravitation – Doubly Averaged

$$\dot{\bar{\boldsymbol{h}}}_p = -\frac{3\mu_p}{4na_p^3h_p^3}\hat{\boldsymbol{H}}_p\cdot(5\boldsymbol{ee}-\boldsymbol{hh})\cdot\widetilde{\hat{\boldsymbol{H}}}_p \tag{3.62}$$

$$\dot{\bar{\boldsymbol{e}}}_p = -\frac{3\mu_p}{4na_p^3h_p^3}\left[\hat{\boldsymbol{H}}_p\cdot(5\boldsymbol{eh}-\boldsymbol{he})\cdot\widetilde{\hat{\boldsymbol{H}}}_p-2\widetilde{\boldsymbol{h}}\cdot\boldsymbol{e}\right] \tag{3.63}$$

where $\hat{\boldsymbol{H}}_p$ is the perturbing bodies angular momentum unit vector.

Solar Radiation Pressure – Alternative Form

The following form is given by Rosengren and Scheeres:[54]

$$\dot{\boldsymbol{h}}_{srp} = -\frac{2\pi(1-\cos\Lambda)}{T_s\cos\Lambda}\widetilde{\hat{\boldsymbol{H}}}_s\cdot\boldsymbol{h} \tag{3.64}$$

$$\dot{\boldsymbol{e}}_{srp} = -\frac{2\pi(1-\cos\Lambda)}{T_s\cos\Lambda}\widetilde{\hat{\boldsymbol{H}}}_s\cdot\boldsymbol{e} \tag{3.65}$$

where:

$$\begin{aligned}\tan\Lambda &= \frac{3\gamma}{2v_{lc}H_s}\\ \gamma &= (1+\rho)(A/m)P_\Phi\\ H_s &= \sqrt{\mu_s a_s(1-e_s^2)}\end{aligned} \tag{3.66}$$

The following terms were not previously defined:

$$\begin{aligned}T_s &: \text{Period of the planet's orbit around the Sun}\\ v_{lc} &: \text{Local circular speed of the object about the planet.}\\ H_s &: \text{Specific angular momentum of the planet about the Sun.}\end{aligned} \tag{3.67}$$

The combined secular equations of orbit angular momentum and eccentricity, including luni-solar tide, earth oblateness and SRP are then:

$$\begin{aligned}\dot{\boldsymbol{h}} = {}& \frac{3nC_{20}}{2a^2h^5}(\hat{\boldsymbol{p}}\cdot\boldsymbol{h})\widetilde{\hat{\boldsymbol{p}}}\cdot\boldsymbol{h} - \frac{3\mu_p}{4na_s^3h_s^3}\hat{\boldsymbol{H}}_s\cdot(5\boldsymbol{ee}-\boldsymbol{hh})\cdot\widetilde{\hat{\boldsymbol{H}}}_s\\ &- \frac{3\mu_m}{4na_m^3h_m^3}\hat{\boldsymbol{H}}_m\cdot(5\boldsymbol{ee}-\boldsymbol{hh})\cdot\widetilde{\hat{\boldsymbol{H}}}_m - \frac{2\pi(1-\cos\Lambda)}{T_s\cos\Lambda}\widetilde{\hat{\boldsymbol{H}}}_s\cdot\boldsymbol{h}\end{aligned} \tag{3.68}$$

$$\begin{aligned}\dot{\boldsymbol{e}} = {}& \frac{3nC_{20}}{4a^2h^5}\left\{\left[1-\frac{5}{h^2}(\hat{\boldsymbol{p}}\cdot\boldsymbol{h})^2\right]\widetilde{\boldsymbol{h}} + 2(\hat{\boldsymbol{p}}\cdot\boldsymbol{h})\widetilde{\hat{\boldsymbol{p}}}\right\}\cdot\boldsymbol{e} - \frac{3\mu_s}{4na_s^3h_s^3}\left[\hat{\boldsymbol{H}}_s\cdot(5\boldsymbol{eh}-\boldsymbol{he})\cdot\widetilde{\hat{\boldsymbol{H}}}_s - 2\widetilde{\boldsymbol{h}}\cdot\boldsymbol{e}\right]\\ &- \frac{3\mu_m}{4na_m^3h_m^3}\left[\hat{\boldsymbol{H}}_m\cdot(5\boldsymbol{eh}-\boldsymbol{he})\cdot\widetilde{\hat{\boldsymbol{H}}}_m - 2\widetilde{\boldsymbol{h}}\cdot\boldsymbol{e}\right] - \frac{2\pi(1-\cos\Lambda)}{T_s\cos\Lambda}\widetilde{\hat{\boldsymbol{H}}}_s\cdot\boldsymbol{e}\end{aligned} \tag{3.69}$$

Similarly to Allan and Cook,[47] we make the simplifying assumption that over long periods $\hat{\boldsymbol{H}}_m = \hat{\boldsymbol{H}}_s$. This is a reasonable assumption as the precession of the moon's

orbit pole completes one period every 18.6 years and is only 5 degrees from the ecliptic. We also consider only circular orbits. To make the following derivations more readable, we define the perturbation constants:

$$\omega_2 = \frac{3nJ_2R_E^2}{2a^2} \tag{3.70}$$

$$\omega_p = \frac{3\mu_p}{4na_p^3h_p^3} \tag{3.71}$$

$$\omega_{srp} = \frac{2\pi(1-\cos\Lambda)}{T_s\cos\Lambda} \tag{3.72}$$

The final form of the equations of motion we wish to linearise are:

$$\dot{\hat{\boldsymbol{h}}} = \omega_2(\hat{\boldsymbol{p}}\cdot\hat{\boldsymbol{h}})\widetilde{\hat{\boldsymbol{p}}}\cdot\hat{\boldsymbol{h}} - (\omega_m+\omega_s)\hat{\boldsymbol{H}}_s\cdot(5\boldsymbol{e}\boldsymbol{e}-\hat{\boldsymbol{h}}\hat{\boldsymbol{h}})\cdot\widetilde{\hat{\boldsymbol{H}}}_s - \omega_{srp}\widetilde{\hat{\boldsymbol{H}}}_s\cdot\hat{\boldsymbol{h}} \tag{3.73}$$

$$\begin{aligned}\dot{\boldsymbol{e}} = {}& \omega_2\left\{\left[1-5(\hat{\boldsymbol{p}}\cdot\hat{\boldsymbol{h}})^2\right]\widetilde{\hat{\boldsymbol{h}}} + 2(\hat{\boldsymbol{p}}\cdot\hat{\boldsymbol{h}})\widetilde{\hat{\boldsymbol{p}}}\right\}\cdot\boldsymbol{e} \\ & - (\omega_s+\omega_m)\left\{\hat{\boldsymbol{H}}_s\cdot(5\boldsymbol{e}\hat{\boldsymbol{h}}-\hat{\boldsymbol{h}}\boldsymbol{e})\cdot\widetilde{\hat{\boldsymbol{H}}}_s - 2\widetilde{\hat{\boldsymbol{h}}}\cdot\boldsymbol{e}\right\} \\ & - \omega_{srp}\widetilde{\hat{\boldsymbol{H}}}_s\cdot\boldsymbol{e}\end{aligned} \tag{3.74}$$

Note, $h=\sqrt{1-e^2}$, and $\boldsymbol{h}=h\hat{\boldsymbol{h}}$, so for circular orbits $h=\sqrt{1-e^2}=1$ and $\hat{\boldsymbol{h}}=\boldsymbol{h}$. The first thing to note is that the equation for $\dot{\boldsymbol{e}}$ is trivially solved for $\boldsymbol{e}=\boldsymbol{0}$ (with our choice of circular orbits). The condition for equilibrium may then be straightforwardly derived from Eq. (3.73) (substituting in $\boldsymbol{e}=\dot{\hat{\boldsymbol{h}}}=0$):

$$\omega_2(\hat{\boldsymbol{p}}\cdot\hat{\boldsymbol{h}})\widetilde{\hat{\boldsymbol{p}}}\cdot\hat{\boldsymbol{h}} + (\omega_s+\omega_m)(\hat{\boldsymbol{H}}_s\cdot\hat{\boldsymbol{h}})\widetilde{\hat{\boldsymbol{H}}}_s\cdot\hat{\boldsymbol{h}} - \omega_{srp}\widetilde{\hat{\boldsymbol{H}}}_s = 0 \tag{3.75}$$

The angular momentum unit vector $\hat{\boldsymbol{h}}$ may be rewritten in terms of the planet obliquity ϵ and the Laplace angle ϕ as:

$$\hat{\boldsymbol{h}} = \frac{1}{\sin\epsilon}\left[\sin(\epsilon-\phi)\hat{\boldsymbol{p}} + \sin\phi\hat{\boldsymbol{H}}_s\right] \tag{3.76}$$

Realising that the vector $\widetilde{\hat{\boldsymbol{p}}} \cdot \hat{\boldsymbol{h}}$ is opposite in direction to vector $\widetilde{\hat{\boldsymbol{H}}}_s \cdot \hat{\boldsymbol{h}}$ in Eq. (3.75) and substituting in Eq. (3.76) into Eq. (3.75) (with the aim of obtaining a scalar expression) gives:

$$\begin{aligned}
&\omega_2 \hat{\boldsymbol{p}} \cdot \left\{ \frac{1}{\sin\epsilon} \left[\sin(\epsilon - \phi)\hat{\boldsymbol{p}} + \sin\phi \hat{\boldsymbol{H}}_s \right] \right\} \widetilde{\hat{\boldsymbol{p}}} \cdot \left\{ \frac{1}{\sin\epsilon} \left[\sin(\epsilon - \phi)\hat{\boldsymbol{p}} + \sin\phi \hat{\boldsymbol{H}}_s \right] \right\} \\
&+ (\omega_s + \omega_m) \hat{\boldsymbol{H}}_s \cdot \left\{ \frac{1}{\sin\epsilon} \left[\sin(\epsilon - \phi)\hat{\boldsymbol{p}} + \sin\phi \hat{\boldsymbol{H}}_s \right] \right\} \widetilde{\hat{\boldsymbol{H}}}_s \cdot \left\{ \frac{1}{\sin\epsilon} \left[\sin(\epsilon - \phi)\hat{\boldsymbol{p}} + \sin\phi \hat{\boldsymbol{H}}_s \right] \right\} \\
&- \omega_{srp} \widetilde{\hat{\boldsymbol{H}}}_s \cdot \{ \frac{1}{\sin\epsilon} \left[\sin(\epsilon - \phi)\hat{\boldsymbol{p}} + \sin\phi \hat{\boldsymbol{H}}_s \right\} = 0
\end{aligned} \tag{3.77}$$

The following results are used:

$$\begin{aligned}
\hat{\boldsymbol{p}} \cdot \hat{\boldsymbol{p}} &= \hat{\boldsymbol{H}}_s \cdot \hat{\boldsymbol{H}}_s = 1 \\
\hat{\boldsymbol{p}} \cdot \hat{\boldsymbol{H}}_s &= \hat{\boldsymbol{H}}_s \cdot \hat{\boldsymbol{p}} = \cos\epsilon \\
\widetilde{\hat{\boldsymbol{p}}} \cdot \hat{\boldsymbol{p}} &= \widetilde{\hat{\boldsymbol{H}}}_s \cdot \hat{\boldsymbol{H}}_s = \boldsymbol{0} \\
\widetilde{\hat{\boldsymbol{p}}} \cdot \hat{\boldsymbol{H}}_s &= -\widetilde{\hat{\boldsymbol{H}}}_s \cdot \hat{\boldsymbol{p}} = \sin\epsilon \hat{\boldsymbol{n}}_{(\hat{p} \times \hat{H}_s)} = -\sin\epsilon \hat{\boldsymbol{n}}_{(\hat{H}_s \times \hat{p})}
\end{aligned} \tag{3.78}$$

Using trigonometric identities and some algebraic manipulation, the equilibrium condition can be rewritten in the following simple scalar form:

$$\omega_2 \sin 2\phi + (\omega_s + \omega_m) \sin 2(\phi - \epsilon) + 2\omega_{srp} \sin(\phi - \epsilon) = 0 \tag{3.79}$$

This agrees with the condition derived by Rosengren.[53] For the geosynchronous SPS case we have $a = 42164.169$km (where a determines the values of ω_2, ω_s, and ω_m). We are only interested in Earth orbiting satellites, therefore the Earth obliquity $\epsilon = 23.4^\circ$ is substituted in. Thus, Eq. (3.79) can be solved for the Laplace plane inclination with respect to the Earth's equator, angle ϕ. To illustrate the affect of the various perturbations on the value of the Laplace inclination, Table 3.3 shows the equilibrium conditions with different perturbations included and the corresponding values of ϕ.

Table 3.3: Equilibrium solutions. Three values of Laplace inclination are given for cases which include SRP as this is the distinguishing property for the SPS orbit dynamics. The examples without SRP are the same for all the different SPS designs.

Perturbations	Equilibrium Condition	Laplace Incl. ϕ (°)
J_2 + Solar Tide	$\omega_2 \sin 2\phi + \omega_s \sin 2(\phi - \epsilon) = 0$	2.84
J_2 + Solar Tide + Lunar Tide	$\omega_2 \sin 2\phi + (\omega_s + \omega_m) \sin 2(\phi - \epsilon) = 0$	7.38
		Cylindrical/Abacus/ISC
J_2 + Solar Tide + SRP	$\omega_2 \sin 2\phi + \omega_s \sin 2(\phi - \epsilon) + 2\ \omega_{srp} \sin(\phi - \epsilon) = 0$	2.85,2.87,3.08
J_2 + Solar Tide + Lunar Tide + SRP	$\omega_2 \sin 2\phi + (\omega_s + \omega_m) \sin 2(\phi - \epsilon) + 2\ \omega_{srp} \sin(\phi - \epsilon) = 0$	7.39,7.40,7.54

In all cases shown in Table 3.3 both solar tide and Earth oblateness are included, as these are the two contributors to the Classical Laplace plane, i.e. the two conflicting forces which create a stable plane. The lunar tide and SRP perturbations are also included. It is clear that the lunar tide has a much more significant impact on the inclination of the stable plane. Also included are values of ϕ for different SPS designs. These are only relevant when the SRP perturbation is included and the different Λ of these designs result in slightly different values of ϕ.

Stability of the Equilibrium Solution

We are interested in the stability of this equilibrium solution, specifically if it is stable to variations in orientation ($\hat{\boldsymbol{h}}$) and spatial variation in the orbit ($\boldsymbol{e}$). We will only consider the case of all the perturbations (the last row in Table 3.3). Rosengren[54] and Allan and Cook[?] can be consulted for further details of the classic Laplace plane solution (i.e. J_2+ solar tide).

In order to study the stability of this equilibrium solution we need to linearise the equations of motion (Eq.s (3.73) and (3.74)) and find the characteristic polynomial. Substituting $\hat{\boldsymbol{h}} = \hat{\boldsymbol{h}}_{eq} + \delta\boldsymbol{h}$ and $\boldsymbol{e} = \delta\boldsymbol{e}$ into Eq.s (3.73) and (3.74), where $\boldsymbol{h}_{eq}$ is the

equilibrium $\boldsymbol{h}$ and δ implies a small variation, and expanding to first order in $\delta\boldsymbol{h}$ and $\delta\boldsymbol{e}$ gives the linearised equations of motion:

$$\dot{\delta\boldsymbol{h}} = \left[\frac{\partial(\dot{\boldsymbol{h}_{eq}} + \delta\boldsymbol{h})}{\partial(\delta\boldsymbol{h})}\right] \cdot \delta\boldsymbol{h} = [\boldsymbol{A}_h] \cdot \delta\boldsymbol{h} \tag{3.80}$$

$$\dot{\delta\boldsymbol{e}} = \left[\frac{\partial(\delta\dot{\boldsymbol{e}})}{\partial(\delta\boldsymbol{e})}\right] \cdot \delta\boldsymbol{e} = [\boldsymbol{A}_e] \cdot \delta\boldsymbol{e} \tag{3.81}$$

where:

$$\frac{\mathrm{d}}{\mathrm{d}t}(\boldsymbol{h}_{eq} + \delta\boldsymbol{h}) = \dot{\delta\boldsymbol{h}} \tag{3.82}$$

(since by definition $\dot{\boldsymbol{h}}_{eq} = 0$). The derivatives are carried out and higher order terms ignored to give the linearised equations of motion:

$$\begin{aligned}\dot{\delta\boldsymbol{h}} = &\left\{\omega_2\left[\widetilde{\hat{\boldsymbol{h}}}_{eq} \cdot \hat{\boldsymbol{p}}\hat{\boldsymbol{p}} - (\hat{\boldsymbol{p}} \cdot \hat{\boldsymbol{h}}_{eq})\widetilde{\hat{\boldsymbol{p}}}\right]\right. && (3.83)\\ &+(\omega_s + \omega_m)\left[\widetilde{\hat{\boldsymbol{h}}}_{eq} \cdot \hat{\boldsymbol{H}}_s\hat{\boldsymbol{H}}_s - (\hat{\boldsymbol{H}}_s \cdot \hat{\boldsymbol{h}}_{eq})\widetilde{\hat{\boldsymbol{H}}}_s\right]\\ &\left.-\omega_{srp}\widetilde{\hat{\boldsymbol{H}}}_s\right\} \cdot \delta\boldsymbol{h} && (3.84)\\ &= [\boldsymbol{A}_h] \cdot \delta\boldsymbol{h}\end{aligned}$$

$$\begin{aligned}\dot{\delta\boldsymbol{e}} = &\left\{-\frac{\omega_2}{2}\left[(1 - 5(\hat{\boldsymbol{p}} \cdot \hat{\boldsymbol{h}}_{eq})^2)\widetilde{\hat{\boldsymbol{h}}}_{eq} + 2(\hat{\boldsymbol{p}} \cdot \hat{\boldsymbol{h}}_{eq})\widetilde{\hat{\boldsymbol{p}}}\right]\right.\\ &-(\omega_s + \omega_m)\left[5\widetilde{\hat{\boldsymbol{h}}}_{eq} \cdot \hat{\boldsymbol{H}}_s\hat{\boldsymbol{H}}_s + (\hat{\boldsymbol{H}}_s \cdot \hat{\boldsymbol{h}}_{eq})\widetilde{\hat{\boldsymbol{H}}}_s - 2\widetilde{\hat{\boldsymbol{h}}}_{eq}\right]\\ &\left.-\omega_{srp}\widetilde{\hat{\boldsymbol{H}}}_s\right\} \cdot \delta\boldsymbol{e} && (3.85)\\ &= [\boldsymbol{A}_e] \cdot \delta\boldsymbol{e}\end{aligned}$$

The linearised equation for the evolution of $\boldsymbol{h}$ is independent of the linearised evolution of $\boldsymbol{e}$. We can find the characteristic polynomials for $[\boldsymbol{A}_h]$ and $[\boldsymbol{A}_e]$. First we rewrite

$[\boldsymbol{A}_h]$ and $[\boldsymbol{A}_e]$ in terms of the angles ϕ, ϵ and substitute in Eq. (3.76):

$$\begin{aligned}[\boldsymbol{A}_h] &= \omega_2(\widetilde{\hat{\boldsymbol{h}}}_{eq} \cdot \hat{\boldsymbol{p}}\hat{\boldsymbol{p}} - \cos\phi\widetilde{\hat{\boldsymbol{p}}}) \\ &+ (\omega_s + \omega_m)(\widetilde{\hat{\boldsymbol{h}}}_{eq} \cdot \hat{\boldsymbol{H}}_s\hat{\boldsymbol{H}}_s - \cos(\epsilon - \phi)\widetilde{\hat{\boldsymbol{H}}}_s) \\ &- \omega_{srp}\widetilde{\hat{\boldsymbol{H}}}_s\end{aligned} \tag{3.86}$$

$$\begin{aligned}[\boldsymbol{A}_e] &= -\frac{\omega_2}{2}\left[(1 - 5(\hat{\boldsymbol{p}} \cdot \hat{\boldsymbol{h}}_{eq})^2)\widetilde{\hat{\boldsymbol{h}}}_{eq} + 2(\hat{\boldsymbol{p}} \cdot \hat{\boldsymbol{h}}_{eq})\widetilde{\hat{\boldsymbol{p}}}\right] \\ &-(\omega_s + \omega_m)\left[5\widetilde{\hat{\boldsymbol{h}}}_{eq} \cdot \hat{\boldsymbol{H}}_s\hat{\boldsymbol{H}}_s + (\hat{\boldsymbol{H}}_s \cdot \hat{\boldsymbol{h}}_{eq})\widetilde{\hat{\boldsymbol{H}}}_s - 2\widetilde{\hat{\boldsymbol{h}}}_{eq}\right] \\ &-\omega_{srp}\widetilde{\hat{\boldsymbol{H}}}_s\end{aligned} \tag{3.87}$$

The characteristic equations including the affects of Earth oblateness, lunisolar gravity, and SRP are derived using symbolic toolbox in MATLAB:

$$\begin{aligned}\lambda_h^2 &= -\omega_{srp}^2 - \omega_2^2\cos^2\phi - \omega_s^2\cos^2(\epsilon - \phi) - \omega_m^2\cos^2(\epsilon - \phi) \\ &- \frac{\omega_2\omega_s}{2}[\cos 2\phi + \cos 2(\epsilon - \phi) + 2\cos 2\epsilon] \\ &- \frac{\omega_2\omega_m}{2}[\cos 2\phi + \cos 2(\epsilon - \phi) + 2\cos 2\epsilon] \\ &- \frac{\omega_2\omega_{srp}}{2}[\cos(\epsilon - \phi) + 3\cos(\epsilon + \phi)] \\ &- 2\omega_s\omega_{srp}\cos(\epsilon - \phi) - 2\omega_m\omega_{srp}\cos(\epsilon - \phi) \\ &- 2\omega_s\omega_m\cos^2(\epsilon - \phi)\end{aligned} \tag{3.88}$$

(3.89)

$$
\begin{aligned}
\lambda_e^2 = & -\frac{\omega_2^2}{4}\left[5\cos^4\phi - 2\cos^2\phi + 1\right] \\
& - \frac{\omega_s^2}{2}\left[7\cos 2(\epsilon-\phi) - 5\right] \\
& - \frac{\omega_m^2}{2}\left[7\cos 2(\epsilon-\phi) - 5\right] \\
& - \frac{\omega_2\omega_s}{16}\left[2 + 3\cos(2\epsilon) + 6\cos(2\phi) + 6\cos 2(\epsilon-\phi) + 15\cos 2(\epsilon-2\phi)\right] \\
& - \frac{\omega_2\omega_m}{16}\left[2 + 3\cos(2\epsilon) + 6\cos(2\phi) + 6\cos 2(\epsilon-\phi) + 15\cos 2(\epsilon-2\phi)\right] \\
& - \omega_{srp}^2 + \frac{\omega_2\omega_{srp}}{4}\left[2\cos(\epsilon-\phi) + \cos(\epsilon+\phi) + 5\cos(\epsilon-3\phi)\right] \\
& + 2\omega_s\omega_{srp}\cos(\epsilon-\phi) + 2\omega_m\omega_{srp}\cos(\epsilon-\phi) \\
& + 2\omega_s\omega_m\cos^2(\epsilon-\phi)
\end{aligned}
\tag{3.90}
$$

The characteristic equations (Eq. (3.88) and (3.90)) are evaluated for the following range of obliquity ($0 < \epsilon < \pi/2$) and Laplace plane inclination ($0 < \phi < \pi$). $\lambda_h^2 < 0$ indicates linear stability with respect to variations in the orbit's orientation. $\lambda_e^2 < 0$ indicates linear stability with respect to variations in the orbit's shape.

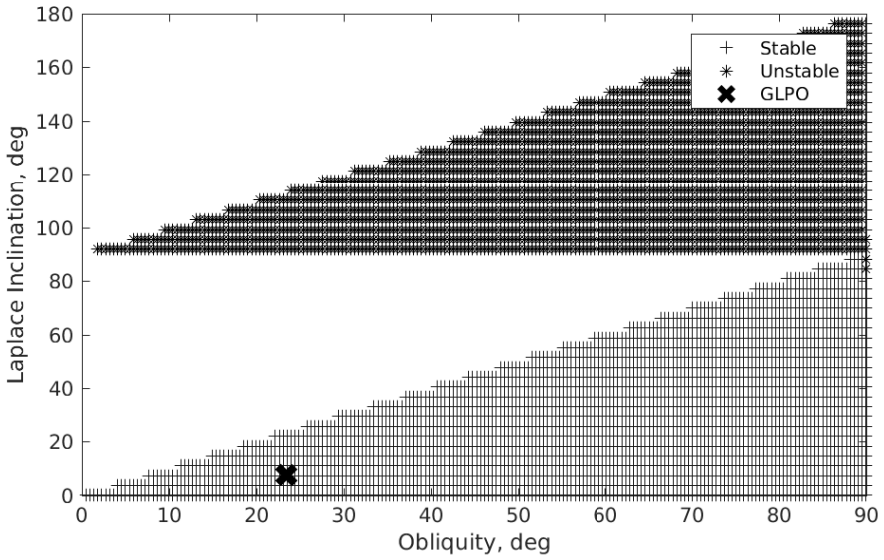

Figure 3.5: The stability and instability domains with respect to angular momentum for the classical and orthogonal Laplace equilibria with oblateness, SRP and luni-solar gravitational perturbations. Every point is a solution to the equilibrium condition. The stable points are where $\lambda_h^2 < 0$, unstable are where $\lambda_h^2 > 0$.

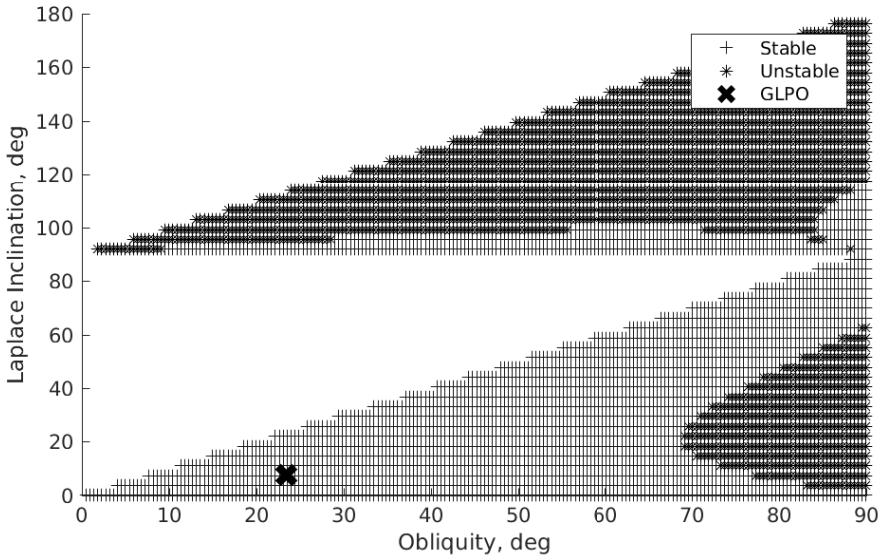

Figure 3.6: The stability and instability domains with respect to eccentricity for the classical and orthogonal Laplace equilibria with oblateness, SRP and luni-solar gravitational perturbations. Every point is a solution to the equilibrium condition. The stable points are where $\lambda_e^2 < 0$, unstable are where $\lambda_e^2 > 0$.

Fig.s 3.5 and 3.6 both illustrate stability regions. They both show the position on the stability plot of the GLPO solution. The stability plots show the full range of obliquities, however, we are only interested in Earth obliquity. The warped Laplace surface in the range $\phi = 0 \rightarrow \epsilon$ is stable. The addition of the lunar gravity has the affect of strengthening the out of plane pull of the Sun (i.e. since we consider $\hat{\boldsymbol{H}}_s = \hat{\boldsymbol{H}}_m$). This means that at a particular altitude, the Laplace inclination will be generally larger than the classic result (see Table 3.3).

We can conclude that the geosynchronous Laplace Plane SPS is stable to both variations in orientation and shape, see cross marker at $\epsilon = 23.4^\circ$ and $\phi = 7.3^\circ$. This is confirmed by the numeric simulations. Although not included in the linear stability analysis, the perturbation due to the microwave beam and the Earth tesseral harmonic J_{22} does not appear to affect the stability of the solution when it is added to the numerical integration.

3.6.9 Initial Conditions for GLPO Solution

To achieve the desired rate of change of mean longitude $\dot{\bar{l}}$, the correct initial value of semimajor axis must be obtained. In the case where initial inclination of $i_0 = 7.5^\circ$ is chosen, a long period oscillation in inclination and ascending node is observed with of approximately $\Delta i = \pm 1.25^\circ$ and $\Delta\Omega = \pm 10^\circ$ about the stable Laplace plane, as found in earlier work.[55] These deviations from the stable Laplace plane, which are caused by the regression of the lunar nodes, can be reduced by choosing the initial orbit plane orientation to be in phase with the nodal precession. Using the empirical method of Friesen et al.,[56] the initial orbit plane orientation for GLPO is found:

$$i_0 = 7.91^\circ \qquad \boldsymbol{h}_0 = \sqrt{1 - e_0^2}\begin{bmatrix} \sin i_0 \sin\Omega_0 & -\sin i_0 \cos\Omega_0 & \cos\Omega_0 \end{bmatrix}$$

$$\Omega_0 = 2.66^\circ \qquad \boldsymbol{e}_0 = \begin{bmatrix} 0 & 0 & 0 \end{bmatrix}$$

3.7 Evaluation of SPS Performance

The results of the long-term orbit propagation may be used to evaluate how an SPS in such an orbit would perform. To achieve this, some SPS performance metrics are defined. First, the distance between the transmitting antenna and rectenna x is evaluated. Variation in this distance causes a fluctuation in the beam coupling efficiency η_t:[20]

$$\eta_t \backsim 1 - \exp(-\tau^2) \tag{3.91}$$

where

$$\tau = \frac{\pi D_T D_R}{4\lambda_\mu x} \tag{3.92}$$

where D_T and D_R are the diameters of the transmitting antenna and rectenna, respectively (illustrated in Fig. 3.2), and λ_μ is the wavelength of beamed radiation. The power received by the ground station can then be calculated according to

$$P_r = P_t \eta_t \cos^2 \alpha \tag{3.93}$$

where P_t is the power transmitted, as given in Table 3.1, η_t is given by Eq. (3.91), and α is the incident angle of the beamed radiation, which can be evaluated knowing the ground station position vector and averaged SPS position vector $\bar{\boldsymbol{r}}$. The off-axis beaming angle β, required to aim the beam at the rectenna, is also evaluated. The limit for the reference antenna chosen was $\beta \leq \pm 3^\circ$.[42]

3.8 Long-Term Orbit Propagation

The results of the long-term SPS orbit propagation for a GLPO and an uncontrolled initially GEO (U-GEO) are presented in Fig. 3.7. U-GEO is considered to understand the long-term natural evolution of an SPS orbit starting in GEO. The implications of the perturbation effects on the orbits for the delivery of power to a single equatorial

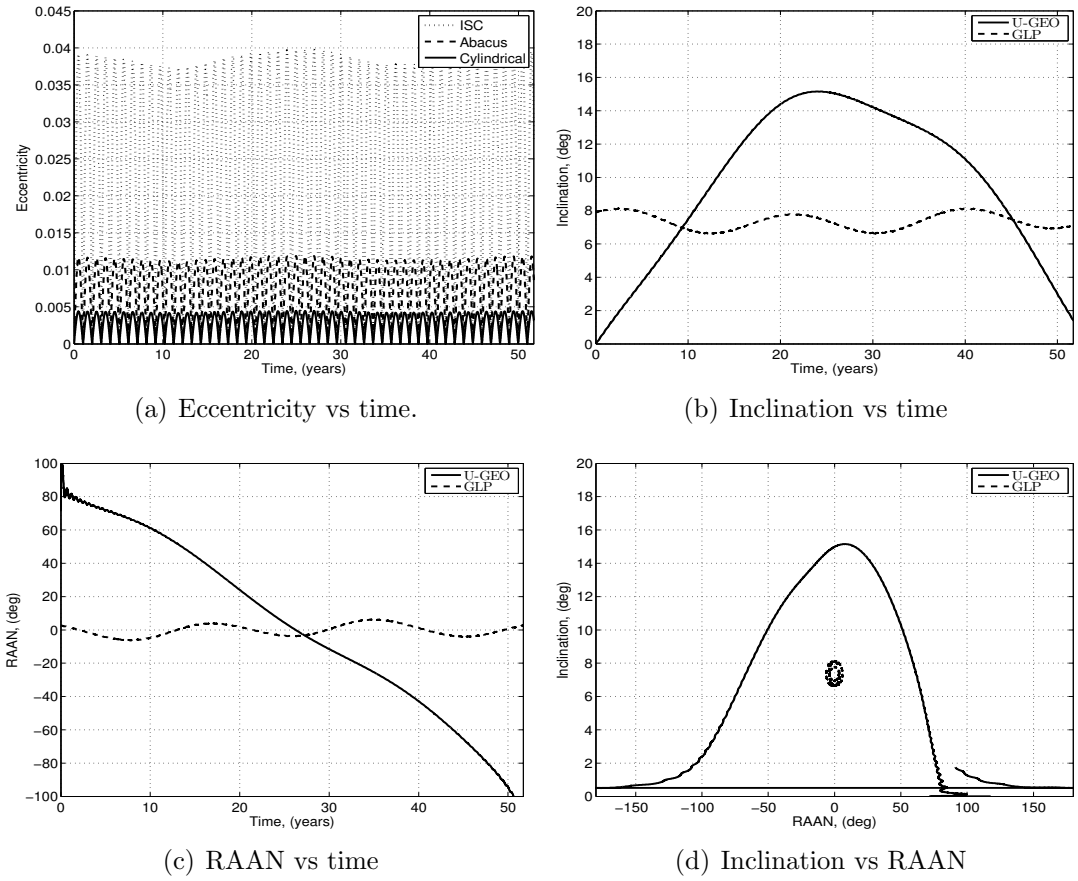

(a) Eccentricity vs time.

(b) Inclination vs time

(c) RAAN vs time

(d) Inclination vs RAAN

Figure 3.7: Long-term orbital element variation.

ground rectenna are assessed. The daily and the long-term evolution of SPS performance parameters for GLPO are given by Fig. 3.8 and 3.9, respectively. The long-term evolution of SPS performance parameters for U-GEO are also given in Fig. 3.10. The case of a fully controlled SPS in GEO (C-GEO) is also considered. Unless otherwise stated, the Abacus SPS has been studied, due to it having the intermediate value of Λ and being most accurately described by the cannonball SRP model (due to its geometry). The singly averaged model is used for all perturbations as this was found to agree well with the numerical integration of the nonaveraged equations of motion (see Appendix B for direct comparison between models).

3.8.1 Eccentricity, *e*

1. *Geosynchronous Laplace Plane Orbit*

The three SPS designs, shown in Fig. 3.1, share similar orbital behavior. The main difference is in their eccentricity evolution due to their different Λ values, defined in Eq. (3.6) and shown in Table 3.2. The effect of solar radiation pressure depends upon Λ. The larger the value of Λ, the greater the amplitude of yearly eccentricity variation (see Fig. 3.7(a)). The other perturbation effects cause minor variations in the amplitude of the yearly eccentricity oscillation.

2. *Uncontrolled Initially GEO*

No significant difference in this behavior is observed between the U-GEO and GLPO cases.

3.8.2 Inclination, *i*

1. *Geosynchronous Laplace Plane Orbit*

The long-term inclination evolution is shown in Fig. 3.7(b). When the initial inclination is chosen to be close to the Laplace plane inclination for the chosen altitude, it is stable and oscillates with a period of 18.6 years due to the moon's nodal motion. The lunar orbital plane is not fixed in the ecliptic plane, but is itself regressing around the pole of the ecliptic with the so-called Saros period of 18.6 years.

2. *Uncontrolled Initially GEO*

The inclination immediately begins to increase and shows long-term periodic motion with period 52.86 years, reaching a maximum after approximately 26 years, then decreasing again. This oscillation is due to the lunisolar gravitational perturbations and agrees well with the results of Allan and Cook,[47] who found the period for inclination variation for a geosynchronous orbiter to be 52.9 years. When started in GEO, the plane of the satellite's orbit is at the obliquity angle (23.4°) to the ecliptic plane. The moon and the sun orbits are not in the same plane, hence their gravity pulls the

satellite out of its initial orbital plane. The stable Laplace plane inclination at geosynchronous altitude is approximately $7.5°$, therefore, when not started at or near to this inclination, the inclination will oscillate around $7.5°$, which explains the maximum value of $15°$. The rate of inclination growth for the first 20 years is approximately $\Delta i = 0.7°$/year.

3.8.3 Right Ascension of the Ascending Node (RAAN), Ω

1. *Geosynchronous Laplace Plane Orbit*

The node oscillates around $0°$ with small amplitude. Again, the period is equal to the Saros period (18.6 years) because this is caused by the nodal motion of the moon. The stable Laplace Plane solution is at $\Omega = 0°$ for all altitudes as this is where the ecliptic, Laplace, and equatorial planes intersect. The stability of the solution in RAAN-inclination space can be seen in Fig. 3.7(d).

2. *Uncontrolled Initially GEO*

The node of the spacecraft regresses due to the combined effects of J_2 and lunisolar perturbations (see Fig. 3.7(c)).

3.9 SPS Performance

3.9.1 Incident Angle of Beamed Radiation, α

1. *Geosynchronous Laplace Plane Orbit*

The motion of the satellite relative to the ground station causes a variation in the absolute value of the incident angle of the beamed power α, as defined in Fig. 3.2. Initially, α varies between $0°$ and $9°$ twice daily as shown in Fig. 3.8. The long-term variation in α for the GLPO is shown in Fig. 3.9. The maximum value of $\alpha = 18°$ is reached after ~ 30 years and is due to the SPS drifting East in longitude by approximately $20°$. In the first $\sim$25 years, the maximum value is $\alpha \sim 10°$.

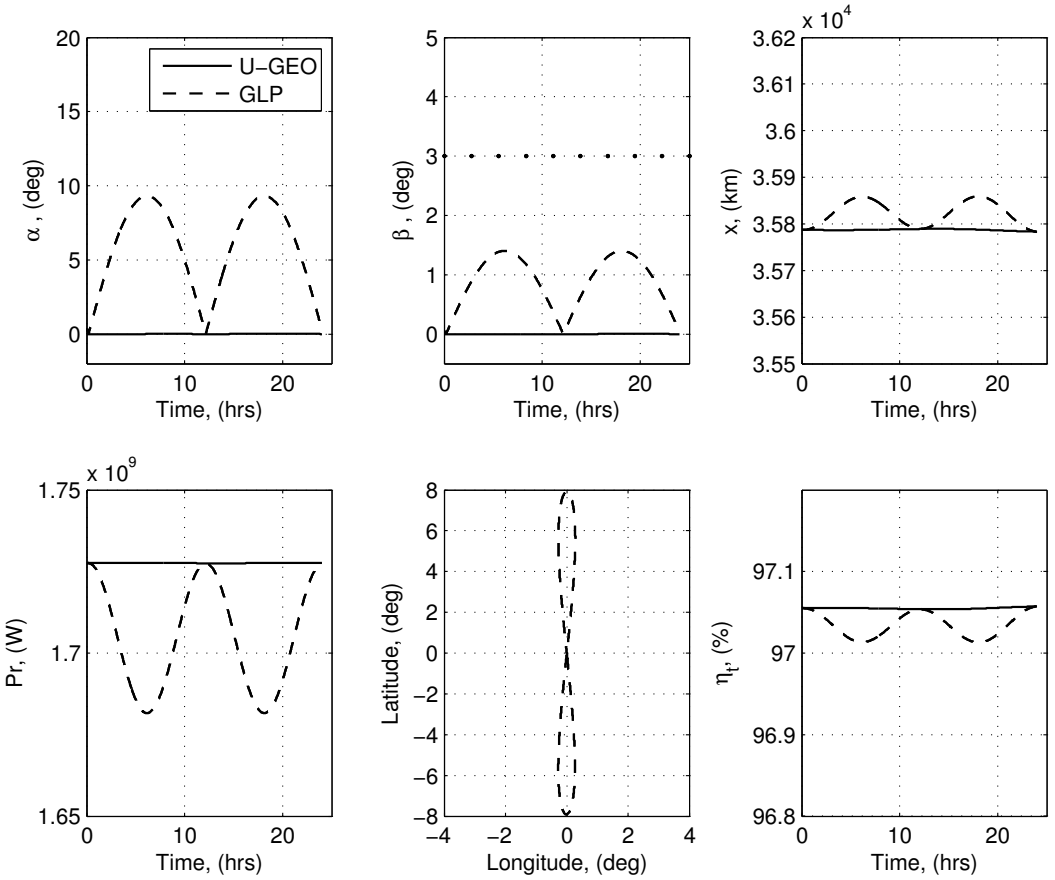

Figure 3.8: Variation of Abacus SPS performance related parameters over one day.

2. *Uncontrolled Initially GEO*

Initially, as shown in Fig. 3.8, $\alpha = 0^\circ$ when the SPS is still in the equatorial plane. The long-term variation in α is shown in Fig. 3.10. In this case, the maximum value of $\alpha = 21^\circ$ is reached after approximately 26 years. This coincides with the maximum inclination.

3.9.2 Off-Axis Beaming Angle, β

1. *Geosynchronous Laplace Plane Orbit*

To continuously beam power, the off-axis beaming angle β must not exceed 3°. This limit is indicated in all plots of β as a dotted line. The GLPO satisfies this constraint over a long period of time (see Fig. 3.9).

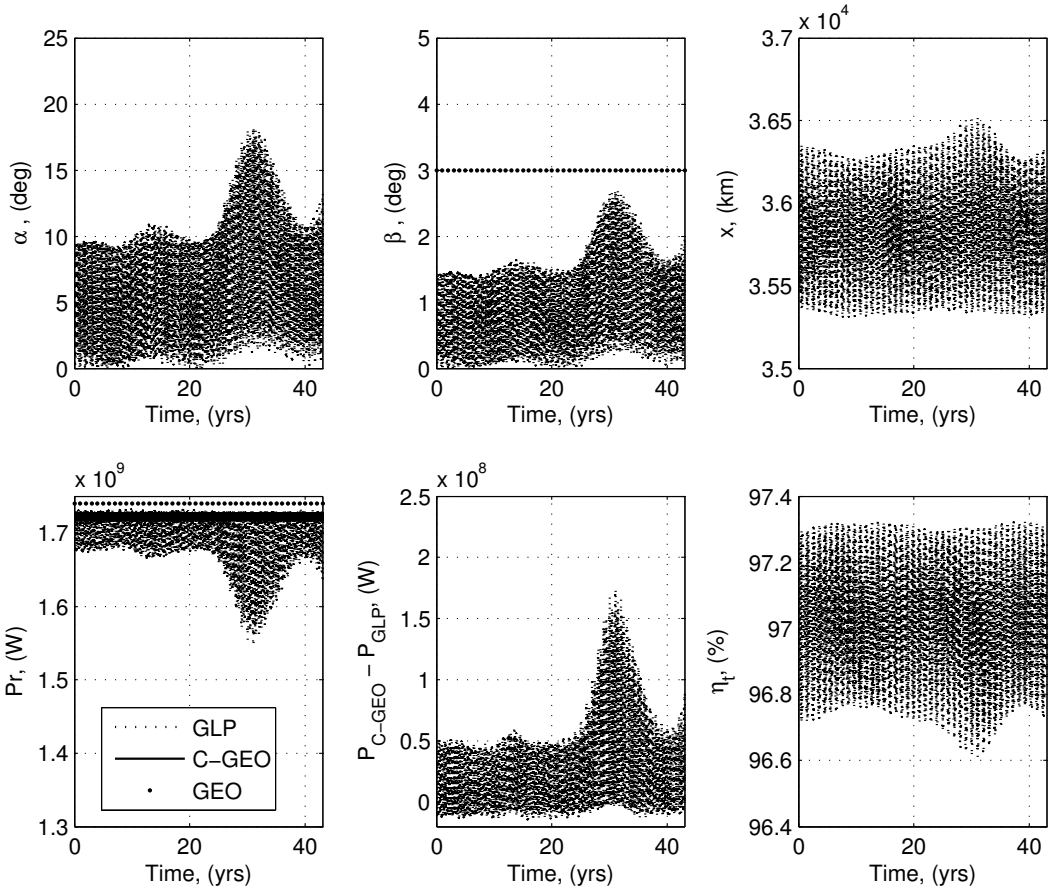

Figure 3.9: Long-term variation in Abacus SPS performance parameters for GLPO.

2. *Uncontrolled Initially GEO*

The β limit is marginally exceeded after ∼25 years (see Fig. 3.10). The SPS would also be operating extremely close to this limit for a period of approximately 5 years.

3.9.3 Inter-Antenna Distance, x

1. *Geosynchronous Laplace Plane Orbit*

The small amplitude oscillation in x is due to the inclination of the orbit. At the ascending and descending node, the value is 35,786 km and this increases slightly when the satellite is either at the "bottom" or "top" of its orbit with respect to the equatorial plane (see Fig. 3.8). The variation in eccentricity caused by SRP causes x to vary, with peak amplitude coinciding with peak eccentricity. The maximum amplitude is dependent upon the maximum value of eccentricity reached and, therefore, the Λ

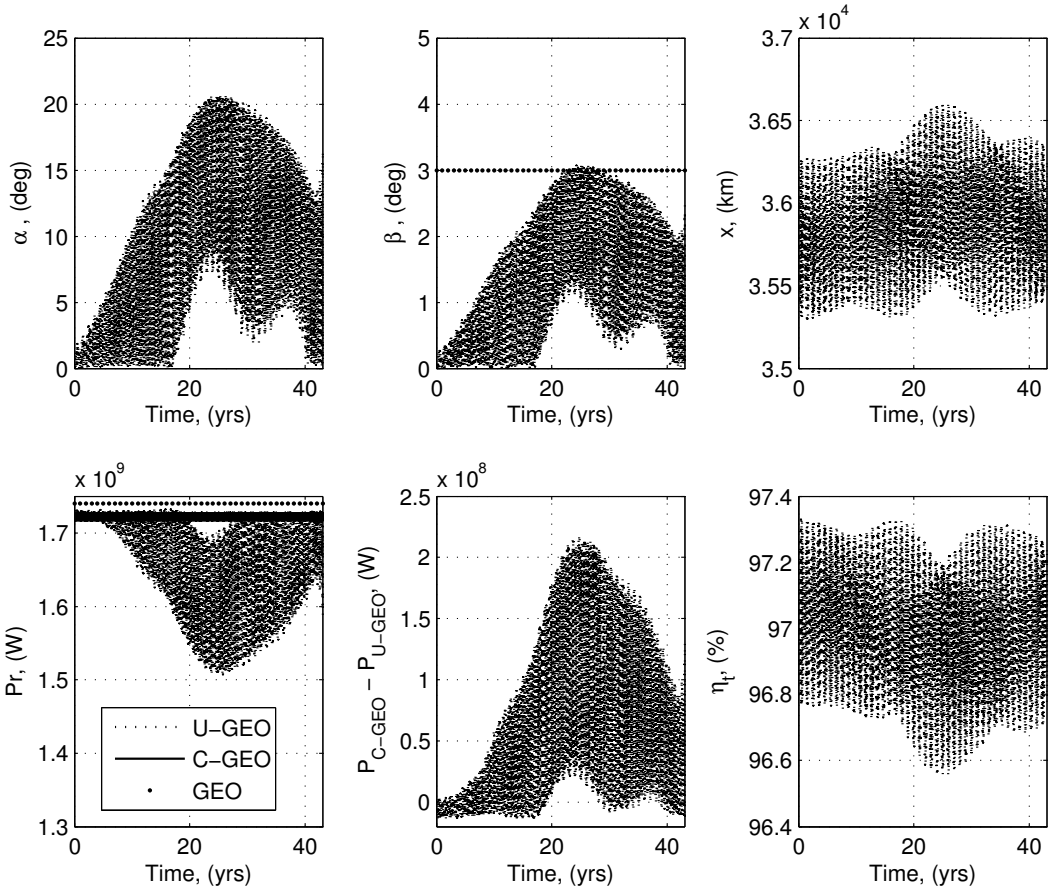

Figure 3.10: Long-term variation in SPS performance parameters for SPS initially in GEO.

value of the SPS.

2. *Uncontrolled Initially GEO*

Similar long-term behavior in x is observed with the exception that, around the time of peak inclination, a small overall increase in x is observed.

3.9.4 Power Received, P_r

1. *Geosynchronous Laplace Plane Orbit*

The power received drops by approximately 45 MW twice per day, as shown in Fig. 3.8, mainly due to the variation in the incident angle α. The long-term variation in α (Fig. 3.9) causes a maximum power loss compared with an ideal controlled GEO SPS (not accounting for engine power consumption, shown by dotted line in Fig. 3.9) of

10% which corresponds to $\alpha = 18^\circ$ and a resultant minimum power P_r(min)=1.55GW. The variation in the beam coupling efficiency also has a small effect on the overall power received. The difference in power received between the C-GEO and the GLPO is shown in Fig. 3.9, and the maximum difference is 170 MW. The average power received over an SPS lifetime of 30 years is 1.70GW. This is only 1.7% less than the ideal GEO case.

2. *Uncontrolled Initially GEO*

The minimum power received over the lifetime of the SPS is P_r(min)=1.50GW. The difference in power received between the C-GEO and the GLPO is shown in Fig. 3.10, and the maximum difference is 220 MW. The average power received over a 30 year lifetime is 1.67GW. This is 3.5% less than the ideal GEO case.

3.9.5 Satellite Ground Track

1. *Geosynchronous Laplace Plane Orbit*

The initial satellite ground track is a figure of eight centered on the equatorial ground station (see Fig. 3.8). The maximum latitude variation is $\pm 8^\circ$ daily. The center of the figure of eight slowly moves along the longitude axis according to the change in the RAAN. The figure of eight ground track moves East and West along the longitude axis over a period of ~ 20 years between $\pm 5^\circ$ (not shown). Over a longer time period, the longitude begins to drift East by a maximum of 20° from the initial longitude. This causes the peak in α after ~ 30 years, after which it appears to drift back westward. Growth in eccentricity causes a distortion in the figure of eight. The eccentricity causes a cyclic change in longitude with a one year period. The amplitude is dependent on the value of Λ as shown for the three SPS designs in Table 3.4. The maximum oscillation in longitude occurs at peak eccentricity.

2. *Uncontrolled Initially GEO*

The daily oscillation in latitude varies as the inclination evolves. At the beginning when $i = 0^\circ$, the latitude oscillation is zero. At the maximum $i = 15^\circ$, the latitude

oscillates between $\pm 15°$. The longitude varies from -10 to $+35°$ over the SPS lifetime. It is the larger variation in longitude which causes the higher values of α for the U-GEO case, along with the higher inclination.

3.9.6 Beam Coupling Efficiency, η_t

1. *Geosynchronous Laplace Plane Orbit*

The variation in η_t for GLPO is reasonably small ($\pm 0.3\%$) for Abacus SPS and indicates that eccentricity control is not required to maintain good efficiency of transmission. The variation of η_t is relatively small for all the values of Λ considered.

2. *Uncontrolled Initially GEO*

No significant difference in the behavior is observed compared to the GLPO case.

3.10 The Microwave and J_{22} Perturbation Effects

The orbit propagation and SPS performance parameters for the full nonaveraged model including the J_{22} and microwave perturbations are shown in Fig. 3.11. The SPS is located at a stable longitude and is assumed to deliver power to a single equatorial rectenna at the same longitude. The Laplace plane solution is therefore shown to be stable to these additional perturbations, with no significant change to the long-term orbital evolution. The power received is actually higher on average and steadier when these perturbations are included. These results confirm that a SPS placed in a GLPO at a stable longitude would require nominal fuel for station keeping. The improved stability of α observed in Fig. 3.11 is actually due to both the microwave and J_{22} perturbations, which act to stabilise the longitude. In the case of the J_{22} perturbation, this is only apparent at one of the stable longitudes. For the microwave perturbation, it always acts to stabilise the longitude. The effects of J_{22} and the microwave perturbations are analysed in the following.

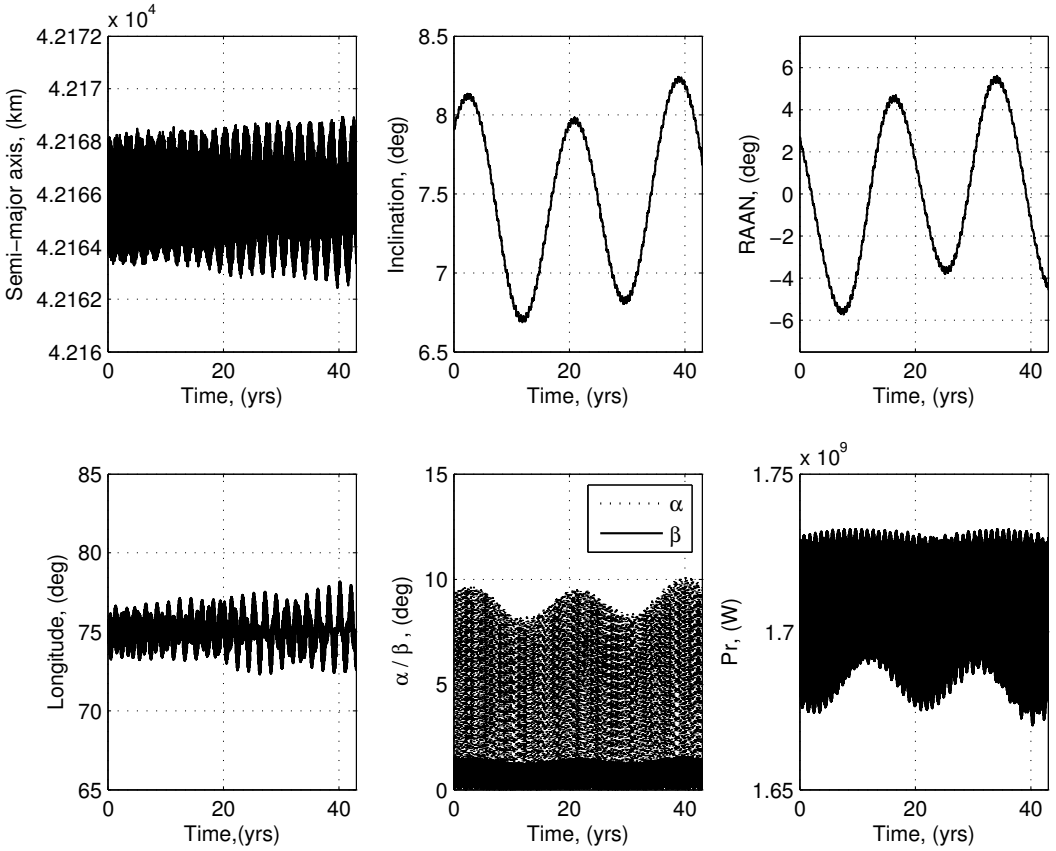

Figure 3.11: Numerical integration of the nonaveraged equations of motion including microwave perturbation and J_{22} perturbations.

3.10.1 Effect of J_{22} on Geosynchronous Satellites and Station Keeping

The equilibrium longitudes for a GLPO are equivalent to those for GEO due to the low eccentricity and relatively low inclination of the SPS orbits. This is shown by following the method given in Chao ([57] Sec. 4.4) for finding the equilibrium longitudes for orbits with nonzero eccentricity and inclination. The analysis here is limited to the J_{22} term; higher order gravity terms are not considered. The following equation is solved for longitude λ:

$$\frac{da}{dt} = 0 = 4na(R_E/a)^2 F_{220} G_{200} \left[-C_{22}\sin 2\lambda + S_{22}\cos 2\lambda\right] \tag{3.94}$$

where F_{lmp} and G_{lpq} are the inclination and eccentricity series gravity harmonic functions, respectively, given in Kaula ([58] Sec. 3.3). Additional terms with higher order

F and G functions have been neglected due to the low eccentricity of the SPS orbits. The averaged values for both the GEO and GLPO solution of e, i, and ω, along with the values of a and n for a geosynchronous orbiter, are substituted in to obtain the equilibrium longitudes. The following results are obtained for both the GLPO and GEO cases:

Stable equilibrium points:

$$\lambda_s = 75.03^\circ\text{E}, 255.03^\circ\text{E} \tag{3.95}$$

Unstable equilibrium points:

$$\lambda_u = 165.03^\circ\text{E}, 345.03^\circ\text{E} \tag{3.96}$$

It is clearly not possible to locate all SPS at the stable equilibrium points. Therefore, the more common situation of maintenance of an SPS at nonequilibrium longitudes is considered. The effect of the J_{22} perturbation on geosynchronous spacecraft is explained clearly by Agrawal,[59] along with a method for calculating the yearly pro-

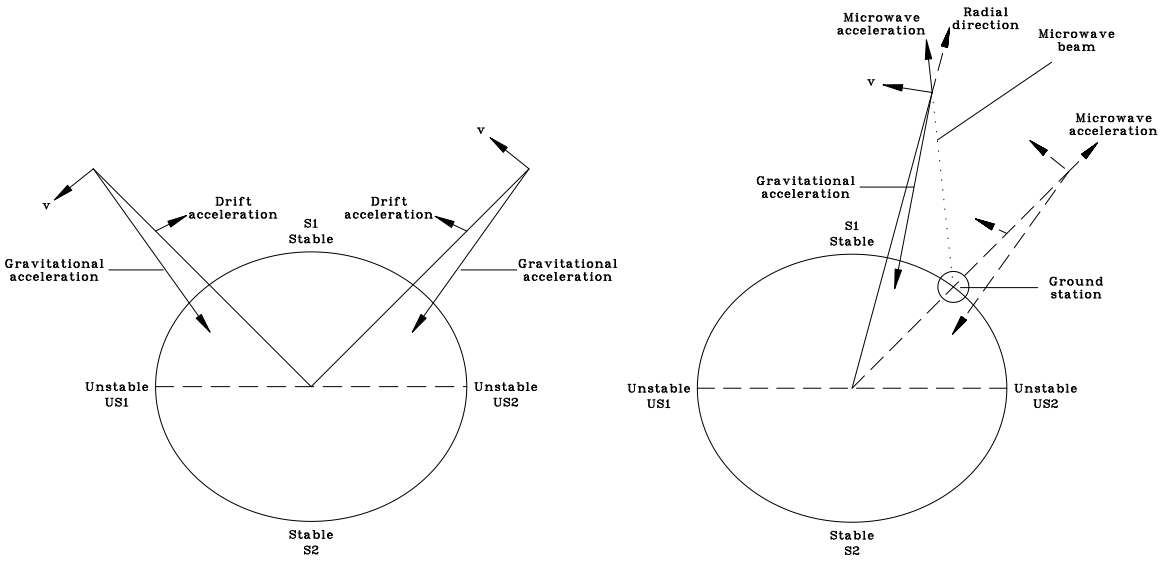

(a) J_{22} (b) J_{22} + Microwave

Figure 3.12: J_{22} and Microwave perturbations. Fig.(a) is based on a figure from Agrawal.[59]

pellant requirements for J_{22} station keeping. The J_{22} effect is briefly reviewed here to analyse the interaction with the SPS microwave perturbation.

The equatorial section of the Earth is shown in Fig. 3.12(a). Because of the bulge, the gravitational force is not always purely radial. This results in a lateral component either along or opposite the velocity direction (both cases shown). For the geosynchronous SPSs we consider, the relative motion between the Earth and the SPS is zero. Therefore, the lateral component of the gravitational force (which is always towards the nearest bulge) either increases or decreases the energy of the orbit continuously. At the stable (S) or unstable (US) points, the gravitational force is purely radial and the longitude drift rate is zero. If, for example, the satellite is between points S1 and US2, the lateral force component is opposite to the velocity direction, reducing the energy of the orbit. A reduction in the energy of the orbit implies a decrease in the semimajor axis, which results in a greater orbital velocity than the geosynchronous rate and, hence, the satellite drifts eastward toward the stable point S1.

The station keeping requirements for control of east-west (EW) drift due to J_{22}, when the SPS is not located in one of the stable equilibrium points, are a function of the longitude. Agrawal[59] derives an equation for determining the Δv costs in meter per second per year:

$$\Delta v_{EW} = 1.74 \sin 2(\lambda - \lambda_s) \tag{3.97}$$

where λ is the longitude of the SPS, and λ_s is the nearest stable longitude. The maximum velocity change required for station keeping is $\Delta v_{EW} = 1.74$ m/s per year, which is required for $(\lambda - \lambda_s) = 45^\circ$. This requirement is approximately the same for both GEO and GLPO. The maximum propellant required for EW station keeping for each SPS in given in Table 3.4.

Table 3.4: Fuel estimates for GEO controlled SPS

SPS	Mass SPS (kg)	Ecc. Fuel (kg/yr)	NS Fuel (kg/yr)	EW Fuel (kg/yr)	Total Fuel (kg/yr)	Fuel Mass (%) [a]
Cylindrical	6.6×10^7	54,000	87,600	3,900	145,500	6.2
Abacus	2.5×10^7	60,000	33,200	1,500	94,700	10.2
ISC	1.7×10^7	139,200	22,600	1,000	162,800	22.3

[a] Fuel Mass(%)=Fuel/(Mass SPS + Fuel). Assuming a 30 year mission lifetime.

3.10.2 Microwave Perturbation

The microwave perturbation is unique to SPS, hence, it is important to consider the effect of this perturbation. When the SPS is aligned in longitude with the ground station (i.e., no longitude drift is present), it simply acts radially. This has the equivalent effect of lowering the Earth's gravitational parameter μ and, consequently, slightly alters the semimajor axis at which geosynchronous rotation is attained.

The effect is more complicated when other perturbations act to change the longitude so that the SPS is no longer aligned with the ground station. It was noted that the magnitude of the microwave perturbing acceleration $\boldsymbol{a}_\mu$ is of similar order to the Earth ellipticity perturbing acceleration $\boldsymbol{a}_{22}$. Hence, the interaction between the two is considered.

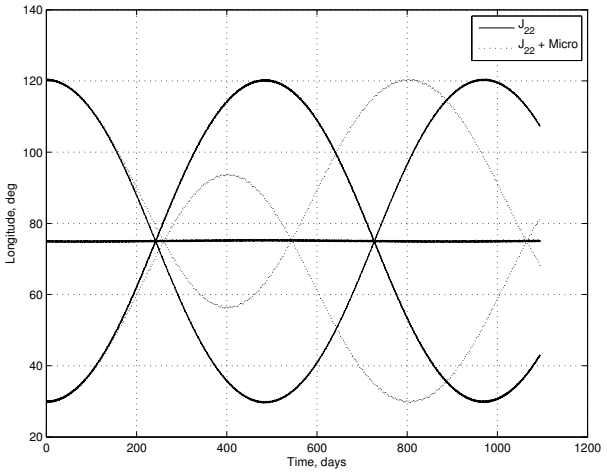

Figure 3.13: Effect of the J_{22} and microwave perturbations on longitude. The $\lambda - \lambda_s = 45^\circ$ case is considered, along with $\lambda = \lambda_s$.

When the longitude of the satellite drifts away from the initial longitude (and that of the ground station), the microwave perturbation is no longer acting radially. In fact, it has a lateral component that increases with increasing drift in longitude (see Fig. 3.12(b)). The lateral component of the microwave acceleration is always opposite to the lateral component of the gravitational force. Therefore, the lateral component of the gravitational force is reduced, causing a reduction in the longitude drift acceleration. This effect only becomes significant once the satellite has already drifted $> 30^{\circ}$ though (see Fig. 3.13). The microwave effect on longitude drift is likely to be extremely limited if we have a small deadband region for longitude control. This may change if the P/m ratio is considerably higher [see Eq. (3.15)] or if the SPS is offset in longitude from its ground station. Offsetting the ground station longitude is unlikely to be worthwhile to attain near propellantless control of J_{22} due to the loss in power from higher α angle and increase in rectenna size necessary, especially when one considers the relatively low propellant requirements for EW station keeping (see Table 3.4).

Whichever direction the longitude drifts, and whatever the source of longitude drift, the microwave perturbation will automatically act to reverse the drift. Although for the P/m ratios for the SPS considered here, this is not enough to fully counteract the effect of J_{22}, the microwave perturbation does reduce the rate of longitude drift (see Fig.3.13). It also changes the period of oscillation in longitude caused by the J_{22} perturbation.

3.11 Controlled Geostationary (C-GEO) - Fuel Requirements and Power Usage

To compare the uncontrolled GLPO with C-GEO, the fuel required to maintain a GEO SPS is calculated. The orbit correction due to SRP and lunisolar gravitation are considered separately. The SRP force primarily effects eccentricity (ecc.) and acts largely in the orbital plane, therefore the position vector $\boldsymbol{r}$ may be held fixed and the acceleration due to SRP $\boldsymbol{a}_{SRP}$ (given by Eq. (3.3)) integrated, to obtain the

Δv_{ecc}. North-South (NS) station keeping is also necessary in GEO. The Δv_{NS} needed to correct the inclination growth is calculated according to

$$\Delta v_{NS} = 2v \sin \Delta i/2 \tag{3.98}$$

where v is the magnitude of the orbital velocity, and Δi is the change in inclination desired, which is obtained from the graph of inclination vs time in Fig. 3.7(b) for U-GEO. The annual fuel requirements are calculated for the three different SPS designs, assuming an $I_{sp} = 3,000$ s, and are given in Table 3.4. In reality, a GEO satellite is controlled by periodically correcting the orbit within a certain tolerance, however, the method adopted gives an approximate mass of fuel required for orbit maintenance.

As discussed earlier, the variation in eccentricity causes a minimal change in the beam coupling efficiency and, hence, the power received. However, as previously observed, the variation in eccentricity due to SRP causes a cyclic change in the longitude. For GEO, the SRP perturbation would need to be counteracted as the variations in longitude $\Delta\lambda$ observed [$\pm 1.3^\circ$ for cylindrical, $\pm 2.5^\circ$ for Abacus, and $\pm 8^\circ$ for ISC] would not be acceptable due to the heavy use of GEO by other users. In the currently unused GLPO, this constraint could be relaxed and, therefore, it is not necessary to control the eccentricity or inclination for the GLPO. The mass of fuel saved depends upon the overall mass of the satellite for inclination control and the Λ value for eccentricity control. The percentage of the overall mass required for fuel shown in the last column of Table 3.4 is particularly large for high Λ SPS, such as the ISC. Such concepts with large, lightweight reflectors would require engines with significantly higher I_{sp} values to operate in GEO without excessive fuel requirements.

To compare the power delivery of the GLPO and the C-GEO, the power necessary for electric ion engines to completely cancel perturbation accelerations to maintain a perfectly controlled GEO SPS is evaluated. The electric ion engine specifications proposed by Wie and Roithmayr[16] for a feasible GEO SPS control system are as-

sumed, which require 30 kW/N. The average power required for engine thrusting for maintaining a GEO is 6.3 MW. Fig. 3.9 shows the power received from a C-GEO SPS, where the power required for the engines is subtracted from the power transmitted. The power from an ideal GEO (no deductions for engine thrusting) is also shown. The power needed to hold the SPS controlled in GEO is calculated by considering unperturbed Keplernian motion and calculating the total perturbing acceleration acting on the SPS. This acceleration is evaluated with Eqs. (3.3), (3.9), and (3.14). The thrust to entirely cancel this is derived from the total perturbation acceleration and is then used to calculate the power required. It is found that the average power delivered from the same SPS only differs by ∼170 MW for the GLPO and C-GEO cases (see lower-central subfigure in Fig. 3.9). Hence, the GLPO SPS offers similar performance to C-GEO in terms of actual power delivered but without the need for a large supply of fuel, because only minimal thrusting is necessary. This may be important because, according to Wie and Roithmayr,[15] little is known about the long-term effect of an extensive plasma (from the large number of electric ion engines required) on geosynchronous satellites with regard to communications, solar cell degradation, etc. GLPO SPS avoids these potential issues by requiring virtually no orbital control thrusting. The only control necessary for GLPO is EW station keeping, which requires at worst 0.2% of the overall mass of the SPS for fuel. It should also be stated that control of an SPS orbit in GLPO would be achievable with currently available electric ion thruster I_{sp} levels. Previous studies of SPS in GEO have assumed high I_{sp} values for SPS control, for example, Ogilvie[60] assumed engines with $I_{sp} = 13,000$s.

3.12 Orbital Debris Risk Reduction

The ultimate aim of SPS research is to eventually have a network of multiple SPSs providing a significant proportion of humanity's energy needs. Consequently, a large number of extremely large satellites would need to launched. Therefore, it is important to attempt to minimise the risk posed by orbit debris, both in terms of the risk posed to

the operation of SPSs by existing debris and the risk that SPSs pose as a large potential source of orbit debris in the future. Avoidance of orbital collisions between SPSs that may be several thousand meters across must be considered, because the debris field of a single SPS, or even a portion of one, could take out the entire geostationary communications system.[28]

3.12.1 Relative Velocities

By launching satellites into GLPO instead of initially equatorial GEO, the average relative velocities between geosynchronous satellites may be greatly reduced below what they would be if all geosynchronous satellites continue to be launched into equatorial orbits. The result being that the violence of potential collisions would be significantly reduced. The discussion that follows summarises the arguments of Friesen et al.,[56] given here for convenience.

Consider a group of satellites to be launched to geosynchronous altitude. If all users launch into initially equatorial orbits or are released from station-kept equatorial orbits at random times, the average relative velocity between the launched objects will be 500 m/s due to the maximum difference in inclination of 15°. If, instead, all the users launch to GLPO, then the average relative velocity between the launched objects would be 45 m/s. This reduces to 3 m/s if they are launched into "matched planes" (described later). If an equal number of users launch to the stable plane as to equatorial GEO orbits, the average encounter velocity will be approximately 375 m/s. The greater the percentage of objects launched into the Laplace plane, the more significant the reduction in average encounter velocity.

Reducing the potential encounter velocities is beneficial in the following ways. First, less damage is likely to be done in the event of a collision. Second, fewer pieces of debris large enough to fragment other satellites are likely to generated by a collision. This in turn reduces the probability of a "collision cascade", whereby large pieces of debris from one collision produce further debris by collision with other

satellites, generating more debris, and so on.

3.12.2 Matched Planes

The planes of all orbits in the Laplace plane precess at the same rate allowing the relative plane motion between satellites in GLPO to be reduced even further.[56] If the current orbit plane orientation of a Laplace plane satellite is carefully observed, and a new satellite is launched into the same orbit plane, the two satellites will maintain a common orbit plane thereafter. Once matched, they remain matched with their orbit planes moving together. Simulations performed by Friesen et al.[56] have shown that satellites in matched plane constellation are capable of maintaining a common plane to within 0.05° for a minimum of 100 years. This is the case whether they start at equal or unequal longitudes and also whether they are launched sequentially or simultaneously.

3.12.3 End of Life Disposal

It is also important to consider the end-of-life disposal options for SPSs. For SPS end-of-life disposal options in GLPO, there are three options as identified by Friesen et al.[56]

1) Turn off satellites and allow them to drift about the stable longitudes. Although collisions will eventually occur, they will be at very low relative velocities and will, on average, tend to damp out the relative motion of these objects until all objects come to rest at the stable longitudes.

2) Maneuver the satellites to the stable longitudes before turning them off. At the stable longitudes, satellites will have near-zero relative velocity, and any motion will quickly be damped out as more satellites are placed at these points.

3) Place objects in a relatively nearby graveyard orbit. Unlike graveyard orbits not in the Laplace plane, a graveyard orbit in the Laplace plane will also have very low

mutual collision velocities. Consequently, objects in the stable plane graveyard orbit are not likely to scatter fragments back through geosynchronous orbit.

3.12.4 Collision Risk with Station-Kept GEO Satellites

There is still a very small collision probability with satellites maintained in the GEO arc if the GLPO SPS crosses the GEO arc at 0° latitude. The GLPO intersects with the equatorial plane twice per orbit at ascending and descending node. However, the SPS in GLPO does not intersect with the GEO ring at ascending/descending node for the majority of the time due to the eccentricity of its orbit (caused by the SRP perturbation). The risk of collisions with station-kept GEO satellites is sensitive to the eccentricity and argument of perigee/longitude of perigee. The times when it may come close to intersecting the GEO ring are either when the eccentricity goes to zero or when the eccentricity is relatively low and the argument of perigee is $\omega \sim 90°$ or 270°. Around these times, careful monitoring of the satellite position and maneuvres may be necessary to avoid collision with station-kept GEO satellites. The frequency and cost of these maneuvres will be the subject of future research. Alternatively, a stable nonzero eccentricity, such as that found by Graf,[38] may minimise the risk of collision with station-kept GEO satellites while having a minimal impact on the beam coupling efficiency.

3.13 Discussion

The main advantages of the geosynchronous Laplace plane orbit are reduction in fuel requirements, due to not having to correct for inclination drift or eccentricity variation; operational robustness, because if the control system were to go offline for any reason, it would not matter because it would stay in that orbit; the major advantages of the GEO SPS (24 h access, low transmitter/receiver relative velocity) are maintained; the risk of orbital debris creation is reduced; and finally, the congestion of GEO

is avoided. As an option that requires minimal control thrusting, the GLPO looks attractive, because it only suffers small losses in power delivered and maintains a stable power supply for the full 30-40 year lifetime. Although not accounted for in this analysis, it is noted that, for GLPO, there will be less power losses compared with C-GEO around winter and summer solstice, where the assumption is made that the solar arrays are oriented perpendicular to the orbital plane and do not track the sun's north-south motion throughout the year. The main disadvantage of GLPO is that the variation of incident angle of the beamed radiation caused by having an inclined orbit means greater daily oscillation in power delivery.

C-GEO delivers comparable average power to the GLPO case as the power required for station keeping engines is not that high and the incidence angle α is maintained near to $0°$. Minimal electronic beam steering is required; the power saved by this has not been accounted for here. Despite offering similar power delivery to the SPS located in GLPO, the C-GEO does require frequent control thrusting over the lifetime of the SPS, and hence on the order of 10^5 kg/year of fuel. Because of the high level of use of GEO, orbital control is necessary for inclination drift and eccentricity variation. The fuel required to do so can compose a significant fraction of the overall mass of the satellite, especially for high Λ SPS. The C-GEO option results in the added complexity and cost of frequent refueling operations. Additionally, the effects of the extensive plasma (produced from the large number of electric ion engines) on geosynchronous satellites with regards to communications and solar cell degradation is as yet poorly understood. GLPO avoids these potential issues.

In the case where the SPS is initially placed in a GEO and left uncontrolled (U-GEO), a useful power source is still obtained, albeit with reduced performance compared to the GLPO option. This option is more demanding of the beam pointing system, with greater off-axis beaming angles required throughout the lifetime. A C-GEO SPS at the end of life would share a similar orbital evolution to the U-GEO. If a large number of SPS are launched, then the orbital evolution from initially equatorial

GEO presents a greater threat of eventually producing orbit debris due to the larger relative velocities between SPSs than the GLPO case.

The Earth tesseral harmonic term J_{22} has not been included in the averaged analysis. This is because a separate resonance-averaging technique would be required to correctly treat this effect. It is important to consider due to the resonance it causes at geosynchronous altitude. This will cause an EW drift in the longitude of the satellite unless the SPS is located in one of the stable "sinks". Otherwise, thrusting would be required to offset the EW longitude drift. In the averaged model, it has been assumed that the SPSs are located in a stable sink. The stability of the GLPO solution to the J_{22} perturbation (when placed at a stable longitude) has been confirmed by including it in the nonaveraged model. The station keeping costs for J_{22} are relatively low. It is noted that this is the only orbital control which is necessary for GLPO.

Because of the use of a very large transmitting antenna for beaming of the microwave energy from orbit to the Earth's surface, there is a reactive force (6N for 500 m 1.78 GW antenna) acting opposite the satellite to ground station beaming direction. This has not been included in the averaged model, however, it is included in the nonaveraged model. It is noted that the magnitude of this perturbation acceleration is comparable to the J_{22} perturbation acceleration. It has been shown that the microwave perturbation acts against longitude drift in either direction. Hence, it acts to stabilise the longitude of the SPS. The magnitude of this effect is dependent on the power transmitted to mass ratio of the satellite.

This study only considers a single geosynchronous satellite delivering power to single equatorial ground station. A number of other configurations involving multiple SPS and multiple ground stations are conceivable and should be investigated in future work. The averaged model is particularly well suited to performing such studies.

To first gain an understanding of the orbital dynamics, the attitude of the SPS has not been considered here. The attitude dynamics of the Abacus SPS in GEO and GLPO shall be considered in the next chapter.

3.14 Novel Contributions

The simulation of the power delivery for SPS operating in different orbits has not been done before. This chapter has shown that GLPO is a feasible orbit location for power transmitters with electronic beam pointing of only +/- 3° to redirect power to the ground station without the need for mechanical re-pointing. Previous transmitting antennas would have required either mechanical repointing or a reflector to redirect the microwave beam (e.g. the Abacus design). Confirming that a SPS placed in GLPO and left completely uncontrolled for the lifetime of the SPS can deliver comparable power levels as a fully controlled GEO SPS is a significant result, and is the main finding of this chapter.

This is the first study to the author's knowledge that shows that the electronic beam pointing technology could be used from a SPS in an uncontrolled GLPO. The power loss due to the SPS not being maintained directly overhead of the rectenna is quantified here over the lifetime an SPS. It is shown that the difference in power delivery from a GLPO compared to a controlled GEO is minimal. This provides evidence that GLPO is feasible for SPS. If the pointing required exceeded the electronic beam pointing technological limit significantly, it would have ruled out using GLPO for a SPS with the electronic beam pointing technology.

Including the orbit perturbation due to the reactive force caused by beaming of microwave power has not been done before in the literature to the author's knowledge. The analysis considers the interaction of the microwave beam orbit perturbation with the J_{22} perturbation in a geosynchronous orbit which is also novel. The finding that the microwave power beam perturbation acts to stabilise the orbit longitude is novel to the author's knowledge.

Additionally, in the orbit dynamics model, the form of the triply averaged secular equations for lunar gravity perturbation has not been presented before to the author's knowledge.

Important observations on the practical implications of placing a huge network of SPS in GEO are made, with the benefits of GLPO quite clear in terms of limiting orbit debris creation. To the authors knowledge, this is the first linking of Friesen's[56] recommended use of GLPO to reduce space debris to SPS, where the consequences are multiplied hugely by the massive size of microwave SPS (1 SPS could wipe out entire GEO satellite communications network if placed in GEO and collided with).

The model constructed allows the simulation of power delivery for an SPS with electronic beam pointing to any number of ground stations, at any latitude. This analysis could be run for any requirements to deliver power to a certain location and evaluate the power delivery from any orbit to that location. The averaged model could be particularly useful for simulating constellations of multiple SPS due to the speed of numerical integration of the averaged equations of motion.

4

Attitude Dynamics of Geosynchronous SPSs

> "The mathematical difficulties of the theory of rotation arise chiefly from the want of geometrical illustrations and sensible images, by which we might fix the results of analysis in our minds."
>
> - James Clerk Maxwell

Although the previous chapter found that the GLPO has many benefits for SPS, including large potential orbit control fuel savings, the attitude dynamics of SPS were not considered. In this chapter, the consequences on the attitude control costs of moving the Abacus SPS from GEO to GLPO are considered, along with the attitude-orbit coupling effects. The SPS is an example of a large space structure. The principal effects of the extremely large size are a large increase in the sensitivity to gravity gradient torques to the extent that this is the dominant disturbing torque even for geosynchronous orbits. Therefore only the gravity gradient torque will be considered here.

4.1 SPS Attitude Dynamics Literature

The attitude dynamics of large geosynchronous SPS have been investigated previously in numerous studies.[60, 15, 19, 16] The previous studies considered a variety of SPS designs all located in GEO.

SPS attitude control is challenging due to the large moments of inertia which mean that attitude control cannot be handled in a conventional manner. Current momentum storage devices are incapable of dealing with the large amount of angular

momentum storage required for kilometre scale spacecraft.[15] The mass of the angular momentum storage system required to maintain 3-axis pointing would be greater than the mass of the satellite.

Instead, researchers have put forward electric propulsion engines for SPS attitude control. Although fuel is required for this approach, it is considered far more robust. It was also found that attitude control could be performed simultaneously with orbit control at essentially no extra cost for some SPS designs. An integrated attitude and orbit control system for the Abacus SPS (shown in Fig. 4.4) located in GEO and oriented perpendicular to the orbital plane (POP) was devised by Wie and Roithmayr[15,16] utilising a large number of electric ion thrusters. It was shown that attitude control could be performed through utilisation of the orbital control thrusting required for maintaining GEO at no additional propellant cost. However, the orbital control costs for an Abacus SPS to operate in GEO were estimated at 93,200 kg/year (no margin included) assuming electric propulsion with $I_{sp} = 3000s$ (see Table 3.4).

A "quasi-inertial" sun-pointing pitch-control concept was developed by Elrod[61] in an attempt to resolve the angular-momentum storage problem of large sun-pointing spacecraft. This concept was further investigated by Juang and Wang.[62] However, as concluded by Wie and Roithmayr,[16] such a free-drift concept is not a viable option for the Abacus satellite due to the large pitch-attitude peak error of 18.8° and the inherent sensitivity with respect to initial phasing and other orbital perturbations. It may however be of interest for alternative SPS designs as the magnitude of the pitch-attitude peak error is dependent on the mass distribution through the ratio $(I_{xx} - I_{yy})/I_{zz}$.

4.2 Solar Radiation Pressure Orbit Control

For SPS in GEO, it was considered necessary to control the dominant SRP orbital perturbation, which if left unchecked would cause a yearly oscillation in eccentricity and consequently, an unacceptably large oscillation in the spacecraft's longitude. Such

an oscillation would risk encroachment upon neighbouring GEO "slots" and interference/collision with other GEO assets. The magnitude of the SRP force and therefore the amplitude of the longitude oscillation is dependent upon the Λ value of the SPS. The integrated orbit-attitude control system for the Abacus SPS in GEO proposed by Wie and Roithmayr[15,16] applied the SRP orbit control thrusting cyclically to cancel the pitch gravity gradient torque simultaneously at no additional cost.

The longitude oscillation due to SRP induced eccentricity variation is still present in GLPO. The difference is that this need not be controlled for a number of reasons: the Laplace plane orbit is stable to variations in eccentricity;[52] the eccentricity has a minimal impact on the beam coupling efficiency of the system; and the SPS is no longer in the overcrowded GEO ring where each satellite must stay within it's allotted longitude "slot". In GLPO the 2-3° longitude oscillation would be acceptable. The SPS in GLPO does not intersect with the GEO ring at ascending/descending node for the majority of the time due to the eccentricity of its orbit (caused by the SRP perturbation). The risk of collisions with station-kept GEO satellites is sensitive to the eccentricity and argument/longitude of perigee. The times when it may come close to intersecting the GEO ring are either when the eccentricity goes to zero or when the eccentricity is relatively low and the argument of perigee is $\omega \sim 90°$ or $270°$. Around these times, careful monitoring of the satellite position and manoeuvres may be necessary to avoid collision with station-kept GEO satellites. The frequency and cost of these manoeuvres will be the subject of future research. However, it is considered likely that the cost in terms of fuel will be significantly less than that required to continuously counteract the SRP force (60,000 kg/year[16]).

Graf[38] considered the possibility of a GLPO with non-zero initial eccentricity, for which it appears the amplitude of the yearly oscillations in eccentricity are decreased for the first decade or so and the eccentricity remains non-zero. Finding a stable eccentricity which does not approach zero annually could potentially offer the lowest probability of intersection with the GEO ring.

4.3 Attitude Dynamics of SPS in the Geosynchronous Laplace Plane

One of the main aims of the attitude dynamics study is to determine if there is an attitude control penalty imparted by locating the SPS in GLPO which may cancel out the orbit control savings. Hence, this study focuses on a re-examination of the attitude dynamics of the Abacus SPS with the novel contribution of directly comparing the attitude control of Abacus in GEO versus the attitude in GLPO.

The model compares the effect of the gravity gradient torque on different SPS designs with different orbit locations and attitude configurations. Calculation of the overall (orbit and attitude) fuel costs for an SPS lifetime is also presented.

4.4 Two Body Formulation and Equations of Motion

The main assumption made in this study is that the mass distributions of the two bodies (Earth and the SPS) are rigid, meaning that we do not account for any deformation in their shape or mass distribution. Fig. 4.1 provides a graphical definition of the problem, with the following section providing a mathematical description.

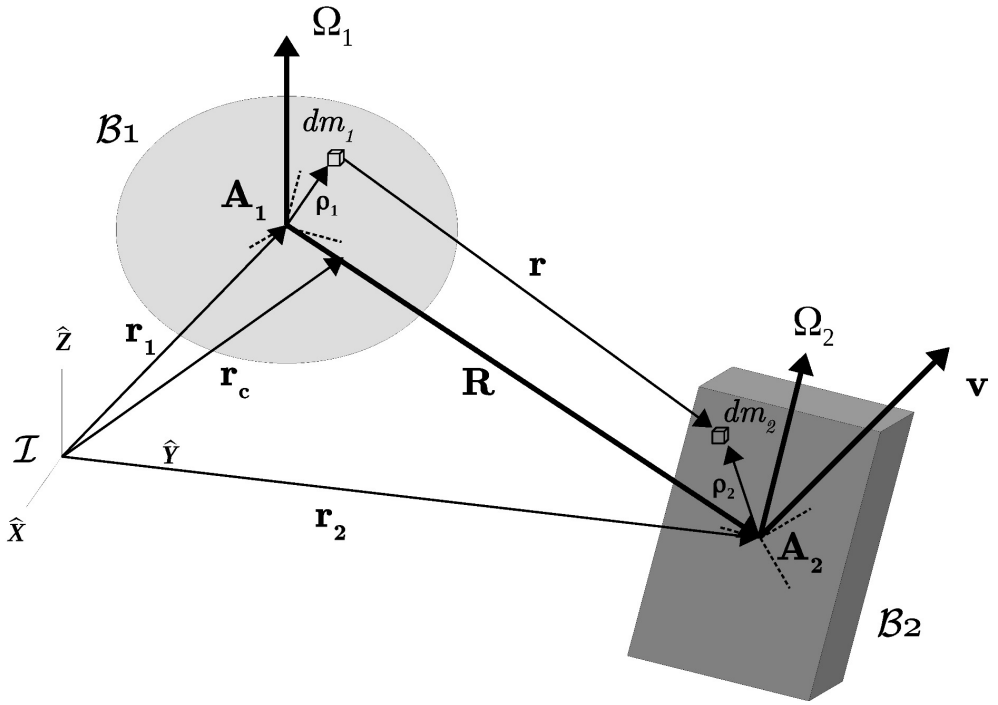

Figure 4.1: The full two body problem illustrating all the degrees of freedom.

$\mathcal{B}_1$	Body 1, the Earth
$\mathcal{B}_2$	Body 2, the Solar Power Satellite
$\mathcal{I}$	Inertial reference frame
$\boldsymbol{r}$	Radius vector between mass elements dm_1 and dm_2
$\boldsymbol{R}$	Radius vector between the origins of bodies 1 and 2
$\boldsymbol{\rho}_1$	Radius vector from the origin of $\mathcal{B}_1$ to dm_1
$\boldsymbol{\rho}_2$	Radius vector from the origin of $\mathcal{B}_2$ to dm_2
$\boldsymbol{\Omega}_1$	Angular velocity of Body 1 relative to $\mathcal{I}$
$\boldsymbol{\Omega}_2$	Angular velocity of Body 2 relative to $\mathcal{I}$
$\boldsymbol{A}_1$	Attitude dyadic from Body 1 frame to $\mathcal{I}$
$\boldsymbol{A}_2$	Attitude dyadic from Body 2 frame to $\mathcal{I}$

4.4.1 Equations of Motion for the Full Two Body Problem

The general problem of two bodies concerns the orbital and rotational motions of two bodies of arbitrary shape. The description of such motion requires the solution of Newton's second law for the orbital motion of the centers of mass of the respective bodies and Euler's equations for the rotational motion. The gravitational force acting on each body consists of contributions from the mutual gravitational interactions between all of the particles comprising Body 1 and all of those comprising Body 2.

The rotational motion, however, will be influenced by the torque produced about appropriate reference axes, where the torque is produced by the mutual gravitational forces between the particles. Consequently, if V represents the mutual gravitational potential between two bodies of masses M_1 and M_2 , then the motion of M_2 relative to M_1 can be described by:

$$\frac{M_1 M_2}{M_1 + M_2}\ddot{\boldsymbol{R}} = -\frac{\partial V}{\partial \boldsymbol{R}} \tag{4.1}$$

$$\boldsymbol{A}_i \left[\boldsymbol{I}_i \cdot \dot{\boldsymbol{\Omega}}_i + \boldsymbol{\Omega}_i \times \boldsymbol{I}_i \cdot \boldsymbol{\Omega}_i\right] = -\frac{\partial V}{\partial \boldsymbol{\theta}_i}; i = 1,2 \tag{4.2}$$

where M_1 and M_2 are the masses of body 1 and 2, $\boldsymbol{I}_i$ are the inertia dyadics of the bodies. The gravitational force is given by the gradient of the mutual gravitational potential, $\partial V/\partial \boldsymbol{R}$. The torque acting on body i is $-\partial V/\partial \boldsymbol{\theta}_i$, where $\boldsymbol{\theta}_i$ represents infinitesimal variations in the attitudes of each body about a specified $\boldsymbol{A}_i$. These equations are still in the inertial frame, although the time derivatives for the rotational equations are chosen in their respective body frames, hence the pre-multiplication by the attitude dyadic, $\boldsymbol{A}_i$. The kinematics of rotation must also be considered. Since the attitude dyadic $\boldsymbol{A}_i$ maps from a body-fixed to an inertial frame, the kinematical equation for it is giving by:

$$\dot{\boldsymbol{A}}_i = \boldsymbol{A}_i \cdot \widetilde{\boldsymbol{\Omega}}_i \tag{4.3}$$

where $\widetilde{\boldsymbol{\Omega}} = \Omega_1(\hat{\boldsymbol{e}}_3\hat{\boldsymbol{e}}_2 - \hat{\boldsymbol{e}}_2\hat{\boldsymbol{e}}_3) + \Omega_2(\hat{\boldsymbol{e}}_1\hat{\boldsymbol{e}}_3 - \hat{\boldsymbol{e}}_3\hat{\boldsymbol{e}}_1) + \Omega_3(\hat{\boldsymbol{e}}_2\hat{\boldsymbol{e}}_1 - \hat{\boldsymbol{e}}_1\hat{\boldsymbol{e}}_2)$. The above equations represent the most general case of the rigid two body problem.

4.4.2 The Mutual Potential

The mutual gravitational potential is considered up to second order only as this is sufficient to model the major perturbation arising from non-spherical mass distributions. The mutual gravity potential for $\mathcal{B}_1$ interacting with $\mathcal{B}_2$ is formulated by the following integration over both volumes:

$$V = -G \int_{\mathcal{B}_1} \int_{\mathcal{B}_2} \frac{dm_1\, dm_2}{r} \tag{4.4}$$

where dm_1 and dm_2 are infinitesimal mass elements in body 1 and 2 respectively. The leading terms of the potential up the fourth order are derived by Ashenberg.[63] The results up to second order are stated here:

$$V^{(0)} = -G \int_{\mathcal{B}_1} \int_{\mathcal{B}_2} \frac{dm_1\, dm_2}{r} = -G\frac{M_1 M_2}{R} \tag{4.5}$$

$$V^{(1)} = -G \int_{\mathcal{B}_1} \int_{\mathcal{B}_2} \frac{\boldsymbol{R}\cdot\Delta\boldsymbol{\rho}}{R^3}\, dm_1\, dm_2 = 0 \tag{4.6}$$

$$V^{(2)} = -\frac{GM_2}{2R^3}(tr\boldsymbol{I}_1 - 3I_{1R}) - \frac{GM_1}{2R^3}(tr\boldsymbol{I}_2 - 3I_{2R}) \tag{4.7}$$

where $I_{iR} = \hat{\boldsymbol{R}}\cdot\boldsymbol{I}_i\cdot\hat{\boldsymbol{R}} = \int_{\mathcal{B}_i}(\rho_i^2 - (\hat{\boldsymbol{R}}\cdot\boldsymbol{\rho})^2)\, dm_i$, $tr\boldsymbol{I}_i = \int_{\mathcal{B}_i} 2\rho_i^2\, dm_i$, and $\Delta\boldsymbol{\rho} = \boldsymbol{\rho}_1 - \boldsymbol{\rho}_2$. Eq. (4.6) reduces to zero when the origins are chosen to coincide with the centres of mass.[63] In Eq. (4.7), originally presented by Schutz,[64] $\boldsymbol{I}_i$ is invariant under rotation. However, I_{iR} depends upon the orientation. Hence, $V^{(2)}$ may be rewritten following the formalism of Ashenberg[63] in terms of the attitude dyadics as:

$$V^{(2)} = -\frac{GM_2}{2R^3}(tr\boldsymbol{I}_1 - 3\hat{\boldsymbol{R}}^T\boldsymbol{A}_1^T\boldsymbol{I}_1\boldsymbol{A}_1\hat{\boldsymbol{R}}) - \frac{GM_1}{2R^3}(tr\boldsymbol{I}_2 - 3\hat{\boldsymbol{R}}^T\boldsymbol{A}_2^T\boldsymbol{I}_2\boldsymbol{A}_2\hat{\boldsymbol{R}}) \tag{4.8}$$

Since we are not assuming that the reference frame is fixed in either $\mathcal{B}_1$ or $\mathcal{B}_2$, the attitude dyadics are required in both terms. To use the Ashenberg method to derive the gradient of the potential, Eq. (4.8) must be expressed in terms of the direction cosines for each body l_i',m_i',n_i':

$$\begin{aligned} V^{(2)} = &-\frac{GM_2}{2R^3}\left[(1-3l_1'^2)I_{1xx} + (1-3m_1'^2)I_{1yy} + (1-3n_1'^2)I_{1zz}\right] \\ &-\frac{GM_1}{2R^3}\left[(1-3l_2'^2)I_{2xx} + (1-3m_2'^2)I_{2yy} + (1-3n_2'^2)I_{2zz}\right] \end{aligned} \tag{4.9}$$

where:

$$
\begin{aligned}
l_1' &= \hat{\boldsymbol{R}}^T \boldsymbol{a}_1^{(1)} = l A_{11}^{(1)} + m A_{12}^{(1)} + n A_{13}^{(1)} \\
m_1' &= \hat{\boldsymbol{R}}^T \boldsymbol{a}_2^{(1)} = l A_{21}^{(1)} + m A_{22}^{(1)} + n A_{23}^{(1)} \\
n_1' &= \hat{\boldsymbol{R}}^T \boldsymbol{a}_3^{(1)} = l A_{31}^{(1)} + m A_{32}^{(1)} + n A_{33}^{(1)} \\
l_2' &= \hat{\boldsymbol{R}}^T \boldsymbol{a}_1^{(2)} = l A_{11}^{(2)} + m A_{12}^{(2)} + n A_{13}^{(2)} \\
m_2' &= \hat{\boldsymbol{R}}^T \boldsymbol{a}_2^{(2)} = l A_{21}^{(2)} + m A_{22}^{(2)} + n A_{23}^{(2)} \\
n_2' &= \hat{\boldsymbol{R}}^T \boldsymbol{a}_3^{(2)} = l A_{31}^{(2)} + m A_{32}^{(2)} + n A_{33}^{(2)}
\end{aligned} \tag{4.10}
$$

With $\boldsymbol{R} = R[l\ m\ n]^T$, $\boldsymbol{A}_1^T = [\boldsymbol{a}_1^{(1)}\ \boldsymbol{a}_2^{(1)}\ \boldsymbol{a}_3^{(1)}]$ the attitude matrix going from the inertial to $\mathcal{B}_1$ frame, and $\boldsymbol{A}_2^T = [\boldsymbol{a}_1^{(2)}\ \boldsymbol{a}_2^{(2)}\ \boldsymbol{a}_3^{(2)}]$ the attitude matrix going from the inertial to $\mathcal{B}_2$ frame, where $\boldsymbol{a}_j^{(i)}$ are the column vectors of $\boldsymbol{A}_i^T$. Also, I_{1xx}, I_{1yy}, and I_{1zz} are the principal moments of inertia of $\mathcal{B}_1$ and I_{2xx}, I_{2yy}, and I_{2zz} are the principal moments of inertia of $\mathcal{B}_2$. The gradient of the mutual gravitational potential may then be computed using the definitions and equations given by Ashenberg.[63] The zeroth order gradient term is given by:

$$
\frac{\partial V^{(0)}}{\partial \boldsymbol{R}} = \frac{G M_1 M_2}{R^3} \boldsymbol{R} \tag{4.11}
$$

The gradient of the first order term is trivially zero. The gradient of the second order mutual potential term (Eq. (4.8)) is given by:

$$
\begin{aligned}
\frac{\partial V^{(2)}}{\partial \boldsymbol{R}} = \frac{3G}{2R^3} \Bigg\{ & \frac{M_2}{R^2} \boldsymbol{R} \left[(1 - 3l_1'^2) I_{1xx} + (1 - 3m_1'^2) I_{1yy} + (1 - 3n_1'^2) I_{1zz} \right] \\
& + M_2 \left[\frac{\partial l_1'^2}{\partial \boldsymbol{R}} I_{1xx} + \frac{\partial m_1'^2}{\partial \boldsymbol{R}} I_{1yy} + \frac{\partial n_1'^2}{\partial \boldsymbol{R}} I_{1zz} \right] \\
& + \frac{M_1}{R^2} \boldsymbol{R} \left[(1 - 3l_2'^2) I_{2xx} + (1 - 3m_2'^2) I_{2yy} + (1 - 3n_2'^2) I_{2zz} \right] \\
& + M_1 \left[\frac{\partial l_2'^2}{\partial \boldsymbol{R}} I_{2xx} + \frac{\partial m_2'^2}{\partial \boldsymbol{R}} I_{2yy} + \frac{\partial n_2'^2}{\partial \boldsymbol{R}} I_{2zz} \right] \Bigg\}
\end{aligned} \tag{4.12}
$$

where terms such as $\partial l_i'/\partial \boldsymbol{R}$ are evaluated with Equation (21) given by Ashenberg.[63] Finally, the total gravitational force between the two bodies is given up to 2^{nd} order as:

$$\frac{\partial V}{\partial \boldsymbol{R}} = \frac{\partial V^{(0)}}{\partial \boldsymbol{R}} + \frac{\partial V^{(2)}}{\partial \boldsymbol{R}} \tag{4.13}$$

which is substituted into Eq. (4.1) to obtain the relative translational motion between the two bodies.

4.4.3 The Mutual Torque

The rotational motion of $\mathcal{B}_1$ or $\mathcal{B}_2$ will be influenced by the mutual torque acting on each body. The torque on $\mathcal{B}_1$ due to $\mathcal{B}_2$ is given to second order by Ashenberg[63] as:

$$\begin{aligned} \boldsymbol{T}_1^{(2)} &= \frac{3GM_2}{R^3} \int_{\mathcal{B}_1} (\boldsymbol{\rho}_1 \cdot \hat{\boldsymbol{R}}) \boldsymbol{\rho}_1 \times \hat{\boldsymbol{R}} \, dm_1 \\ &= \frac{3GM_2}{R^3} \begin{bmatrix} m_1' n_1' (I_{1zz} - I_{1yy}) \\ l_1' n_1' (I_{1xx} - I_{1zz}) \\ l_1' m_1' (I_{1yy} - I_{1xx}) \end{bmatrix} = -\frac{\partial V}{\partial \boldsymbol{\theta}_1} \end{aligned} \tag{4.14}$$

where $\boldsymbol{\rho}_1$ is the radius vector from the origin of $\mathcal{B}_1$ to the mass elements dm_1. Similarly the torque on $\mathcal{B}_2$ due to $\mathcal{B}_1$ is:

$$\begin{aligned} \boldsymbol{T}_2^{(2)} &= \frac{3GM_1}{R^3} \int_{\mathcal{B}_2} (\boldsymbol{\rho}_2 \cdot \hat{\boldsymbol{R}}) \boldsymbol{\rho}_2 \times \hat{\boldsymbol{R}} \, dm_2 \\ &= \frac{3GM_1}{R^3} \begin{bmatrix} m_2' n_2' (I_{2zz} - I_{2yy}) \\ l_2' n_2' (I_{2xx} - I_{2zz}) \\ l_2' m_2' (I_{2yy} - I_{2xx}) \end{bmatrix} = -\frac{\partial V}{\partial \boldsymbol{\theta}_2} \end{aligned} \tag{4.15}$$

where $\boldsymbol{\rho}_2$ is the radius vector from the origin of $\mathcal{B}_2$ to the mass elements dm_2. Equations (4.14) and (4.15) for the torque are substituted into the right hand side of the rotational equations of motion for each body (Eq. (4.2)). Physically, the direction cosines (l_i', m_i', n_i') are quantifying the relative attitude between $\mathcal{B}_1$ and $\mathcal{B}_2$.

4.5 Linear Stability Analysis of Gravity Gradient Torque

Linear stability analysis of the gravity gradient torque on a rigid body in a circular orbit is well known and detailed derivations can be found in Schaub Section 4.63 p193[65] and Hughes Section 9.2 p293.[66] This will not be reproduced here, except to provide the stability conditions this analysis provides and evaluate those conditions for different SPS. This analysis can only be applied to SPS which are configured to rotate at the orbit rate (Cylindrical, Sun-Tower, Tethered).

The attitude stability conditions for a rigid body in a circular orbit as derived by Schaub[65] are:

$$1.\ (1 + 3k_Y + k_Y k_R)^2 > 16 k_Y k_R \tag{4.16}$$

$$2.\ k_R k_Y > 0 \tag{4.17}$$

$$3.\ k_R < k_Y \tag{4.18}$$

where:

$$k_R = \frac{I_2 - I_1}{I_3};\ \ k_Y = \frac{I_2 - I_3}{I_1} \tag{4.19}$$

where the indices indicate which of the orbit axes that moment of inertia lies along, see Fig. 4.2.

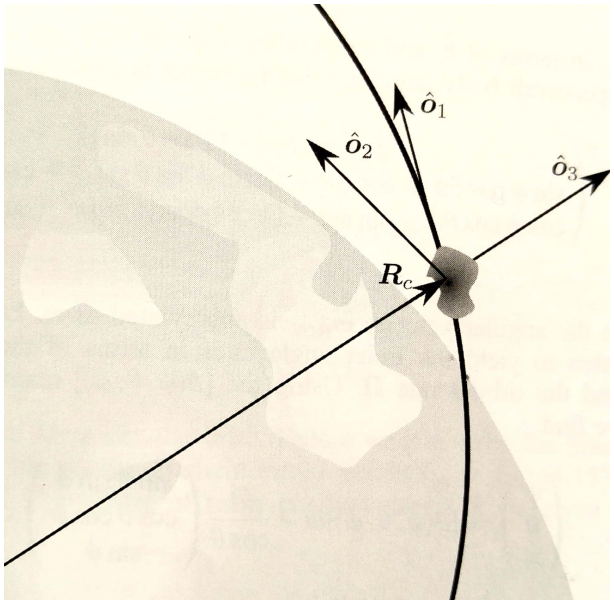

Figure 4.2: Orbit frame axes, Figure from Schaub.[65]

All three stability conditions are shown in Fig. 4.3. The unstable regions are shaded while the stable regions I and II are white.

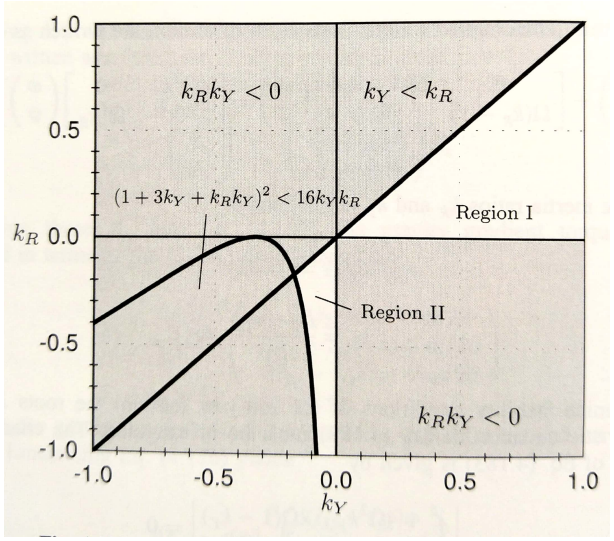

Figure 4.3: Orbit frame axes, Figure from Schaub.[65]

The linearised analysis of the gravity gradient torque only guarantees neutral stability of the linearised system. In Fig. 4.3 region I is the only truly stable region. Region II is unstable if damping effects are included.[67] The stability conditions Eq. (4.17)

and (4.18) can be written in terms of the moments of inertia as:

$$I_2 \geq I_3 \geq I_1 \tag{4.20}$$

This condition means that the spacecraft must be rotating around its maximum moment of inertia at the orbit rate with its minimum axis aligned with the gravity field as it orbits the Earth, and the intermediate axis along the direction of travel. Whether or not the different SPS designs satisfy this condition is stated in Table 4.1.

Table 4.1: Stability analysis for SPS in circular orbits subject to gravity gradient torque.

	Sun-Tower	Cylindrical	Tethered
I_{min}[kgm^2]	2.0319×10^{15}	3.6317×10^{13}	1.205×10^{13}
I_{int}[kgm^2]	1.694×10^{16}	2.3848×10^{14}	1.010×10^{14}
I_{max}[kgm^2]	1.695×10^{16}	2.5133×10^{14}	1.017×10^{14}
$\boldsymbol{I}_2$[kgm^2]	$\begin{bmatrix} I_{min} & 0 & 0 \\ 0 & I_{int} & 0 \\ 0 & 0 & I_{max} \end{bmatrix}$	$\begin{bmatrix} I_{int} & 0 & 0 \\ 0 & I_{max} & 0 \\ 0 & 0 & I_{min} \end{bmatrix}$	$\begin{bmatrix} I_{min} & 0 & 0 \\ 0 & I_{int} & 0 \\ 0 & 0 & I_{max} \end{bmatrix}$
$I_2 \geq I_1 \geq I_3$	$\surd$	$\times$	$\surd$
k_R	0.0049	-0.9016	0.0539
k_Y	0.8806	-0.8044	0.8872
Condition 1	$\surd$	$\times$	$\surd$
Condition 2	$\surd$	$\surd$	$\surd$
Condition 3	$\surd$	$\surd$	$\surd$

The neutrally stable region II corresponds to having $I_2 < I_1$ and $I_2 < I_3$, i.e. the spacecraft spinning about its minimum axis of inertia which is a maximum kinetic energy state. With damping, this will degrade to a pure spin about the maximum axis of inertia.[67] Therefore gravity gradient satellites are typically long and skinny structures rotating about the maximum axis of inertia with the minimum axis of inertia aligned with the Earth pointing direction.

Both the Tethered and Suntower SPS's satisfy the stability conditions and hence are linearly stable to the gravity gradient torque. The Cylindrical SPS is shown to be unstable in its proposed configuration. Despite the low attitude fuel costs associated

with the Cylindrical SPS (see Table 4.4), this is not a stable attitude orientation. The Sun Tower and Tethered SPS both have low attitude control costs and are linearly stable to gravity gradient torque and therefore appear more attractive from an attitude dynamics perspective. Both can be operated in GEO or GLPO with virtually no fuel required for attitude control thrusting.

Importantly, both of these gravity gradient SPS can operate in GLPO with nominal fuel required for both orbit and attitude control. Thus they offer linearly stable and near propellant-less SPS structures.

Some SPS designs are sun-pointing and cannot be configured in the gravity gradient orientation. We consider one such SPS further, the Abacus SPS.

4.6 System Properties

4.6.1 Abacus Solar Power Satellite - Geometry and Mass Distribution

The Abacus SPS is chosen for this study due to its well documented[16] geometry and mass distribution properties (see Appendix B for the Abacus mass breakdown). It is an example of a Type I SPS. It consists of three major components: a large solar array, a transmitting antenna, and an Earth-pointing reflector that moves relative to the solar array. The dimensions and configuration of Abacus are indicated in Fig. 4.4. It is important to note that the transmitting antenna is fixed to the solar array, whereas the reflector is fastened to the solar array with two rotational joints that allow the reflected microwave beam to be pointed at a particular point on the Earth's surface. The first of these is an azimuth roll-ring that permits rotation once per orbit about the solar-array pitch axis, nominally perpendicular to the Earth's equatorial plane, and the second is a set of ballscrew activated links that change the tilt of the reflector. For a SPS in GEO, this may be set to a constant offset so that the beam can be aimed at different latitudes depending on the location of the ground receiving station. For the GLPO with it's inclination of 7.5°, the tilt of the reflector will need

to be varied throughout one orbit by a maximum of $\beta \sim 1.5^\circ$ according to Fig. 3.11 (assuming power delivery to an equatorial location).

The mass of each major component along with the total mass of the SPS are given in Table 4.2. As noted by Wie and Roithmayr,[16] the reflector's mass and inertia may be neglected in the attitude analysis as it constitutes less than 4% of the total mass. This allows the Abacus SPS to be treated as a single body rather than a multibody spacecraft. When the Abacus SPS is regarded as a rigid single body, the spacecrafts moments and products of inertia for a set of axes fixed in the solar array do not vary with time. Additionally, when the asymmetrical mass distribution of the reflector is omitted, the principal axes of inertia of the spacecraft with respect to the spacecrafts mass center are parallel to the roll, pitch, and yaw axes illustrated in Fig. 4.4. The moments of inertia for these axes may therefore be considered as the principal moments of inertia and are given in Table 4.2.

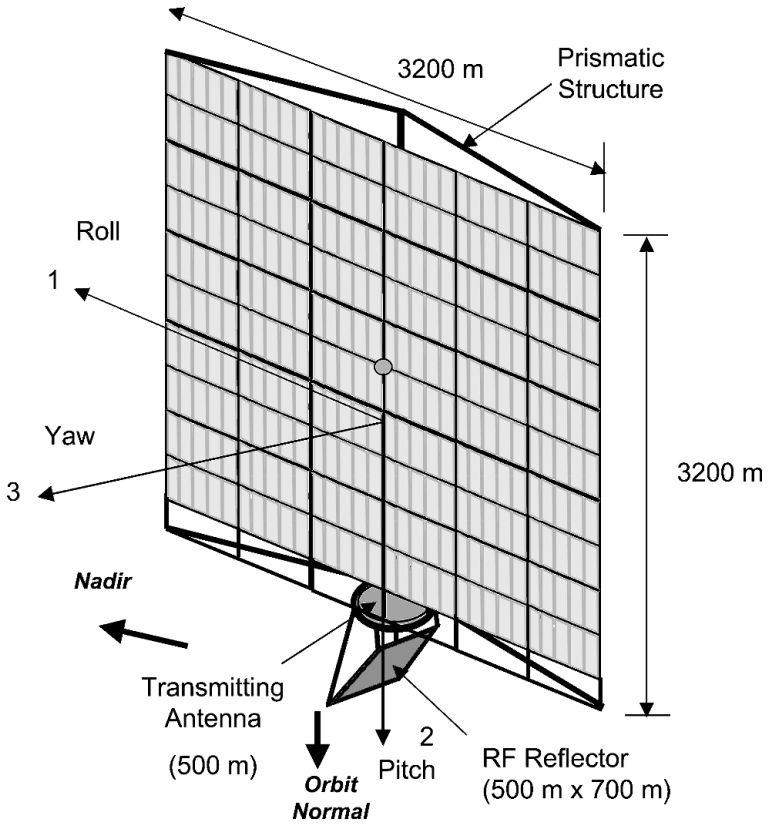

Figure 4.4: Abacus SPS configuration.[40] Figure from Wie and Roithmayr.[16]

Table 4.2: Mass properties for 1.2-GW Abacus SPS as given by Wie.[16]

Parameter	Value
Solar array mass	21×10^6 kg
Transmitting antenna mass	3×10^6 kg
Reflector mass	0.8×10^6 kg
Total mass	$M_2 = 25 \times 10^6$ kg
Roll inertia	$I_{2xx} = 2.8 \times 10^{13}$ kg.m^2
Pitch inertia	$I_{2yy} = 1.8 \times 10^{13}$ kg.m^2
Yaw inertia	$I_{2zz} = 4.6 \times 10^{13}$ kg.m^2

4.6.2 Reference Attitude Orientation

To maintain the sun-pointing of the large solar array, the SPS must rotate counter-clockwise at a rate of 1°/day about the pitch axis which is perpendicular to orbit plane (POP). North-south tracking of the sun by the SPS solar array is not considered here, instead the SPS solar array may be oversized slightly to account for losses due to variation of the solar beta angle.

4.7 Attitude Evolution

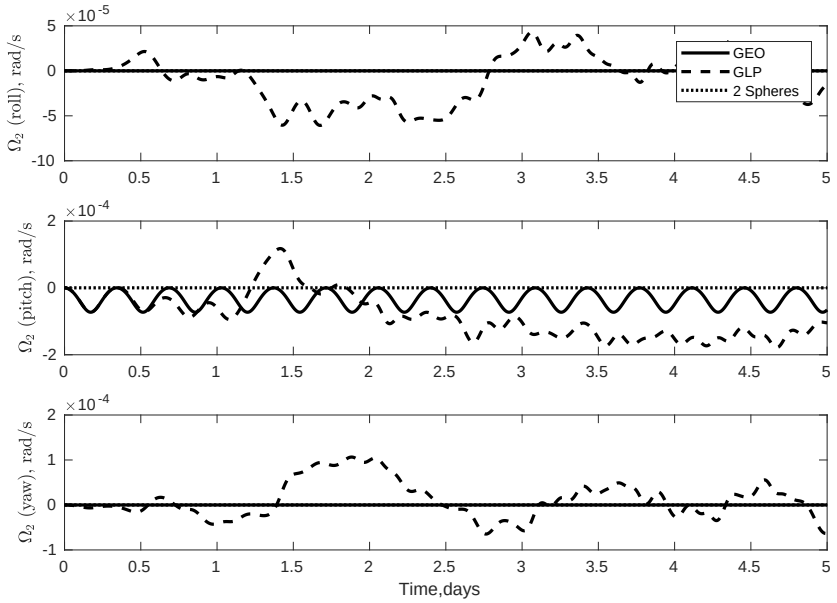

Figure 4.5: Angular velocity for Abacus POP. Where the dotted line is not visible it is coincident with the GEO case.

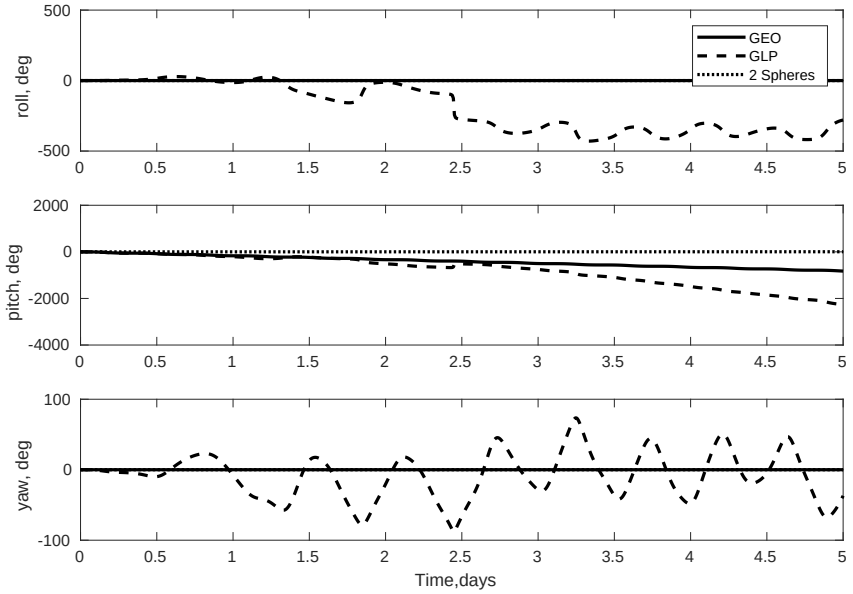

Figure 4.6: Euler angles for Abacus POP.

The angular velocity and attitude evolution are shown in Fig. 4.5 and 4.6 respectively. To illustrate the desired attitude, the inertia dyadics of both the Earth and the SPS are set to represent spherical mass distributions. This is labelled as the '2 Spheres' case, which involves a change in only the pitch angle of 1°/day.

Considering only the rotation around the pitch axis, for both the GEO and GLPO the attitude of the SPS diverges from the reference attitude by more 90° in the pitch axis in less than 1 orbit. This is due to the torque induced about the SPS center of mass, as described by Eq. (4.15) and labelled as 'pitch torque' in Fig. 4.7. This implies that if the attitude were left uncontrolled, the SPS would suffer high losses due to no longer pointing at the Sun. It would completely lose power beyond 90° as only one face of Abacus is covered with solar arrays. This confirms that the attitude must be actively controlled for the Abacus SPS to be a useful resource. For GEO, the pitch angle continues to increase at the same rate while the roll and yaw angles remain at zero. The torque acts solely around the pitch axis for the GEO case.

4.8 Gravity Gradient Torque Cancellation

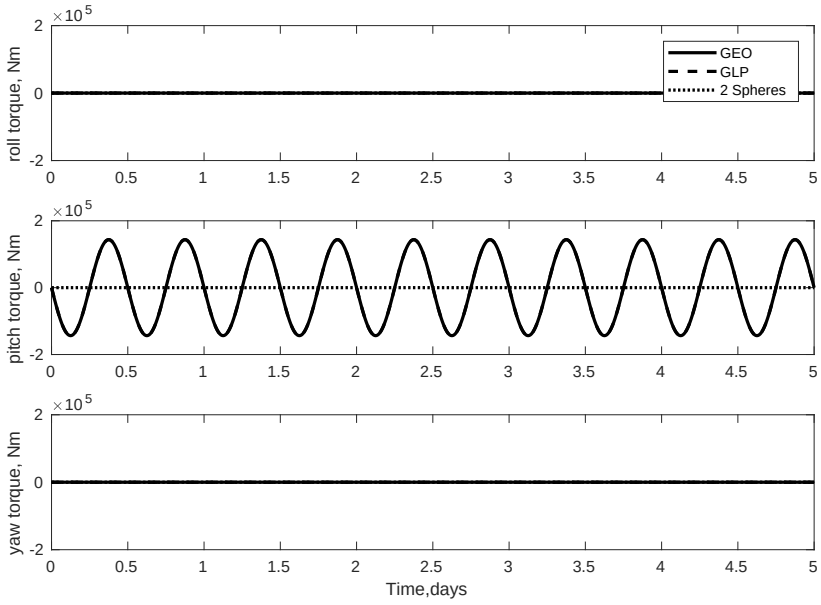

Figure 4.7: Torque acting on Abacus POP.

The variation of the torque acting on the SPS is shown in Fig. 4.7. Clearly the largest torque acting is the gravity gradient torque about the pitch axis. It is a cyclic disturbance torque with a peak value of approximately 143,000 Nm, which is in agreement with Wie and Roithmayr[16] for the Abacus SPS. This is too large to be dealt with using conventional momentum storage devices. Instead electric ion thrusters should be used.

The average force, F_{Thrust}, that must be provided by thrusters to cancel the gravitational torque is determined from the torque on body 2, $\boldsymbol{T}_2^{(2)}$, by dividing by each component by the relevant moment arm. It is assumed that the thrusters are placed at the location which maximises the moment arm. The fuel required to cancel out the gravitational torque over a given period of time Δm_{AC} may be calculated as follows:

$$\begin{aligned} \frac{dm}{dt} &= \frac{F_{Thrust}}{I_{sp} g_0} \\ \int dm &= \frac{F_{Thrust}}{I_{sp} g_0} \int dt \\ \Delta m_{AC} &= \frac{F_{Thrust} t}{I_{sp} g_0} \end{aligned} \tag{4.21}$$

where an $I_{sp} = 3000s$ is assumed, $g_0 = 9.8m/s^2$. Table 4.3 shows the fuel requirements for cancellation of gravitational torques per year for the Abacus SPS in GEO and GLPO. Also shown are the average forces required. Use of present day electric ion thrusters would require a large number of thrusters to produce the necessary force. For example, for the control system proposed by Wie and Roithmayr for Abacus[16] they calculate 500 1N thrusters would be necessary, however, the electric ion thrusters with the capabilities they assumed still do not exist. The highest performance electric ion thrusters to the author's knowledge are NASA's Evolutionary Xenon Thrusters (NEXT)[68] which are capable of 236 mN thrust requiring 6.9 kW. Approximately 2000 of these would be required for an equivalent control system. Wie[16] also makes the point that worldwide production (in 2005) of Xenon was only $40,000$ kg.

Table 4.3: GEO vs GLPO comparison.

Orbit	GEO	GLPO
F_{Thrust} (N)	60	60
Δm_{AC} (kg/yr)	61,445	61,445
NS station-keeping (kg/yr)	32,000	~ 0
Maximum Collector loss (%)	8.2 %	3.8 %
Average Rectenna Loss (%)	~ 0 %	1.4 %

4.9 SRP Torque Cancellation

A calculation of the fuel required to offset the SRP torque for each SPS design is given in Table 4.4. The method used to estimate the fuel required to offset the SRP torque is given below. The force due to SRP acting on the SPS is given by Wie[16] as:

$$F_{SRP} = P(1+\rho)A_{cs} \tag{4.22}$$

where $P = 4.5 \times 10^{-6}$ N/m^2 is the nominal SRP constant, ρ is the overall surface reflectance (0 for a blackbody and 1 for a mirror), and A_{cs} is the cross-sectional area with respect to incoming sunlight. This force imparts a torque, $\boldsymbol{\tau}_{SRP}$ on a body when there is an offset between the centre of mass (COM) and centre of pressure (COP), $\boldsymbol{r}_{MP}$:

$$\boldsymbol{\tau}_{SRP} = \boldsymbol{F}_{SRP} \times \boldsymbol{r}_{MP} \tag{4.23}$$

The force required to cancel this torque can be calculated using the moment arm r_{arm} of the specific SPS for generating a counter-torque around the appropriate axis:

$$F_{control} = \tau_{SRP}(avg)/r_{arm} \tag{4.24}$$

Although the SRP torque is higher for SPS than normal spacecraft, SPS also have much larger moment arms available to counteract the torque, hence the $F_{control}$ is generally < 1N. The fuel required to cancel out the SRP torque over a given period

of time may be calculated as follows:

$$\begin{aligned} \frac{dm}{dt} &= \frac{F_{control}}{I_{sp}g_0} \\ \int dm &= \frac{F_{control}}{I_{sp}g_0} \int dt \\ \Delta m_{AC,SRP} &= \frac{F_{control}t}{I_{sp}g_0} \end{aligned} \tag{4.25}$$

where an $I_{sp} = 3000s$ is assumed, and $g_0 = 9.8m/s^2$. Table 4.4 shows the results for cancelling SRP torque for 1 year for various SPS designs.

The Abacus SPS is the only one that we can assume has a constant cross sectional area with respect to the sun, as it is the only sun-pointing design. The other designs considered have a varying cross-sectional area. In this analysis this has been averaged for each design over the course of 1 year. It was also necessary to account for the variations in the distance between the centre of mass (COM) and the centre of pressure (COP) which affects the moment arm of the SRP disturbance torque.

This simple SRP torque calculation is also not valid for multi-body SPS with rotating reflectors, such as ISC and the Sandwich SPS, therefore they are not included in this analysis.

4.10 Comparison of SPS Designs

Of the 30 or so SPS designs, many are not well enough defined to calculate their principle moments of inertia for this comparing the attitude dynamics. The method of this chapter assumes a rigid single body for the Abacus SPS. Therefore we are limited to SPS which we can reasonably treat as a single body to perform the same attitude control calculations, and those for which detailed mass properties are available in the literature.

SPS such as the sandwich SPS and ISC cannot be treated with this method as they consist of multiple bodies, i.e. a transmitting antenna/photovoltaics assembly

linked to large rotating reflectors by a boom. Detailed analysis of the ISC attitude control accounting for the effects of body structural flexibility, gravitation and solar radiation pressure disturbances was performed by Glaese and McDonald.[19] Their detailed model found that a fuel mass of $\Delta m_{AC}(\text{Total}) = 111{,}244$ kg/yr was required for attitude control. They also calculated the orbit station-keeping requirements at 132,337 kg/yr, which is similar to our result for ISC in Chapter 3 of 162,800 kg/yr (the difference is mostly due to different values of I_{sp}). Glaese notes that their propellant calculations take no advantage of the opportunity to combine orbit and attitude control thrusting and that 'it is probable that most or all of the station-keeping force could be combined with attitude and pointing control.' This is also assumed by Wie and Roithmayr in their study of Abacus.[16]

The model of this chapter was applied to the Sun tower, Cylindrical, and Tethered SPS designs. The results of this analysis are presented in Table 4.4. The Abacus SPS has the largest attitude control costs. The Sun-Tower and Tethered SPSs are both intentionally designed to take advantage of the gravity gradient torque for stabilisation. The Cylindrical SPS is purposely made near axi-symmetric specifically to minimise the gravity gradient torque. Hence, these latter 3 designs exhibit near zero fuel requirements for cancelling gravity gradient torque. Cancelling the SRP disturbance torque is also shown to require a very small amount of fuel relative to the masses of the SPSs ($< 1\%$ of the overall SPS mass for 30 years of fuel supply). It is also shown that the GLPO actually reduces attitude control costs compared to GEO when the SRP torque is considered.

Table 4.4: Attitude control costs of SPS in GEO/GLPO for gravity gradient (GG) and solar radiation pressure (SRP). The mass properties and moment arms for each SPS are given.

	Abacus	Sun-Tower	Cylindrical	Tethered
Mass[kg]	2.500×10^7	6.160×10^7	6.600×10^7	2.000×10^7
I_{min}[kgm^2]	1.800×10^{13}	1.415×10^{12}	3.632×10^{13}	1.205×10^{13}
I_{int}[kgm^2]	2.800×10^{13}	1.694×10^{16}	2.385×10^{14}	1.010×10^{14}
I_{max}[kgm^2]	4.600×10^{13}	1.695×10^{16}	2.513×10^{14}	1.017×10^{14}
$\boldsymbol{I}_2$[kgm^2]	$\begin{bmatrix} I_{max} & 0 & 0 \\ 0 & I_{int} & 0 \\ 0 & 0 & I_{min} \end{bmatrix}$	$\begin{bmatrix} I_{min} & 0 & 0 \\ 0 & I_{int} & 0 \\ 0 & 0 & I_{max} \end{bmatrix}$	$\begin{bmatrix} I_{int} & 0 & 0 \\ 0 & I_{max} & 0 \\ 0 & 0 & I_{min} \end{bmatrix}$	$\begin{bmatrix} I_{min} & 0 & 0 \\ 0 & I_{int} & 0 \\ 0 & 0 & I_{max} \end{bmatrix}$
r_x[m]	2263	260	3335	1769
r_y[m]	1600	28838	3335	1200
r_z[m]	1600	28839	750	1300
$\boldsymbol{\Omega_2}(t_0)$[rad/s]	[0 0 2π/1 yr]	[0 0 2π/1day]	[0 0 2π/1day]	[0 0 2π/1day]
COM-COP [m]	200	369	300	217
F_{SRP}[N]	60	101	55	35
GEO				
Δm_{AC}(GG) [kg/yr]	61,445	470	0	8
Δm_{AC}(SRP) [kg/yr]	7,371	499	2,631	1,570
Total [kg/yr]	68,816	969	2,631	1,578
30 yr fuel as % of M_{sps}	8.26	0.05	0.12	0.24
GLPO				
Δm_{AC}(GG) [kg/yr]	61,445	470	0	8
Δm_{AC}(SRP) [kg/yr]	7,726	345	1,861	1,059
Total [kg/yr]	69,171	815	1,861	1,067
30 yr fuel as % of M_{sps}	8.30	0.04	0.09	0.16

The attitude control fuel costs do not necessarily render any of the SPS designs considered as infeasible in the future. However, we consider present day technology, then the Abacus and the ISC SPS are not feasible. Abacus and ISC (see Glaese[19]) have the highest percentage of its overall mass required of fuel for attitude control. Abacus requires 8.3% of its overall mass for a 30 year supply of propellant, while ISC requires 19.6%.[19] This is not unrealistic from a mass point of view (if it is economically feasible to launch a SPS with mass of the order 10^7kg, then launching that amount of fuel is not unreasonable). However, it would require significant engineering to store the large mass of propellant required to supply control over an SPS lifetime. Storage of this mass of propellant has never been attempted before. Alternatively, a refuelling strategy would need to be devised, adding additional engineering issues and risk.

4.11 GEO vs GLPO: Orbit and Attitude Dynamics

In both the GEO and GLPO case the primary torque is the cyclic gravity gradient pitch torque. No additional fuel is required in GLPO compared to GEO as shown in Table 4.3. This is an important result which suggests that there is no attitude

dynamics penalty for locating Abacus SPS in GLPO compared to GEO.

For the Abacus design, as with all SPS designs, the high area to mass ratio of the SPS causes an orbital perturbation due to solar radiation pressure. This SRP perturbation causes a yearly oscillation in eccentricity and hence, an oscillation of 2.5° in longitude (see Sec. 3.11), which must be controlled in GEO. Coincidentally, the force of the SRP perturbation (60 N) for Abacus[16] is approximately equal to the average value of force required to cancel the pitch gravity gradient torque (given the maximum moment arm of Abacus), see Table 4.3. Therefore, Wie[16] considers applying the SRP cancellation force in a cyclic manner to achieve pitch control at essentially no extra cost. This suggests that the geometry of any SPS design for operation in GEO should be adjusted so that the thrust for controlling gravity gradient is equal to the thrust required for SRP orbit control.

Attitude control is essential for both GEO and GLPO. East-west station-keeping is also necessary, although this represents a relatively small fuel cost, especially for SPS near the stable longitude points. It will also be approximately equivalent in GEO or GLPO depending on the chosen longitude and therefore it is not considered here. For GLPO the SRP orbit control is not strictly necessary (see Sec. 4.3). As neither North-South station-keeping or SRP cancellation is required for GLPO, the fuel costs reduce down to what is required for attitude control.

For the Abacus SPS, when both orbit and attitude control are taken into consideration, GLPO has lower fuel requirements overall by approximately 32,000 kg/yr. Over a 30 year lifetime the Abacus SPS in GLPO requires 8.3% of it's overall mass in fuel*. This is entirely for attitude control (orbital control costs are near zero). In GEO, Abacus requires 18.5% of it's overall mass in fuel, which includes the North-South station-keeping essential to maintain GEO, and attitude/SRP orbit control. The GLPO solar collector losses are lower than in GEO due to the fact that the GLPO is nearer to the ecliptic plane. Thus the cosine losses for the solar array are

*Fuel mass(%)=Fuel mass/(M_{sps} + Fuel mass) for a 30 year lifetime

lower in GLPO over the course of the year as the solar beta angle varies. GLPO incurs additional losses due to non-zero incidence angle of the beamed power on the rectenna on the ground. This is due to the SPS not being fixed directly overhead as it is for GEO. If an equatorial rectenna is assumed, the average loss in power received is relatively low for GLPO. The greater solar collector losses in GEO are approximately balanced out by the additional rectenna losses from GLPO. SPS in GLPO experiences approximately a day and a half more eclipse time annually than SPS in GEO. Once these factors are accounted for both orbit options offer approximately equivalent power delivery.

Once the attitude control issue is considered alongside the orbit control costs, the fuel savings for Abacus POP in GLPO are significant compared to Abacus POP in GEO.

It is likely that the decision to place a SPS in GEO or GLPO will also come down to other factors as well. For instance, the intended location of the power delivery on the Earth's surface is important. As stated by Ogilvie, for delivering power to higher latitudes, locating the SPS in GLPO requires an increased rectenna size (13.9% larger for 34° latitude[39]) incurring higher costs as a result. Hence, GLPO is more suited to delivering power to lower latitude regions.

With the Abacus design in GLPO there is also the added complexity of having to vary the tilt of the microwave reflector throughout the orbit to maintain the power delivery. As such, GLPO is more suited to a retro-directive phased array transmitting antenna system.[69] Such a system allows electronic beam steering without the need for mechanical pointing of the transmitting antenna.

4.12 Modification of the Mass Distribution and Attitude Orientation

In this section the benefits of modifying the mass distribution of the Abacus SPS and the attitude orientation are considered.

GLPO will offer greater savings for SPSs which can minimise the pitch gravity

gradient torque through inertia balancing, i.e. designing the SPS to minimise ($I_{2xx} - I_{2yy}$), see Eq. (4.14). For instance, if we set $I_{2xx} = I_{2yy}$, then the pitch torque is zero for both GEO and GLPO. This is referred to as 2 dimensional inertia balancing (2-DIB) by Ogilvie[70] and may be achieved simply by altering the dimensions of the solar array. Alternatively, the cylindrical SPS design (see Fig. 3.1(a)) may be used, which naturally has $I_{2xx} = I_{2yy}$.

Gravity gradient stabilised SPS designs, such as the Sun Tower SPS take advantage of the pitch gravity gradient torque rather than trying to minimise it.

To instead rotate around the maximum moment of inertia of the SPS, the SPS solar array may be oriented in the orbital plane (IOP). The angular velocity of the SPS is in this case $\Omega_2 = [0\ 0\ n]$, where n is the orbital rate. Consequently the transmitting antenna is Earth-pointing, removing the need for the microwave reflector. With the large solar array IOP, a system of solar reflectors would be necessary to redirect the Sun's rays onto the surface of the solar array. The reflector system would impart a torque unless a symmetrical design is utilised. The design and analysis of a reflector system is not considered here but shall be addressed in future work. In this orientation the SPS with 2-DIB in GLPO could operate virtually propellant-less.

For SPS in GEO with 2-DIB and oriented IOP, the gravitational torque also disappears entirely. However, the SRP orbit perturbation must still be controlled for GEO in addition to the NS station-keeping, which would remain unchanged. The SRP orbit perturbation may be more complex due to the interaction with the reflector system. However, it is likely to be more costly to control due to the higher reflectivity of the solar reflector system. Therefore, an IOP SPS in GEO with 2-DIB does not appear to offer significant fuel savings overall.

Another advantage of the IOP SPS orientation is that a retro-directive phased array antenna could be used with no need for movement/rotation between the antenna and solar array. Also, the solar arrays would be approximately edge on to the solar wind, minimising damage from micro-meteorites and increasing the solar array life-

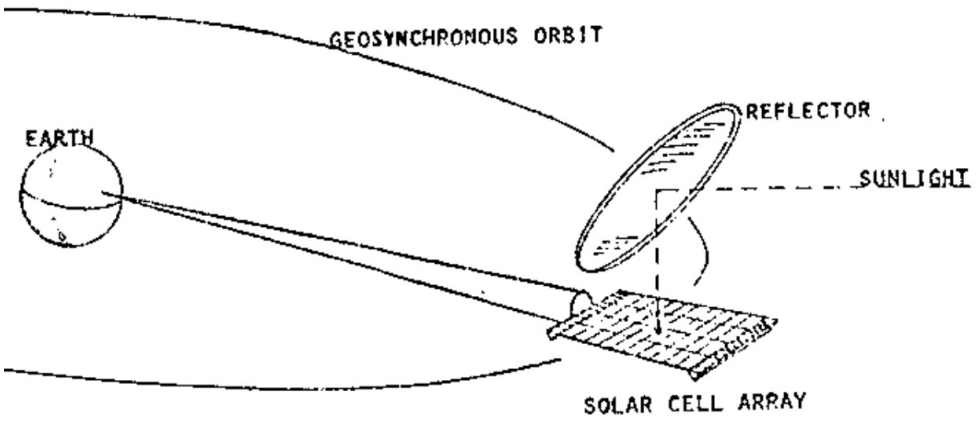

Figure 4.8: Gravity gradient stabilised SPS, original figure from Bowden.[71]

time. The idea of orienting the solar arrays IOP has been proposed before by Bowden in 1981[71] (see Fig. 4.8) and was referred to as a gravity gradient stabilised SPS. That study assumed the use of a large monolithic free-flying reflector to maintain illumination of the solar arrays. Instead, a modular reflector system attached to the main solar array could be designed.

4.13 Orbit-Attitude Coupling

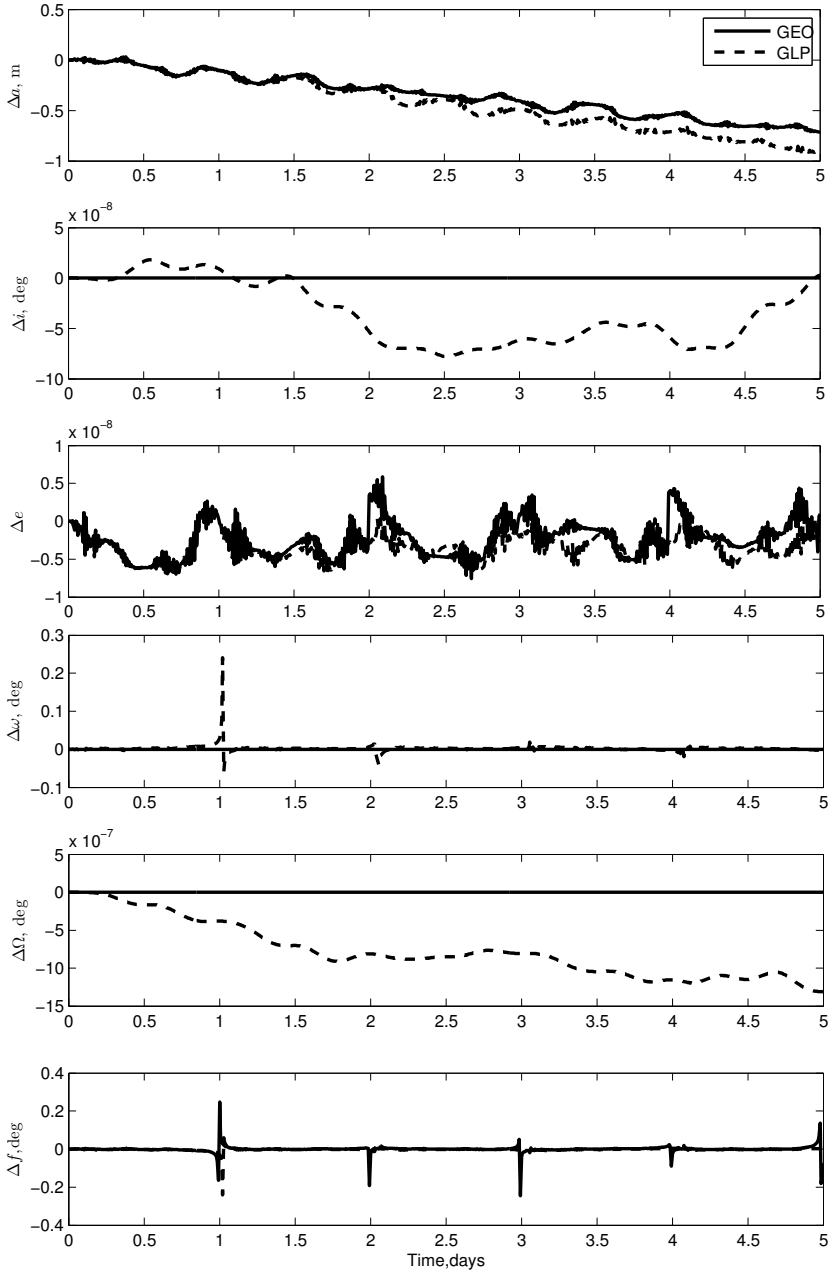

Figure 4.9: Differences between coupled and uncoupled orbital elements for both GEO and GLPO.

In considering the orbital and attitude motion of a satellite orbit about an attracting body, it is normal practice to assume that the orbit is Keplerian and then the attitude is studied separately. For purely gravitational interactions these motions are generally

assumed to be uncoupled. In fact there is always weak gravitational coupling between the two, such that a change in attitude will perturb the orbit and vice versa. For a normal sized spacecraft orbiting the Earth, treating the two independently is a reasonable assumption. However, as stated by Sincarsin and Hughes,[72] the magnitude of this coupling is governed by the spacecraft's mass distribution and orientation, and its size relative to its orbit radius. Hence, for SPS scale spacecraft it is worthwhile to examine the effect of the coupling. Therefore the coupling between orbit and attitude motion is fully accounted for by the model used here. We are only considering gravitational attraction between the two body's (no other disturbances are considered at this stage).

To examine the effect of the attitude on the orbital elements the coupled case is compared with the uncoupled case. For the uncoupled case, the right hand side of Eq. (4.2) is set equal to zero. Fig. 4.9 shows the differences in orbit elements between the coupled and uncoupled cases for both GEO and GLPO.

For the GEO case, the coupling of attitude into the orbit causes changes in the in-plane orbit elements: semi-major axis a, eccentricity e, argument of perigee ω, and true anomaly f. The GLPO case also experiences variation in the out-of-plane orbit elements inclination i, and right ascension of the ascending node Ω.

Measurable variations in the orbit parameters are observed when the gravitational coupling between the attitude and orbit dynamics is accounted for (see Fig. 4.9). The orbital perturbations observed are too small to indicate a serious control problem, however, they would need to be considered in the operation of a SPS. For the investigations of the dynamics of SPS designs at an early research stage it is reasonable to decouple the equations of motion.

4.14 SPS Flexibility

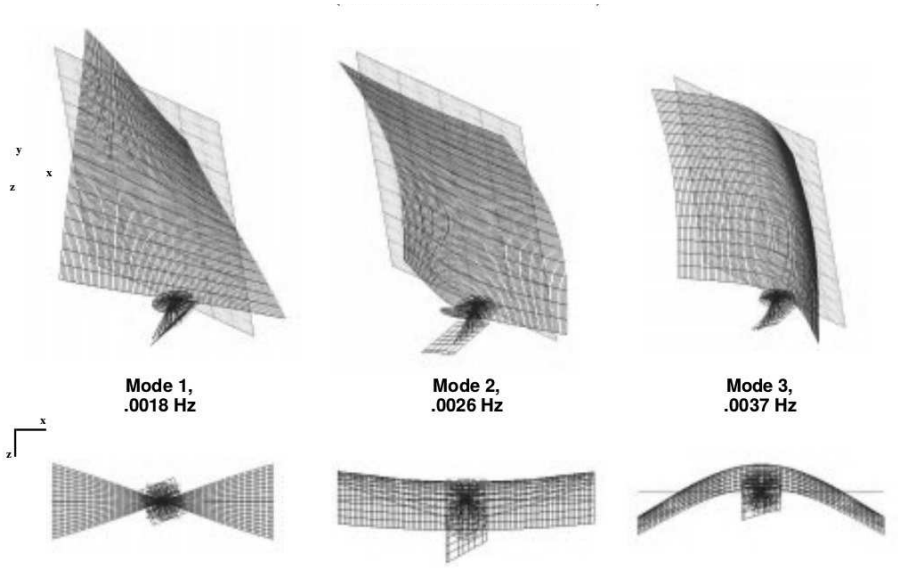

Figure 4.10: Abacus modes of vibration, original Figure Tim Collins at NASA LaRC.

In the case where the gravity gradient torque is cancelled by continuous control thrusting, for Abacus, we still are left with a body rotating around its minimum axis of inertia (see Sec. 4.6.2). SPS are designed to be built in space and therefore do not need to be structurally rigid. The natural modes of vibration of the Abacus structure are shown in Fig. 4.10. Wie[16] discussed the issue in terms of developing a controller that avoids exciting these modes by avoiding exciting the natural frequencies (first three modes are noted in Fig. 4.10). However, the issue of maintaining a large flexible structure in a minimum inertia axis spin does not appear to have been considered in the literature. The flexible nature of the structure provides an obvious route for energy to be dissipated. Thereby one would expect that over time the Abacus SPS would start to tumble and dissipate energy before settling in a major inertia axis spin. In the subsequent chapter this issue is addressed by constructing a model for energy dissipation and using it to investigate the dynamics of the Abacus SPS in geosynchronous orbits with both energy dissipation and gravity gradient acting.

The interaction of the gravity gradient force and the SPS structure (or any struc-

ture on the scale of SPS) is a complex issue that has been treated in the literature recently by Liu et al.[73] and Zhao et al.[74] for the ISC and a general flat plate structure (similar to Abacus), respectively. Liu et al. show that the vibration frequencies of the SPS change with the pitch angle under the effect of gravity-gradient force. For the ISC some interesting behaviours are observed when the fundamental structural mode of the SPS is close to the orbital angular velocity. For example, a buckling instability of the structure was found to occur at a certain range for the pitch angle. They propose a structural stiffness design criteria for the ISC to avoid this instability.

For satellites of a more normal size than SPS, the impact of the gravity-gradient force on the flexible structure is often neglected. This simplification was also made for early SPS studies whereby the structural vibration was either treated using a linear model (LM)[75,76,77] or using a finite element model.[78,79] Using the LM, Glaese and McDonald[75] proposed a design for a sun-pointing control system for the ISC SPS. Zhou and Fan[77] proposed a composite control method for the vibration suppression of a tethered SPS. The vibration control of flexible structures has been studied extensively by He et al.,[80] He and Ge,[81] He and Zhang,[82] and He and Ge.[83] Using the finite element method, Ishimura et al.[78] studied the stability of the orbit and attitude dynamics of the tethered SPS, including both the gravity gradient and structural vibration.

The issue of control structure interaction is a concern with km scale platforms. For example, the Abacus SPS has a 3.2.x 3.2 km platform whose lowest structural mode is about 0.002 Hz. The dynamics and control of similar structures have been investigated in the literature extensively,[84,85,86] with active structural vibration control being a topic of continuing practical interest.[73]

Wie and Roithmayr[16] state that the most appropriate way to deal with this problem is to avoid the conditions under which it occurs in the first place, which may be achieved by employing a control bandwidth lower than 1×10^{-5} Hz in systems that control the orbit and attitude. As stated by Zhao et al.,[74] the primary challenge is

the design of control frequencies away from several major structural frequencies.

The impact of the flexibility of the SPS structure is very dependent upon the specific SPS design. The focus of this thesis is on the utility of the GLPO for SPS compared to GEO rather than focusing on detailed control design for a particular SPS. Therefore a full analysis of the flexible modes of specific SPS and all the potential related control issues has not been considered here. For an in depth analysis of the SPS flexibility related issues in the literature, for the ISC refer to Liu et al.[73] and for Type I SPS refer to Zhao et al.[74]

The assumption that the SPS's are rigid bodies has been made in this chapter in order to compare the gravity gradient and SRP torques affects on SPS in GEO vs SPS in GLPO.

5

Accounting for Energy Dissipation

> "Nearly four centuries of experience since Galileos time has shown that it is frequently useful to depart from the real and to construct a model of the system being studied; some of the complications are stripped away, so a simple and generalized mathematical structure can be built up out of what is left. Once that is done, the complicating factors can be restored one by one, and the relationship suitably modified. To try to achieve the complexities of reality at one bound, without working through a simplified model first, is so difficult that it is virtually never attempted and, we can feel certain, would not succeed if it were attempted."
>
> - Isaac Asimov

5.1 Motivation

The first principles of mechanics require that a freely rotating top must evolve to the spin state that minimises the rotational kinetic energy, for a fixed angular momentum. This spin state can be attained by adjustment of mass distribution and/or alteration of the rotation axis.

The state of rotation about the maximum inertia axis is the minimal energy state. Spin about the minimum inertia axis corresponds to the maximal energy state. A body will dissipate energy to get rid of the excessive energy and evolve towards a spin around the maximum inertia axis regardless of the initial spin state.

This process was evident in 1958 when Americas first artificial satellite Explorer I began to carry out what were at the time unexpected manoeuvres. Explorer I was a very elongated body with four flexible antennas attached. After orbit insertion, the plan was to stabilise the satellite by rotating it around its longest dimension

(i.e. minimum inertia axis). This decision was made based on the assumption that the spacecraft could be treated as a rigid body. A rigid body is stable to small perturbations about principle axis spins around the maximum and minimum moments of inertia. It is only unstable to rotations about the intermediate axis of inertia. In this case, unstable means that the amplitude of a small perturbation grows exponentially with time. For a rigid body, the solutions that start out near an equilibrium point for minimum or maximum inertia spins stay near the equilibrium point forever, i.e. they are Lyapunov stable.

However, it proved impossible to maintain the spacecraft in the desired spin state, Explorer persistently deviated from the simple rotation and went into a wobble, exhibiting slowly changing complex rotation. The rotation around the minimum inertia axis was not stable to perturbation due to energy dissipation through the flexible appendages. The rotation state was evolving toward the minimal kinetic energy state (with the angular momentum being fixed). This was an early lesson in dangers of not accounting for the effect of energy dissipation. The rigid body assumption was invalid and compromised the successful operation of the spacecraft.

In the case of SPS, the scale of the structures requires that they be constructed on-orbit. This in turn relaxes the need for strong, rigid structures to withstand launch. Therefore, the structures will be very flexible. This flexibility will necessitate the consideration of energy dissipation on the rotational dynamics. The model developed in this chapter aims to address that need and to assess the rotational dynamics of a geosynchronous SPS subject to energy dissipation and gravity gradient torque (both in GEO and GLPO).

5.2 Energy Dissipation Modeling Approaches

In Kaplan's text 'Modern Spacecraft Dynamics and Control',[87] three methods for modeling energy dissipation are summarised. These methods are the subject of the work by Likins[88] where he reviews their use in the literature and directly compares

them for a specific example of modeling rotational motion with energy dissipation.

The first is a rigid spacecraft model with an 'energy sink' incorporated. The 'energy sink' method requires that we assume the spacecraft has no moving parts which dissipate energy. In fact there must be some motion in order to cause the dissipation, however, this is ignored in the analysis and Euler's equations for rigid body motion are assumed to be appropriate. The first integral of these equations is a statement of conservation of rotational energy which cannot in fact be satisfied when dissipation is present. The argument can be made that motion over any single precession cycle is nearly the same as that of a rigid body with the same rotational energy and momenta. This argument is then applied repeatedly over each cycle with incremental reductions in rotational energy each time. This approximation is the basis of the energy sink method. The major difficulty with the energy sink method is the appropriate selection of a dissipation rate. This tends to require some physical insight, and often some empirical knowledge of the system. As the SPSs we are considering are early stage designs, it is not possible to gain the necessary empirical knowledge to ensure a feasible dissipation rate is selected. The idealised energy sink violates Newtons laws by producing changes in motion without applying forces.

The second utilises a modal model, i.e. motions are described in terms of the normal modes of deformation of a slightly flexible, lightly damped structure (i.e. stiff with high k_D and low c_D). This modeling approach requires significant modification between different SPS designs and hence has not been employed here as we wish to compare different designs.

The final method involves the modeling of dampers analytically and is referred to as the 'discrete parameter' method. This is the method that we choose to model SPS motion. The reasons for choosing this method are that it allows the building in of a mechanism for energy dissipation while also allowing external forces and torques to be incorporated, and the equations of motion allow analysis of rotational behaviour for arbitrary initial angular velocity. The discrete parameter method does have dis-

tinct disadvantages when trying to accurately model complex spacecraft structural elements which act essentially as unspecified dampers. This is mainly due to the virtual impossibility of obtaining valid empirical data on the properties of equivalent spring-dampers to mimic the structural elements correctly. However, the discrete parameter method may be used for the initial design/evaluation of SPSs as it allows a qualitative understanding of the dynamics of a system to be obtained. We are utilising it simply to provide a mechanism that dissipates energy slowly over time rather than trying to precisely model particular system elements. The symmetric configuration of spring mass dampers chosen allows the centre of mass of the system to be preserved.

5.3 Effects of Energy Dissipation

For a rotating body, vector $\boldsymbol{l}$ of the total angular momentum is proportional to the momentary angular velocity $\boldsymbol{\omega}$, but generally deviates from $\boldsymbol{\omega}$ in direction. Both vectors $\boldsymbol{l}$ and $\boldsymbol{\omega}$ have a common direction only if the body rotates about one of the three mutually orthogonal axes called principal axes of inertia. Principal axes of inertia exist for every body. For symmetrical bodies manufactured of a homogeneous material, the principal axes of inertia coincide with the axes of symmetry.

The primary effects of energy dissipation are as follows:

1. The major inertia axis of a body and its angular velocity $\boldsymbol{\omega}$ tend to align along its angular momentum $\boldsymbol{l}$.

2. A rotating body will attain its minimum energy spin state by dissipating energy. An object initially in a minor or intermediate axis spin will undergo complex rotation before evolving towards a major axis spin.

Although energy is dissipating, the magnitude and direction (with respect to an inertial reference frame) of angular momentum $\boldsymbol{l}$ is conserved in the absence of external torques. When modeling energy dissipation, any mechanism for energy dissipation

should not cause a shift in the principal axis frame so that it remains straightforward to incorporate external torques/forces.

5.4 Multiple Spring Damper Model

The method of Hughes[66] Section 3.4 may be employed whereby a mechanism for energy dissipation is incorporated into the equations of motion through the addition of a spring-mass damper (see Fig. 5.1). The method of Hughes is modified here to incorporate multiple spring mass dampers. The reason for additional dampers is that with only one damper, it is possible that the damper will remain unexcited if the spin is about the damper axis. If only a single damper were utilised (and it was aligned so that it was not parallel with any of the principal axes of the body) movement of the damper mass would also cause a shift in the principal axes frame $\mathcal{F}_p$. To preserve the principal axes frame regardless of the damper movements and have a system which is able to dissipate energy regardless of the orientation of the initial angular velocity vector, the configuration shown in Fig. 5.2 is used.

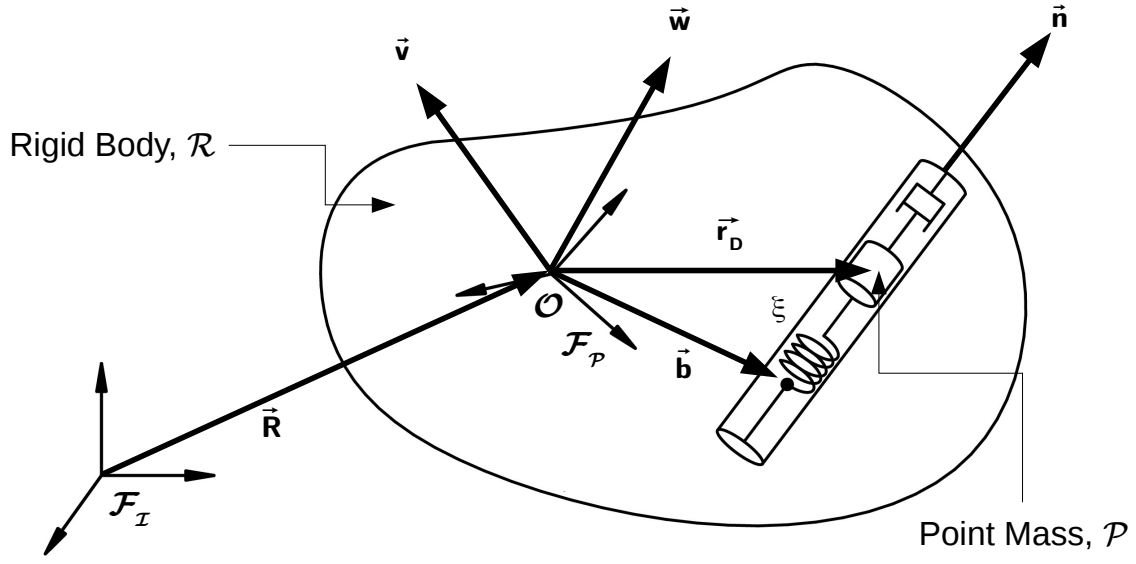

Figure 5.1: Spinning rigid body $\mathcal{R}$, with an internal point mass damper $\mathcal{P}$.

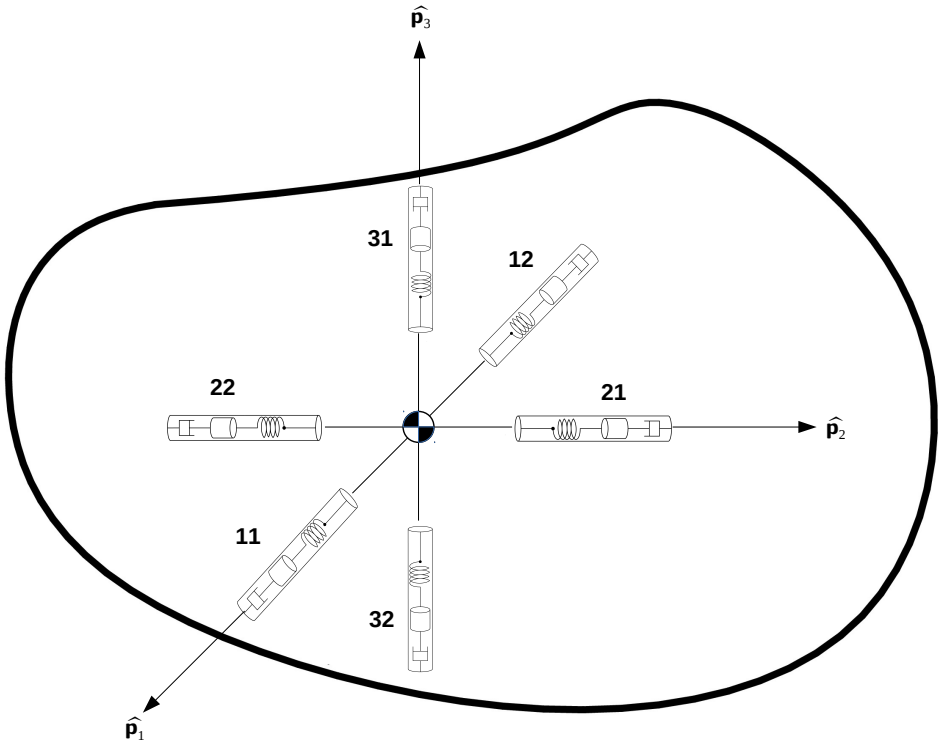

Figure 5.2: Rigid body $\mathcal{R}$, with 6 internal point mass dampers.

The rigid body $\mathcal{R}$ is augmented here to include multiple point mass dampers $\mathcal{P}_{ij}$*. Two dampers are placed symmetrically with respect to the centre of mass of $(\mathcal{R}+\mathcal{P}_{ij})$ along each principal axis. Each point mass is constrained to move in a rectilinear slot with respect to $\mathcal{R}$. The motion of this point mass is damped by a linear viscous damper (with damping constant, $c_{d,ij}$), $\mathcal{P}_{ij}$ is also connected to $\mathcal{R}$ by a linear spring (spring constant, $k_{d,ij}$). The natural modes of the SPS (for Abacus, see Fig. 4.10) may be used to obtain an approximate value to use for $k_{d,ij}$:

$$k_{d,ij} \sim 4\pi^2 f_n^2 m_{d,ij} \tag{5.1}$$

where f_n is the natural frequency, and $m_{d,ij}$ is the mass chosen for $\mathcal{P}_{ij}$. The interaction between $\mathcal{R}$ and $\mathcal{P}_{ij}$ provides a mechanism for dissipating the energy of $\mathcal{R}$. As discussed

*The indices $i = 1 \rightarrow 3$ indicates the principal axis the damper lies along; $j = 1,2$ indicates placement of the damper in the positive and negative direction respectively

earlier, the effects of energy dissipation can be crucial to the nature of the motion. The position of $\mathcal{P}_{ij}$ with respect to $\mathbf{0}$ is given by:

$$\underset{\rightarrow}{\boldsymbol{r}}_{d,ij} = \underset{\rightarrow}{\boldsymbol{b}}_{ij} + \xi_{ij}\,\underset{\rightarrow}{\hat{\boldsymbol{n}}}_{ij} \tag{5.2}$$

where $\xi_{ij} = 0$ corresponds to a relaxed spring with position vector $\underset{\rightarrow}{\boldsymbol{b}}_{ij}$, and the unit vector $\underset{\rightarrow}{\hat{\boldsymbol{n}}}_{ij}$ defines the direction of $\mathcal{P}_{ij}$'s travel ($\underset{\rightarrow}{\hat{\boldsymbol{n}}}_{ij} \cdot \underset{\rightarrow}{\hat{\boldsymbol{n}}}_{ij} = 1$). The masses of $\mathcal{R}$ and $\mathcal{P}_{ij}$ are respectively, m_b and $m_{d,ij}$, therefore the total system mass is:

$$m = m_b + \sum_{i,j=1}^{3,2} m_{d,ij} \tag{5.3}$$

In total 6 dampers are added as illustrated in Fig. 5.2 to provide a fully 3 dimensional mechanism for energy dissipation. The first and second moments of inertia of the system with respect to $\mathbf{0}$ are:

$$\underset{\rightarrow}{\boldsymbol{c}}(t) = \underset{\rightarrow}{\boldsymbol{c}}_b + \sum_{i,j=1}^{3,2} m_{d,ij}\,\underset{\rightarrow}{\boldsymbol{r}}_{d,ij} \tag{5.4}$$

$$\underset{\rightarrow}{\boldsymbol{J}}(t) = \underset{\rightarrow}{\boldsymbol{J}}_b + \sum_{i,j=1}^{3,2} m_{d,ij}(r_{d,ij}^2\,\underset{\rightarrow}{\boldsymbol{U}} - \underset{\rightarrow}{\boldsymbol{r}}_{d,ij}\,\underset{\rightarrow}{\boldsymbol{r}}_{d,ij}) \tag{5.5}$$

where $\underset{\rightarrow}{\boldsymbol{U}}$ is the identity matrix and $\underset{\rightarrow}{\boldsymbol{c}}_b$ and $\underset{\rightarrow}{\boldsymbol{J}}_b$ are the first and second moments of inertia of $\mathcal{R}$ around $\mathbf{0}$ given by:

$$\underset{\rightarrow}{\boldsymbol{c}}_b = \int_{\mathcal{R}} \underset{\rightarrow}{\boldsymbol{r}}\,\sigma(\underset{\rightarrow}{\boldsymbol{r}})dV \tag{5.6}$$

$$\underset{\rightarrow}{\boldsymbol{J}}_b = \int_{\mathcal{R}} (r^2\,\underset{\rightarrow}{\boldsymbol{U}} - \underset{\rightarrow}{\boldsymbol{r}}\,\underset{\rightarrow}{\boldsymbol{r}})\sigma(\underset{\rightarrow}{\boldsymbol{r}})dV \tag{5.7}$$

where $\sigma(\underset{\rightarrow}{\boldsymbol{r}})$ is the mass density at position $\underset{\rightarrow}{\boldsymbol{r}}$ and dV is an element of volume at $\underset{\rightarrow}{\boldsymbol{r}}$ (see Fig. 5.3). The total mass of $\mathcal{R}$ is:

$$m_b = \int_{\mathcal{R}} \sigma(\underset{\rightarrow}{\boldsymbol{r}})dV \tag{5.8}$$

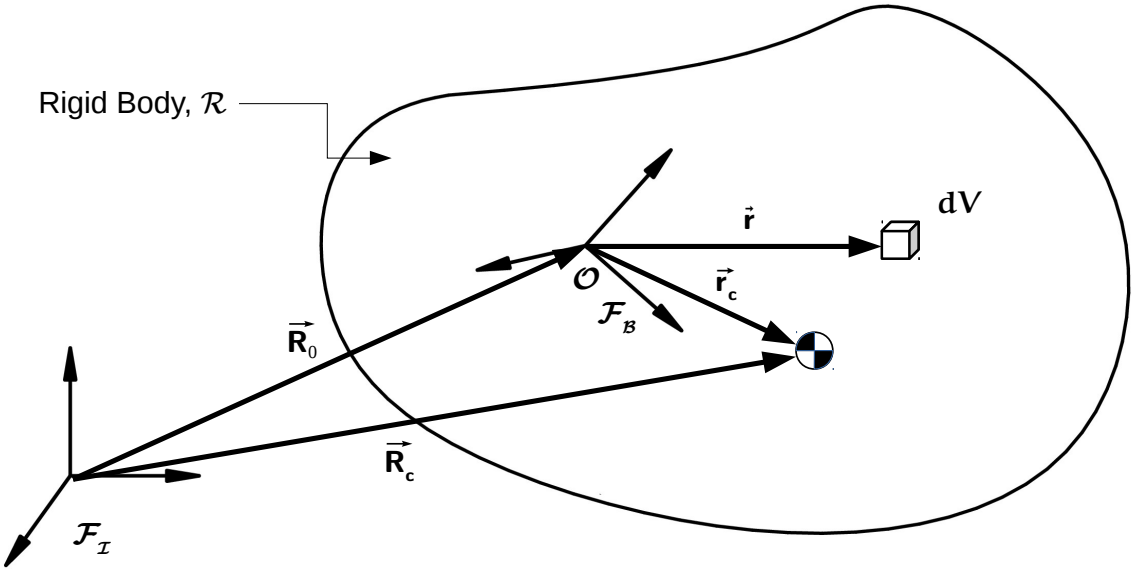

Figure 5.3: Rigid body.

We choose the centre of mass of $\mathcal{R} + \mathcal{P}_{ij}$ to be coincident with point **0**. Consequently $\underrightarrow{c}_b = \underrightarrow{c}(t_o) = 0$. The latter is true due to the choice of $\xi_{ij} = 0$ for all dampers giving an initially symmetric distribution of damper masses around the centre of mass.

5.4.1 Vectorial Motion Equations for Damped System

The absolute velocity of **0** is denoted by $\underrightarrow{v}$, while the absolute angular velocity of $\mathcal{R}$ is denoted by $\underrightarrow{\omega}$. Hence, the velocity at a point $\underrightarrow{r}$ in $\mathcal{R}$ is $\underrightarrow{v} + \underrightarrow{\omega} \times \underrightarrow{r}$ and the velocity of $\mathcal{P}_{ij}$ is $\underrightarrow{v} + \underrightarrow{\omega} \times \underrightarrow{r}_{d,ij} + \dot{\xi}_{ij}\,\underrightarrow{\hat{n}}_{ij}$. Consequently the momenta of $\mathcal{R}$ and $\mathcal{P}_{ij}$ are:

$$\underrightarrow{p}_b = \int_{\mathcal{R}} (\underrightarrow{v} + \underrightarrow{\omega} \times \underrightarrow{r}) dm = m_b\,\underrightarrow{v} + \underrightarrow{\omega} \times \underrightarrow{c}_b \tag{5.9}$$

$$\underrightarrow{p}_{d,ij} = m_{d,ij}(\underrightarrow{v} + \underrightarrow{\omega} \times \underrightarrow{r}_{d,ij} + \dot{\xi}_{ij}\,\underrightarrow{\hat{n}}_{ij}) \tag{5.10}$$

The total momenta of the system is then:

$$\underrightarrow{p} = \underrightarrow{p}_b + \sum_{i,j=1}^{3,2} \underrightarrow{p}_{d,ij} = m\,\underrightarrow{v} - \underrightarrow{c} \times \underrightarrow{\omega} + \sum_{i,j=1}^{3,2} m_{d,ij}\dot{\xi}_{ij}\,\underrightarrow{\hat{n}}_{ij} \tag{5.11}$$

For the later development of the system equations of motion we are interested in the component of $\underrightarrow{p}_{d,ij}$ along the axis $\underrightarrow{\hat{n}}_{ij}$, which we denote by $p_{n,ij}$:

$$p_{n,ij} = \underrightarrow{\hat{n}}_{ij} \cdot \underrightarrow{p}_{d,ij} = m_{d,ij}(\underrightarrow{\hat{n}}_{ij} \cdot \underrightarrow{v} - \underrightarrow{\hat{n}}_{ij} \times \underrightarrow{b}_{ij} \cdot \underrightarrow{\omega} + \dot{\xi}_{ij}) \tag{5.12}$$

Similarly, the absolute angular momentum of $\mathcal{R}$ around $\mathbf{0}$ is:

$$\begin{aligned} \underrightarrow{l}_b &= \int_{\mathcal{R}} \underrightarrow{r} \times (\underrightarrow{v} + \underrightarrow{\omega} \times \underrightarrow{r})dm \\ &= \underrightarrow{c}_b \times \underrightarrow{v} + \underrightarrow{J}_b \cdot \underrightarrow{\omega} \end{aligned} \tag{5.13}$$

and the total absolute angular momentum of $(\mathcal{R} + \sum_{i,j=1}^{3,2} \mathcal{P}_{ij})$ about $\mathbf{0}$ is:

$$\begin{aligned} \underrightarrow{l} &= \underrightarrow{l}_b + \sum_{i,j=1}^{3,2} (\underrightarrow{r}_{d,ij} \times \underrightarrow{p}_{d,ij}) \\ &= \underrightarrow{c} \times \underrightarrow{v} + \underrightarrow{J} \cdot \underrightarrow{\omega} + \sum_{i,j=1}^{3,2} m_{d,ij}\dot{\xi}_{ij}(\underrightarrow{b}_{ij} \times \underrightarrow{\hat{n}}_{ij}) \end{aligned} \tag{5.14}$$

The other dynamical quantity of interest is the kinetic energy:

$$\begin{aligned} T \triangleq\ & \frac{1}{2}\int_{\mathcal{R}} (\underrightarrow{v} + \underrightarrow{\omega} \times \underrightarrow{r}) \cdot (\underrightarrow{v} + \underrightarrow{\omega} \times \underrightarrow{r})dm \\ & + \frac{1}{2}\sum_{i,j=1}^{3,2} m_{d,ij}(\underrightarrow{v} + \underrightarrow{\omega} \times \underrightarrow{r}_{d,ij} + \dot{\xi}_{ij}\,\underrightarrow{\hat{n}}_{ij}) \cdot (\underrightarrow{v} + \underrightarrow{\omega} \times \underrightarrow{r}_{d,ij} + \dot{\xi}_{ij}\,\underrightarrow{\hat{n}}_{ij}) \\ & = \frac{1}{2} m\,\underrightarrow{v} \cdot \underrightarrow{v} + \frac{1}{2}\underrightarrow{\omega} \cdot \underrightarrow{J} \cdot \underrightarrow{\omega} - \underrightarrow{v} \cdot (\underrightarrow{c} \times \underrightarrow{\omega}) \\ & + \sum_{i,j=1}^{3,2} \left\{ \frac{1}{2} m_{d,ij}\dot{\xi}_{ij}^2 - m_{d,ij}\dot{\xi}_{ij}(\underrightarrow{\hat{n}}_{ij} \times \underrightarrow{b}_{ij}) \cdot \underrightarrow{\omega} + m_{d,ij}\dot{\xi}_{ij}\,\underrightarrow{v} \cdot \underrightarrow{\hat{n}}_{ij} \right\} \end{aligned} \tag{5.15}$$

Considering the forces and torques acting on the system $\mathcal{R}$, the external force and torque are $\underset{\rightarrow}{f}$ and $\underset{\rightarrow}{g}$, and $\mathcal{P}_{ij}$ exerts a force $-\underset{\rightarrow}{f}_{d,ij}$. Through Newton's Third Law, $\mathcal{R}$ exerts a force $\underset{\rightarrow}{f}_{d,ij}$ on $\mathcal{P}_{ij}$*. The motion equations for $\mathcal{P}_{ij}$ and $\mathcal{R}$, respectively, may now be written:

$$\underset{\rightarrow}{\dot{p}}_{d,ij} = m_{d,ij}\,\underset{\rightarrow}{\ddot{r}}_{d,ij} = \underset{\rightarrow}{f}_{d,ij} = -\underset{\rightarrow}{\hat{n}}_{ij}(c_{d,ij}\dot{\xi}_{ij} + k_{d,ij}\xi_{ij}) + \underset{\rightarrow}{f}_{con,ij} \tag{5.16}$$

where $(\underset{\rightarrow}{\hat{n}}_{ij} \cdot \underset{\rightarrow}{f}_{con,ij} = 0)$

$$\underset{\rightarrow}{\dot{p}}_{b} = \underset{\rightarrow}{f} - \sum_{i,j=1}^{3,2} \underset{\rightarrow}{f}_{d,ij} \tag{5.17}$$

$$\underset{\rightarrow}{\dot{l}}_{b} + \underset{\rightarrow}{v} \times \underset{\rightarrow}{p}_{b} = \underset{\rightarrow}{g} - \sum_{i,j=1}^{3,2} (\underset{\rightarrow}{r}_{d,ij} \times \underset{\rightarrow}{f}_{d,ij}) \tag{5.18}$$

where $\underset{\rightarrow}{f}_{con,ij}$ is the constraining force normal to the direction of $\mathcal{P}_{ij}$'s travel. Summing Eq. (5.16) and Eq. (5.17) gives:

$$\underset{\rightarrow}{\dot{p}} = \underset{\rightarrow}{f} \tag{5.19}$$

Substitution of Eq. (5.18) into Eq. (5.14) yields (after reduction using earlier definitions):

$$\underset{\rightarrow}{\dot{l}} + \underset{\rightarrow}{v} \times \underset{\rightarrow}{p} = \underset{\rightarrow}{g} \tag{5.20}$$

Then the last motion equation is found from Eq. (5.12) and Eq. (5.16):

$$\begin{aligned}
\dot{p}_{n,ij} &= \underset{\rightarrow}{\dot{\hat{n}}}_{ij} \cdot \underset{\rightarrow}{p}_{d,ij} + \underset{\rightarrow}{\hat{n}}_{ij} \cdot \underset{\rightarrow}{\dot{p}}_{d,ij} \\
&= (\underset{\rightarrow}{\omega} \times \underset{\rightarrow}{\hat{n}}_{ij}) \cdot \underset{\rightarrow}{p}_{d,ij} + \underset{\rightarrow}{\hat{n}}_{ij} \cdot (-\underset{\rightarrow}{\hat{n}}_{ij}(c_{d,ij}\dot{\xi}_{ij} + k_{d,ij}\xi_{ij}) + \underset{\rightarrow}{f}_{con,ij}) \\
&= \underset{\rightarrow}{\omega} \cdot \underset{\rightarrow}{\hat{n}}_{ij} \times \{m_{d,ij}(\underset{\rightarrow}{v} + \underset{\rightarrow}{\omega} \times \underset{\rightarrow}{r}_{d,ij} + \dot{\xi}_{ij}\,\underset{\rightarrow}{\hat{n}}_{ij})\} - c_{d,ij}\dot{\xi}_{ij} - k_{d,ij}\xi_{ij} \\
&= m_{d,ij}\,\underset{\rightarrow}{\omega} \cdot \underset{\rightarrow}{\hat{n}}_{ij} \times \{\underset{\rightarrow}{v} - \underset{\rightarrow}{r}_{d,ij} \times \underset{\rightarrow}{\omega}\} - c_{d,ij}\dot{\xi}_{ij} - k_{d,ij}\xi_{ij}
\end{aligned} \tag{5.21}$$

*External forces on $\mathcal{P}_{ij}$ may also be included if so desired, although here it is not deemed necessary as the damper masses are only there to provide a dissipation mechanism according to the spin state of $\mathcal{R}$.

where $\underset{\rightarrow}{\hat{n}}_{ij} \cdot \underset{\rightarrow}{\hat{n}}_{ij} = 1$, $\underset{\rightarrow}{\hat{n}}_{ij} \cdot \underset{\rightarrow}{f}_{con,ij} = 0$, and the inertial frame time derivative is $\dot{\underset{\rightarrow}{\hat{n}}}_{ij} = \mathring{\underset{\rightarrow}{\hat{n}}}_{ij} + \underset{\rightarrow}{\omega} \times \underset{\rightarrow}{\hat{n}}_{ij} = (\underset{\rightarrow}{\omega} \times \underset{\rightarrow}{\hat{n}}_{ij})$. * The time derivative of $\underset{\rightarrow}{\hat{n}}_{ij}$ with respect to the rotating frame $\mathring{\underset{\rightarrow}{\hat{n}}}_{ij} = 0$ because we assume that the rectilinear slots which the dampers move in are fixed in the rigid body.

The change in kinetic energy during the motion is given by analogy with Eq. (67) in Section 3.2 of Hughes[66] for a continuum:

$$\begin{aligned}
\dot{T} &= \int_{\mathcal{R}} (\underset{\rightarrow}{v} + \underset{\rightarrow}{\omega} \times \underset{\rightarrow}{r}) \cdot d\underset{\rightarrow}{f} + \sum_{i,j=1}^{3,2} (\underset{\rightarrow}{v} + \underset{\rightarrow}{\omega} \times \underset{\rightarrow}{r}_{d,ij} + \dot{\xi}_{ij} \underset{\rightarrow}{\hat{n}}_{ij}) \cdot \underset{\rightarrow}{f}_{d,ij} \\
&= \underset{\rightarrow}{v} \cdot \int_{\mathcal{R}} d\underset{\rightarrow}{f} + \underset{\rightarrow}{\omega} \cdot \int_{\mathcal{R}} \underset{\rightarrow}{r} \times d\underset{\rightarrow}{f} \\
&+ \sum_{i,j=1}^{3,2} \left\{ \underset{\rightarrow}{v} \cdot \underset{\rightarrow}{f}_{d,ij} + \underset{\rightarrow}{\omega} \cdot \underset{\rightarrow}{r}_{d,ij} \times \underset{\rightarrow}{f}_{d,ij} + \dot{\xi}_{ij} \underset{\rightarrow}{\hat{n}}_{ij} \cdot \underset{\rightarrow}{f}_{d,ij} \right\} \\
&= \sum_{i,j=1}^{3,2} \left\{ \underset{\rightarrow}{v} \cdot (\underset{\rightarrow}{f} - \underset{\rightarrow}{f}_{d,ij}) + \underset{\rightarrow}{\omega} \cdot (\underset{\rightarrow}{g} - \underset{\rightarrow}{r}_{d,ij} \times \underset{\rightarrow}{f}_{d,ij}) + \underset{\rightarrow}{v} \cdot \underset{\rightarrow}{f}_{d,ij} \right. \\
&\left. + \underset{\rightarrow}{\omega} \cdot \underset{\rightarrow}{r}_{d,ij} \times \underset{\rightarrow}{f}_{d,ij} + \dot{\xi}_{ij} \underset{\rightarrow}{\hat{n}}_{ij} \cdot \underset{\rightarrow}{f}_{d,ij} \right\} \\
&= \underset{\rightarrow}{f} \cdot \underset{\rightarrow}{v} + \underset{\rightarrow}{g} \cdot \underset{\rightarrow}{\omega} - \sum_{i,j=1}^{3,2} \left\{ c_{d,ij} \dot{\xi}_{ij}^2 + k_{d,ij} \xi_{ij} \dot{\xi}_{ij} \right\}
\end{aligned} \tag{5.22}$$

The term $k_{d,ij}\xi_{ij}\dot{\xi}_{ij} = \dot{V}_{ij}$ is the rate of change of the potential energy stored in the spring, $V_{ij} = 1/2 k_{d,ij} \xi_{ij}^2$. Hence, the change in the total energy $E = T + \sum_{i,j=1}^{3,2} V_{ij}$ is:

$$\dot{E} = \underset{\rightarrow}{f} \cdot \underset{\rightarrow}{v} + \underset{\rightarrow}{g} \cdot \underset{\rightarrow}{\omega} - \sum_{i,j=1}^{3,2} c_{d,ij} \dot{\xi}_{ij}^2 \tag{5.23}$$

which shows that the energy increases as work is done by $\underset{\rightarrow}{f}$ and $\underset{\rightarrow}{g}$ but decreases through dissipation in the damper.

*the overcircle notation $\mathring{}$ indicates a time derivative in a rotating frame.

5.4.2 Scalar Motion Equations

To deduce the scalar motion equations, the vectors must be expressed in terms of their components. We choose to express all vectors in the body principal axes frame $\mathcal{F}_p$, the under-arrow notation is subsequently dropped. The formalism of Hughes[66] is used for consistency, bold font symbols are column matrices of the components of the vector form (under-arrow) expressed in the chosen reference frame. Matrix operations using this notation are explained in Appendix C. Note that $\hat{\boldsymbol{n}}_{ij}, \boldsymbol{b}_{ij}, \boldsymbol{c}_b$, and $\boldsymbol{J}_b$ are constant when expressed in $\mathcal{F}_p$. For clarity, $\boldsymbol{\omega}$ is the angular velocity vector of the frame $\mathcal{F}_p$ with respect to the $\mathcal{F}_\mathcal{I}$ as expressed in $\mathcal{F}_p$. The velocity $\boldsymbol{v}$ is the velocity of $\mathcal{R} + \sum_{i,j=1}^{3,2} \mathcal{P}_{ij}$ with respect to $\mathcal{F}_\mathcal{I}$ as expressed in $\mathcal{F}_p$. The momenta and kinetic energy are as follows:*

$$\boldsymbol{p} = m\boldsymbol{v} - \boldsymbol{c}^\times \boldsymbol{\omega} + \sum_{i,j=1}^{3,2} m_{d,ij} \dot{\xi}_{ij} \hat{\boldsymbol{n}}_{ij} \tag{5.24}$$

$$\boldsymbol{l} = \boldsymbol{c}^\times \boldsymbol{v} + \boldsymbol{J}\boldsymbol{\omega} + \sum_{i,j=1}^{3,2} m_{d,ij} \dot{\xi}_{ij} \boldsymbol{b}_{ij}^\times \hat{\boldsymbol{n}}_{ij} \tag{5.25}$$

$$p_{n,ij} = m_{d,ij} (\hat{\boldsymbol{n}}_{ij}^T \boldsymbol{v} - \hat{\boldsymbol{n}}_{ij}^T \boldsymbol{b}_{ij}^\times \boldsymbol{\omega} + \dot{\xi}_{ij}) \tag{5.26}$$

$$\begin{aligned} T = {} & \frac{1}{2} m \boldsymbol{v}^T \boldsymbol{v} + \frac{1}{2} \boldsymbol{\omega}^T \boldsymbol{J} \boldsymbol{\omega} - \boldsymbol{v}^T \boldsymbol{c}^\times \boldsymbol{\omega} \\ & + \sum_{i,j=1}^{3,2} \left\{ \frac{1}{2} m_{d,ij} \dot{\xi}_{ij}^2 - m_{d,ij} \dot{\xi}_{ij} \hat{\boldsymbol{n}}_{ij}^T \boldsymbol{b}_{ij}^\times \boldsymbol{\omega} + m_{d,ij} \dot{\xi}_{ij} \boldsymbol{v}^T \hat{\boldsymbol{n}}_{ij} \right\} \end{aligned} \tag{5.27}$$

$$\dot{E} = \boldsymbol{f}^T \boldsymbol{v} + \boldsymbol{g}^T \boldsymbol{\omega} - \sum_{i,j=1}^{3,2} c_{d,ij} \dot{\xi}_{ij}^2 \tag{5.28}$$

The structure of these equations may be stated in terms of the system inertia matrix $\boldsymbol{\mathcal{M}}$, where we write out the values for each damper explicitly for clarity, defined as follows:

*See Appendix C for definition of $\boldsymbol{a}^\times$ and $\boldsymbol{a}^T\boldsymbol{b}$.

$$\boldsymbol{\mathcal{M}} \triangleq \begin{bmatrix} m\boldsymbol{U} & -\boldsymbol{c}^{\times} & m_{d,11}\boldsymbol{n}_{11} & m_{d,12}\boldsymbol{n}_{12} & m_{d,21}\boldsymbol{n}_{21} & m_{d,22}\boldsymbol{n}_{22} & m_{d,31}\boldsymbol{n}_{31} & m_{d,32}\boldsymbol{n}_{32} \\ \boldsymbol{c}^{\times} & \boldsymbol{J} & m_{d,11}\boldsymbol{b}_{11}^{\times}\boldsymbol{n}_{11} & m_{d,12}\boldsymbol{b}_{12}^{\times}\boldsymbol{n}_{12} & m_{d,21}\boldsymbol{b}_{21}^{\times}\boldsymbol{n}_{21} & m_{d,22}\boldsymbol{b}_{22}^{\times}\boldsymbol{n}_{22} & m_{d,31}\boldsymbol{b}_{31}^{\times}\boldsymbol{n}_{31} & m_{d,32}\boldsymbol{b}_{32}^{\times}\boldsymbol{n}_{32} \\ m_{d,11}\boldsymbol{n}_{11}^{T} & -m_{d,11}\boldsymbol{n}_{11}^{T}\boldsymbol{b}_{11}^{\times} & m_{d,11} & 0 & 0 & 0 & 0 & 0 \\ m_{d,12}\boldsymbol{n}_{12}^{T} & -m_{d,12}\boldsymbol{n}_{12}^{T}\boldsymbol{b}_{12}^{\times} & 0 & m_{d,12} & 0 & 0 & 0 & 0 \\ m_{d,21}\boldsymbol{n}_{21}^{T} & -m_{d,21}\boldsymbol{n}_{21}^{T}\boldsymbol{b}_{21}^{\times} & 0 & 0 & m_{d,21} & 0 & 0 & 0 \\ m_{d,22}\boldsymbol{n}_{22}^{T} & -m_{d,22}\boldsymbol{n}_{22}^{T}\boldsymbol{b}_{22}^{\times} & 0 & 0 & 0 & m_{d,22} & 0 & 0 \\ m_{d,31}\boldsymbol{n}_{31}^{T} & -m_{d,31}\boldsymbol{n}_{31}^{T}\boldsymbol{b}_{31}^{\times} & 0 & 0 & 0 & 0 & m_{d,31} & 0 \\ m_{d,32}\boldsymbol{n}_{32}^{T} & -m_{d,32}\boldsymbol{n}_{32}^{T}\boldsymbol{b}_{32}^{\times} & 0 & 0 & 0 & 0 & 0 & m_{d,32} \end{bmatrix}$$

The momenta and energy can now be expressed concisely in terms of $\boldsymbol{\mathcal{M}}$:

$$\boldsymbol{\varrho} = \boldsymbol{\mathcal{M}}\boldsymbol{\mathcal{V}} \tag{5.29}$$

$$T = \frac{1}{2}\boldsymbol{\mathcal{V}}^{T}\boldsymbol{\mathcal{M}}\boldsymbol{\mathcal{V}} \tag{5.30}$$

where

$$\begin{aligned} \boldsymbol{\varrho} &\triangleq \begin{bmatrix} \boldsymbol{p} & \boldsymbol{l} & p_{n,11} & p_{n,12} & p_{n,21} & p_{n,22} & p_{n,31} & p_{n,32} \end{bmatrix}^{T} \\ \boldsymbol{\mathcal{V}} &\triangleq \begin{bmatrix} \boldsymbol{v} & \boldsymbol{\omega} & \dot{\xi}_{11} & \dot{\xi}_{12} & \dot{\xi}_{21} & \dot{\xi}_{22} & \dot{\xi}_{31} & \dot{\xi}_{32} \end{bmatrix}^{T} \end{aligned} \tag{5.31}$$

Finally, the motion equations themselves, i.e. the scalar equivalents of Eq. (5.19),(5.20), and (5.21) are:

$$\dot{\boldsymbol{p}} = -\boldsymbol{\omega}^{\times}\boldsymbol{p} + \boldsymbol{f} \tag{5.32}$$

$$\dot{\boldsymbol{l}} = -\boldsymbol{\omega}^{\times}\boldsymbol{l} - \boldsymbol{v}^{\times}\boldsymbol{p} + \boldsymbol{g} \tag{5.33}$$

$$\dot{p}_{n,ij} = m_{d,ij}\boldsymbol{\omega}^{T}\hat{\boldsymbol{n}}_{ij}^{\times}(\boldsymbol{v} - \boldsymbol{r}_{d,ij}^{\times}\boldsymbol{\omega}) - c_{d,ij}\dot{\xi}_{ij} - k_{d,ij}\xi_{ij} \tag{5.34}$$

The above, Eq. (5.32)-(5.34) are numerically integrated for $\boldsymbol{p}, \boldsymbol{l}$, and p_n while simultaneously solving the algebraic equations (5.24) through (5.26) for $\{\boldsymbol{v}, \boldsymbol{\omega}, \dot{\xi}\}$. This is the key for implementation of this model. In terms of $\boldsymbol{\mathcal{M}}$, this solution takes the form:

$$\boldsymbol{\mathcal{V}} = \boldsymbol{\mathcal{M}}^{-1}\boldsymbol{\varrho} \tag{5.35}$$

This may be performed using the left divide matrix operation in MATLAB, i.e. $\boldsymbol{\mathcal{V}} = \boldsymbol{\mathcal{M}} \backslash \boldsymbol{\varrho}$. The initial conditions depend on the particular application of the model.

We choose the centre of mass of $\mathcal{R} + \mathcal{P}_{ij}$ to be coincident with point $\mathbf{0}$. Consequently $\boldsymbol{c}_b, \boldsymbol{c}(t_o) = 0$. The latter is true due to the choice of $\xi_{ij} = 0$ for all dampers giving an initially symmetric distribution of damper masses around the centre of mass. Initially, it will be assumed that the external force and torque are zero ($\boldsymbol{f} = \boldsymbol{g} = \mathbf{0}$) to conduct a number of tests on the model before it is applied to modeling SPS motion.

The equations of motion are based upon those given by Hughes[66] Section 3.4 for a rigid body with a single spring-mass damper. The novelty of the model used in this thesis lies in the particular configuration of multiple spring-dampers, as shown in Fig. 5.2. The spring-damper masses are placed at equal distance from the centre of mass, with two along each principal axis of the body. To the author's knowledge, this particular configuration of spring-mass dampers has not been applied before to satellite attitude dynamics. The benefit of this model is that it can be used across multiple SPS designs without alteration. If a single mass damper was used then the placement and properties would need to be calculated for each different SPS. The multidamper model allows for a straightforward comparison of the attitude motion/stability for multiple SPS designs. It also allows the stability of the motion to be checked with small departures around an arbitrary spin axis. In the literature,[66] the single damper model must be configured to each rotation being considered.

5.5 Short Axis Mode

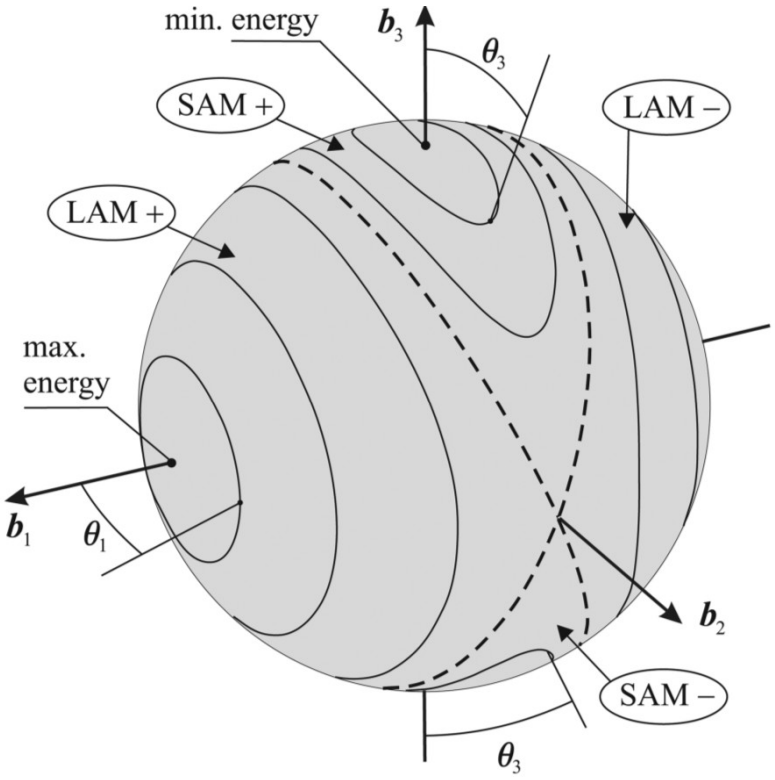

Figure 5.4: Angular momentum vector $\boldsymbol{l}$ evolution on a l =constant sphere in the body frame. Dashed lines mark the separatrices as borderlines between four rotation modes. Nutation angle θ_i is shown. Figure from Breiter.[89]

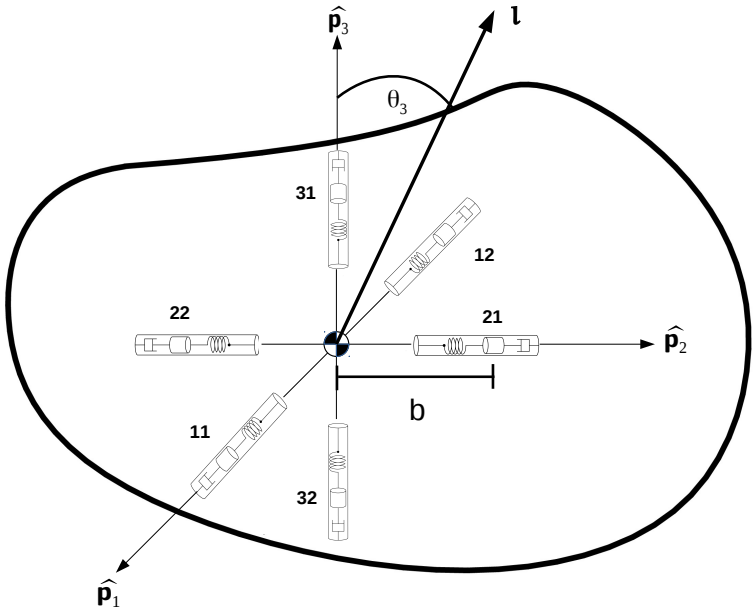

Figure 5.5: Spinning rigid body $\mathcal{R}$, with 6 internal point mass dampers. The angular momentum $\boldsymbol{l}$ and the nutation angle θ are illustrated.

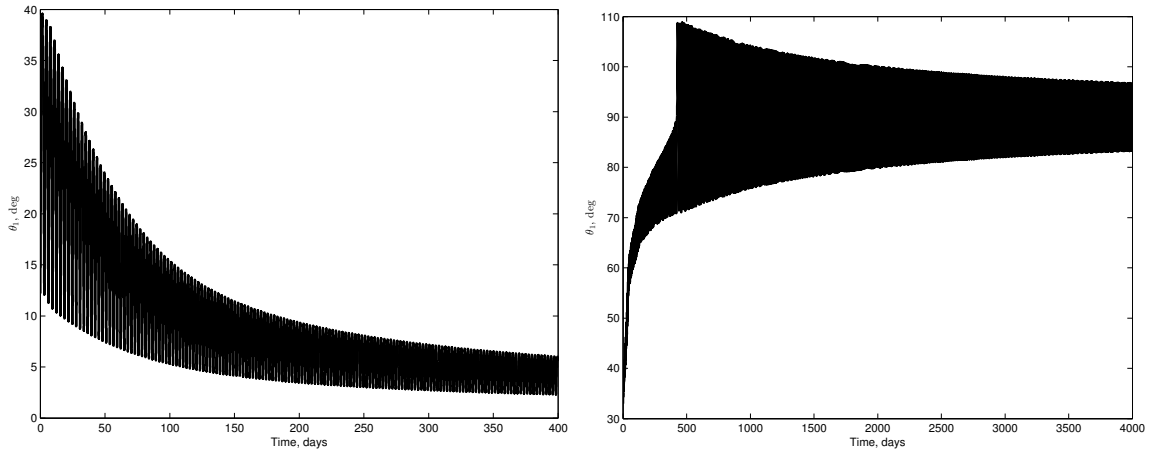

(a) SAM: Angle θ_3 between $\boldsymbol{l}$ and $\hat{\boldsymbol{p}}_3$.

(b) LAM: Angle θ_1 between $\boldsymbol{l}$ and $\hat{p}_1$.

Figure 5.6: Nutation angle evolution.

An initial test of the energy dissipation model is to start the body in a short axis mode (SAM) rotation state and observe if it will damp towards a purely major axis spin. SAM is an excited rotated state near to a major axis spin, i.e. the angular momentum vector $\boldsymbol{l}$ circulates around the major principal axis of inertia (see Fig. 5.4). The body axis frame $\{\boldsymbol{b}_1, \boldsymbol{b}_2, \boldsymbol{b}_3\}$ shown in Breiter's illustration (Fig. 5.4) is considered to be

aligned with the principal axis frame $\{\hat{\boldsymbol{p}}_1, \hat{\boldsymbol{p}}_2, \hat{\boldsymbol{p}}_3\}$. Only the SAM+ and LAM+ cases shall be considered ($\pm$ depends on the sign of the scalar product of $\boldsymbol{l}$ and the principal axis of interest).

To examine a SAM case, the following initial angular velocity vector is used (the magnitude of the angular velocity is $\omega_0 = 2\pi/P$, where P is the period of rotation of the body.):

$$\boldsymbol{\omega}_0 = \left[\delta \quad 0 \quad \sqrt{(\omega_0^2 - \delta^2)}\right]$$

where $\delta = 2 \times 10^{-5}$rad is a small error which gives an initial nutation angle of $\theta_3 \sim 30^\circ$ (see Fig. 5.6(a)), i.e. chosen to initiate a SAM. Note, the convention that $I_3 > I_2 > I_1$ is used here.

To observe how a nearly rigid body evolves towards a stable major axis spin the nutation angle is plotted in Fig. 5.6(a). The nutation angle is defined as the angle between the angular momentum vector $\boldsymbol{l}$ and the principal axis of interest (taken to be $\hat{\boldsymbol{p}}_3$ for the SAM case, see Fig. 5.5) and is calculated as follows:

$$\theta_i = \cos^{-1}\left\{\frac{\boldsymbol{l} \cdot \hat{\boldsymbol{p}}_i}{l}\right\} \tag{5.36}$$

where $\hat{\boldsymbol{p}}_i$ is a principal axis of the body and one of the axes of $\mathcal{F}_p$ (see Fig. 5.2), and l is the magnitude of $\boldsymbol{l}$. The nutation angle decays exponentially:

$$\theta_3(t) = \theta_3(t_0) \exp\{-t/\tau_D\} \tag{5.37}$$

where τ_D is the damping time. Eq. (5.37) may be fitted to $\theta_3(t)$ in order to obtain τ_D. The time taken to damp to a major axis spin is dependent on the damper parameters and $\theta_3(t_0)$. This result confirms that the model has achieved the objective of modeling the damping towards major axis spin. It is confirmed that $\boldsymbol{l}$ and $\boldsymbol{\omega}$ align by plotting the angle between them in Fig. D.3 in Appendix D.

The angular momentum of body ($\mathcal{R} + \sum_{i,j=1}^{3,2} \mathcal{P}_{ij}$) should be conserved with respect

to the inertial reference frame $\mathcal{F}_\mathcal{I}$. This can be calculated by: *

$$^{\mathcal{I}}\boldsymbol{l} = \boldsymbol{A}\ ^{\mathcal{P}}\boldsymbol{l} \tag{5.38}$$

where $\boldsymbol{A}$ is the attitude dyadic mapping from $\mathcal{F}_\mathcal{P}$ to $\mathcal{F}_\mathcal{I}$ given by Eq. (1.6), and $^{\mathcal{P}}\boldsymbol{l} = \boldsymbol{l}$ is the angular momentum expressed in $\mathcal{F}_\mathcal{P}$ given by Eq. (5.25). Both the magnitude and direction of the angular momentum must be conserved in the absence of external torque, this is validated in Figures E.1 and E.3 in Appendix E.

The total energy of the system may be calculated:

$$E = T + \sum_{i,j=1}^{3,2} V_{ij} \tag{5.39}$$

where T is the kinetic energy of the system given by Eq. (5.27), and $V_{ij} = 1/2 k_{d,ij} \xi_{ij}^2$ is the potential energy of each spring. For the model to perform its function, the energy should decrease unless the object is in a principal axis spin around the major axis of inertia. This is validated in Fig. E.5 in Appendix E.

The rate of energy dissipation can be controlled through the choice of damper parameters, specifically, $c_{d,ij}$ as can be seen through Eq. (5.28). The mass of the dampers $m_{d,ij}$ is selected to be small compared to the mass of the rigid body, the moments of inertia are monitored to ensure that there is no reordering of the order of moments of inertia due to damper movements.

*Previously the subscript $^{\mathcal{P}}$ has been omitted.

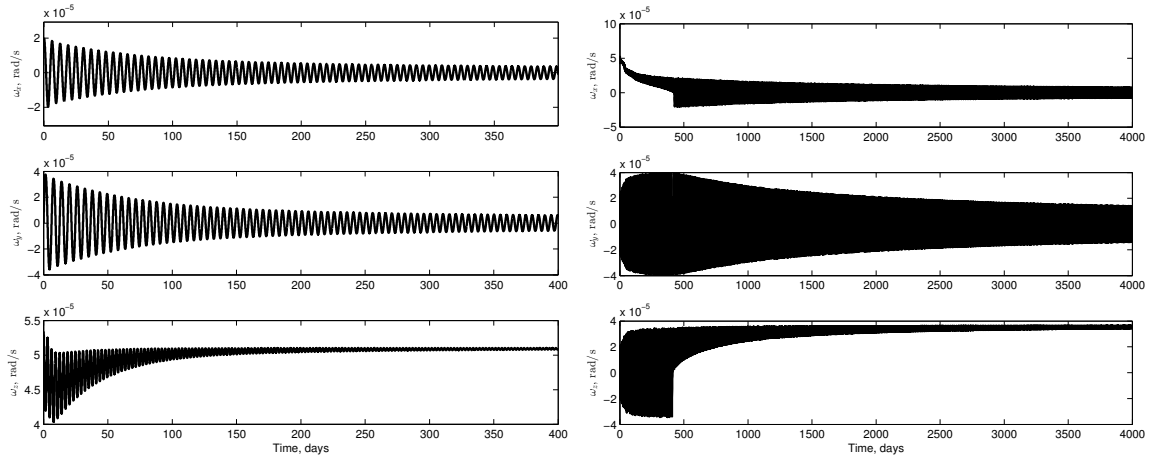

(a) SAM (b) LAM

Figure 5.7: Angular velocity components for $\boldsymbol{f} = \boldsymbol{g} = \boldsymbol{0}$.

5.6 Long Axis Mode

A long axis mode (LAM) is an excited rotated state near to a minor axis spin. The initial angular velocity vector in this case is:

$$\boldsymbol{\omega}_0 = \begin{bmatrix} \sqrt{(\omega_0^2 - \delta^2)} & 0 & \delta \end{bmatrix}$$

where again it is assumed that $I_3 > I_2 > I_1$. The expected instability of LAM is clearly observed as the body quickly begins to tumble (see Fig. 5.6(b)). After tumbling for a period, the body then begins to damp towards a major axis spin. The conservation of angular momentum is validated in Fig. E.2 and E.4 in Appendix E. It is confirmed that $\boldsymbol{l}$ and $\boldsymbol{\omega}$ align by plotting the angle between them in Fig. D.4 in Appendix D.

5.7 Addition of External Forces and Torques

To account for the effect of external forces or torques, $\boldsymbol{f}$ and $\boldsymbol{g}$ respectively, they must be in expressed in the principal axis frame $\mathcal{F}_p$. To assess rotational stability of SPS in geosynchronous orbits the Earth's central gravity field is added. The position vector $\boldsymbol{R}(t)$ between the central body and the spacecraft in $\mathcal{F}_p$ may be found by numerically

integrating the following equation:

$$\begin{aligned}\mathring{\boldsymbol{R}} &= \dot{\boldsymbol{R}} - \boldsymbol{\omega} \times \boldsymbol{R} \\ &= \boldsymbol{v} - \boldsymbol{\omega} \times \boldsymbol{R}\end{aligned} \tag{5.40}$$

where, it should be noted that the left hand side is the time derivative with respect to the rotating $\mathcal{F}_{\mathcal{P}}$ frame. The force acting on the $\mathcal{R} + \sum_{i,j=1}^{3,2} \mathcal{P}_{ij}$ system due to a central body is given by:

$$\boldsymbol{f} = -\frac{GMm}{R^3}\boldsymbol{R} = -\frac{\partial V^{(0)}}{\partial \boldsymbol{R}} \tag{5.41}$$

where M is the mass of the central body, and m is the mass of $\mathcal{R} + \sum_{i,j=1}^{3,2} \mathcal{P}_{ij}$. The gravity gradient torque is calculated in $\mathcal{F}_p$ with the expression given by Hughes[66] *:

$$\boldsymbol{g} = \frac{3GM}{R^3}\begin{bmatrix}(I_3 - I_2)c_{23}c_{33} \\ (I_1 - I_3)c_{33}c_{13} \\ (I_2 - I_1)c_{13}c_{23}\end{bmatrix} \tag{5.42}$$

where I_i are the principal moments of inertia of $\mathcal{R} + \sum_{i,j=1}^{3,2} \mathcal{P}_{ij}$ and the direction cosines are given by:

$$\begin{bmatrix}c_{13} & c_{23} & c_{33}\end{bmatrix}^T = -\frac{\boldsymbol{R}}{R} \tag{5.43}$$

Note, this equation is equivalent to Eq. (4.15) except for slightly different notation. In this case only the attitude of the second body (the SPS) is considered.

Example results of the 6 damper system with gravitational force and torque are analysed for the Abacus SPS orbiting the Earth in both GEO and GLPO subsequently.

*This is the same expression as Eq. (4.15) but with slightly different notation to be consistent with Hughes.

5.8 Geosynchronous SPS with Energy Dissipation

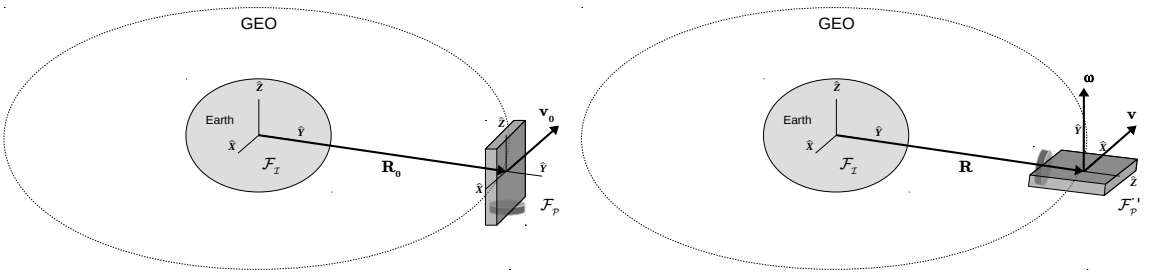

(a) Initial orientation. (b) Final orientation.

Figure 5.8: Abacus attitude state in GEO.

This section considers the rotational motion of the Abacus SPS when it is placed in a geosynchronous orbit (either GEO or GLPO) with a small out-of-plane error in position and with zero spin ($\boldsymbol{\omega}_0 = \mathbf{0}$) and no attitude control. The moments of inertia of the Abacus SPS inertia are assigned as follows:

$$I_1 = 2.8 \times 10^{13} \text{kg m}^2$$
$$I_2 = 4.6 \times 10^{13} \text{kg m}^2$$
$$I_3 = 1.8 \times 10^{13} \text{kg m}^2$$

so $I_2 > I_1 > I_3$, i.e. the moments of inertia are labelled to indicate which of the principal axes $\{\hat{\boldsymbol{p}}_1, \hat{\boldsymbol{p}}_2, \hat{\boldsymbol{p}}_3\}$ that they are aligned with (it is convenient to drop the normal convention here). The initial orientation this corresponds to is shown in Fig. 5.8(a).

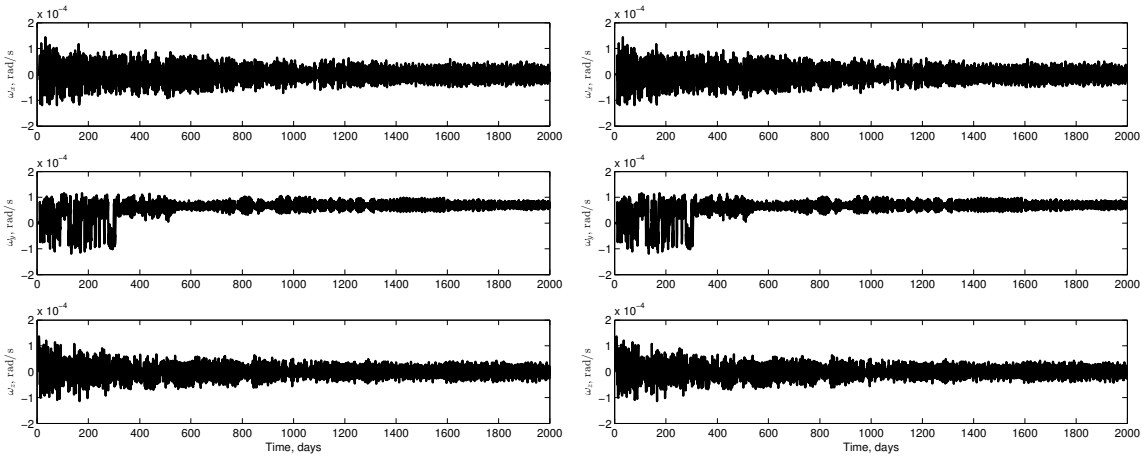

(a) GEO (b) GLPO

Figure 5.9: Angular velocity $\boldsymbol{\omega}$ components in $\mathcal{F}_p$.

Regardless of the initial orientation, the spacecraft will eventually rotate around its maximum moment of inertia at the orbit rate n_{GEO} ($\omega_y = n_{GEO} = 7.292 \times 10^{-5}$rad/s in Fig. 5.9) and align its minimum moment of inertia with the local vertical ($R_z = a_{GEO} = 42,164$km in Fig. 5.10). This result shows that the naturally stable attitude configuration for the Abacus satellite is as shown in Fig. 5.8(b). This is essentially a gravity gradient stabilised attitude. The dampers continue moving (as damper parameters for underdamped motion are selected) and dissipating energy until the minimum energy state is reached. The movement of the dampers causes fluctuations in the moments of inertia of $\mathcal{R} + \sum_{i,j=1}^{3,2} \mathcal{P}_{ij}$, as shown in Fig. D.5. However, no re-ordering of moments of inertia is observed, this is due to the small value of $m_{d,ij}$ chosen ($m_{d,ij} << m_b$).

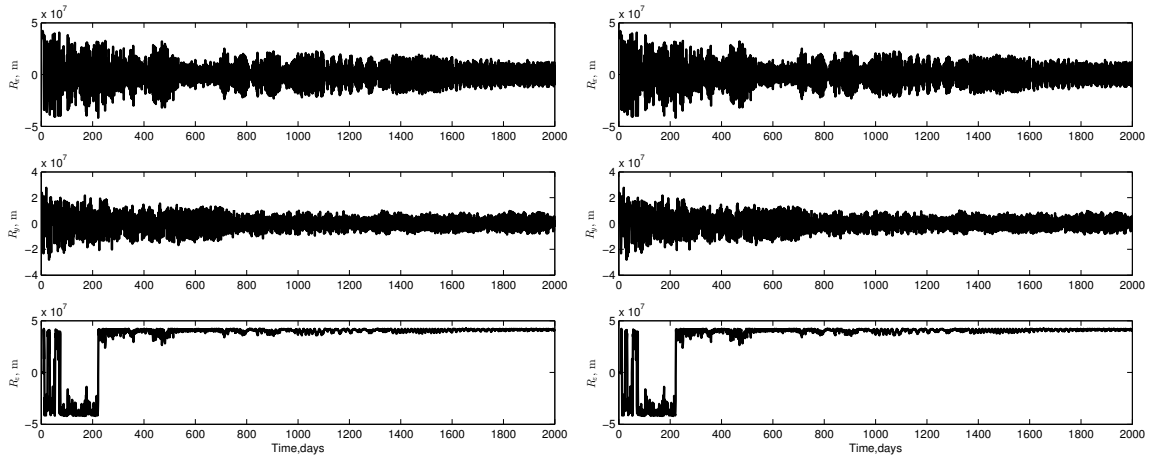

(a) GEO (b) GLPO

Figure 5.10: Position vector $\boldsymbol{R}$ components in $\mathcal{F}_p$.

The dynamics of the Abacus SPS in GEO and GLPO are very similar when energy dissipation and gravity gradient are considered. The main difference is in the velocity components (see Fig. 5.11). In the GEO case, the satellite is in the orientation shown in Fig. 5.8. In the GLPO case, the v_x component of velocity (see Fig. 5.11(b)) is observed to alternate between positive and negative values. This indicates that the SPS is flipping 180° around the $\hat{\boldsymbol{p}}_3$ axis (i.e. the Earth pointing minimum axis of inertia). This is due to the non-pitch components of the gravity gradient torque which are non-zero for a SPS in GLPO. However, if the simulation is run out for longer, this flipping ceases. By incorporating a simple mechanism by which energy can be dissipated (as it would be for a large flexing structure), the natural dynamics of the system have been identified.

For such large scale spacecraft, it would be sensible to adhere to these natural dynamics, rather than continually fighting against them. Locating SPS in GLPO certainly does this from an orbit dynamics perspective. For the attitude dynamics, rotating around the maximum inertia axis at the orbit rate with the minimum axis earth pointing, and intermediate axis parallel to the orbit plane, is the lowest energy configuration. As mentioned in Section 4.12, this configuration, as shown in Fig. 5.8(b), has been proposed previously by Bowden[71] and was found to minimise

attitude control costs * in Section 4.12 (see Fig. 4.8).

5.9 Gravity Gradient Stabilised SPS

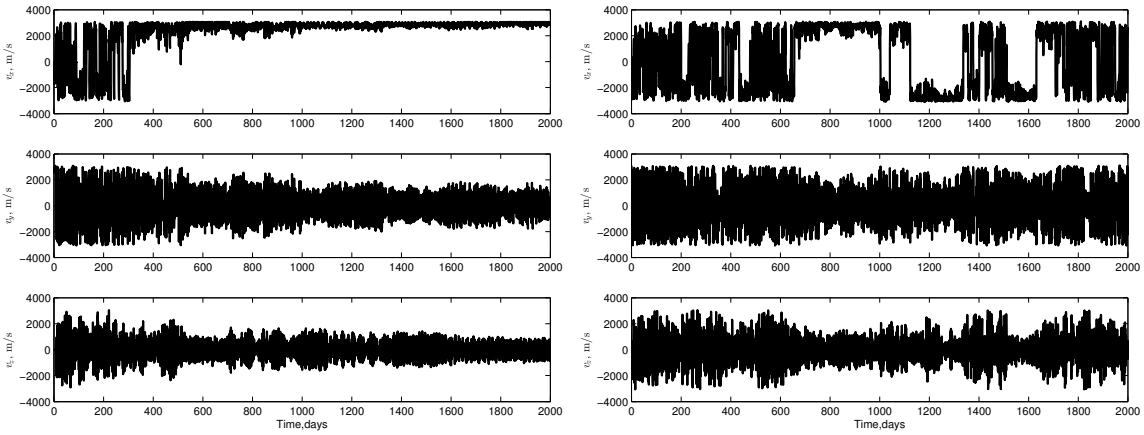

(a) GEO (b) GLPO

Figure 5.11: Velocity $\boldsymbol{v}$ components in $\mathcal{F}_p$.

In this section the attitude dynamics of the Abacus SPS when it is initialised near the stable orientation (with a small error in the position vector) are analysed. The stable orientation shall be referred to as the gravity gradient stabilised orientation (GGSO) from this point onwards. The moments of inertia of the Abacus SPS inertia are assigned as follows:

$$I_1 = 1.8 \times 10^{13} \text{kg m}^2$$

$$I_2 = 2.8 \times 10^{13} \text{kg m}^2$$

$$I_3 = 4.6 \times 10^{13} \text{kg m}^2$$

and the initial angular velocity is $\boldsymbol{\omega}_0 = [0\ 0\ n_{GEO}]$. Both GEO and GLPO cases are considered (for GLPO the initial orientation is imparted). Earth oblateness is not included here. †

*Previously referred to as the in-orbit-plane (IOP) configuration

†It is not necessary to include $\partial V/\partial R^{(2)}$ as it causes a very small out of plane component R_z compared to the much larger oscillation in the R_x and R_y caused by the first order term $\partial V/\partial R^{(0)}$.

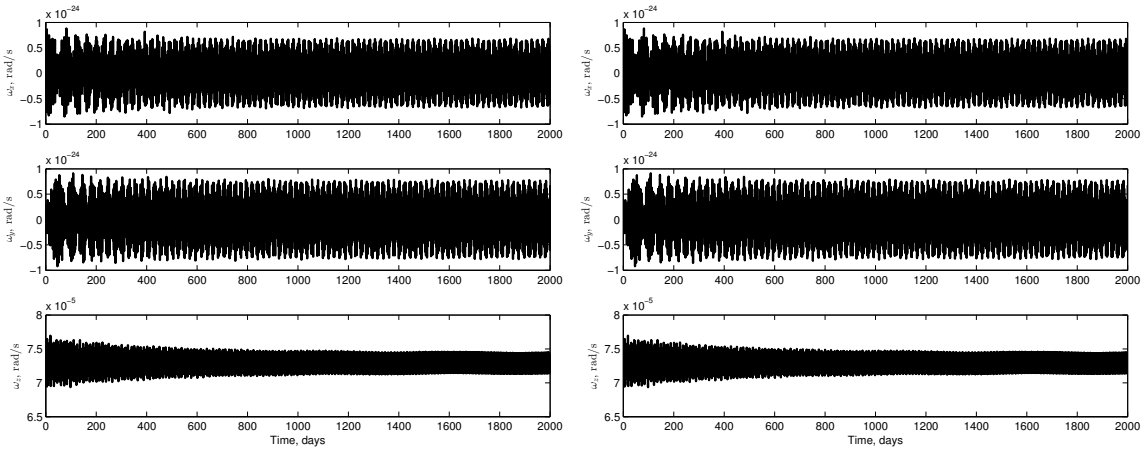

(a) GEO (b) GLPO

Figure 5.12: Angular velocity $\boldsymbol{\omega}$ components in $\mathcal{F}_{\mathcal{P}}$ for GGSO.

In stability analysis, it is considered sufficient to study the response to a small initial deviation, because stability is not influenced by the magnitude of the disturbance.[90] Therefore a small deviation $\Delta R_z = 1 \times 10^{-13}$m is included in the initial conditions for the GGSO SPS in GEO and GLPO.

The ω_x and ω_y components in Fig. 5.12 are very small compared to ω_z for both GEO and GLPO. The small disturbance does not appear to cause significant growth in these components indicating that this is a stable orientation. However, a more in-depth study incorporating other disturbance torques and thorough attitude stability analysis is necessary to confirm this. However, the fact that the SPS will end up in close to this orientation regardless of initial orientation (see Section 5.8) is also a good indicator that this is a stable orientation.

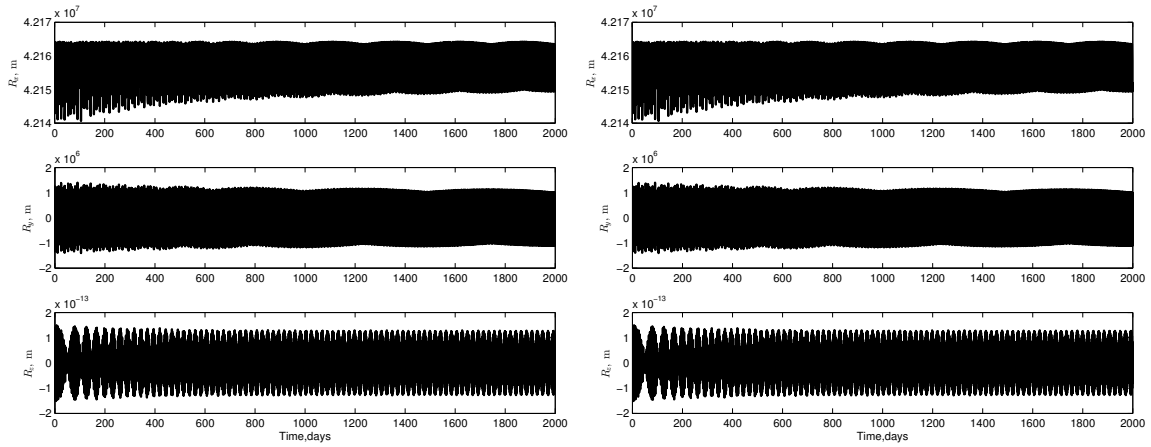

(a) GEO (b) GLPO

Figure 5.13: Position $\boldsymbol{R}$ components in $\mathcal{F}_{\mathcal{P}}$ for GGSO.

The components of $\boldsymbol{R}$ shown in Fig. 5.13, indicate that there is a significant oscillation in the x-y plane. The position in the $\mathcal{F}_{\mathcal{P}}$ frame can be used to find the attitude deviation angle Δ (plotted in Fig. 5.15), where:

$$\Delta = \cos^{-1}\left\{\frac{\boldsymbol{R}\cdot\hat{\boldsymbol{p}}_1}{R}\right\} \tag{5.44}$$

where $\hat{\boldsymbol{p}}_1$ is used to calculate the deviation angle from ideal attitude as the minimum axis should be aligned with $\boldsymbol{R}$, i.e. minimum axis Earth pointing. For both GEO and GLPO, Δ remains small and bounded (see Fig. 5.15) when subject to a small initial perturbation indicating this is a stable attitude.

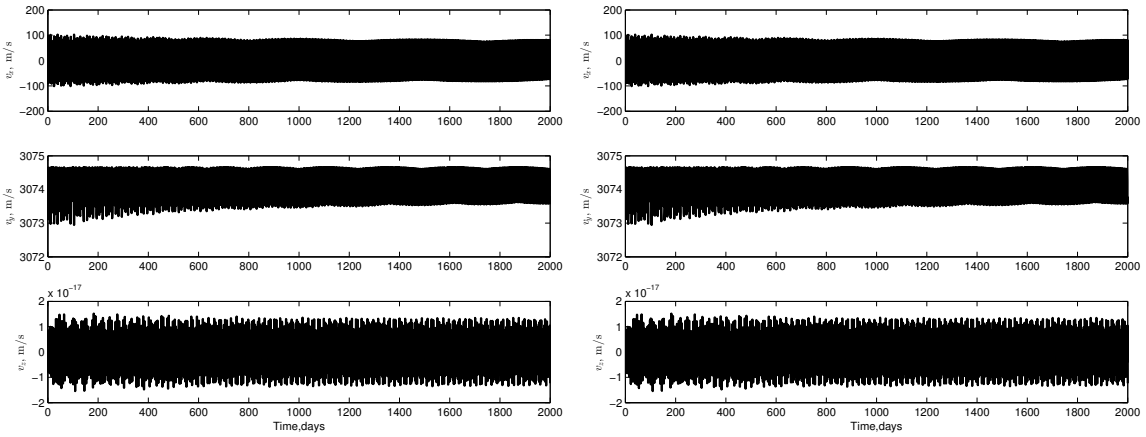

(a) GEO (b) GLPO

Figure 5.14: Velocity $\boldsymbol{v}$ components in $\mathcal{F}_{\mathcal{P}}$ for GGSO.

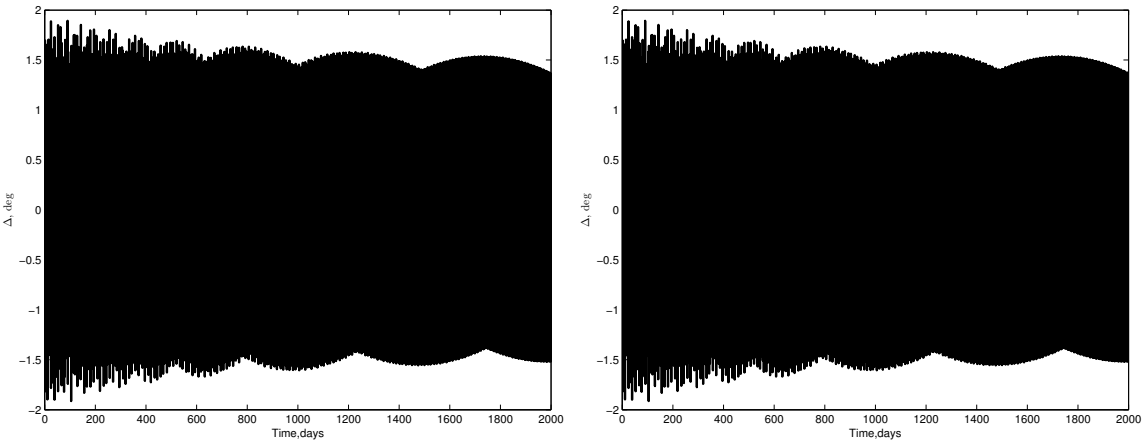

(a) GEO (b) GLPO

Figure 5.15: Attitude deviation from ideal.

5.10 Discussion

5.10.1 Gravity Gradient Stabilised SPS Advantages and Disadvantages

Although the idea of a gravity gradient stabilised SPS is not novel, a conceptually simple model has been developed which allows the attitude dynamics to be qualitatively assessed. Given more detailed information about SPS designs the model would offer quantitative predictions on attitude stability.

Bowden[71] noted some benefits unique to the gravity gradient stabilised orientation (GGSO). It removes the need for a slip-ring or microwave reflector as the transmitting antenna is now always Earth-pointing without the need for reorientation. This is important because the slip-ring, passing electricity generated by the solar arrays to the converter/antenna, was acknowledged as a major engineering challenge and single point of failure of the original Type I SPS designs. Removing the need for the microwave reflector of the Abacus design also eliminates a serious engineering challenge. For accurate pointing, the degree of flatness required of the microwave reflector may not be feasible in any case for such a large diameter reflector. In GLPO and with the sun-pointing orientation, the microwave reflector would have to be continually reoriented throughout the orbit to maintain power beaming to the ground station. With the GGSO the microwave antenna will be Earth pointing and no mechanical redirection of the antenna would be necessary (electronic beam pointing with retrodirective phased array can be used). Another advantage is that the gravity gradient forces provide tension to keep the array of solar cells taut in the radial direction, so that the supporting structure would not be necessary along this axis offering mass savings.

As was previously mentioned in Section 4.12, placing the array in the orbital plane positions the solar cells approximately edge-on to the solar wind, thus minimising damage from micro-meteorites and increasing solar-cell lifetime. Other advantages, such as easier assembly in orbit, lower position keeping propellant requirements, possibilities for decreasing necessary solar cell area, and longer solar cell life, may make this design superior. One side could be solar arrays with the other side radiator material (which will naturally never be sun-pointing). A high level of solar concentration would therefore be possible without the thermal issues associated with the Type III sandwich SPS. This would allow a significant reduction in the size of the platform for the same energy collected, although a trade-off study would be necessary to determine the optimal size of solar array platform, area of reflectors (sun concentration level),

and mass of radiator material required.

The obvious issue with the gravity gradient stabilised SPS is that the solar arrays are not sun-pointing (see Fig. 4.8). Hence, some method of redirecting sunlight onto the platform becomes necessary. Bowden[71] envisaged single large reflector (see Fig. 4.8). The method for determining the necessary reflector diameter for full illumination of the solar array is given by Bowden.[71]

In some ways, this transfers the dynamics issues onto another body, the reflector. However, the high cost and mass components are on the solar array/transmitting antenna portion which is a now in a dynamically stable position. The reflectors may be extremely lightweight, and could even be attached in a very lightweight structure designed to maximise solar insolation of the solar array platform while minimising the torque imparted on the structure due to solar radiation pressure. Another option may be a swarm of smaller free flying reflectors rather than a single large one. If the free flying option is used, the same light that the reflectors are redirecting onto the solar array platform also provides a force which keeps the solar array and mirror/s separated by displacing each a convenient distance out of the orbital plane away from each other.[71]

In the case that SPS is to used as a long-term power source then having the majority of the mass (the solar array platform and transmitting antenna) in a dynamically stable position, with only nominal orbit and attitude control necessary, is certainly an attractive prospect. Replacement reflectors could be then launched as required. Whether a single large reflector or a formation of smaller reflectors is optimal is not clear. The best way to address the solar redirection issue is an interesting problem for future research.

5.10.2 Energy Dissipation Model

Accurate tuning of the damping time would require empirical measurements of the system. However, the model has captured qualitatively the dynamics of the system.

A systematic method for obtaining appropriate damper parameters $\{k_{d,ij}, c_{d,ij}, m_{d,ij}\}$ for any rotating system is the next step. Accurately determining the appropriate rate of energy dissipation for precise modeling is difficult.

At this stage the rotational dynamics with energy dissipation has not been combined with the orbital dynamics to keep the model as simple as possible. The full orbit and attitude dynamics, with all the perturbing forces and torques, as well as the energy dissipation mechanism could be combined.

5.10.3 Further Applications of Energy Dissipation Model

The model developed could also be applied to analysing the dynamics of other SPS designs. Initially only a Type I SPS (Abacus) has been considered. The Type III Sandwich SPS may also be assessed with this model, although modifications would be necessary due to the complications which would arise from the large, lightweight rotating reflectors as well as the long and flexible interconnecting tethers. Sandwich type SPS such as the ISC (see Fig. 3.1(c)) would likely need to be considered as multi-bodied entities, as Glaese[19] did with numerical simulations of the ISC dynamics in GEO.

The model could also be used to analyse the dynamics of the free flying reflector of Bowden's gravity gradient concept[71] (see Fig. 4.8). This would involve incorporating the external torques due to solar radiation pressure and the control torques necessary to rotate the reflector appropriately throughout the orbit to maximise the solar radiation redirected down onto the solar array.

6

Conclusions and Future Work

6.1 Conclusions

The geosynchronous Laplace plane orbit (GLPO) has been confirmed as a viable alternative to the conventional geostationary Earth orbit (GEO) nominally proposed for the large solar power satellite (SPS). The numerical and semi-analytical simulations of the orbital motion of an SPS illustrate that it will remain within range of an equatorial ground receiving station throughout its 30-40 year lifetime without active control (assuming a stable longitude). The average power received over the lifetime is only 1.7% less than for an ideal GEO case (where the SPS remains directly above the ground receiver and is unperturbed) but with fuel savings in the order of 10^5 kg/year.

The orbital evolution of an uncontrolled initially GEO SPS results in lower performance than SPS in GLPO. The average power received is 3.5% less than the ideal GEO case. Compared with GLPO, this orbital evolution increases the likelihood of orbital debris production when a large network of SPSs is considered. Any station-kept GEO SPS will eventually follow a similar orbital evolution once its fuel supply is exhausted.

Although only nominal orbit control is necessary in GLPO, active control of the SPS attitude may be required to maintain sun pointing of the large solar arrays/concentrators. Due to the large moments of inertia of SPS satellites, gravity gradient is the dominant disturbance torque even at geosynchronous altitude.

Attitude control should be passive through gravity gradient, or if active, through electric ion thrusters. Depending on the mass distribution and attitude configuration,

counteracting the dominant gravity gradient torque may be slightly more expensive in GLPO compared to GEO. For Abacus SPS in GLPO additional components of torque are induced around the roll and yaw axes that are not present for the GEO case. Alternatively, the SPS may take advantage of the gravity gradient torque for attitude stabilisation.

Large space structures such as SPS will be constructed in-space, consequently, a lower rigidity of structure is probable compared to conventional current day satellites which must withstand launch intact. This lower rigidity will lead to significant flexing of the structure, and inevitably internal energy dissipation. The large planar platforms of Type I SPS such as Abacus may be oriented in such a way that both orbit and attitude control costs are minimised. Conventionally, these platforms of solar arrays are designed to rotate perpendicular to the orbit plane and be sun-pointing. The alternative in-orbit-plane (IOP) configuration, also known as the gravity gradient stabilised orientation (GGSO) is shown to be superior from a dynamic stability perspective. An initial study indicates that this is a dynamically stable rotational state for both GEO and GLPO.

Besides offering nominal attitude control requirements, GGSO offers numerous other benefits including: placing the array IOP positions the solar cells approximately edge-on to the solar wind and micro-meteorites, increasing solar-cell lifetime. Assembly is easier in orbit. High solar concentration is possible too, as one side of the structure may be used for radiators. Hence, one recommendation of this work is that gravity gradient stabilised SPS of Bowden be re-examined for use in GLPO. Also, instead of a large free-flying reflector, the feasibility of incorporating a lightweight structure to mount multiple reflectors should also be investigated.

The most significant result of the research in this thesis is proving that a SPS can operate in GLPO with nominal orbit control and yet still deliver almost equivalent power to the Earth's surface as the same SPS would in a controlled GEO.

6.1.1 Implications of the Results of the Thesis

The systems analysis performed in Chapter 2 quantified the benefit in terms of energy to cost ratio of utilising the GLPO compared to any other circular orbit. It also showed that a range of inclined geosynchronous orbits are also superior to GEO (for $a = 42,164$km and $0 < i < 14^{\circ}$. The sensitivity analysis performed highlighted that the size of the rectenna has the greatest impact on the Energy to cost ratio. This implies that choosing sites where rectenna size can be maximised is crucial to the performance of a SPS system.

The dynamics results of this thesis indicate that from an orbit-attitude dynamics perspective, gravity gradient (GG) SPS designs in the GLPO are the superior solution. Attitude and orbit stability is obtained, with near propellant-less operation of the SPS. Operational robustness is naturally achieved with this solution as it will never drift far from its stable attitude-orbit configuration. The need for production and on-board storage of extremely large quantities of propellant ($\sim 100,000$ kg/yr) is removed, along with the potential complications of performing re-fuelling operations. Over a 30 year lifetime, GG SPS in the GLPO would save approximately 1 million kg of fuel for orbit-attitude maintenance. Even if we consider a very optimistic value of specific launch cost in the future of \$100/kg, that still amounts to an additional cost of \$100 million per SPS system. It has been proven that SPS can operate in GLPO rather than GEO without incurring additional attitude control costs or suffering from significant reduction in the power delivered when Earth oblateness is considered. The Sun-Tower and Tethered SPS have been shown to be compatible with GG operation in GLPO. These designs can operate with nominal propellant for orbit-attitude control.

Certain designs have been shown to be unstable in their proposed attitude configuration, such as the Abacus and Cylindrical SPSs. The orbit and attitude stability of the various SPS studied is summarised in Table 6.1.

Table 6.1: Summary of SPS designs in GLPO.

	Abacus	Sun-Tower	Cylindrical	Tethered	ISC	Sandwich
Sun-pointing reflectors/PV	√	√	×	×	√	√
Concentration	×	×	×	×	√	√
PMAD Issue	√	√	√	×	×	×
Orbit stability						
$\lambda_h^2 < 0$	√	√	√	√	√	√
$\lambda_e^2 < 0$	√	√	√	√	√	√
Attitude Stability						
$I_2 \geq I_1 \geq I_3$	×	√	×	√	×	√

Table 6.2 shows the fuel requirements for a 30 year lifetime for 5 different SPS designs in GEO. The orbit station-keeping costs are near zero for the same designs in GLPO. Only minor differences in the attitude control costs are observed for these SPS operating in GLPO (see Table 4.4). The Sun-Tower, Cylindrical, and Tethered SPS offer near propellant-less operation in GLPO. The Abacus and ISC still require a significant mass of fuel for attitude control in GLPO.

Table 6.2: Summary of SPS designs in GEO.

	Abacus	Sun-Tower	Cylindrical	Tethered	ISC
Orbit Station-keeping (% Overall Mass)	10.2	10.4	6.2	10.7	22.3
Attitude Control (% Overall Mass)	8.3	~ 0	~ 0	~ 0	19.6[19]

The most significant result of the thesis is proving that gravity gradient stabilised SPS designs can operate in GLPO with virtually no propellant with minimal reduction in the power that the SPS can deliver compared to operation in GEO.

6.1.2 Recommendations On Future SPS Designs

Table 6.1 indicates that only 3 of the SPS designs considered offer orbit and attitude stability: Sun-Tower, Tethered, and Sandwich SPS. The Abacus and Cylindrical SPS designs have been shown to be in unstable attitude configurations which should exclude them from further consideration in the author's opinion.

The more major engineering challenges associated with SPS that can be removed or reduced in scope, the more realistic a near term demonstration/prototype of SPS becomes. As acknowledged in the report on SPS by the IAA,[7] a demonstration SPS is necessary to prove the various technologies and persuade investors to provide the significant capital to build a GW scale SPS. With this in mind, one of the 3 designs which are stable in orbit-attitude should be selected for the purpose of a demonstration SPS.

For a practical version of SPS to be realised, the system must initially be made as simple and operationally robust as possible. Tethered SPS appears the best option for a demonstration SPS for this reason. It is virtually propellant-less, highly modular, with no single point of failure (multiple tethers rather than one). It does not involve any large rotating components to complicate the dynamics, and it is in a naturally stable attitude configuration. It uses the sandwich panel but without sun concentration which is the source of the thermal issues with the sandwich design. It would allow many of the important technical components of SPS to be demonstrated without over complication of the design. The major drawback is that it is out of sunlight twice a day and only collects certain percentage of the sun's light.

The most promising SPS design in the long term is the sandwich SPS, however, detailed research is required to investigate the multi-body dynamics of this design and overcome the overheating of the sandwich component. It satisfies the orbit and attitude stability requirements while offering considerably more efficient power collection than the Sun-Tower or Tethered SPS due to it's large sun-tracking reflectors. Working prototypes of the sandwich module (the defining component of the sandwich SPS) have been built and tested at the Naval Research Laboratory.[11] The advantages and disadvantages of each SPS considered in this thesis are summarised in Table 6.3.

Table 6.3: Advantages and disadvantages of different SPS designs.

	Advantages	Disadvantages
Abacus	Sun-pointing solar array collects maximum amount of sunlight with 0 angle of incidence Only one lightweight moving part, the reflector which redirects the microwave beam	Not a stable attitude configuration Optically flat large reflector required Requires $\sim 10^6$ kg orbit-attitude fuel over 30 year lifetime
Cylindrical	Axisymmetric which minimises gravity gradient torque Transmitting antenna near COM which reduces SRP torque	Not a stable attitude configuration Majority of sunlight collected has non-zero angle of incidence necessitating larger solar array area
ISC	Separation of PV and transmitting antenna Avoids thermal issue of sandwich SPS by separating PVs and transmitting antenna, allowing higher sun concentration	Not a stable attitude configuration Complex multi-body dynamics Requires $\sim 10^6$ kg of orbit-attitude fuel over 30 year lifetime[19]
Sandwich	Extremely modular Rated most technically feasible by IAA[7] Working prototype sandwich modules exist[11]	Thermal issue - combining PVs with transmitting antenna leads to issue with radiating heat Complex multi-body dynamics Interconnecting tethers represent single point of failure
Sun-Tower	Nominal orbit-attitude control required Stable attitude configuration	Requires extremely long (55 km) tether backbone to avoid self-shadowing of PV panels Worse PMAD issue than any other SPS, power must be transferred a maximum of 55 km Tether backbone is single point of failure for system
Tethered	Extremely modular Nominal orbit/attitude control required Multiple tethers offer attitude control method No moving parts	Power outages throughout day when PV arrays not in sunlight - not suitable for base--load power

6.2 Future Work

It is the author's opinion that GLPO should also be considered more widely for current day satellites as an alternative to GEO. There are considerable costs associated with operating a satellite in GEO in terms of the propellant required to maintain the satellite in its 'box'. The propellant requirement is largely driven by the need to correct out-of-plane perturbations due to luni-solar gravitational attraction, and the orbital plane is maintained in a quasi-stationary state by periodic thrusting. The lifetime of the satellite is limited by this requirement, and the need to have sufficient propellant for an end-of-life transfer to a graveyard orbit. Operating in GLPO would remove these requirements. Cost-benefit analysis would be necessary to determine if the particular satellite system should be adapted to operate in GLPO rather than GEO. It should certainly be considered as it may offer significant extra operational lifetime to satellites. Additionally, the Laplace plane is not limited to Earth. It is a natural phenomenon which exists for any planet with oblateness and obliquity. The possibility of operating satellites in the Laplace plane of Mars to support future in-situ

missions may be worth considering.

As a general result, the combination of a GGSO in GLPO is an interesting prospect. This allows extremely large structures to be built at geosynchronous altitude with basically no orbit-attitude control required. In the long-term, building large space structures at geosynchronous altitude should seriously consider the GLPO, not only for the fuel savings but also to limit the orbit debris problem at that altitude. This is important considering how valuable a resource the geosynchronous altitude is. If the prospect of operating a SPS (or other large space structure) in GGSO is not beneficial overall, then it may still be a sensible orientation to use in the intermediate stages of on-orbit construction. Additionally, such a configuration may be a good option for a demonstrator SPS mission, eliminating some of the more complicated issues surrounding construction and operation of a large geosynchronous SPS (such as the 'slip-ring' and orbit-attitude control system).

Initially only the force of gravity due to a central attracting body (the Earth) and the torque caused by this force acting on a non-point mass have been incorporated into the spring-damper rotational dynamics model. The effect of adding other disturbance torques should be assessed. In the case that there is an offset between the centre-of-pressure of incoming sunlight and the centre-of-mass of the SPS, the solar radiation pressure will cause a torque. This will probably be larger than conventional satellites due to the high area to mass ratio of SPSs and larger moment arms possible. The transmission of the microwave beam to the Earth's surface may also induce a torque depending on the geometry of the SPS. The stability of the GGSO to these additional torques should be confirmed. The solar radiation pressure gradient torque, which was identified by Sincarsin as a potential problem for SPS and other large spacecraft, should be investigated for modern SPS designs. This is caused when the SPS passes into penumbra/umbra and there is uneven distribution of solar radiation causing a torque. For very large spacecraft solar-pressure-gradient torque can become significant and can produce a solar torque in penumbra greater than that experienced

in full sunlight. It can even dominate gravity-gradient torque, both in magnitude and angular impulse, for some spacecraft.[91]

Straightforward calculation of both orbit station-keeping and gravity-gradient torque cancellation propellant requirements have been performed. However, this thesis has primarily focussed on simulating the uncontrolled dynamics of SPSs. The next logical step is the development of optimal control laws for different SPS designs. Comprehensive attitude stability analysis should be carried out for candidate SPS designs. The equations of motion of the spring-damper model could be linearised so that stability conditions could be derived (i.e conditions on the ratios of the moments of inertia).

The foundations have been laid to develop equations of motion which incorporate energy dissipation, mutual gravity gradient torque, disturbance torques (SRP, microwave beaming etc.) as well as all of the orbit perturbations. This thesis has generally considered the orbital and rotational dynamics separately (which was shown to be a reasonable assumption), however, for a more complete understanding of the dynamics of SPS systems, and for detailed stability analysis it may be beneficial to reassess this. The orbit perturbation equations may be incorporated into the energy-dissipation model to assess the full dynamics of SPS systems. The full orbit-attitude dynamics model will allow for the most appropriate orbit and attitude configurations to be identified for candidate SPS designs.

Along with more detailed analysis of the GGSO attitude mode, other possible attitude modes for SPS deserve further research. The quasi-inertial pointing mode of Elrod[61] and the quasi-sun pointing mode of Sincarsin[72] should be re-examined, with the application to modern SPS designs investigated. Previously, these attitude modes have only been considered in GEO or geosynchronous ecliptic plane orbits. The feasibility of their application in GLPO should also be considered.

The spring-damper model for energy-dissipation has potential non-SPS applications. For instance, it could be used to model the rotational motion of asteroids or comets. Study of comets and asteroids rotation states may provide much information

about their recent history and internal structure. The spring-damper model could offer a conceptually simple way to approximate the internal stress induced by non-uniform rotation, which leads to energy dissipation in asteroids. In order to apply the energy-dissipation model to the asteroid rotation state modelling, the physical properties of the asteroid must be related to the parameters of the spring mass damper system. The kinetic energy of rotation decreases at a rate equal to that of energy losses in the material. Therefore, the elastic energy stored in a tumbling body should be calculated first, followed by the energy-dissipation rate, using the material quality factor. From the energy-dissipation rate the appropriate spring-damper parameters could be calculated to simulate the motion.

Another application of the spring-damper model is for the investigation of attitude control by moving mass actuators. Moving masses present some advantages over traditional methods for controlling spacecraft attitude. They require no propellant and are not affected by the Earth's magnetic field as others methods can be. This idea has been previously proposed and tested for cubesats, to the author's knowledge it has not been widely considered for large space structures. Such a method may help to enable sun-pointing modes by reducing the mass of propellant required, although whether or not it is feasible is yet to be determined.

I

Appendices

A

Orbit Dynamics Model

A.1 Partial Derivatives

The partials of the singly averaged potentials for substitution into Eqs. (3.54) and (3.55), respectively, are given by

$$\frac{\partial \overline{\mathcal{R}}^*_{SRP}}{\partial \boldsymbol{h}} = 0 \qquad \frac{\partial \overline{\mathcal{R}}^*_{SRP}}{\partial \boldsymbol{e}} = \frac{3}{2}\sqrt{\frac{a}{\mu}}\frac{\gamma}{d_s^2}\hat{\boldsymbol{d}}_s$$

$$\frac{\partial \overline{\mathcal{R}}^*_{20}}{\partial \boldsymbol{h}} = \frac{3nC_{20}}{4a^2h^5}\left\{[1-\frac{5}{h^2}(\hat{\boldsymbol{p}}\cdot\boldsymbol{h})^2]\boldsymbol{h} + 2(\hat{\boldsymbol{p}}\cdot\boldsymbol{h})\hat{\boldsymbol{p}}\right\} \qquad \frac{\partial \overline{\mathcal{R}}^*_{20}}{\partial \boldsymbol{e}} = \frac{3nC_{20}}{4a^2h^5}\left[1-(\hat{\boldsymbol{p}}\cdot\boldsymbol{h})^2\right]\boldsymbol{e}$$

$$\frac{\partial \overline{\mathcal{R}}^*_{s}}{\partial \boldsymbol{h}} = -\frac{3\mu_s}{2nd_s^3}(\hat{\boldsymbol{d}}_s\cdot\boldsymbol{h})\hat{\boldsymbol{d}}_s \qquad \frac{\partial \overline{\mathcal{R}}^*_{s}}{\partial \boldsymbol{e}} = \frac{3\mu_s}{2nd_s^3}\left[5(\hat{\boldsymbol{d}}_s\cdot\boldsymbol{e})\hat{\boldsymbol{d}}_s - 2\boldsymbol{e}\right]$$

$$\frac{\partial \overline{\mathcal{R}}^*_{m}}{\partial \boldsymbol{h}} = -\frac{3\mu_m}{2nd_m^3}(\hat{\boldsymbol{d}}_m\cdot\boldsymbol{h})\hat{\boldsymbol{d}}_m \qquad \frac{\partial \overline{\mathcal{R}}^*_{m}}{\partial \boldsymbol{e}} = \frac{3\mu_m}{2nd_m^3}\left[5(\hat{\boldsymbol{d}}_m\cdot\boldsymbol{e})\hat{\boldsymbol{d}}_m - 2\boldsymbol{e}\right]$$

where all the symbols used have been previously defined in the text.

A.2 Comparison of Averaged and Nonaveraged Dynamics

The nonaveraged model, singly averaged model, and doubly averaged model are compared in Fig. A.1 (where the double averaging is only over the lunisolar gravitational perturbations). For propagations of the order of 50 years, the integration of the averaged equations of motion is several hundred times faster than the integration of the nonaveraged equations of motion. The singly averaged model more closely matches the non-averaged model. The averaged models still qualitatively capture the long-term motion of the satellite and would be well suited to future studies involving multiple

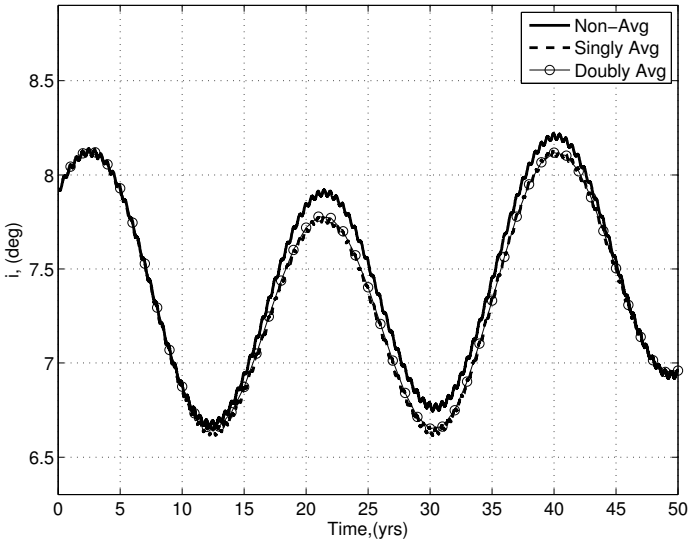

(a) Inclination vs time.

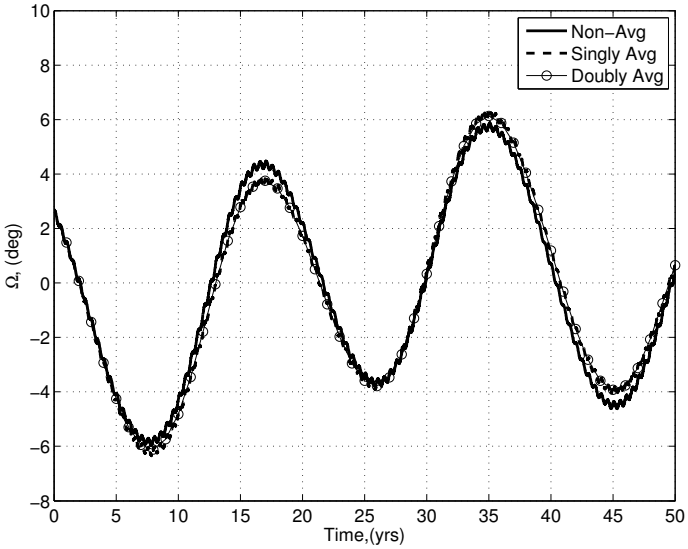

(b) RAAN vs time

Figure A.1: Comparison of singly averaged dynamics and nonaveraged dynamics.

satellite constellations.

B

Abacus Solar Power Satellite

Abacus/Reflector Concept

ENTECH Concentrators, Solid State, 1200 MW Delivered from GEO

System Element	*Mass (MT)*	*Comments*
RF Transmitter Array		Devices, Structure; Input Power = 3614 MWe
Transmitter Elements	1156	Diameter = 500 meters; 83903 Thousand Solid State Devices
Transmitter Planar Array	1612	Mass = 8.21 kg/m2
Transmitter Array Structure	281	Composite Truss Structure @ 1.43 kg/m2
Reflector and Bearing Struct	844	Only Applicable to Reflector Concepts
Transmitter Thermal Control	0	Integrated, Some TC Included in Transmitter Element Mass
Add'l Structure Allowance	117	Allowance = 3%
Solar Conversion		SLA, 1 wing(s) with array dimensions = 1772 m x 6200 m
Solar Concentrators/Arrays	4317	Unit Height = 40 m, Width = 200 m, Mass = 3.664 MT, Power = 3.346 MW
Add'l Structure Allowance	129	Allowance = 3%
Telecomm & Command	3	One set per solar array node (38 sets)
Add'l Structure Allowance	0	Allowance = 3%
Integrating Structure	3563	Abacus, Total Length = 1772 meters
PMAD		Cabling & Power Conversion, SPG Power = 3941 MWe; Advanced PMAD
Cabling	173	Total Length = 3162 km @ 0.055 kg/m, Voltage = 100 kV
Array Converter Mass	3544	Mass based on 1178 Converters (1000 V to 100 kV), 3.346 MW Power Out
Transmitter PMAD Mass	4362	Mass Includes Voltage Convertors, Switches, Harness & PMAD Thermal , 3.61 GW
Rotary Joints, Switches, Etc.	1	Thruster Switches Only
Attitude Control/Pointing		Sensors, Computers, Control Effectors
Dry Mass	452	Thrusters, CMG's, Sensors etc. at each solar collector
Propellant	665	Delta V = 50 m/s per year for 10 years
Add'l Structure Allowance	14	Allowance = 3%
SEP Propulsion	831	LEO-GEO Transfer Stages
Dry Mass	3815	Thruster Power = 50 kWe (8 Hall Thrusters, Isp = 2000 sec)
Propellant	7361	Krypton
Add'l Structure Allowance	114	Allowance = 3%
Expendable Solar Arrays	664	Thin Film Arrays, 500 W/kg
Payload Mass	0	
Satellite Launched Mass (MT)	33187	ETO Payloads = 40 MT per launch (830 Launches)
Satellite Orbited Mass (MT)	25162	At 35786 km

Rectenna Diameter (m) 7450

Harvey Feingold 5/26/00

Figure B.1: Mass breakdown of Abacus components.[40]

C

Matrix Operations

The following are operations between vectors which are expressed in a particular frame of reference as matrices:

$$\begin{aligned} \boldsymbol{a}^T\boldsymbol{b} &= [a_1 \ a_2 \ a_3] \begin{bmatrix} b_1 \\ b_2 \\ b_3 \end{bmatrix} \\ &= a_1b_1 + a_2b_2 + a_3b_3 \end{aligned} \tag{C.1}$$

$$\boldsymbol{a}^\times = \begin{bmatrix} 0 & -a_3 & a_2 \\ a_3 & 0 & -a_1 \\ -a_2 & a_1 & 0 \end{bmatrix} \tag{C.2}$$

This may also be represented by:

$$\widetilde{\boldsymbol{a}} = a_1(\hat{\boldsymbol{e}}_3\hat{\boldsymbol{e}}_2 - \hat{\boldsymbol{e}}_2\hat{\boldsymbol{e}}_3) + a_2(\hat{\boldsymbol{e}}_1\hat{\boldsymbol{e}}_3 - \hat{\boldsymbol{e}}_3\hat{\boldsymbol{e}}_1) + a_3(\hat{\boldsymbol{e}}_2\hat{\boldsymbol{e}}_1 - \hat{\boldsymbol{e}}_1\hat{\boldsymbol{e}}_2) \tag{C.3}$$

where a_i are the components of the vector and $\hat{\boldsymbol{e}}_1\hat{\boldsymbol{e}}_2$ is a dyad:

$$\hat{\boldsymbol{e}}_1\hat{\boldsymbol{e}}_2 = \hat{\boldsymbol{e}}_1\hat{\boldsymbol{e}}_2^T \tag{C.4}$$

$$= \begin{bmatrix} 1 \\ 0 \\ 0 \end{bmatrix} [\, 0\ 1\ 0\,]$$

$$= \begin{bmatrix} 0 & 1 & 0 \\ 0 & 0 & 0 \\ 0 & 0 & 0 \end{bmatrix} \tag{C.5}$$

D

Energy Dissipation Model Additional Results

D.1 SAM and LAM

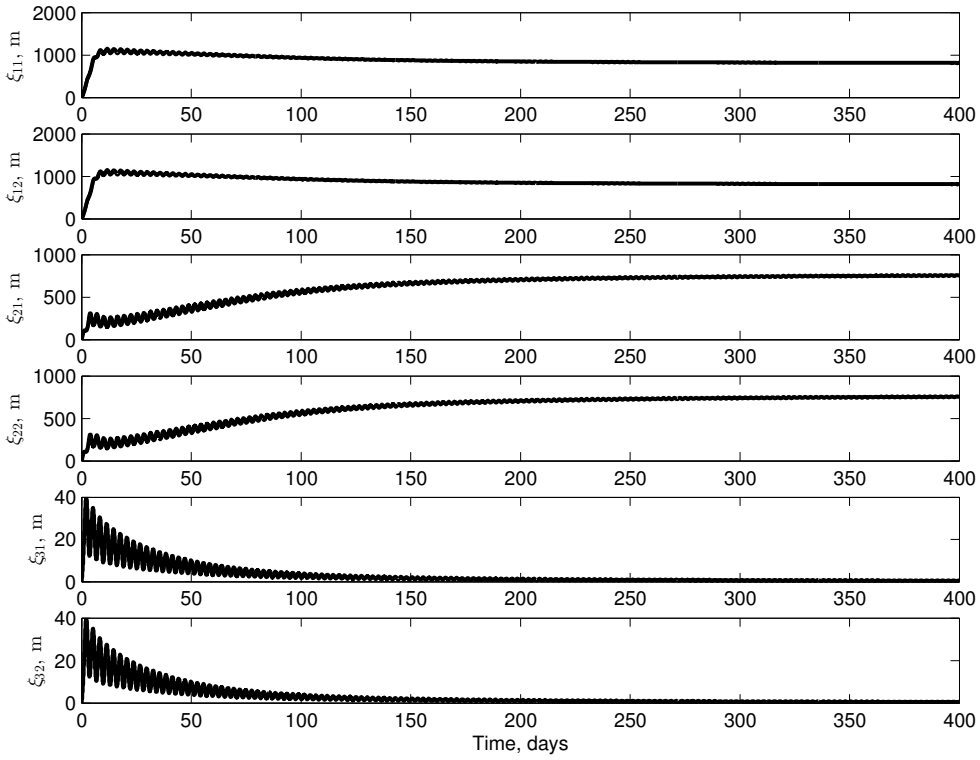

Figure D.1: SAM damper displacements.

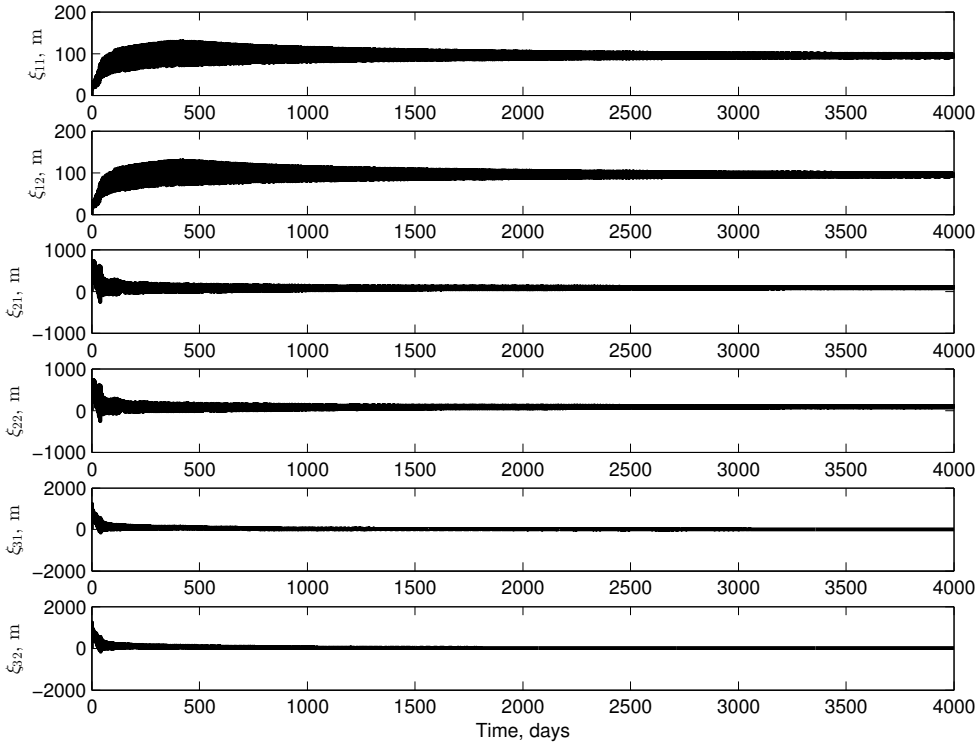

Figure D.2: LAM damper displacements.

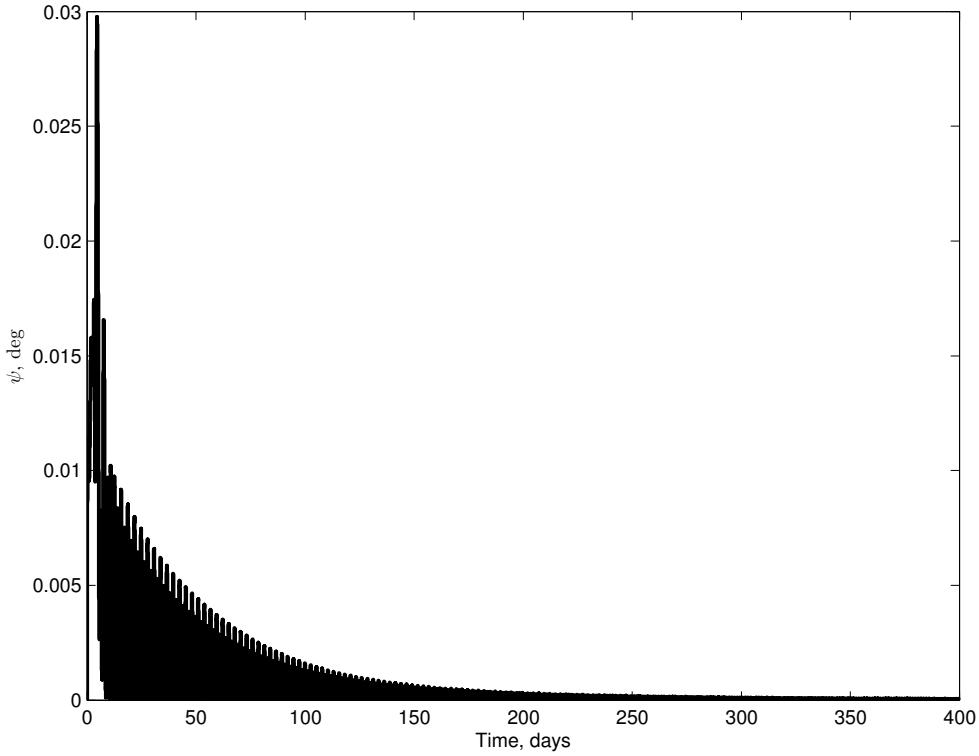

Figure D.3: SAM: Angle between $\boldsymbol{l}$ and $\boldsymbol{\omega}$.

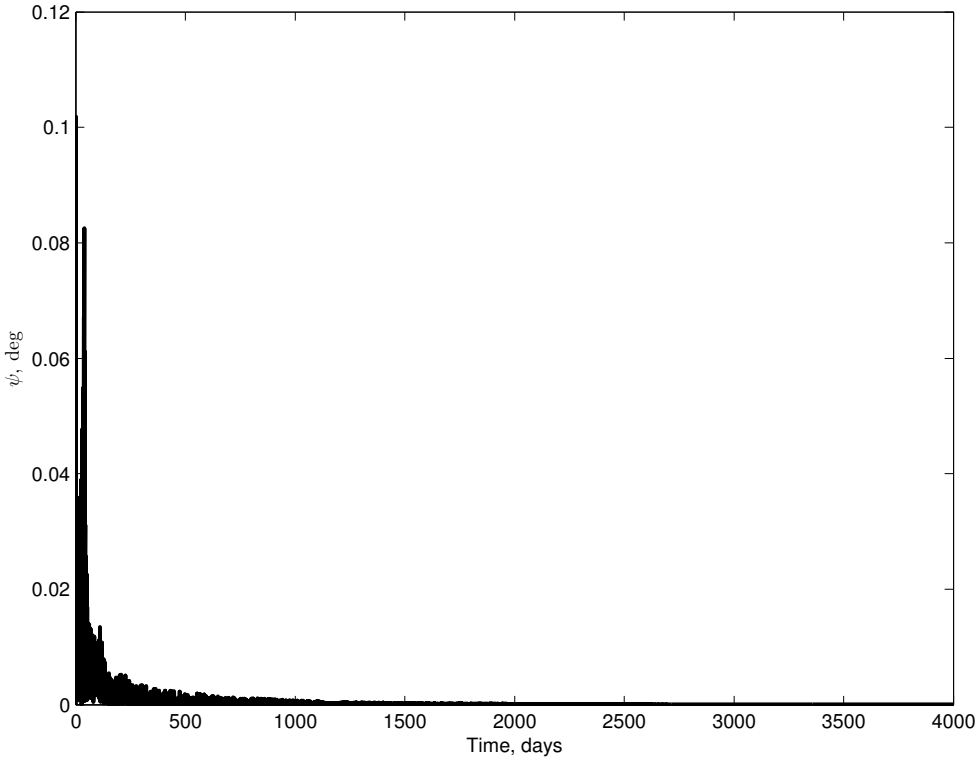

Figure D.4: LAM: Angle between $\boldsymbol{l}$ and $\boldsymbol{\omega}$.

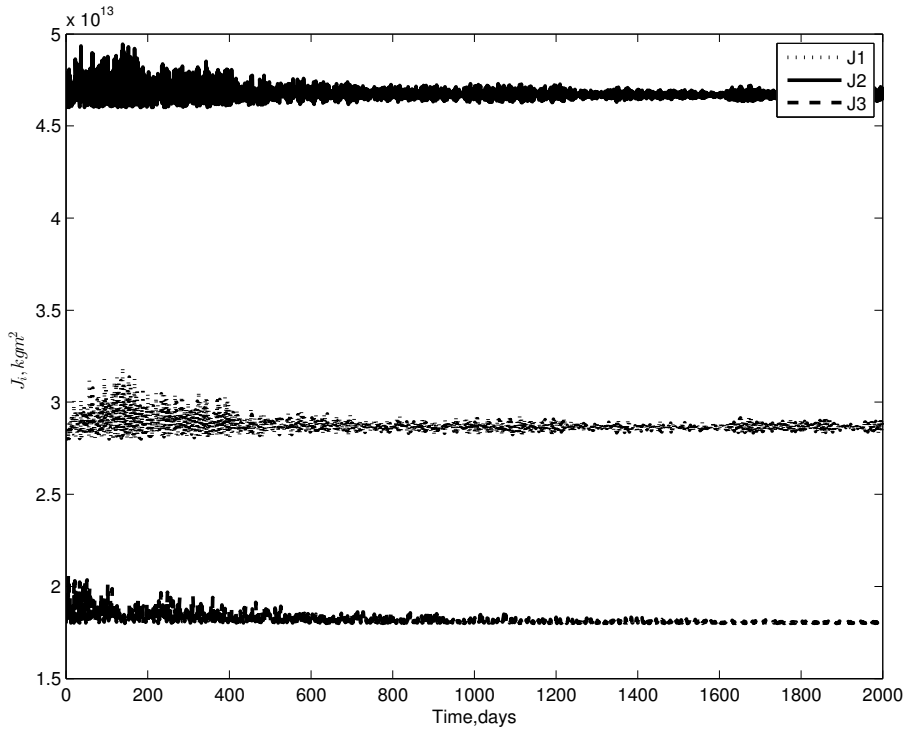

Figure D.5: Inertia dyadic diagonal elements.

E

Angular Momentum and Energy

In the absence of external torques ($\boldsymbol{g} = \mathbf{0}$) the magnitude of the angular momentum of the system l should be conserved. In an inertial reference frame, the direction of the angular momentum vector should also be constant. To confirm that this, $\frac{l_0 - l(t)}{l_0}$ is plotted versus time in Fig E.1(b). The variation in the magnitude of the angular momentum vector l is less than the integration tolerance. The direction of the angular momentum vector $\boldsymbol{l}$ is shown to be conserved in Fig. E.3.

Once the body reaches a maximum axis rotation state, it has reached the minimum rotational kinetic energy state. The total kinetic energy is shown for SAM in Fig. E.5(a) and the total energy (as given by Eq. (5.39)) in Fig. E.5(b). The total kinetic energy is shown for LAM in Fig. E.6(a) and the total energy in Fig. E.6(b).

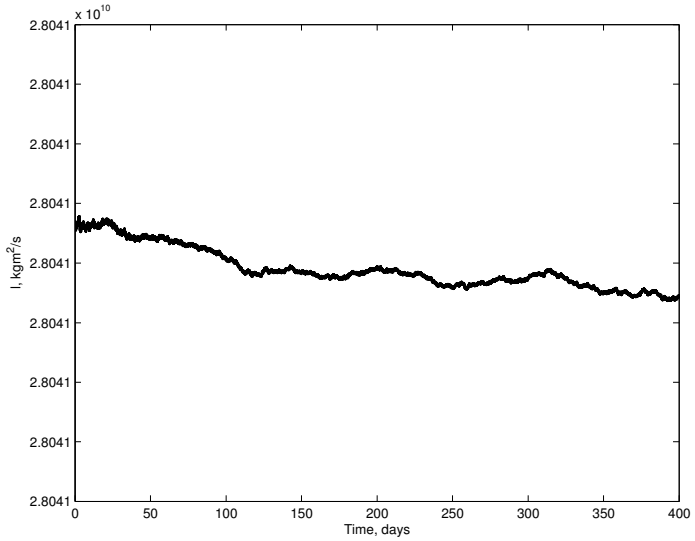

(a) Magnitude of angular momentum.

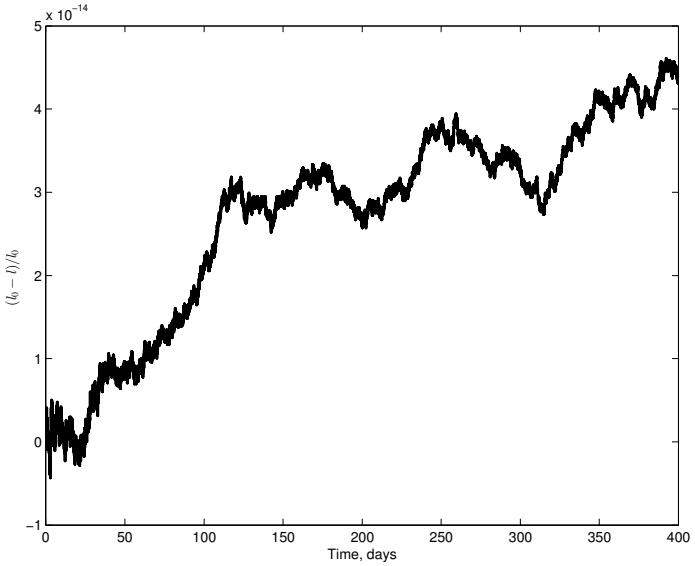

(b) $(l_0 - l)/l_0$ versus time.

Figure E.1: Validation of the conservation of angular momentum for the SAM case.

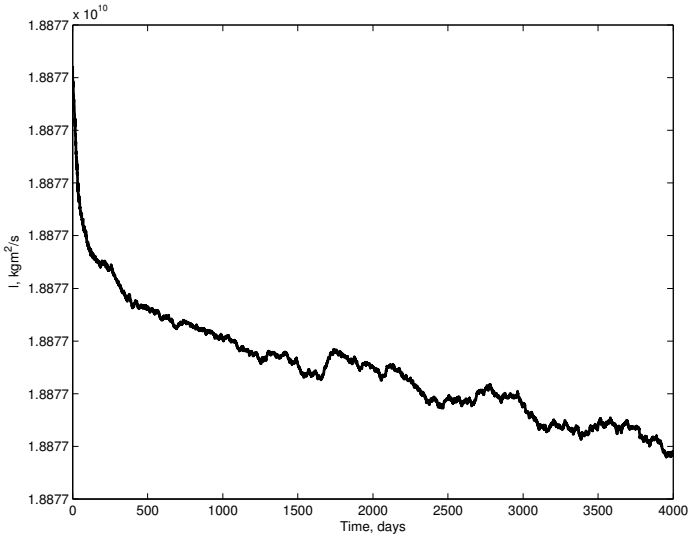

(a) Magnitude of angular momentum.

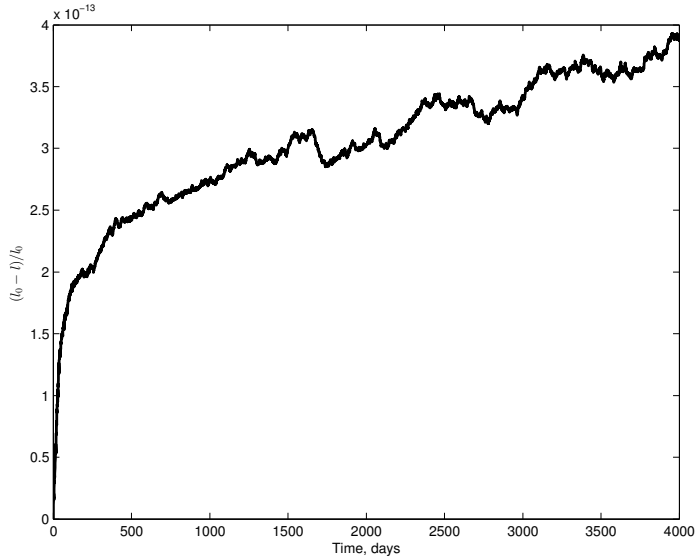

(b) $(l_0 - l)/l_0$ versus time.

Figure E.2: Validation of the conservation of angular momentum for the LAM case.

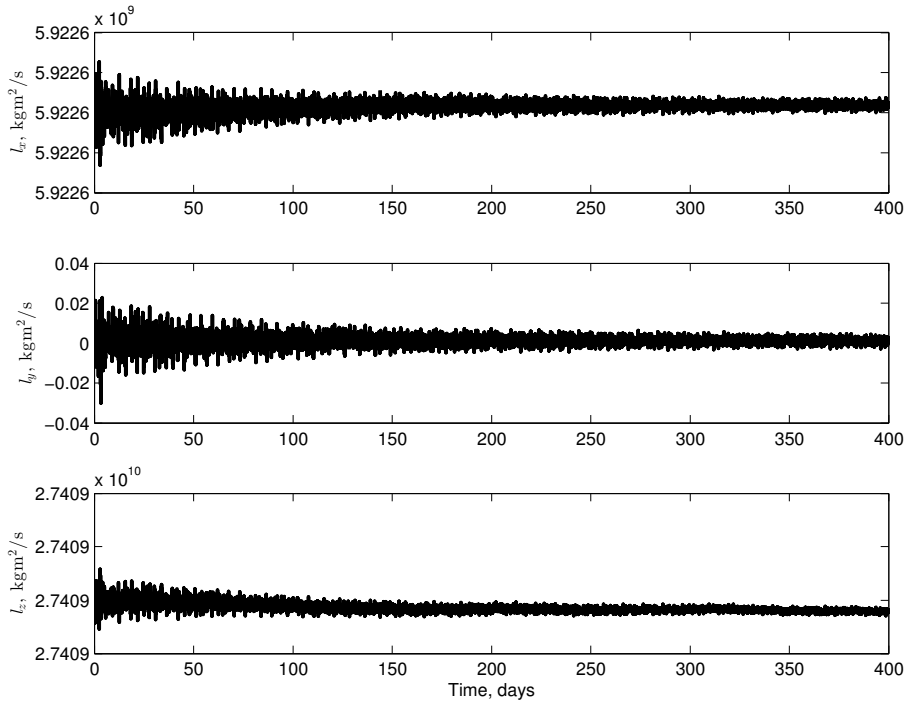

Figure E.3: Angular momentum components in $\mathcal{F}_{\mathcal{I}}$ for SAM test case.

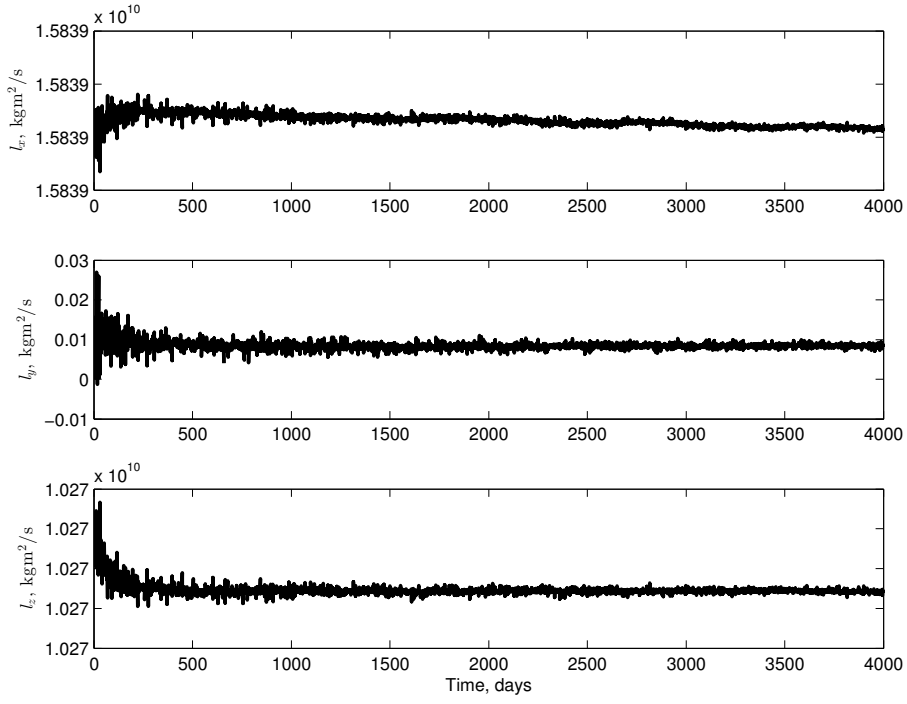

Figure E.4: Angular momentum components in $\mathcal{F}_{\mathcal{I}}$ for LAM test case.

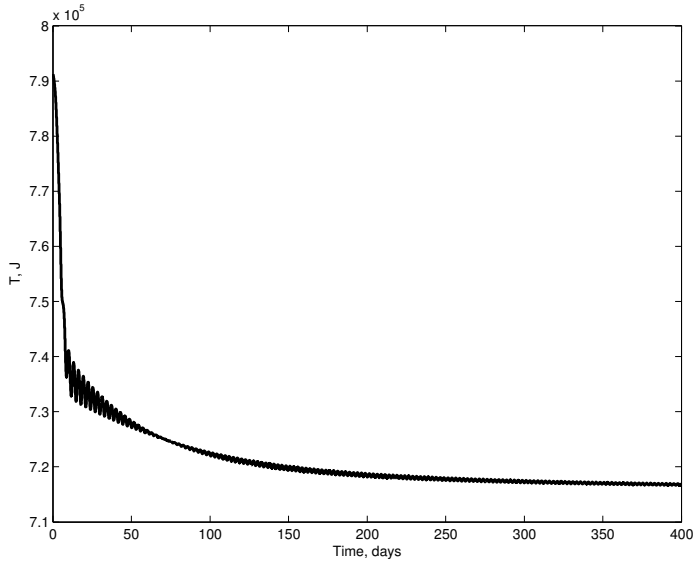

(a) Total kinetic energy.

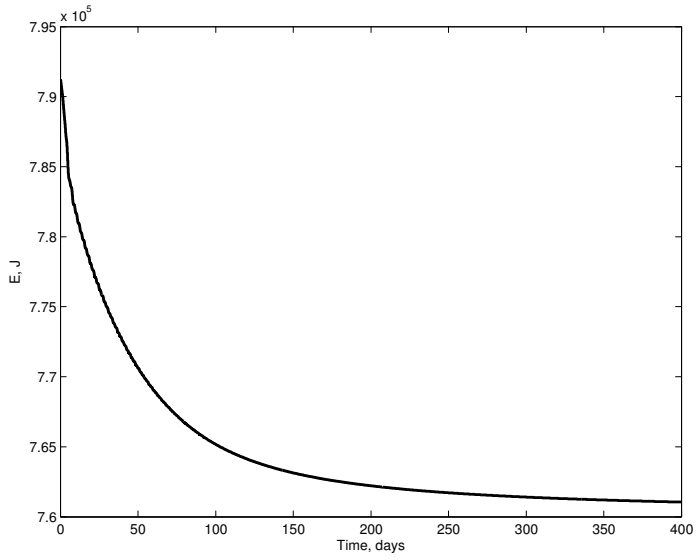

(b) Total energy.

Figure E.5: Energy for SAM case.

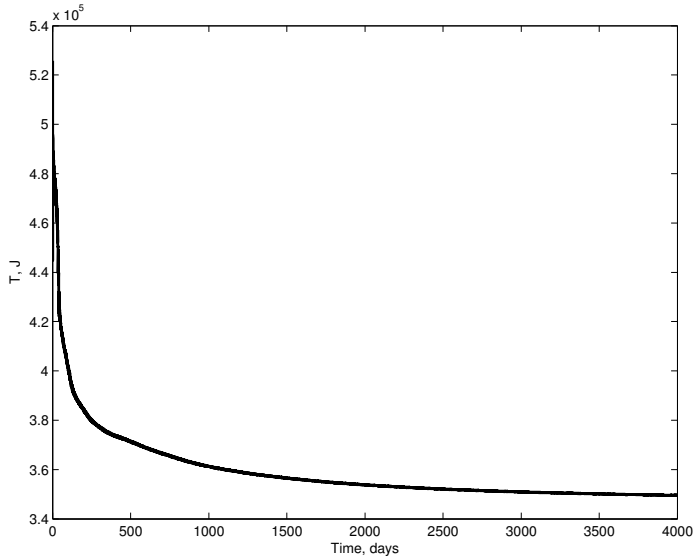

(a) Total kinetic energy.

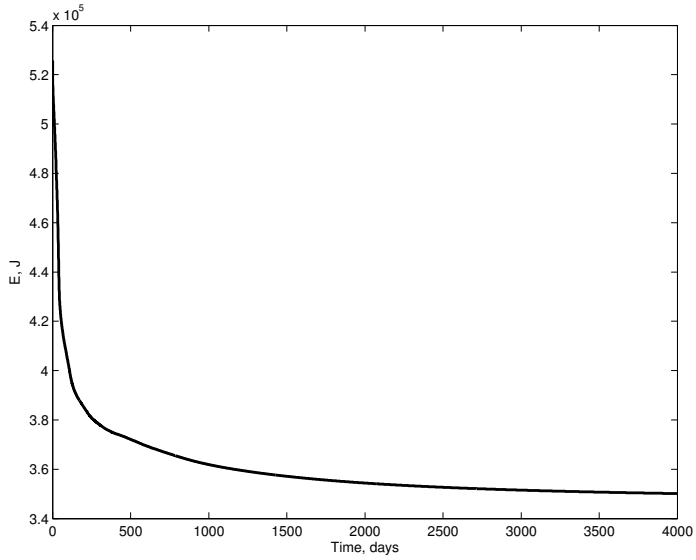

(b) Total energy.

Figure E.6: Energy for LAM case.

Bibliography

[1] Glaser, P., "Power from the Sun: Its Future," Science, Vol. 162, No. 3856, November 1968, pp. 857–861, doi:10.1126/science.162.3856.857.

[2] "Satellite Power System (SPS) Concept Development and Evaluation Program, Reference System Report," Tech. rep., NASA and US Department of Energy, 1978.

[3] The Final Proceedings of the Solar Power Satellite Program Review, 1980.

[4] Mankins, J. C., "A Fresh Look at Space Solar Power: New Architecture, Concepts, and Technologies," Acta Astronautica, Vol. 41, No. 4-10, 1997, pp. 347–359, doi:10.1016/S0094-5765(98)00075-7.

[5] "Space-Based Solar Power as an Opportunity for Strategic Security: Phase 0 Architecture Feasibility Study," Tech. rep., National Security Space Office, Washington, DC, 2007.

[6] Corporation, N. G., "Space Solar Power Initiative Established by Northrop Grumman and Caltech," April 2015.

[7] Mankins(Ed.), J. and Kaya(Ed.), N., "Space Solar Power: The First International Assessment of Space Solar Power," Tech. rep., International Academy of Astronautics, 2011.

[8] Council, N. R., Laying the Foundation for Space Solar Power: An Assessment of NASA&039;s Space Solar Power Investment Strategy, The National Academies Press, Washington, DC, 2001.

[9] R. Taton, C. W., editor, The General History of Astronomy, Vol. Vol.2: Planetary astronomy from the Renaissance to the rise of Astrophysics. Part B: The eighteenth and nineteenth centuries, Cambridge University Press, 1995.

[10] Goldstein, H., Classical Mechanics, Addison-Wesley, Reading, MA, 1980.

[11] Jaffe, P. I., A sunlight to microwave power transmission module prototype for space solar power, Ph.D. thesis, University of Maryland, 2013.

[12] Maynard, O. E., "Solid State SPS Microwave Generation and Transmission Study," Tech. Rep. NASA CR-3338, NASA, November 1980, Vol. I, Phase II Final Report prepared for MSFC under contract NAS 8-33157.

[13] 61st International Astronautical Congress, Multiobjective Optimisation of Integrated Space-Based and Terrestrial Solar Energy Systems, Prague, 2010.

[14] Gershman, R. and Seybold, C., "Propulsion Trades for Space Science Missions," Acta Astronautica, Vol. 45, No. 4-9, 1999, pp. 541–548.

[15] Wie, B. and Roithmayr, C., "Integrated Orbit, Attitude, and Structural Control Systems Design for Space Solar Power Satellites," Tech. rep., NASA Langley Research Center, Hampton, Virginia, 2001, NASA Contract NAS1-00122.

[16] Wie, B. and Roithmayr, C., "Attitude and Orbit Control of a Very Large Geostationary Solar Power Satellite," Journal of Guidance, Control and Dynamics, Vol. 28, No. 3, 2005, pp. 439–451, doi:10.2514/1.6813.

[17] "Solar Cell and Array Technology for Future Space Science Missions," Tech. rep., NASA, 2002.

[18] Seboldt, W. and Reichert, M., "System Concepts, Architectures and Technologies for Space Exploration and Utilisation," Tech. rep., DLR, 1999.

[19] Glaese, J. R. and McDonald, E. J., "Space Solar Power Multi-Body Dynamics and Controls, Concepts for the Integrated Symmetrical Concentrator Configuration," Tech. Rep. NAS8-00151, NASA, 2000.

[20] Goubau, G. and Schwering, F., "On the Guided Propagation of Electronmagnetic Wave Beams," IRE Transactions on Antennas and Propagation, Vol. 9 (3), 1961, pp. 248–256, doi: 10.1109/TAP.1961.1144999.

[21] Brown, W. C. and Eves, E. E., "Beamed microwave power transmission and its application to space," IEEE Transactions on Microwave Theory and Techniques, Vol. 40, No. 6, Jun 1992, pp. 1239–1250.

[22] McSpadden, J. O. and Mankins, J. C., "Space solar power programs and microwave wireless power transmission technology," IEEE Microwave Magazine, Vol. 3, No. 4, Dec 2002, pp. 46–57.

[23] Jaffe, P., "Space Solar Power: Naval Research Laboratory Sandwich Panel Research and Development Status Update," International Space Solar Power Symposium, 2011.

[24] "Space X: Capabilities and Services," `http://www.spacex.com/about/capabilities`, Accessed: 2018-04-12.

[25] Martin, J. A., Donnahue, B. B., and Henley, M. W., "In-Space Transportation for GEO Space Solar Power Satellites," Tech. Rep. NAS8-98244, NASA, 1999.

[26] Wiesel, W. E. and Alfano, S., "Optimal Many-Revolution Orbit Transfer," Journal of Guidance, Control and Dynamics, Vol. 8, 1985, pp. 155–157.

[27] Wertz, J. R., Space Mission Analysis and Design, Microcosm Press and Springer, 3rd ed., 1999.

[28] Potter, S., Bayer, M., Davis, D., Born, A., McCormick, D., Dorazio, L., and Patel, P., "Space Solar Power Satellite Alternatives and Architectures," 47th

AIAA Aerospace Sciences Meeting Including the New Horizons Forum and Aerospace Exposition, Boeing Company, 5-8 January 2009, AIAA 2009-462, doi: 10.2514/6.2009-462.

[29] Vallado, D. A., Fundamentals of Astrodynamics and Applications, Microcosm Press and Springer, 3rd ed., 2007.

[30] Wie, B., Space Vehicle Dynamics and Control, AIAA Education Series, AIAA, 1998.

[31] "Construction costs for most power plant types have fallen in recent years," https://www.eia.gov/todayinenergy/detail.php?id=31912, Accessed: 2018-04-25.

[32] Sobol, I., "Global sensitivity indices for nonlinear mathematical models and their Monte Carlo estimates," Mathematics and Computers in Simulation, Vol. 55, No. 1, 2001, pp. 271 – 280, The Second IMACS Seminar on Monte Carlo Methods.

[33] Saltelli, A., "Making best use of model evaluations to compute sensitivity indices," Computer Physics Communications, Vol. 145, No. 2, 2002, pp. 280 – 297.

[34] Saltelli, A., Annoni, P., Azzini, I., Campolongo, F., Ratto, M., and Tarantola, S., "Variance based sensitivity analysis of model output. Design and estimator for the total sensitivity index," Computer Physics Communications, Vol. 181, No. 2, 2010, pp. 259 – 270.

[35] Herman, J. and Usher, W., "SALib: An open-source Python library for Sensitivity Analysis," The Journal of Open Source Software, Vol. 2, No. 9, jan 2017.

[36] Electric Power From Orbit: A Critique of a Satellite Power System, The National Academies Press, Washington, DC, 1981.

[37] Mankins, J., "SPS-ALPHA: The First Practical Solar Power Satellite via Arbitrarily Large Phased Array," 2012.

[38] Graf, O., "Orbital Motion of the Solar Power Satellite," Tech. Rep. N78-1548, Analytical and Computational Mathematics, Inc., 1978.

[39] "Satellite Power System Concept Definition Study. Vol. III." Tech. Rep. SD 78-AP-0023-3, Rockwell International, April 1978.

[40] Carrington, C. and Feingold, H., "Space Solar Power Systems Integration, Analysis and Modeling," Space Solar Power Technical Interchange Meeting No.3, 2000.

[41] Glaser, P., "Satellite Solar Power Station," Solar Energy, Vol. 12, 1969, pp. 353–361, doi: 10.1016/0038-092X(69)90049-8.

[42] Little, F., Kokel, S., Rodenback, C., Chang, K., and Arndt, G., "Development of a Retrodirective Control Transmitter for Wireless Power Transmission," Radio Science Bulletin, , No. 311, 2004, pp. 38–46.

[43] Tamayo, D., Burns, J., Hamilton, D., and Nicholson, P., "Dynamical Instabilities in High-Obliquity Systems," The Astronomical Journal, Vol. 145:54, March 2013, pp. 1–12, doi: 10.1088/0004-6256/145/3/54.

[44] Laplace, P., "Traité de mécanique céleste," de l'Imprimerie Crapelet, Vol. 4, 1805.

[45] Rosengren, A. J., Scheeres, D. J., and McMahon, J. W., "Long-term dynamics and stability of GEO orbits: the primacy of the Laplace plane," Advances in Space Research, Vol. 53, April 2014, pp. 1219–1228, doi: 10.1016/j.asr.2014.01.034.

[46] Ulivieri, C., Circi, C., Ortore, E., Bunkheila, F., and Todino, F., "Frozen Orbital Plane Solutions for Satellites in Nearly Circular Orbit," Journal of Guidance, Control and Dynamics, Vol. 36, No. 4, 2013, pp. 935–945, doi: 10.2514/1.59734.

[47] Allan, R. and Cook, G., "The long-period motion of the plane of a distant circular orbit," Proceedings of the Royal Society of London A, Vol. 280, 1964, pp. 97–109, doi: 10.1098/rspa.1964.0133.

[48] Rosengren, A. J. and Scheeres, D., "Long-term dynamics of high area-to-mass ratio objects in high-Earth orbit," Advances in Space Research, Vol. 52, 2013, pp. 1545–1560, doi: 10.1016/j.asr.2013.07.033.

[49] Rosengren, A. J. and Scheeres, D., "On the Milankovitch Orbital Elements for Perturbed Keplerian Motion," Celestial Mechanics and Dynamic Astronomy, Vol. 118, 2014, pp. 197–220, doi:10.1007/s10569-013-9530-7.

[50] Scheeres, D., Orbital Motion in Strongly Perturbed Environments: Applications to Asteroid, Comet and Planetary Satellite Orbiters, Springer-Praxis Books in Astronautical Engineering, 2012, doi:10.1007/978-3-642-03256-1.

[51] Mignard, F. and Hénon, M., "About an Unsuspected Integrable Problem," Celestial Mechanics and Dynamic Astronomy, Vol. 33(3), July 1984, pp. 239–250, doi: 10.1007/BF01230506.

[52] Tremaine, S., Touma, J., and Namouni, F., "Satellite Dynamics on the Laplace Surface," The Astronomical Journal, Vol. 137, 2009, pp. 3706–3717, doi: 10.1088/0004-6256/137/3/3706.

[53] Rosengren, A., Scheeres, D., and McMahon, J., "The classical Laplace plane as a stable disposal orbit for geostationary satellites," Advances in Space Research, 2014, 1219-1228.

[54] Rosengren, A. and Scheeres, D., "Laplace Plane Modifications Arising from Solar Radiation Pressure," The Astrophysical Journal, , No. 786, 2014, 13pp.

[55] McNally, I., Scheeres, D. J., Radice, G., and Ceriotti, M., "Orbital Dynamics of

Large Solar Power Satellites," Presented at the 64th International Astronautical Congress, Beijing, CN, 23-27 September 2013, IAC-13-C3.1.7.

[56] Friesen, L. J., Kessler, D. J., and Zook, H. A., "Reduced debris hazard resulting from a stable inclined geosynchronous orbit," Advances in Space Research, Vol. 13, No. 8, 1993, pp. 231–241, doi: 10.1016/0273-1177(93)90596-4.

[57] Chao, C. C., Applied Orbit Perturbations and Maintenance, The Aerospace Press / AIAA, 2005, pp 46-52.

[58] Kaula, W. M., Theory of Satellite Geodesy, Blaisdell Publishing Company, Waltham, MA, 1966, pp 30-37.

[59] Agrawal, B. N., Design of Geosynchronous Spacecraft, Prentice-Hall, 1986, pp 83-91.

[60] Ogilvie, R. E., "The Final Proceedings of the Solar Power Satellite Program Review: SPS Attitude Control and Stationkeeping-Requirements and Tradeoffs," Tech. rep., Rockwell International, Lincoln, Nebraska, April 1980, pp 168-171.

[61] Elrod, B. D., "A quasi-inertial attitude mode for orborbit spacecraft," Journal of Spacecraft and Rockets, Vol. 9, No. 12, 1972, pp. 889–895.

[62] Juang, J. N. and Wang, S. J., "An investigation of quasi-inertial attitude control for a solar power satellite," Space Solar Power Review, Vol. 3, No. 4, 1982, pp. 337–352.

[63] Ashenberg, J., "Mutual gravitational potential and torque of solid bodies via inertia integrals," Celestial Mechanics and Dynamic Astronomy, Vol. 99, 2007, pp. 149–159.

[64] Schutz, B., "The mutual potential and gravitational torques of two bodies to fourth order," Celestial mechanics, Vol. 24, No. 2, 1981, pp. 173–181.

[65] Schaub, H. and Junkins, J. L., Analytical Mechanics of Space Systems, AIAA Education Series, Reston, VA, 2nd ed., October 2009.

[66] Hughes, P. C., Spacecraft Attitude Dynamics, Dover Publications, Inc., 1986, 2004.

[67] Junkins, J. and Turner, J., Optimal spacecraft rotational maneuvers, Studies in astronautics, Elsevier, 1986.

[68] Herman, D. A., "NASAs Evolutionary Xenon Thruster (NEXT) Project Qualifi cation Propellant Throughput Milestone: Performance, Erosion, and Thruster Service Life Prediction After 450 kg," Tech. Rep. NASA/TM2010-216816, NASA, 2010.

[69] Chernoff, R. C., "Large active retrodirective arrays for space applicatons," IEEE Trans. Antennas Propag., Vol. AP-27, No. 4, July 1979, pp. 489–496.

[70] Ogilvie, R. E., "Attitude control of large solar power satellites," AIAA Guidance and Control Conference, August 1978, AIAA Paper 78-1266.

[71] Bowden, M. L., "A Gravity Gradient Stabilized Solar Power Satellite Design," AIAA 19th Aerospace Sciences Meeting, , No. AIAA-81-0362, 1981.

[72] Sincarsin, G. B. and Hughes, P. C., "Gravitational Orbit-Attitude Coupling For Very Large Spacecraft," Celestial Mechanics, Vol. 31, 1983, pp. 143–161.

[73] Liu, Y., Wu, S., Radice, G., and Wu, Z., "Gravity-Gradient Effects on Flexible Solar Power Satellites," Journal of Guidance, Control and Dynamics, , No. 3, 2018, 773-778.

[74] Zhao, Y., Zhang, J., Zhang, Y., Zhang, J., and Hu, Q., "Gravitational force and torque on a solar power satellite considering the structural flexibility," Acta Astronautica, 2017, 322-337.

[75] Glaese, J. R. and McDonald, E. J., "Space Solar Power Multi-Body Dynamics and Controls, Concepts for the Integrated Symmetrical Concentrator Configuration," Tech. Rep. NAS8-00151, NASA, 2000.

[76] Ogilvie, R. E., "Attitude control of large solar power satellites," AIAA Guidance and Control Conference, August 1978, AIAA Paper 78-1266.

[77] Zhou, D. and Fan, J. X., "Boundary Control in the Attitude Maneuvering of Tethered Space Solar Power Satellite," Journal of Vibration Engineering, Vol. 26, No. 1, 2013, pp. 41–47, (in Chinese).

[78] Ishimura, K., Natori, M., and Wada, M., "Stability Analysis and Decentralized System Design of Large Space Structures Based on Potential Field," 13th International Conference on Adaptive Structures and Technologies, 2003, pp. 413–423, edited by E. J. Breitbach, L. F. Campanile, and H. P. Monner, CRC PRess, Boca Raton, FL.

[79] Ishimura, K. and Higuchi, K., "Coupling between structural deformation and attitude motion of large planar space structures suspended by multi-tethers," Acta Astronautica, Vol. 60, No. 8, 2007, pp. 691 – 710.

[80] He, W., Ouyang, Y., and Hong, J., "Vibration Control of a Flexible Robotic Manipulator in the Presence of Input Deadzone," IEEE Transactions on Industrial Informatics, Vol. 13, No. 1, Feb 2017, pp. 48–59.

[81] He, W. and Ge, S. S., "Cooperative control of a nonuniform gantry crane with constrained tension," Automatica, Vol. 66, 2016, pp. 146 – 154.

[82] He, W., Zhang, S., and Ge, S. S., "Adaptive Control of a Flexible Crane System With the Boundary Output Constraint," IEEE Transactions on Industrial Electronics, Vol. 61, No. 8, Aug 2014, pp. 4126–4133.

[83] He, W. and Ge, S. S., "Vibration Control of a Flexible Beam With Output Constraint," IEEE Transactions on Industrial Electronics, Vol. 62, No. 8, Aug 2015, pp. 5023–5030.

[84] Santini, P., "Stability of flexible spacecrafts," Acta Astronautica, Vol. 3, No. 9, 1976, pp. 685 – 713.

[85] Kumar, V. K. and Bainum, P. M., "Dynamics of a Flexible Body in Orbit," Journal of Guidance, Control, and Dynamics, Vol. 3, No. 1, 1980, pp. 90–92.

[86] Zhendong, H. and Jiazhen, H., "Modeling and analysis of a coupled rigid-flexible system," Applied Mathematics and Mechanics, Vol. 20, No. 10, Oct 1999, pp. 1167–1174.

[87] Kaplan, M. H., Modern Spacecraft Dynamics and Control, John Wiley & Sons, 1976.

[88] Likins, P. W., "Effects of Energy Dissipation on the Free Body Motions of Spacecraft," JPL Technical Report No. 32-860, 1966.

[89] Breiter, S. and Murawiecka, M., "Tumbling asteroid rotation with the YORP torque and inelastic energy dissipation," Monthly Notices of the Royal Astronomical Society, Vol. 449, No. 3, May 2015, pp. 2489–2497.

[90] Tewari, A., Atmospheric and Space Flight Dynamics: Modeling and Simulation with MATLAB and Simulink, Birkhauser Basel, 1st ed., 2007.

[91] Sincarsin, G. B. and Hughes, P. C., "Torque from Solar Radiation Pressure Gradient During Eclipse," J. Guidance, Vol. 6, No. 6, 1983, pp. 511–517.